UNIVERSITY OF CAPE TOWN
IYUNIVESITHI YASEKAPA • UNIVERSITEIT VAN KAAPSTAD

DEPARTMENT OF CIVIL ENGINEERING

STRUCTURAL ENGINEERING AND MECHANICS

Dissertation in partial fulfilment of:

Master of Science in Engineering

FINITE ELEMENT MODELLING OF VOIDED SLAB BRIDGE DECKS USING ORTHOTROPIC PLATE THEORY

By

Warrick de Kock

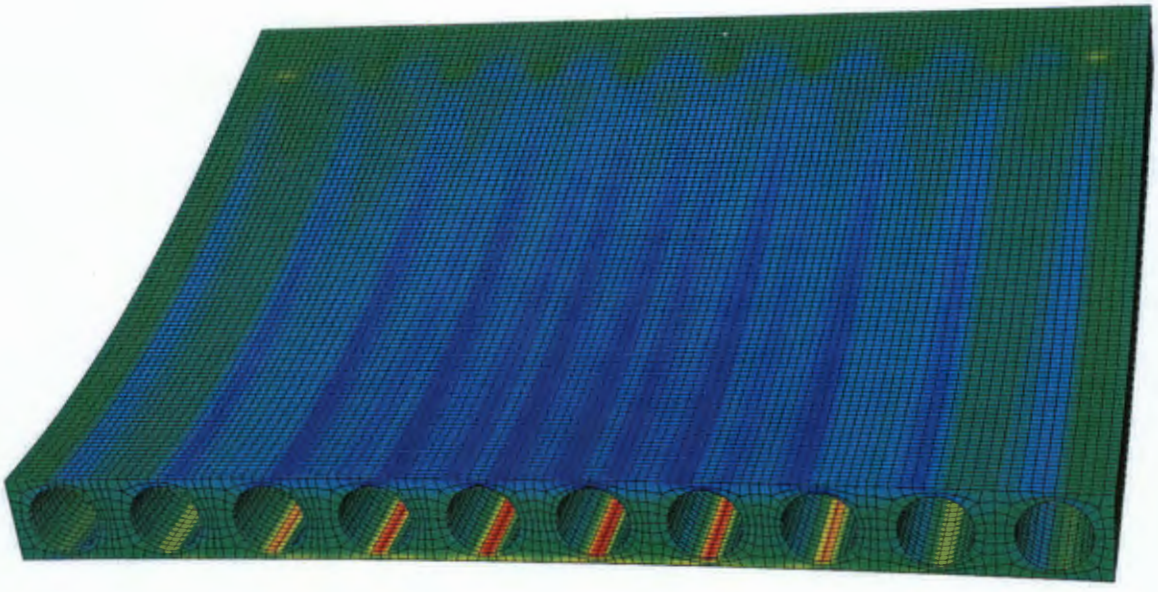

Supervisor: Professor Pilate Moyo

November 2015

PLAGIARISM DECLARATION

I know the meaning of plagiarism and declare that all the work in the document, save for that which is properly acknowledged, is my own.

Signature: Signed

Date: 19/11/2015

"The greatest enemy of knowledge is not ignorance, it is the illusion of knowledge"

- **Stephen Hawking**

ACKNOWLEDGEMENTS

I would like to thank the following individuals for their help, support and contribution to the completion of this research:

- My supervisor, Professor Pilate Moyo, for his guidance and motivation that have been crucial to the outcomes of this research. It was a privilege to study under your supervision.
- My parents and brother for their unwavering support and encouragement for which I am grateful.

ABSTRACT

Circular voids are often incorporated into concrete bridge decks to reduce their self-weight without greatly reducing the flexural stiffness. Incorporating voids within a slab offers many advantages over a conventional solid concrete slab, for example a lower total cost of construction, reduced material use, and enhanced structural efficiency. The advantages of this topology are obvious, however the voids within the slab complicate the analysis of the structure.

The incorporation of the voids within the slab results in different flexural stiffness in the longitudinal and transverse directions, resulting in an orthotropic slab. Another feature which distinguishes voided slabs from other common bridge types is the deformable nature of their cross-sections, which influences the load distribution of the structure. The need for a method of analysis which accounts for the orthotropic behaviour and deformable nature of the cross-section has been suggested by many in the past.

The idealisation of voided slabs as an orthotropic plate has been the subject of extensive research. When modelling a voided slab as an orthotropic plate, it is necessary to calculate the reduction in the longitudinal and transverse stiffness due to the presence of the voids. Several equivalent plate parameters, which take on numerous forms, have been suggested by various authors to account for the effect of the voids. No research has been reported in technical literature to compare these different methods employing orthotropic plate parameters. Key shortcomings to these methods include the lack of definition of the suggested equivalent plate parameters, and the geometrical parameters of voided slabs which influence their behaviour.

In an attempt to address these limitations, the aim of this study is to verify and validate the effect of the void diameter ratio and void spacing on the structural behaviour of voided slabs, which are the main influences on the orthotropic behaviour and cross-section deformation. The different methods of analysis using orthotropic plate theory suggested by various authors employing equivalent plate parameters are compared and discussed. The objectives of the study were achieved based on the finite element approach using ABAQUS.

Finite element models with a void diameter to slab depth ratio range of 0.5 to 0.9, and a void spacing range of 0.9m to 2.7m were considered and analysed. Comparisons were made of the longitudinal and transverse stress distribution results from these models in order to draw conclusions. Results from solid models using both isotropic and orthotropic materials based on the equivalent plate parameters suggested from literature are also presented for comparison in order to verify the methods suggested by the technical literature for the analysis of voided slab bridge decks.

Results of the finite element modelling show that the addition of voids causes large variations to the transverse stress distribution from the typical parabolic transverse stress distribution shape, leading to large peak transverse stresses in the flanges above and below the voids. These variations are due to the

deformable nature of the cross-section. The voids also lead to a stress raising effect on the longitudinal stresses.

It was found that an increase in void diameter to slab thickness ratio results in a rapid increase in both the longitudinal and transverse stresses, which shows that there is an increase in orthotropic behaviour and deformation of the cross-section with an increase in void diameter ratio. From the results it can be concluded that the optimal void diameter ratio is between 0.6 and 0.8. This range of void diameter ratios allow for greater efficiency due to reduced dead load and material use, without generating excessive stresses due to cellular distortion resulting from excessively thin and flexible flanges above and below the voids.

The spacing of the voids was found to have minimal effect on the stress distributions for a logical void spacing. These results show that the orthotropic behaviour and deformation of the cross-section are more sensitive to variations in void diameter ratio than the spacing of the voids. The void diameter ratio should therefore form the basis of the equivalent plate parameters for the use of orthotropic plate theory.

The use of a solid orthotropic plate to idealise a voided slab showed reasonable agreement with the results from three-dimensional models, with some discrepancies in the different authors' methods noted. The net effect of using a two-dimensional analysis is the averaging out of the stress transverse distribution, which cannot predict the peak stresses around the voids. The orthotropic models compared more favourably with the 3D model than the isotropic models with increasing void diameter ratio.

The results presented have shown that the incorporation of voids begins to affect the structural behaviour of the slab once the void diameter ratio exceeds 0.6, and the orthotropic behaviour becomes considerable. The stress raising effect of the voids should therefore be accounted for in the analysis of a voided slab once the void diameter ratio exceeds 0.6. It is recommended that a solid isotropic slab can be used to idealise a voided slab when the void diameter to slab depth ratio is less than 0.6. When the void diameter ratio is greater than 0.6, the transverse stiffness should be evaluated independently from the longitudinal stiffness, and orthotropic models are more suitable.

For higher void diameter ratios, the method employed by Sen *et al.* (1994), which employs a reduced depth solid orthotropic slab in conjunction with stress multipliers, was found to be the most accurate method for idealising voided slabs. It is evident from this study, that while a three-dimensional finite element model may be too complex for everyday use, it may be extremely valuable for determining the local effects due to the presence of the voids.

TABLE OF CONTENTS

LIST OF FIGURES

LIST OF TABLES

1. INTRODUCTION

1.1. Overview of Voided Slab Bridge Decks

Reinforced concrete bridges can take on various forms, including solid slabs, beam and slabs, cellular decks and voided slabs, with solid slabs being the most popular (Jackson, 2008). Solid bridge deck slabs are common due to their simplicity, in-situ workability and the ability of the slab to distribute concentrated loads in two directions (Faridoon & Nazar, 2011). Cast in-situ solid slab bridges are simple to construct and are structurally efficient when the span of the bridge is less than 10-12m. However, as the span becomes larger, the dead weight of the solid slab becomes excessive and a solid slab becomes uneconomical (Jackson, 2008).

A common method of overcoming this problem is through the use of voided reinforced concrete slabs. In a voided slab, voids replace the tensile concrete in the centre of the slab, thus decreasing the dead weight and increasing the structural efficiency of the slab in bending. The voids within the slab are typically circular in shape and are placed in the longitudinal direction as shown in Figure 1.1. The circular shape makes the voids simple to fabricate and ensures that it is relatively easy to achieve compaction of the concrete under the void during casting (Kim & Kand, 2012). A typical cross-section and plan view of a voided slab bridge deck is shown in Figure 1.1.

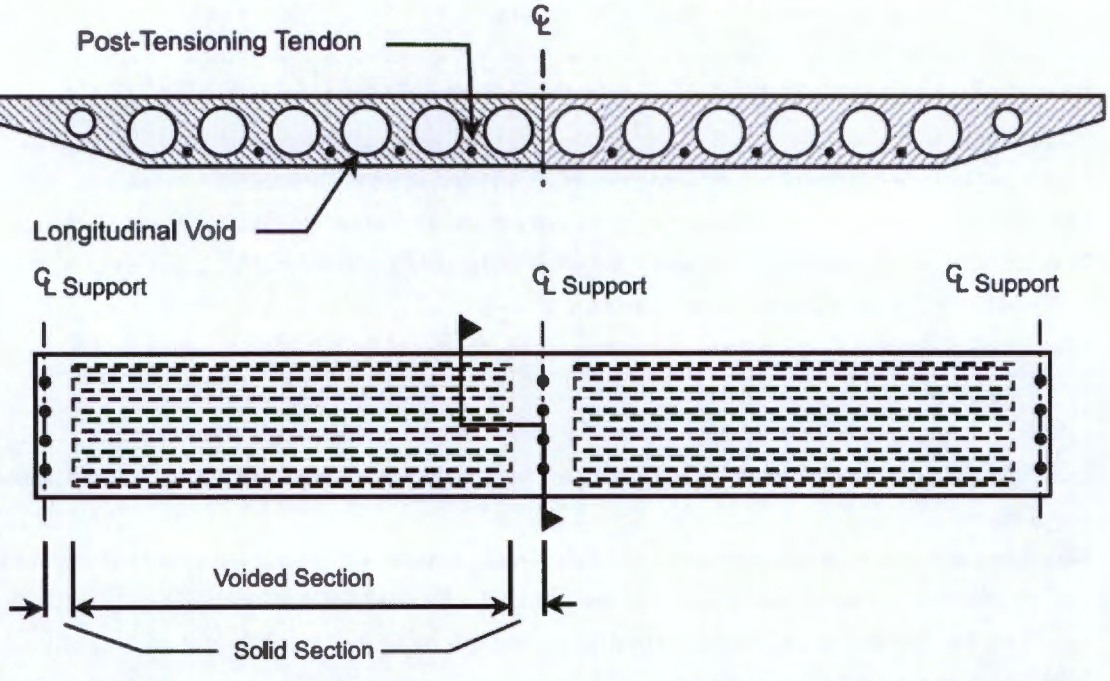

Figure 1.1 - Typical cross-section and plan view of a voided slab bridge deck (Scollard & Bartlett, 2003).

A voided slab can typically reduce the amount of concrete used by between 30% and 50% resulting in an increase in the flexural capacity compared to a solid slab of the same thickness. As a result they can be lighter, stronger, and thinner than regular solid reinforced concrete slabs (Oline & Sen, 1987). The reduced dead weight means that voided slabs can have a typical span of 15m, compared to a span of 10m

for conventional solid slabs (Biswas, 1986). The span length can be increased to 25m through the use of prestressing (Biswas, 1986).

The decreased dead load of voided slabs results in an increased flexural capacity, however the effects of the voids can have a negative effect on the shear resistance, punching shear capacity, deflections, transverse flexural resistance, and fire resistance of the slab. Theoretical models show the shear strength of voided slabs is around 60% to 80% of a solid slab with the same depth (Lai, 2010). This can be countered by discontinuing the voids around areas of high shear such as supports to create incorporated transverse beams.

Incorporating voids within a slab offers many advantages over a conventional solid concrete slab such as a lower total cost of construction, reduced material use, enhanced structural efficiency and decreased construction time (Lai, 2010). Decreased concrete material and weight leads to less reinforcing steel and prestressing. The decreased weight of the deck slab also leads to lower construction costs of downstream components such as piers, abutments and foundations. However, it should be noted that the cost of including the voids within the slab can often outweigh the costs that are saved during construction due to the more complex design that is required (Benaim, 2008).

1.2. Background

The concept of decreasing the dead load of a structure is ancient, with one of the earliest examples being the nearly 2000 year old Pantheon in Rome, which consists of a coffered unreinforced concrete dome. In the past 100 years, this concept has been extended to applications in reinforced concrete allowing for structures to span greater distances with a reduced thickness. Typical examples of reducing the dead load in reinforced concrete include voided, waffle, hollow-core and BubbleDeck slabs.

Waffle slabs are constructed by using removable forms, whereas voided, hollow-core and BubbleDeck slabs use voided forms to incorporate voids within the element. Hollow-core slabs were invented in the 1950's (Fellinger *et al.,* 2005), and consist of a prefabricated pre-stressed slab incorporating longitudinal voids. Hollow-core slabs remain a popular system for floor slab construction, however they can only be used in one-way spanning applications. BubbleDeck slabs were invented in the 1990's (BubbleDeck UK, 2008), and consist of spherical voids placed between the top and bottom reinforcing layers within the slab. The result is a two-way spanning biaxial slab that acts in a similar manner to a solid slab.

Voided slab bridge decks incorporating longitudinal voids have been popular since the 1960's for medium span bridges and have been used in various countries such as the United Kingdom, Canada, USA, Australia and South Africa. Most of the research involving the application of voided slabs in bridge deck construction took place between 1970 and 1990 and focused on developing appropriate structural models to describe the structural behaviour of voided slabs (Jackson, 2008). This research

focused on modelling voided slabs as solid orthotropic plates with adjustments to the longitudinal and transverse flexural rigidities in order to account for the effects of the voids. Forms of analysis such as grillage and finite element models have also been used successfully for the analysis of voided slab bridge decks.

1.3. Objectives of Research

The objectives of this study are to improve on the understanding of the structural behaviour of voided slab bridge decks and the current forms of analysis used in their idealisation. The following are the key objectives of the study:

- To understand the structural behaviour of voided slab bridge decks, and to verify the current forms of analysis which govern their design.
- To determine the effect of the void diameter ratio on the structural behaviour of voided slab bridge decks.
- To determine the effect of the void spacing on the structural behaviour of voided slab bridge decks.
- To verify the suitability of using an orthotropic plate, and the associated equivalent orthotropic plate parameters, for the idealisation of voided slab bridge decks.

These objectives will be achieved through the use of a three-dimensional finite element model which can accurately predict the effects of the voids on the structural behaviour of voided slab bridge decks. By achieving the objectives of this study, the analysis and design of voided slab bridge decks can be approached with greater accuracy and efficiency.

1.4. Limitations and Scope of Research

This study will be limited to the investigation of the structural behaviour of a single span slab type bridge deck with circular longitudinal voids incorporated at mid-depth. No curvature, skews, or prestressing will be considered in this study.

1.5. Plan of Development

This report consists of six chapters, structured as follows:

Chapter 1 gives an introduction and background to the research, and the objectives of the study.

Chapter 2 provides the results of an in-depth literature review that focuses on the salient information regarding voided slabs, the structural behaviour of voided slabs, typical structural analysis methods employed for voided slabs, and past research pertaining to voided slabs.

Chapter 3 presents finite element modelling techniques relevant to the analysis of voided slabs, which includes orthotropic material models, typical element types, and various types of analyses.

Chapter 4 describes the methodology of the finite element modelling used in the study, including material parameters, boundary conditions, and geometrical parameters. The modelling is divided into three phases, which relate to the objectives of this study, namely the effects of the void diameter ratio, the effect of the void spacing, and the suitability of using an orthotropic plate for the idealisation of voided slabs.

Chapter 5 reports the findings and observations of the study, with a discussion relating to the objectives of the study. The results of each phase are presented individually.

Chapter 6 summarises the research presented in this report, draws conclusions, and gives recommendations for future research.

2. LITERATURE REVIEW

2.1. Forms of Voided Slabs

There are various forms of voided concrete structures that have been developed, all of which use the principle of reducing the dead weight of the slab by introducing voids within the concrete. The most common forms of incorporated voided structures are voided slab bridge decks, BubbleDeck slabs and Hollow-core slabs.

2.1.1. Voided Slab Bridge Decks

Voided slab bridge decks consist of cylindrical forms placed in the longitudinal direction of the bridge deck. The result is a cross-section that consists of top and bottom flanges above and below the voids with webs separating the voids. The diameter of the voids depends on the deck thickness, and can be as large as 80% of the deck thickness (Jofriet *et al.*, 1983). The structural behaviour of voided slabs is mainly influenced by the ratio of the void diameter to the slab thickness. Void diameters that exceed 60% of the deck thickness require additional consideration of the effect of the voids on the flexural rigidity of the slab, while void diameters less than 60% can be analysed much like a solid slab with reduced weight (Hambly, 1991). The spacing of the voids should generally be between 750mm and 1500mm (Benaim, 2008). O'Brien & Keogh (1999) concluded that the spacing of voids has little effect on transverse and longitudinal rigidities of voided slabs, providing a logical spacing of less than 3m is used.

Voided slab bridges typically have a rather utilitarian appearance, which can be altered by varying the form of the side cantilevers and the deck depth. Curved soffits can also be incorporated through the use of different sizes of voids across the width to vary their appearance. Significant weight saving can be achieved by using relatively long transverse cantilevers giving the bridge a spine beam form (Jackson, 2008). The slab may also be provided with haunches at intermediate supports, allowing the slab to span further (Benaim, 2008). A typical voided deck cross-section with a spine form is shown in Figure 2.1.

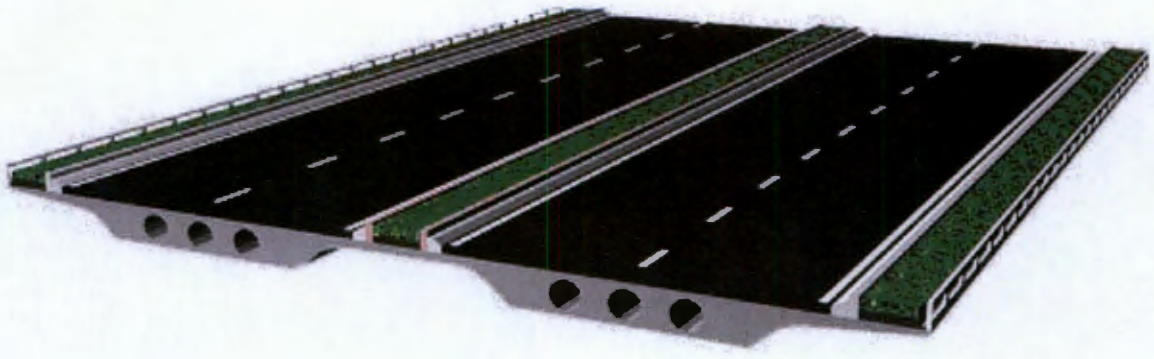

Figure 2.1 - Twin spine voided slab bridge deck (Diaz *et al.*, 2010).

Voided bridge decks can be prestressed, which provides an economic means for longer spans without a significant increase in slab depth. Longitudinal prestressing tendons are located in the webs between the voids. The common layout of the tendons in the longitudinal direction is parabolic, with negative eccentricities in the mid-span and positive eccentricities in the support zones. Two prestressed tendons placed vertically at the centre of the webs is preferred at the end of the deck where one tendon may be swept up to carry a proportion of the shear force, while the other may be kept low to tie in the final concrete shear strut (Benaim, 2008). Two tendons also provide a more even distribution of anchorage forces on the end face of the deck, reducing the equilibrium reinforcement required. Voided slabs can also be prestressed transversely. Figure 2.2 shows a typical layout of transverse prestressing in a voided slab bridge deck.

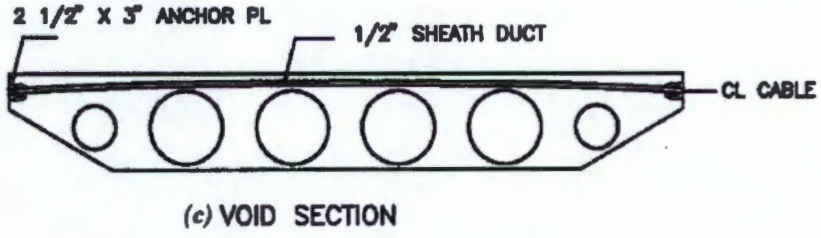

Figure 2.2 - Typical transverse prestressing layout of a voided slab (Sen *et al.*, 1993).

When longitudinal voids are incorporated within concrete bridge decks, a number of additional considerations are required during construction. The main concern are the buoyancy forces acting upon the void formers during casting. Major difficulties, such as the voids floating during casting, can arise when these forces are not satisfactorily provided for, sometimes requiring the entire deck to be demolished and reconstructed. It is therefore essential that the arrangement be properly designed and that the void formers be sufficiently rigid, sealed and tied down before casting the concrete (Latimer, 2011). Metal tie-down straps or reinforcement bars are usually adequately distributed along the length of the formers during construction to resist these buoyancy forces. The tie-down straps are used to anchor void formers to the bottom reinforcement, however in most cases the reinforcing is not heavy enough to resist the buoyancy forces, in which case the tie-down straps should be secured below the soffit formwork.

Another approach is to anchor the voids to the reinforcement, and then pour the first layer of concrete enclosing the bottom layer of steel, providing the weight to resist flotation (Benaim, 2008). Casting can be continued before this lower layer has partially set. Although this technique is effective, it requires very good control of the casting process to avoid creating a horizontal cold joint. In order to reduce the buoyancy forces during concreting, concrete should be placed and compacted in layers on either side of the void formers rather than full depth (Latimer, 2011). Concreting voided decks requires more care than for solid slabs, as there is the risk of incomplete filling and compaction beneath the voids. Consequently voided slab construction is a slower and more labour-intensive operation. The placement sequence must thus be carefully considered to ensure that the concrete is well compacted and that no

cold joints develop. The normal method for decks with circular voids is to work across the deck, filling one web and observing the concrete flowing out from beneath the adjacent void (Benaim, 2008).

The choice of material for the void formers is very important. They should be adequately robust to ensure they do not deform due to the buoyancy forces. They usually require internal bracing to ensure that they maintain their shape. The void formers should also be sealed to prevent the ingress of water or grout, and should have drainage outlets at their low points (Latimer, 2011). Voided slabs within South Africa are generally constructed using hollow thin walled steel sections placed within the slab. It is also common to use expanded polystyrene which has the advantage of being light and easy to cut.

Figure 2.3 - Example of a voided slab bridge deck during construction showing steel void formers, reinforcement, and longitudinal prestressing ducts (Latimer, 2011).

2.1.2. BubbleDeck Slabs

BubbleDeck slabs consist of hollow plastic spheres cast into the concrete to create a grid of void forms inside the slab. BubbleDeck slabs are similar in principle to voided bridge deck slabs, with the main distinction being that bubble deck slabs use hollow plastic bubbles or ellipsoids as opposed to longitudinal cylinders used in voided slabs. The plastic bubbles result in a two-dimensional arrangement of voids which reduce the self-weight of the slab. The two-dimensional arrangement of the voids allows for loads to be distributed in an arbitrary direction as opposed to a one-way spanning slab with longitudinal voids. It is important to note the voids formed by the bubbles are not prismatic as in voided bridge decks, they are discrete volumes in a two-dimensional array so they do not detract from the slab strength and stiffness in the way that a prismatic void would (BubbleDeck UK, 2008). The spheres also allow for flexible design in the layout of the slab which can easily be adapted to fit irregular or curved layouts. Figure 2.4 shows the structure of a typical BubbleDeck slab.

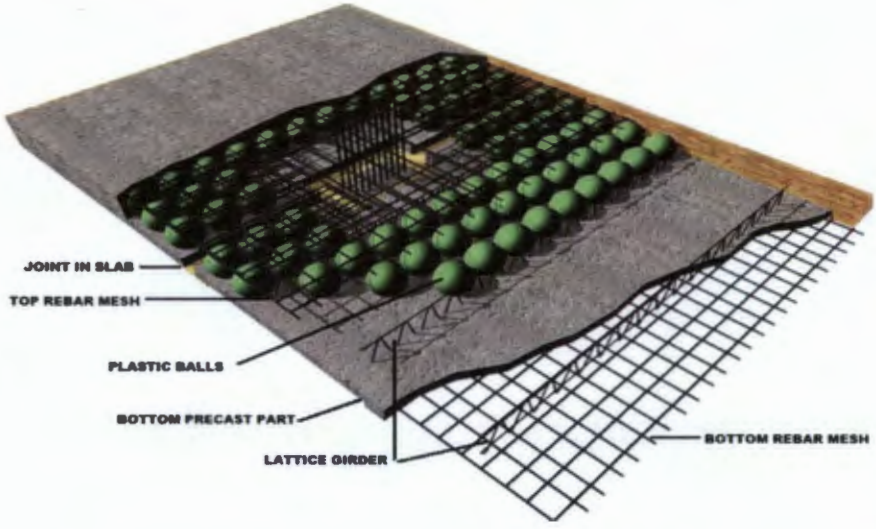

Figure 2.4 – Typical structure of a BubbleDeck Slab (Bokil, 2010).

The structural behaviour of BubbleDeck slabs is influenced by the ratio of the bubble diameter to the slab thickness. Thorough investigations made at universities in Germany, Netherlands and Denmark concluded that bubble deck slabs act like solid slabs (Bokil, 2010). Bokil (2010) found that a BubbleDeck slab had 87% of the bending stiffness of a similar solid slab, but only used 66% of the concrete volume (Bokil, 2010). As with voided bridge deck slabs, BubbleDeck slabs have a reduced resistance to shear, transverse flexure and fire, as well as an increase in deflection compared to conventional solid slabs.

BubbleDeck slabs were first proposed by Jorgen Breuning in the 1990's (Bokil, 2010). Since their introduction, BubbleDeck slabs have become popular in a number of countries due to the savings that can be achieved from the reduced material use and enhanced structural efficiency. Figure 2.5 below shows a world map of the usage of the bubble deck system in various countries.

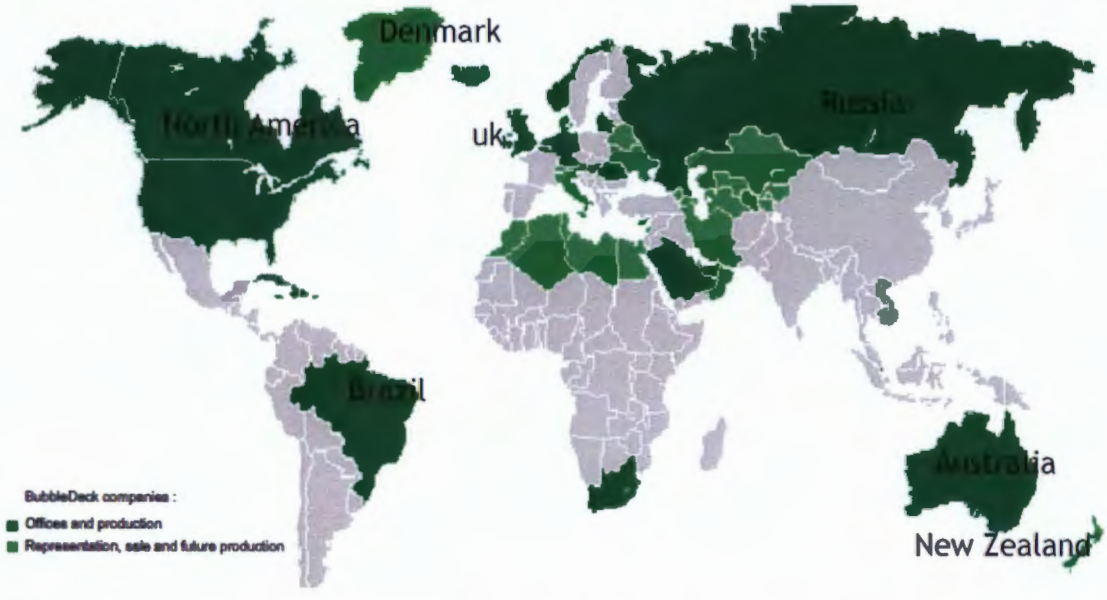

Figure 2.5 - World map showing the usage of BubbleDeck Slabs by country (Bokil, 2010).

The primary application of BubbleDeck slabs is in the construction of floor slabs in multi-story buildings. One of the largest structures that has used BubbleDeck slabs is the Le Coie Hotel in Great Britain (Bokil, 2010). The structure comprises 7 800m^2 of Bubble Deck floor slabs between 3 and 6 stories high supported on in-situ reinforced concrete columns. Over R7.5m of savings were realised as a direct result of incorporating BubbleDeck technology into this project, amounting to a 3% saving off the total project cost (Bokil, 2010). Although uncommon, BubbleDeck slabs can also be used in bridge applications, as shown in Figure 2.6.

Figure 2.6 - Application of BubbleDeck Technology in bridge decks (Bokil, 2010).

2.1.3. Hollow Core Slabs

Hollow Core slabs are pre-fabricated prestressed concrete slabs that contain tubular voids that extend throughout the full length of the slab. Hollow Core slabs were first proposed during the 1950's (Fellinger *et al.,* 2005). The slabs consist of pre-cast units of typically 1.2m wide. The cross-sectional depth depends on the intended span and ranges between 150mm to 400mm, reaching spans up to 16m (Fellinger *et al.,* 2005). A typical cross-section of a Hollow Core slab is shown in Figure 2.7. As with voided slab bridge decks, the main disadvantage of Hollow Core slabs is a reduction in shear capacity, transverse flexure, and fire resistance.

Hollow Core slabs are manufactured by tensioning the prestressing strands on long benches. Concrete is then cast using a moulding and casting machine that moves along the bench. Once the concrete has reached sufficient strength, the prestressing strands are cut releasing the prestressing force into the slab. The slab can then be cut into elements of the desired length (Fellinger *et al.*, 2005).

The voids within the slab reduce the self-weight of the structure, and due to the ease of construction associated with precast slabs, Hollow Core slabs provide an economic means of construction. They are widely used for floors and roofs of office, residential, commercial and industrial buildings. Precast Hollow Core slabs are typically not used in bridge applications.

Due to the automated method of construction, Hollow Core slabs contain no transverse or shear reinforcement. The pre-stressing strands are also the only reinforcement provided in the longitudinal direction. Therefore in order to simplify their design, it is generally assumed that hollow core slabs behave like simply supported beams (Pajari, 2009). This simplification means that the mechanical model of a hollow core slab is a number of parallel I-beams. To get an impression of the behaviour of a large floor subjected to a uniformly distributed load, it is sufficient to study a longitudinal cut taken from one slab unit, resulting in a single prestressed I-section such as the one shown in Figure 2.7.

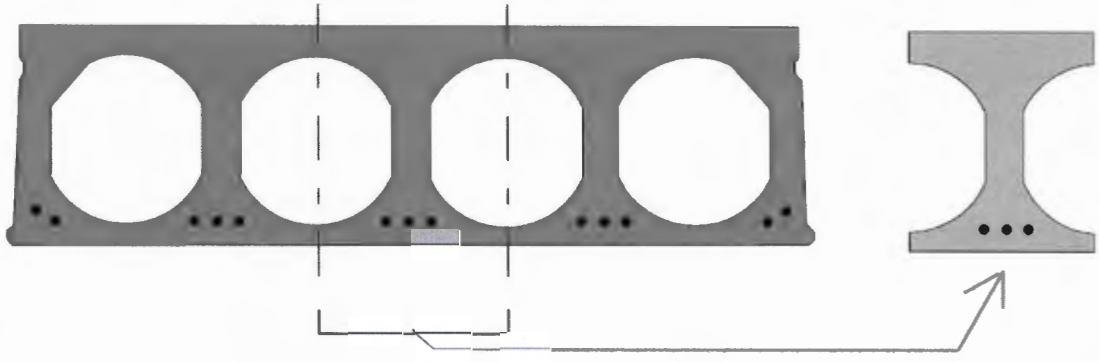

Figure 2.7 - Typical cross-section of a prestressed Hollow Core slab and an I-section used for structural analysis (Pajari, 2009).

2.2. Structural Behaviour of Voided Slabs

2.2.1. Orthotropic Plate Theory

Plate theory is typically used to describe the structural behaviour of slab type structures. Plate theory can therefore be used to describe the structural behaviour of voided slabs by making an allowance for the effect of the voids. By considering a solid plate made of an anisotropic material that can account for the effect of the voids in each direction independently, plate theory can be used to describe the structural behaviour of orthotropic slabs such as voided slabs.

A plate is defined as a structural component having two of its dimensions significantly larger than the third, namely its thickness. The elastic structural analysis of a plate is carried out by considering the state of stress at the middle plane of a plate. All the stress components are expressed in terms of the deflection w of the plate in the thickness direction z which is a function of the two coordinates x and y in the plane of the plate (Ryall, 2008). The stresses and strains in the plate can be calculated by considering the curvature of the plate in planes parallel to the xz and yz planes, as shown in Figure 2.8. By considering the curvature of the plate, a differential equation can be obtained that relates the stresses and strains in the plate to the applied bending moment and flexural rigidities (Timoshenko & Woinowsky-Krieger, 1959).

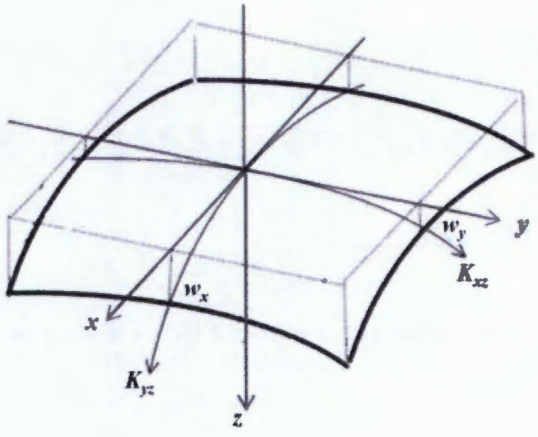

Figure 2.8 - Curvature of a plate in planes parallel to the xz and yz planes (adapted from Diaz *et al.*, 2010).

The idealisation of a uniform solid slab deck as a plate model is straightforward, as the plate model can be given the same depth and material properties as the original slab. When plate theory is applied to voided slabs, the effects of the voids within the slab result in additional factors that require careful consideration. The main consideration is that the flexure rigidity of the plate in the x and y directions are different due to the presence of the voids, resulting in an orthotropic plate. If a conventional isotropic plate model is assumed, the plate will have the same thickness in either direction, resulting in a stiffness that is the same in the x and y direction, which is clearly not correct for a voided slab.

The longitudinal stiffness of a voided slab can be calculated in the usual manner as the cross-section is constant along the length of the bridge, and can be calculated by subtracting the moment of

inertia of the voided section from the solid section based on a mid-depth neutral axis. Transversely, the structure behaves quite differently due to the varying cross-section along the width of the bridge. The varying nature of the transverse cross-section makes it difficult to calculate the transverse stiffness of a voided slab.

According to Hambly (1991), slabs with a void diameter of less than 60% of the slab depth can be modelled as isotropic, where the transverse stiffness is assumed to be equal to the longitudinal stiffness. For voids of larger diameter, the orthotropic nature of the slab should be incorporated in the analysis, and the longitudinal and transverse stiffness's should be calculated independently by using adjusted flexural rigidities in orthogonal directions. Typical forms of analysis that are relevant to orthotropic plates such as voided slabs include grillage analysis and finite element analysis using orthotropic plate theory, which are discussed in Section 2.2.3.

The orthotropic nature of voided slabs can be accounted for by considering an elastic modulus in the orthogonal direction that accounts for the presence of the voids. Therefore a solid plate can be used to model a voided slab with the effect of the voids entering the model through the elastic moduli in either direction. This results in a solid plate made of an anisotropic material. The plate thickness can then be defined and the flexural rigidities in the orthogonal directions can be accounted for by calculating elastic moduli in the orthogonal directions based on the plate thickness. Thus a solid plate of thickness t can be used to idealise the flexural response of an orthotropic voided slab by using an anisotropic material with different elastic moduli in the longitudinal and transverse directions.

In order to define the orthotropic plate behaviour, the flexural rigidities in the x and y direction (D_x and D_y), as well as the torsional rigidities (D_{xy} and D_{yx}) need to be defined. This is normally done by using rigidity factors in the relevant directions. If a structure is to be analysed through a two-dimensional plate idealisation, these rigidity factors could have a significant effect on the accuracy of the analysis. The rigidity factors should therefore model the actual structure as closely as possible without requiring complex calculations. Numerous bending and torsional rigidity factors have been proposed by various authors, which are summarised in Table 2.1. These factors are based on studies using voids of various sizes and spacing, and therefore are based on voided slab properties such as void diameters, void spacing, and slab thickness. These factors can be used to define the anisotropic material used for the analysis of voided slabs which can account for their orthotropic nature.

The factors proposed by Aster (1968), Bakht *et al.* (1981b), O'Brien & Keogh (1999) and Elliott & Clarke (1982) are similar. The rigidity in the longitudinal direction is calculated by subtracting the stiffness of the voided circular portion from the stiffness of the solid rectangular section. The transverse stiffness is calculated based on the ratio of the void diameter to slab depth. The factors proposed by Jofriet *et al.* (1973) and Diaz *et al.* (2010) are based on the reduction in the moment of inertia in each direction from that of the equivalent solid slab. The factors proposed by Pama *et al.* (1975) include the thickness of the webs and number of voids, which relate to the spacing of the voids.

The torsional rigidity factors proposed by Bakht *et al.* (1981b) and O'Brien & Keogh (1999) can be obtained by calculating the torsional rigidity of the equivalent solid slab, and multiplying it by a factor obtained from Table 2.2, which is based on the void diameter to spacing and void diameter to slab thickness ratios. The factors are based on the assumption that the neutral axis is at a constant depth and located at mid depth. If this is not the case, then the neutral axis can be adjusted using the parallel axis theorem in the conventional manner. It is important to recognise the approximate nature of the equivalent orthotropic plate parameters, which are not obtained from theoretical analysis but semi empirically from tests and analyses of voided models.

Table 2.1 - Flexural rigidity factors proposed by various authors (Kim and Kang, 2012).

Author	D_x	D_y	$D_{xy} = D_{yx}$
Aster (1968)	$E\left[\frac{t^3}{12} - \frac{\pi d^4}{64s}\right]$	$\frac{Et^3}{12}\left[1 - 0.59\left(\frac{d}{t}\right)^3\left(\frac{d}{s}\right)\right]$	$\frac{(E_x + E_y)/2}{2(1+\nu)}$
Bakht *et al.* (1981b) & O'Brien & Keogh (1999)	$E\left[\frac{t^3}{12} - \frac{\pi d^4}{64s}\right]$	$\frac{Et^3}{12}\left[1 - 0.95\left(\frac{d}{t}\right)^4\right]$	Table 2.2
Elliot & Clarke (1982)	$E\left[\frac{t^3}{12} - \frac{\pi d^4}{64s}\right]$	$\frac{Et^3}{12}\left[1 - \left(\frac{d}{t}\right)^4\right]$	$\frac{Gt^3}{12}\left[1 - 0.85\left(\frac{d}{t}\right)^4\right]$
Jofriet *et al.* (1973) & Diaz *et al.* (2010)	$D_{solid}\frac{I_x}{I_{solid}}$	$D_{solid}\frac{I_x}{I_{solid}}$	$v\sqrt{D_x D_y}$
Pama *et al.* (1975)	$\frac{Et^3}{12}\left[1 - \frac{3\pi\left(\frac{d}{t}\right)^4\left(\frac{t}{t_{web}}\right)}{16\left(1 + \left(\frac{d}{t_{web}}\right)\right)}\right]$	$\frac{Et^3}{12}\left[1 - \left(\frac{d}{t}\right)^3\right]$	$\frac{Et^3}{12}\left[\frac{3n\left(1 + \frac{d}{t_{web}}\right)\left(1 + \frac{d}{t}\right)\left(1 - \frac{d^2}{t^2}\right)}{4n\left(1 + \frac{d}{t_{web}}\right)\left(\frac{t}{t_{web}}\right)\left(1 - \frac{d^2}{t^2}\right)}\right]$

Where D_x, D_y and D_{xy} are the flexural rigidities per unit width (N/m^2), E is the modulus of elasticity (GPa), ν is Poisions ratio, t is the thickness of the voided slab (m), t_{web} is the width of the webs between the voids, D is the void diameter (m), s is the distance between void centres (m), and n is the number of voids.

Table 2.2 - Torsional rigidity factors for voided slabs (Ward & Cassell, 1974).

$\frac{d_v}{d}$	$\frac{d_v}{s_v}$ = 0.9	0.8	0.7	0.6	0.5
0.90	0.45	0.48	0.51	0.56	0.62
0.85	0.55	0.58	0.61	0.64	0.69
0.80	0.64	0.66	0.68	0.71	0.75
0.75	0.70	0.72	0.74	0.77	0.80
0.70	0.76	0.78	0.79	0.82	0.84
0.65	0.81	0.82	0.84	0.86	0.88
0.60	0.85	0.86	0.87	0.89	0.90

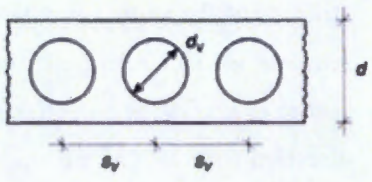

To the author's knowledge, no comprehensive study has been reported in technical literature to compare the results of the different parameters proposed in Table 2.1 in order to idealise a voided slab as an orthotropic plate. A study of this nature would be required to confirm the applicability of orthotropic plate theory for the idealisation of voided slab bridge decks.

The orthotropic plate analogy which can account for the effect of the voids within a slab can therefore be developed as follows, which is based on the approach by Diaz *et al.* (2010). The analogy is based on the Reissner-Mindlin theory of plates, which is an extension of the Kirchhoff-Love plate theory that takes into account shear deformations through the thickness of the plate. The theory is based on curvatures that are induced on a plate when subject to pure bending, such as the one in Figure 2.9 below.

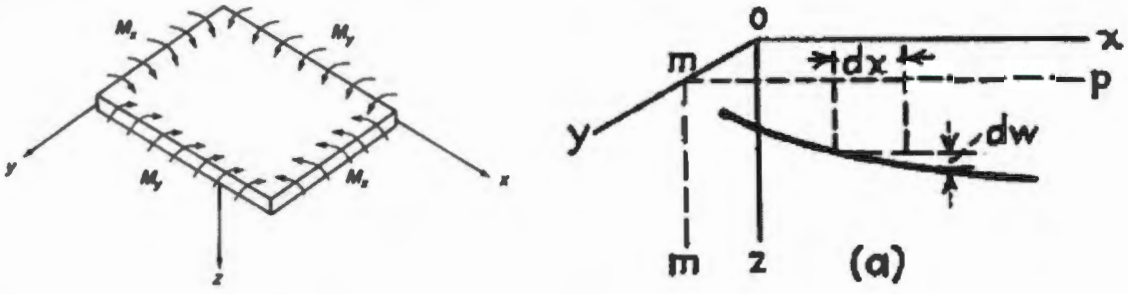

(a) (b)

Figure 2.9 - (a) Plate element subject to pure bending and (b) curvature of plate in the *xz* plane (Timoshenko & Woinowsky-Krieger, 1959).

The following terms can be used to represent the curvature of the middle surface of a plate subjected to pure bending (Timoshenko & Woinowsky-Krieger, 1959):

$$\frac{1}{r_x} = \frac{d^2w}{dx^2} \qquad \frac{1}{r_y} = \frac{d^2w}{dy^2} \qquad \frac{1}{r_{xy}} = \frac{d^2w}{dxdy} \tag{2.1}$$

The first two terms represent the curvature of the plate in a plane parallel to the *xz* and *yz* planes respectively, and the last term is a quantity used to represent the twist of the surface with respect to the *x* and *y* axes. *w* denotes small deflections of the plate in the *z* direction. The first expression is similar to the expression used in determining the curvature of a beam in bending using the Euler-Bernoulli beam theory. Using the curvatures, the strain vector due to bending at a distance *z* from the neutral surface can be expressed as:

$$\varepsilon_b = \left(-z\frac{d^2w}{dx^2} \quad -z\frac{d^2w}{dy^2} \quad -2z\frac{d^2w}{dxdy}\right) \tag{2.2}$$

By using Hooke's law, the stress vector at a distance *z* from the neutral surface can be expressed as:

$$\sigma_b = D_b(\varepsilon_x \quad \varepsilon_y \quad \tau_{xy}) \tag{2.3}$$

Where D_b is the constitutive matrix of the material, which for isotropic and orthotropic elements can be expressed as follows:

$$D_{b,i} = \begin{pmatrix} \frac{E}{1-v^2} & \frac{vE}{1-v^2} & 0 \\ \frac{vE}{1-v^2} & \frac{E}{1-v^2} & 0 \\ 0 & 0 & G \end{pmatrix} \quad \text{and,} \quad D_{b,o} = \begin{pmatrix} \frac{E_x}{1-v_{xy}v_{yx}} & \frac{v_{yx}E_y}{1-v_{xy}v_{yx}} & 0 \\ \frac{v_{xy}E_y}{1-v_{xy}v_{yx}} & \frac{E_y}{1-v_{xy}v_{yx}} & 0 \\ 0 & 0 & G_{xy} \end{pmatrix} \tag{2.4}$$

Where $G = \frac{E}{2(1+v)}$ is the shear modulus of the material.

Having obtained an expression for the bending stresses in the plate, the bending moments can be obtained through integration. The bending moment in x direction can be determined as follows:

$$M_x = \int_{-h/2}^{h/2} \sigma_x z d_z = \int_{-h/2}^{h/2} D_b z^2 \frac{d^2w}{dx^2} d_z = -D_b \frac{h^3}{12} \frac{d^2w}{dx^2} \tag{2.5}$$

The same procedure can be followed to determine M_y, and the shearing stress τ_{xy} can be integrated to give the twisting moment M_{xy}. The generalised force vector can then be expressed as follows:

$$M = \widehat{D_b}\, \widehat{\varepsilon_b} \tag{2.6}$$

Where $M = (M_x \quad M_y \quad M_{xy})$ and the generalised strain vector $\widehat{\varepsilon_b} = \left(-\frac{d^2w}{dx^2} \quad -\frac{d^2w}{dy^2} \quad -2\frac{d^2w}{dxdy}\right)$. $\widehat{D_b}$ is called the flexural rigidity of the plate and can be defined as follows for isotropic and orthotropic materials:

$$D_{b,i} = \begin{pmatrix} \frac{EI_y}{1-v^2} & \frac{vEI_y}{1-v^2} & 0 \\ \frac{vEI_x}{1-v^2} & \frac{EI_x}{1-v^2} & 0 \\ 0 & 0 & G \end{pmatrix} \quad \text{and,} \quad D_{b,o} = \begin{pmatrix} \frac{E_xI}{1-v_{xy}v_{yx}} & \frac{v_{yx}E_yI}{1-v_{xy}v_{yx}} & 0 \\ \frac{v_{xy}E_yI}{1-v_{xy}v_{yx}} & \frac{E_yI}{1-v_{xy}v_{yx}} & 0 \\ 0 & 0 & G_{xy} \end{pmatrix} \tag{2.7}$$

Where I is the moment of inertia per unit length and can be expressed as:

$$I = \frac{h^3}{12} \tag{2.8}$$

As the voided slab is represented by an equivalent solid slab, the expression of the orthotropic mechanical parameters of the equivalent slab need to be obtained. This is done by assuming $1 - v^2 \approx 1$ and $1 - v_{xy}v_{xy} \approx 1$, it can then be concluded that:

$$E_x = \frac{I_y}{I}E \qquad E_y = \frac{I_x}{I}E \qquad E_{xy} = \frac{I_x}{I}G \tag{2.9}$$

Due to the complexity in calculating I_x and I_y, the values of E_x, E_y, and E_{xy} can be obtained using the orthotropic plate parameters suggested in Table 2.1. While E_x, E_y, and E_{xy} can be determined uniquely, there are two different expressions for v_{yx}. Therefore the average value is chosen, which is calculated as follows:

$$v_{xy} = \frac{I_x + I_y}{2I_y}v \tag{2.10}$$

Since the height of the equivalent orthotropic slab is different from the voided slab, a fictitious orthotropic material density must be defined to ensure that the weight of both slabs is the same:

$$\rho_f = \rho_r \frac{A_{r,x}}{A_{f,x}} \tag{2.11}$$

Where ρ_r is the actual concrete density and ρ_f is the fictitious orthotropic material density, and $A_{r,x}$ and $A_{f,x}$ are the areas of the voided cross-section and the equivalent fictitious solid slab. By using this analogy, the stresses and strains in the plate model can be determined.

It should be noted that when using this method, the stresses and strains that are determined relate to the equivalent solid slab model, and not that of the voided slab. Therefore once the kinematics and moment-curvature relations of the orthotropic solid slab have been created, the expressions that relate the stress and force values of the orthotropic solid model with the ones of the actual voided slab must be developed.

Diaz *et al.* (2010) proposed a method in which the stresses and strains are converted between the equivalent solid slab and voided slab by considering the equilibrium of forces between the two models. Sen *et al.* (1994) and Jofriet *et al.* (1973) proposed using factors to convert the stresses and strains between the two models. No other authors have suggested the need to convert the stresses obtained from the equivalent orthotropic models to the actual voided slab. The method of Diaz *et al.* (2010) is presented below, and the conversion factors used in the methods of Sen *et al.* (1994) and Jofriet *et al.* (1973) are summarised in Section 2.4.

The conversion of the forces and moments from the equivalent solid slab to the voided slab using the equilibrium method suggested by Diaz *et al.* (2010) can be used to obtain the in-plane membrane forces and the stresses resulting from flexure. The membrane forces and bending stresses can be determined as follows:

By establishing equality of the membrane forces in the two slabs in the longitudinal direction, as shown in Figure 2.10, it can be seen that:

$$N_x = \sigma_{r,x,m} A_{r,x} = \sigma_{f,x,m} A_{f,x} \tag{2.12}$$

Where $\sigma_{r,x,m}$ and $\sigma_{f,x,m}$ are the membrane stresses in the longitudinal direction for the actual voided slab and fictitious orthotropic solid slab respectively. From here, the membrane longitudinal stress in the real voided slab can be expressed as:

$$\sigma_{r,x,m} = \frac{A_{r,x}}{A_{f,x}} \sigma_{f,x,m} = \frac{\rho_r}{\rho_f} \sigma_{f,x,m} \tag{2.13}$$

The same can be concluded for the membrane stresses in the transverse direction using Figure 2.11. However, the cross-section in the transverse section is not constant due to the solid webs in between the voids. Therefore, the worst case is considered where the cross-sectional area is the lowest at the centreline of the void. At this point the membrane transverse stress in the voided slab can be expressed as:

$$\sigma_{r,y,m} = \frac{A_{r,y}}{A_{f,y}} \sigma_{f,y,m} = \frac{h}{e_1+e_2} \sigma_{f,x,m} \tag{2.14}$$

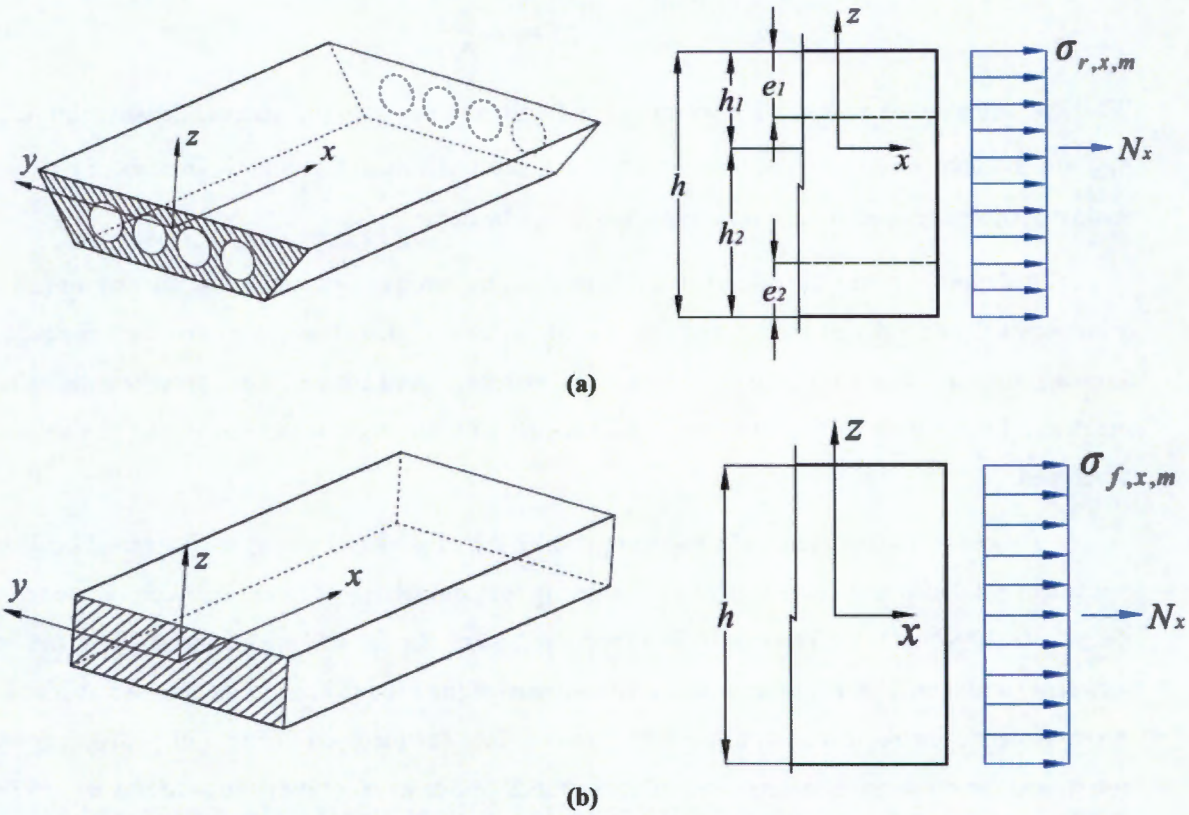

Figure 2.10 - Membrane stress in the longitudinal direction (a) in the voided slab and (b) the fictitious orthotropic solid slab (Diaz *et al.*, 2010).

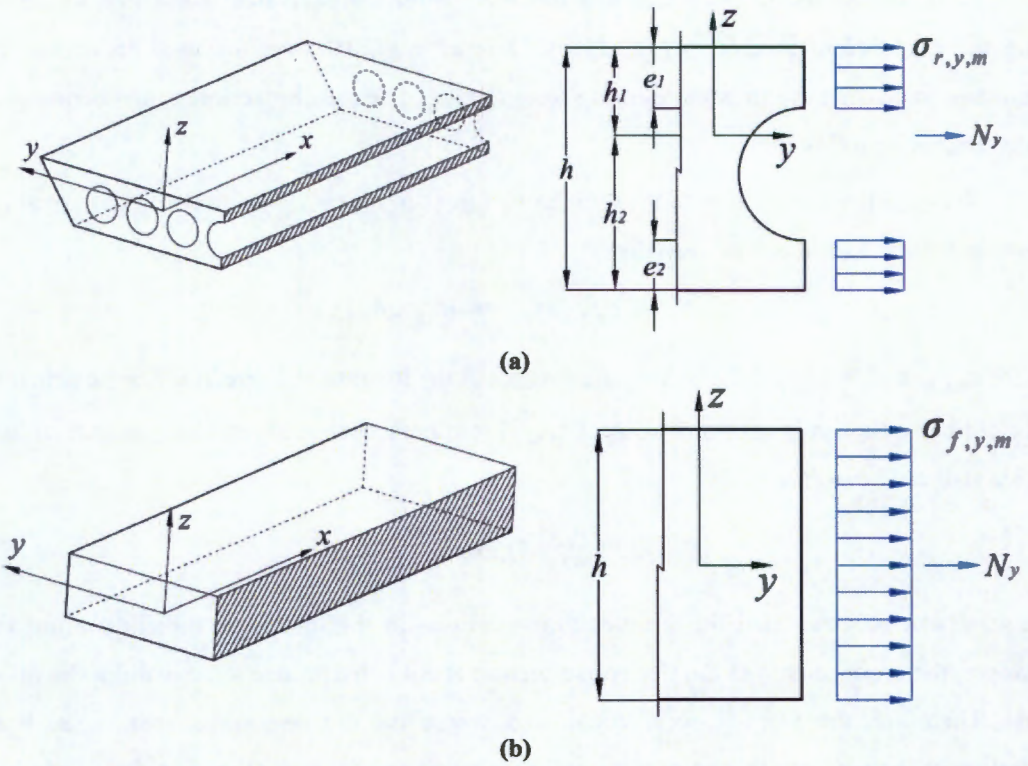

Figure 2.11 - Membrane stress in the transverse direction in (a) the voided slab and (b) the fictitious orthotropic solid slab (Diaz *et al.*, 2010).

The bending stresses in either direction can be obtained by considering moment equilibrium. By considering Figure 2.12, the following relationship can be determined:

$$M_y = \sigma_{r,x,b,i} W_{r,y} = \sigma_{f,x,b,i} W_{f,y} \tag{2.15}$$

Where i represents the top fibre for $i = 1$ and the bottom fibre for $i = 2$ and $\sigma_{r,x,b,i}$ and $\sigma_{f,x,b,i}$ are the bending stresses in the longitudinal direction for the actual voided slab and fictitious orthotropic solid slab respectively. $W_{r,y}$ and $W_{f,y}$ are the strength modului in the transverse direction for the actual and orthotropic materials and can be defined as follows:

$$W_{r,y} = \frac{I_{r,y}}{h_i} \qquad \text{and} \qquad W_{f,y} = \frac{I_{f,y}}{h/2} = \frac{h^3/12}{h/2} = \frac{h^2}{6} \tag{2.16}$$

Where $I_{r,y}$ is the moment of inertia per unit length of the voided slab about the y axis and h_i is defined in Figure 2.12. Using Equation 2.15, the stress in the voided slab in the longitudinal direction can be expressed as:

$$\sigma_{r,x,b,i} = \frac{\sigma_{f,x,b,i} W_{f,y}}{W_{r,y}} = \frac{h_i h^2}{6 I_{r,y}} \sigma_{f,x,b,i} \tag{2.17}$$

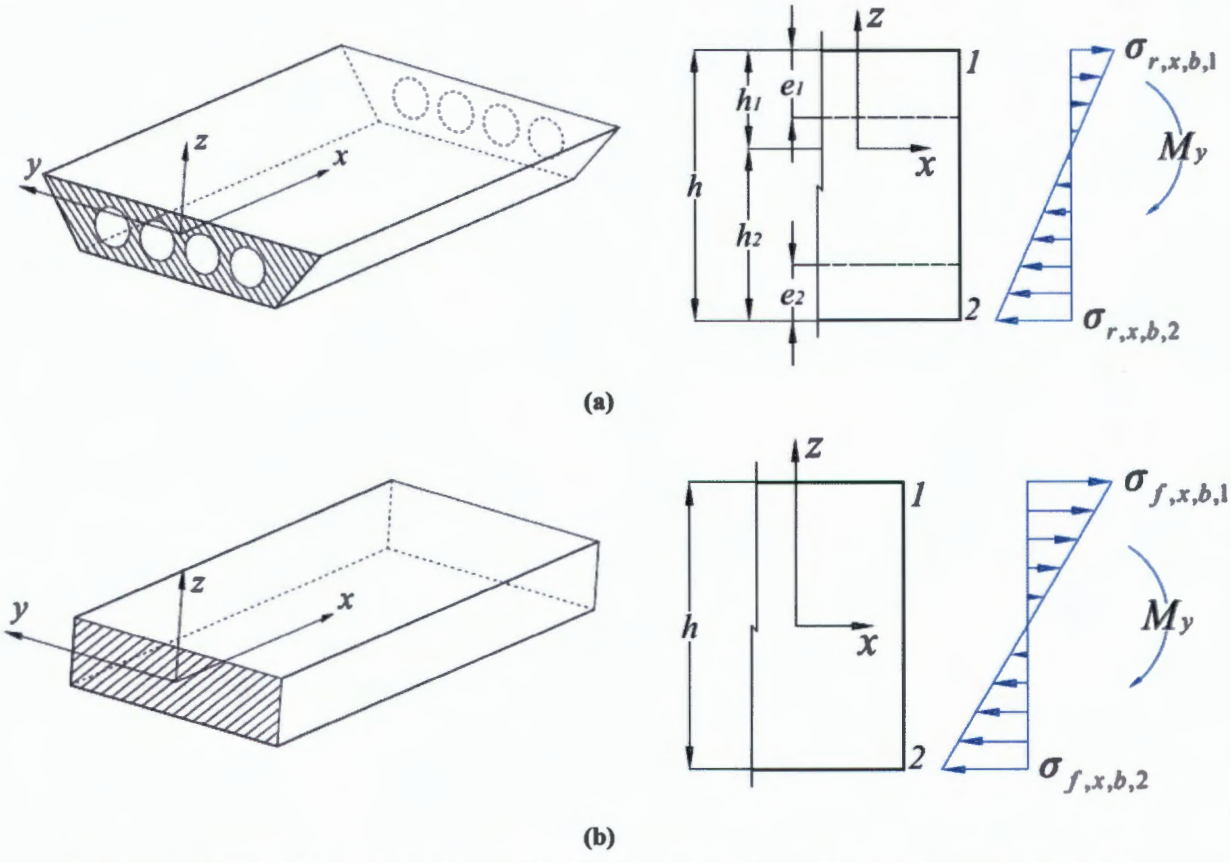

Figure 2.12 - Bending stress in the longitudinal direction in (a) the voided slab and (b) the fictitious orthotropic solid slab (Diaz *et al.*, 2010).

Using the same force equilibrium and Figure 2.13 below, the bending stresses about the transverse axis for the voided slab can be determined:

$$M_x = \sigma_{r,y,b,l} W_{r,x} = \sigma_{f,y,b,l} W_{f,x} \tag{2.18}$$

$W_{r,x}$ and $W_{f,x}$ are the strength modului in the x direction for the actual voided slab and orthotropic solid slab and can be defined as follows:

$$W_{r,x} = \frac{I_{r,x}}{h_l} = \frac{\frac{{e_1}^3}{12} + e_1\left(h_1 - \frac{e_1}{2}\right)^2 + \frac{{e_2}^3}{12} + e_2\left(h_2 - \frac{e_2}{2}\right)^2}{h_l} \quad \text{and} \quad W_{f,x} = \frac{I_{f,x}}{h/2} = \frac{h^3/12}{h/2} = \frac{h^2}{6} \tag{2.19}$$

Where $I_{r,x}$ is the moment of inertia per unit length about the longitudinal axis of the voided slab and h_1 h_2, e_1, and e_2 are defined in Figure 2.13.

Using Equation 2.18, the stress in the voided slab in the transverse direction can be expressed as:

$$\sigma_{r,y,b,l} = \frac{\sigma_{f,y,b,l} W_{f,x}}{W_{r,x}} = \frac{2h_l h^2}{{e_1}^3 + {e_2}^3 + 12\left[e_1\left(h_1 - \frac{e_1}{2}\right)^2 + e_2\left(h_2 - \frac{e_2}{2}\right)^2\right]} \sigma_{f,y,b,l} \tag{2.20}$$

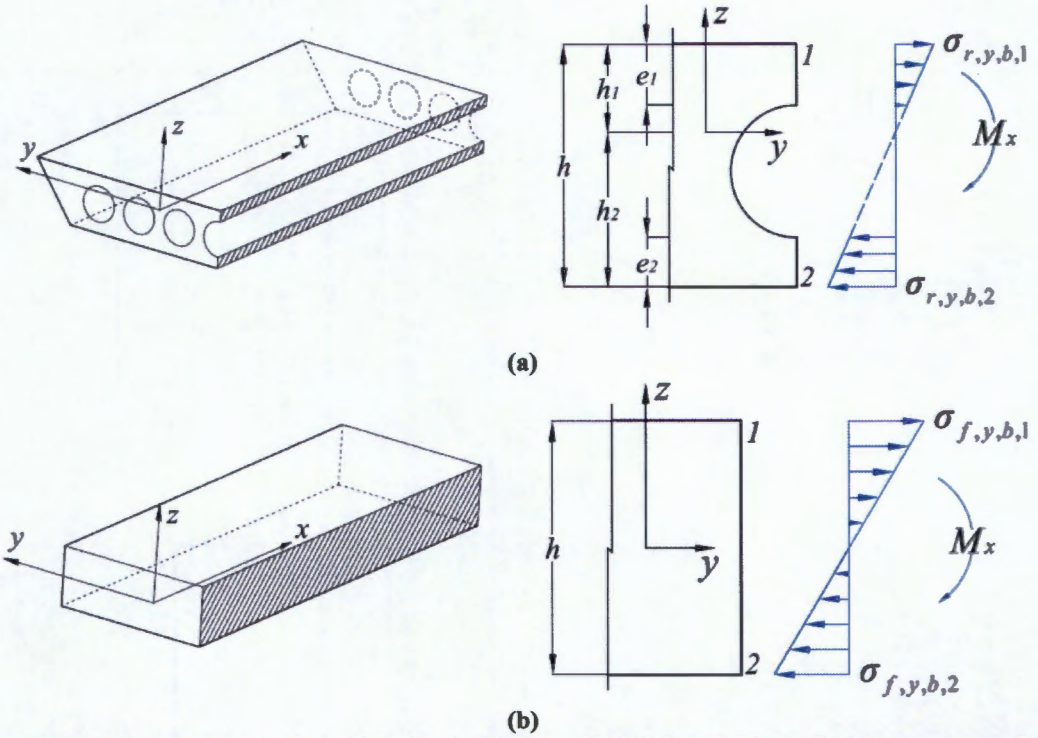

Figure 2.13 - Bending stress in the *y* direction in (a) the voided slab and (b) the fictitious orthotropic solid slab (Diaz *et al.*, 2010).

Once the membrane and bending stresses have been calculated, they can be combined to obtain the total stresses $\sigma_{r,x,t,l}$ and $\sigma_{r,y,t,l}$:

$$\sigma_{r,x,t,l} = \sigma_{r,x,m,l} + \sigma_{r,x,b,l} \tag{2.21}$$

$$\sigma_{r,y,t,l} = \sigma_{r,y,m,l} + \sigma_{r,y,b,l} \tag{2.22}$$

The finite element approach using the orthotropic plate analogy developed by Diaz *et al.* (2010) for voided slabs can be summarised in the following steps:

- The voided slab is replaced by an equivalent fictitious solid slab consisting of an anisotropic material. The effect of the voids is included in the model by using a modified elastic moduli in the transverse and longitudinal directions, resulting in an orthotropic plate.
- Using the generalised force vector and the bending moments acting on the slab in conjunction with the modified flexural rigidity of the plate, the curvature of the equivalent plate in bending can be determined.
- From the curvature the stress and strain in the equivalent plate can be calculated.
- Using the equality of forces between the voided and equivalent fictitious slabs, the stresses in the voided slab can then be determined.

These results allow for the global design and definition of the voided slab bridge deck.

It is also important to note that deformations due to transverse shear are neglected using solid orthotropic plates. A true solution of an orthotropic plate incorporating shear deformations, although possible, is too complex (Bakht *et al.*, 1981). Therefore orthotropic plate methods are applicable only to those cellular structures such as voided slabs which have small void diameter to slab depth ratios or transverse diaphragms in sufficient numbers to prevent the local bending of the flanges and webs due to shear deformations (Bakht *et al.*, 1981).

2.2.2. Effect of Voids on Structural Behaviour

2.2.2.1. Flexural Behaviour

A conventional solid slab under flexure is able to distribute the applied loading in two directions. However, the discontinuous nature of the voids in the transverse direction of a voided slab results in a decrease in the transverse distribution of forces when compared to a solid slab. A voided slab therefore behaves more like a one way than a two way spanning structure.

The effect of the voids on the longitudinal flexural behaviour of a structure can be studied by looking at the position of the voids within the slab, which is shown in Figure 2.14 below. Voided slabs are designed so that the voided zone is situated in the tensile concrete layer between the concrete compression zone and tensile reinforcement. In reinforced concrete design, it is typical to assume that only the compressive concrete contributes to flexural stiffness in bending, and the tensile concrete is neglected. As the voids are designed to be located in the tensile concrete, the addition of the voids to the slab has minimal effect on the strength in flexure. However, if the slab is highly stressed, the stress block may enter the voided zone. Laboratory tests have proven that anything up to 20% encroachment has a trivial effect on the performance of the structure (Lai, 2010).

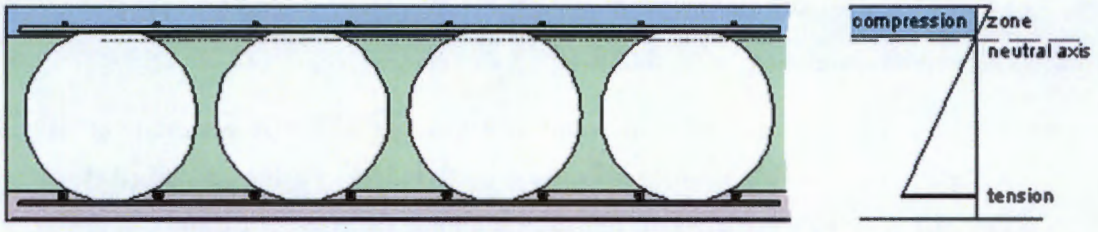

Figure 2.14 – Position of voids within a reinforced concrete element under flexure (Bokil, 2010).

The voids also lead to a reduction in the moment of inertia of the structure, which is due to the reduction in concrete cross-section. The reduction in moment of inertia increases exponentially with an increase in void diameter (Hambly, 1991). The moment of inertia of a voided slab with the voids located at mid-depth can be calculated by subtracting the moment of inertia of the voids from that of the solid slab, as shown in Equation 2.23 (Donohoe and Keogh, 2000).

$$I = I_{slab} - I_{voids} = \frac{bd^3}{12} - \frac{n\pi {d_v}^4}{64} \tag{2.23}$$

Where b is the width of the slab, d is the depth of the slab, n is the number of voids, and d_v is the diameter of the voids. Figure 2.15 shows the reduction of moment of inertia when the void diameter is increased keeping the slab depth constant. It can be seen that the moment of inertia varies by 5% as the void diameter increases from 0 to 0.6 of the slab depth. Once the void diameter exceeds 0.6 of the slab depth, the moment of inertia decreases exponentially. Therefore the voids can have a considerable effect on the stiffness of the structure, depending on the void diameter ratio, and can affect the structural behaviour of the slab under flexure.

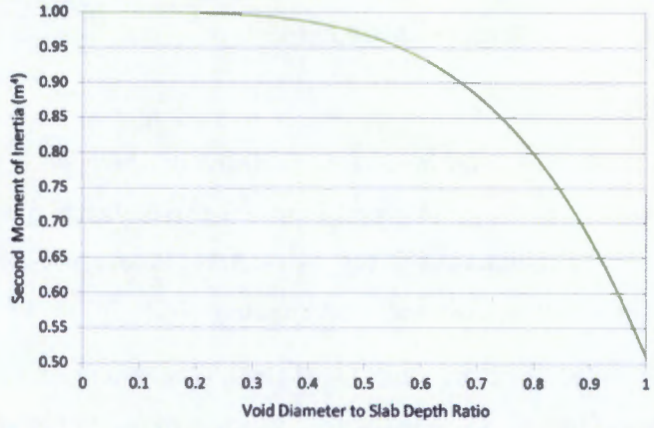

Figure 2.15 - Comparison of moment of inertia versus void diameter to slab depth ratio.

2.2.2.2. Shear Behaviour

The shear resistance of concrete slabs is directly related to the area of the concrete cross-section, therefore the voids within a voided slab can significantly decrease the slabs resistance to shear compared to a conventional solid slab. Theoretical models show the shear strength of voided slabs is around 60% to 80% of a solid slab with the same depth (Lai, 2010). This is usually countered by discontinuing the voids around areas of high shear such as supports to create incorporated transverse beams.

According to Jackson (2008), provided the void diameters are less than 60% of the slab thickness, the voided slab can be analysed as a solid slab without considering the reduced transverse shear resistance. If larger voids are required, the reduced shear must be accounted for. The shear capacity can be increased by omitting the voids in high shear areas and through the use of shear links provided in the webs between the voids. These shear links can be designed as for a flanged beam using the minimum web thickness (Jackson, 2008).

2.2.2.3. Cellular Distortion of Cross-section

As the void diameter to slab thickness ratio increases, a voided slab starts to behave in a more similar manner to a cellular structure, with flanges above and below the voids. This behaviour is characterised by the deformable nature of the web and flange type cross-section, with the flanges and webs bending about their own local axis, causing the cross-section to act in a similar manner to a Vierendeel frame (Jackson, 2008). This deformation is known as cellular distortion and can result in an increase in local stresses within the flanges and webs. The neglect of cellular distortion can lead to an underestimation of both longitudinal and transverse moments and shear forces (Bakht *et al.*, 1981a).

The need for a method of analysis which takes into account the deformable nature of the cross-section has been stressed by many authors (Bakht *et al.*, 1981a). However opinions differ with regard to the influence of cellular distortion, and the need to account for it in the analysis. Cellular distortion, which results from transverse shear deformation, is mainly influenced by the ratio of the diameter of the voids to the slab thickness, as it affects the thickness of the webs and flanges (Hambly, 1991).

If there are several transverse diaphragms in cellular type bridges that are sufficient to prevent cellular distortion, the structure can be idealised without consideration of cellular distortion. However due to the continuous nature of the longitudinal voids in a voided slab, diaphragms cannot be easily accommodated. The absence of transverse diaphragms reduces the cross-sections ability to resist distortion, thus increasing the transverse flexibility of the structure, and reducing the ability of the structure to distribute loads in the transverse direction (Bakht *et al.*, 1981a). Consequently higher concentrations of longitudinal and transverse moments and shear forces occur than those predicted by an analysis which neglects cellular distortion.

Figure 2.16 shows the effects of cellular distortion on the cross-section of cellular and voided type structures. It can be seen that an increase in deformation results from the flexure of the flanges and webs about their own axes. Plane sections do not remain plane and the flexibility of the cross-section increases, thereby affecting the manner in which the load effects are distributed transversely in the structure.

Aster (1968) proposed that transverse cellular distortion can be accounted for in an orthotropic plate model through the use of a reduced transverse rigidity factor, such as those in Table 2.1. Since the transverse cell distortion depends upon transverse shear rather than moments, it is open to question

whether cellular distortion can be accounted for by decreasing the values of the transverse rigidity. Bakht *et al.* (1981a) concluded that the representation of cell distortion by an equivalent reduction of the flexural rigidity of the transverse medium as proposed is unlikely to realistically represent the cell distortion effects and can lead to erroneous results. Hambly (1991) stated that the effect of cellular distortion can be neglected provided the void diameters are less than 60% of the slab thickness and transverse steel is provided in the top and bottom flanges. However, as this is rarely the case for modern day voided slabs, a method which accounts for the effects of cross-section distortion is required.

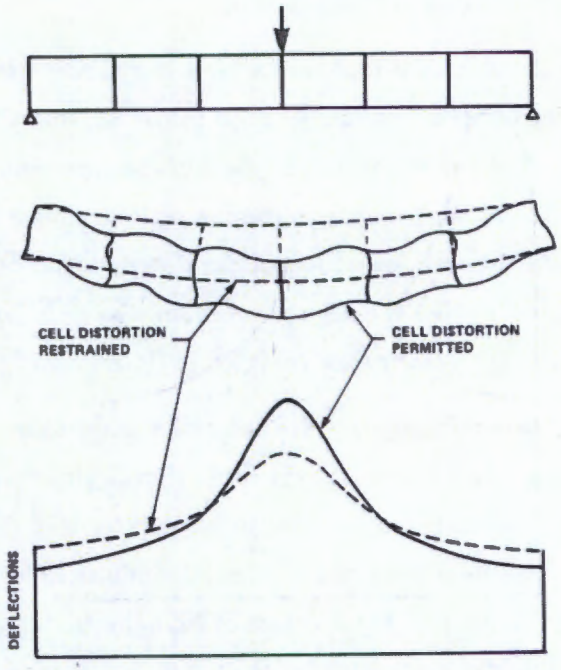

Figure 2.16 - Effect of cross-section distortion on cellular and voided slab structures (Bakht *et al.*, 1981a).

Bakht *et al.* (1981a) proposed that the effect of cell distortion can be accounted for by providing a measure of the increase in the longitudinal and transverse moments and shear forces due to cellular distortion which can be used in conjunction with a simplified method of analysis which neglects cell distortion. The methodology proposed by Bakht *et al.* (1981a) can be summarised as follows.

The moments and shear forces, neglecting cellular distortion, can be obtained using a simplified orthotropic plate analysis using rigidity factors to account for the effect of the voids. Three non-dimensional parameters, which are used to characterise the transverse distribution of the longitudinal moments and deflections of the voided slab cross-section, can be calculated using the following simple equations:

$$\alpha = \frac{D_{xy} + D_{yx} + D_x + D_y}{2(D_x D_y)^{0.5}} \tag{2.24}$$

$$\theta = \frac{b}{L}\left[\frac{D_x}{D_y}\right]^{0.25} \tag{2.25}$$

$$\delta = \frac{\pi^2 b}{L}\left[\frac{D_x}{s_y}\right]^{0.5} \tag{2.26}$$

Where D represents the rigidity factors in the relevant directions, b is the width of the deck, L is the span length, and S_y is the product of the shear modulus and the equivalent transverse shear area per unit length. Once the distribution coefficients have been obtained, magnifiers are calculated which can be used to account for the influence of cellular distortion. These magnifiers are defined as the ratio of the maximum intensity of the moments and shears in a structure if cell distortion is considered to the maximum intensity if cell distortion is absent. Two magnifiers are considered, namely γ_m and γ_s, which account for the increase in moments and shears due to cellular distortion respectively.

Bakht *et al.* (1981a) developed charts that use α, θ, and γ and the number of loaded lanes from which the values of γ_m and γ_s can be easily obtained. The charts were developed by investigating the effect of various void diameters and spacing ratios, as well as loading configurations, in order to determine their effect on cellular distortion. Once the values of the magnifiers and the distribution factors have been determined, it is possible to ascertain the increase of the longitudinal moments and shear forces due to the effect of transverse cell distortion using the magnifiers.

The results obtained using this methodology showed that the effects of void ratio and spacing had a minor effect on distortion, and their effects can be neglected. However the maximum void diameter to slab thickness used was only 0.75, therefore the results are only applicable to voided slabs with low void diameter ratios, and the influence of cell distortion with larger void diameter ratios is still open to question. The parameter having the greatest effect on the magnifiers was the number of loaded lanes. When all lanes are loaded, γ_m and γ_s never exceed 1.04, suggesting that in these bridges the neglect of cell distortion can cause the governing longitudinal moment intensity to be underestimated by at most 4%. For single lane loaded conditions the underestimation can be as high as 17%.

Bakht *et al.* (1981a) demonstrated that γ_m decreased with increasing eccentricity of load from the bridge centre line and also with the increase in the number of lines of wheels. When the longitudinal moments under a concentrated load increases, to maintain overall statics, it is accompanied by a reduction of longitudinal moments in other transverse locations. It can be readily visualised that under the action of several concentrated loads, the effects near any one concentrated load are relatively less severe than if there was only one load on the bridge. In the extreme case of an infinite number of loads on a transverse section, a uniformly distributed load, the two magnifiers would both be equal to 1.0. This result shows that the influence of cross-section distortion is primarily dependent on the loaded lane conditions, and the number of loaded lanes. Bakht *et al.* (1981b) used this result to conclude that the effect of cellular distortion becomes excessive when the loading is less than 2/3 of the bridge width.

Other methods that can be used to account for cellular distortion include using a grillage idealisation and assigning equivalent shear areas to transverse beams, which allows for shear deformation to be included in the analysis. A shear weak plate using transverse shear rigidity factors can also be used. Various transverse shear rigidity factors have been proposed by researchers, however Bakht *et al.*, (1981a) found that the proposed factors did not compare well with experimental results, and

further research is required on the proposed shear factors and their application for shear deformation of voided slabs. Cellular distortion can also be modelled by considering the voided slab to act like a cellular slab and make use of a shear-flexible grillage analysis (Hambly, 1991).

2.2.3. Structural Analysis of Voided Slabs

Structural analysis consists of simplified mathematical modelling of the response of a structure to applied loading and boundary conditions. Such models are based on idealisations of the structural behaviour of the structure and are, therefore, imperfect to some extent, depending upon the simplifying assumptions in the modelling (Ryall, 2008). Consequently the assessment of structural responses is the best estimate that can be obtained in view of the assumptions implicit in the modelling of the system. The following are methods that have been suggested for the structural analysis of voided bridge deck slabs. Examples using these forms of analysis are presented in Section 2.3.

2.2.3.1. Grillage Analysis

Grillage analysis is a method of modelling bridge decks in two dimensions. It involves the idealisation of a bridge slab as a mesh of discrete interconnected longitudinal and transverse beams located in one plane (O'Brien & Keogh, 1998). The grillage analogy is popular as it is easy to comprehend and use, relatively inexpensive, and has been proven to be reliably accurate for a wide variety of bridge types (Hambly, 1991). The representation of a bridge as a grillage is ideally suited to carrying out the necessary calculations associated with analysis and design on a computer, and it can be used in cases where the bridge exhibits complicating features such as a heavy skew, edge stiffening and deep haunches over supports (Qaqish, 2008). Figure 2.17 shows a grillage model used to idealise a slab type bridge.

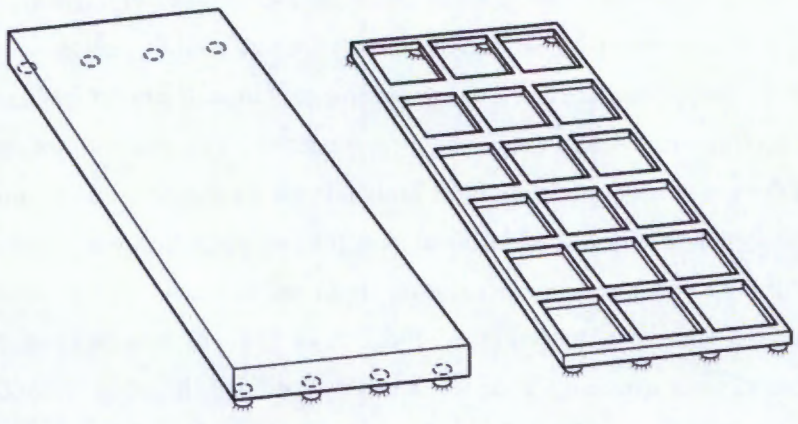

Figure 2.17 - Grillage idealisation of a slab type bridge (Ryall, 2008)

In a grillage model, the dispersed bending and torsional stiffness's in every region of the slab are assumed to be concentrated into the nearest equivalent grillage beam (Shanmugam & Narayanan, 2008). The longitudinal stiffness of the structure is concentrated in the longitudinal beams, and the transverse stiffness in the transverse beams. Thus each longitudinal or transverse grillage beam element must have

the same moment of inertia and torsional constants that resemble the longitudinal and transverse bending and twisting behaviour of the portion of the bridge being represented. Each longitudinal and transverse beam can be defined by its flexural stiffness, torsional stiffness, and length. Ideally the beam stiffness's should be such that when the bridge deck and equivalent grillage are subject to identical loads, the two structures deflect identically, and the moments, shear forces and torsions in any grillage beam should be equal to the resultants of the stresses in the cross-section of the part of the deck the beam represents (Hambly, 1991). The accuracy of the results depends on the effort put into the discretisation of the system into a two-dimensional grid (Bapat, 2009).

Defining the stiffness of each grillage element is straight forward, and can be calculated by considering the moment of inertia of a beam, where the width of the beam is replaced by the width of the portion of the slab the element represents. The moment of inertia is calculated about the neutral axis of the deck. A similar procedure can be done to calculate the torsional constants of the slab. The elements of the grid are assumed to be rigidly connected, so that the angles between elements connected together at a node remain unchanged. Both torsional and bending moment continuity then exist at the nodal point of a grid. The direct stiffness method can then be used to relate the element forces and displacements with a stiffness matrix.

The logical choice of the location of the grillage beams depends on the mesh density, which affects the computational cost and accuracy of the idealisation. Hambly (1991) recommends that longitudinal members should be spaced with a maximum separation of a quarter of the effective span length. The number of transverse beams can then be chosen to achieve a 1:1.5 ratio with the number of longitudinal beams (Ryall, 2008). There is little point in placing members closer than 2 to 3 times the deck depth as local dispersion of loads is not considered (Hambly, 1991). The mesh density should be sufficiently dense to allow the grillage to deflect in a smooth surface. A finer mesh can also be utilised in areas of rapid load changes such as isolated point loads and over supports.

A logical choice for the longitudinal beams of a voided slab would be to have one beam replace a portion of the slab that extends from the middle of one web to the next. The stiffness of the beam can then be calculated by considering the stiffness of the solid portion less the stiffness of the voided section. The calculation of the stiffness on the transverse beams is complicated by the fact that the cross-sectional area is not constant through the width of the slab due to the presence of the webs between the voids.

A conservative assumption that is made in grillage models of voided slabs is to assume that the slab behaves isotropically and the transverse stiffness is equal to the longitudinal stiffness. This assumption is sufficient for design purposes for voided slabs with void diameters less than 60% of the deck thickness. For larger void sizes, a shear-flexible grillage is more suited (Hambly, 1991). Another assumption is to calculate the stiffness at the point of minimum cross-section area, at the middle of one of the voids. The transverse stiffness will then be the result of the solid sections above and below the voids. However, this assumption could prove to be too conservative as it neglects the webs in between

the voids. The flexural rigidities of the beams in a grillage idealisation can also be obtained by multiplying the beam spacing by the rigidity factors proposed for orthotropic plate analysis in Section 2.2.1. Figure 2.18 below shows a typical grillage model of a voided slab bridge deck.

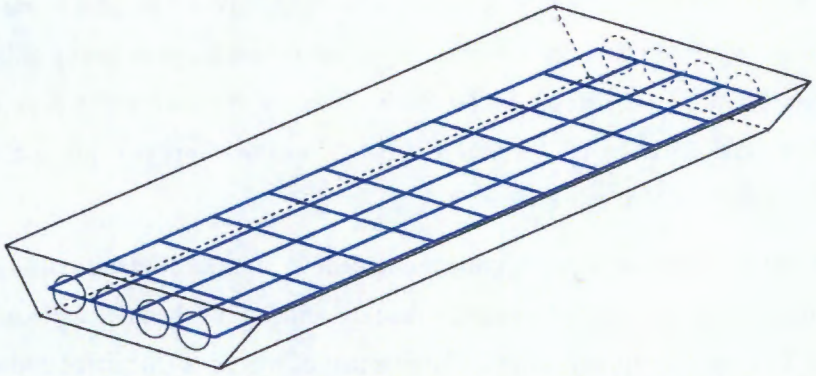

Figure 2.18 - Typical grillage model of a voided slab bridge deck (Diaz *et al.*, 2010).

A shortcoming of using grillage models to analyse slab type decks is that the moment in any beam is solely proportional to the curvature of the beam in one plane, while in a slab the moment in any direction depends on the curvature of the slab in two orthogonal planes. Local effects and coupling of the slab are also not correctly accounted for. A grillage analogy is also unable to account for the effects of transverse cell distortion experienced by voided slabs. However, a grillage analogy with shear-weak transverse beams has been verified by more rigorous analysis and is regarded to be an efficient and versatile method for the analysis of cellular and voided structures which can account for the effects of shear deformation (Bakht *et al.*, 1981). A grillage model is only an approximation of the actual behaviour, however grillage results of sufficient accuracy have been obtained for the analysis of voided slab bridge decks (Hambly, 1991).

2.2.3.2. Shear-Flexible Grillage Analysis

Grillage models can be used to analyse voided slabs with small void diameter to slab depth ratios with sufficient accuracy. However, for larger void diameter ratios, the slab may not behave like a plate but more like a cellular deck, whose behaviour can be more accurately investigated using a shear-flexible grillage. A shear-flexible grillage differs from a typical grillage analogy as it takes into account the deformations due to shear and torsion by assigning equivalent shear areas to transverse members (Hambly, 1991).

A shear-flexible grillage, which is typically used for the analysis of cellular decks, is more appropriate for voided slabs when the void diameter exceeds 60% of the deck thickness (Hambly, 1991). In this method, the cylindrical voids of a voided slab can be replaced by square section voids of the same cross-sectional area, resulting in a cellular structure with top and bottom slabs separated by vertical webs. The square voids are considerably more flexible than circular voids, resulting in an underestimation of the stiffness, therefore this is a conservative assumption.

A shear-flexible grillage uses the same principal of dividing the structure into a mesh of longitudinal and transverse beams as a standard grillage. The longitudinal beams are coincident with the vertical webs of the cellular deck and the transverse members are spaced closer than a quarter of the distance between points of contra-flexure (Hambly, 1991).

Longitudinal bending is considered by cutting the cellular deck between the webs, resulting in a number of I-beams. The longitudinal bending and shear stresses can be determined using beam theory for an I-beam subjected to the same curvature as the deck. Transverse bending, which is the flexure of the top and bottom slabs in unison about a common centre of gravity, is considered by calculating the transverse moment of inertia based on the slab thicknesses and lever arms to the centroid. The torques in a cellular deck can be considered by again cutting the deck into I-beams. The torsion in the deck is due to the opposed shear flows in the top and bottom slabs, as well as the shear flows in the webs. The torque is resisted by the torsional stiffness of the top and bottom slabs of the grillage members, and the shear area of the longitudinal grillage members, which should have the same area as the vertical webs. A shear-flexible grillage can also approximate Vierendeel truss behaviour, which can be used to describe the transverse behaviour of a voided slab, where the vertical shear force causes the slabs and webs to flex independently out of plane (Hambly, 1991).

A shear-flexible grillage is not the most theoretically rigorous analogy of cellular decks available, however it has the benefit of being applicable to a wide variety of structures, of being relatively inexpensive in user and processing time, and being relatively simple to comprehend (Hambly, 1991).

2.2.3.3. Finite Element Analysis

The finite element method is a numerical procedure for the approximate solution of problems in continuum mechanics in which the actual structure is represented as an assemblage of finite elements interconnected at a finite number of nodal points (Abdelraouf & Matlock, 1972).

The finite element method involves subdividing the actual structure into a suitable number of sub-regions that are called finite elements. These elements can be in the form of line elements, two-dimensional planar elements and three-dimensional elements. The intersection of two elements results in nodes, which are assigned degrees of freedom in the form of displacements and rotations. Each element has its own shape, thickness, material properties and governing equations. The choice of element properties is critical and if incorrect, the results can be far more inaccurate than those predicted by simpler analysis methods (Hambly, 1991). The subdivision of the model into elements depends on the geometry of the structure, the local features such as stress concentrations and the convergence properties of the model solution (Qaqish, 2008).

The entire procedure of the finite element method involves subdividing the structure into an equivalent system of finite elements, choosing a suitable displacement function, deriving a stiffness matrix using the principles of mechanics, formulating a global stiffness matrix for the entire structure, solving the resulting differential equations to determine the displacements of the nodes, and computing the stresses and strains from the nodal displacements (Ryall, 2008).

The advantages of finite element analysis include that it can be used to model irregularly shaped bodies composed of different materials, handle complex loading and boundary conditions, handle both geometric and material non-linear behaviour and can include dynamic effects (Qaqish, 2008). The finite element method also removes the need to calculate or estimate geometric and material properties of the structure, and therefore reduces the number of assumptions that need to be made in order to idealise a structure. The finite element method is the most powerful analytical method available, however it is cumbersome and expensive to use (Hambly, 1991).

The finite element method is a systematic and uniform procedure for the analysis of structures regardless of the type. Since the basic principle of subdivision of a structure into simple elements can be applied to structures of all forms and complexity, there is no logical limit to the type of structure that can be analysed, provided the appropriate element types and stiffness's are used (Hambly, 1991). Therefore the finite element method can be utilised for the analysis of voided slab bridge decks. Figure 2.19 shows the finite element method applied to the analysis of a voided slab bridge deck.

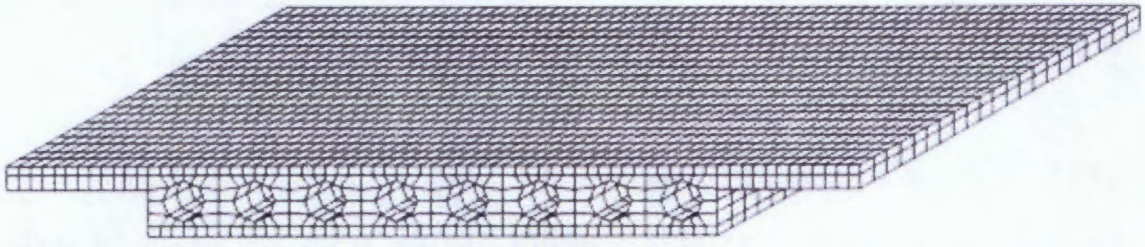

Figure 2.19 - Finite element model of a voided slab bridge deck incorporating wide transverse cantilevers (O'Brien and Keogh, 1998).

Modern software packages with user-friendly graphical input make it fairly straightforward to produce three-dimensional finite element models with several thousand degrees of freedom, allowing complex structures to be analysed with a simple computer. It should also be kept in mind that the finite element method is a numerical method based on numerous assumptions and simplifications (Jukic & Ekfeldt, 2012). Therefore the accuracy of the model will be based on these assumptions and simplifications, and the model may be required to be calibrated to ensure the accuracy of the results.

2.2.3.4. Upstand Grillage and Finite Element Models

O'Brien & Keogh (1998) investigated the accuracy of the grillage analogy for voided slabs incorporating wide transverse cantilevers. The study found the plane grillage analogy to be an inaccurate method for linear elastic analysis of structures in which there are variations in the vertical position of the neutral or

centroidal axis, such as slabs with wide transverse cantilevers, or voided slabs where the voids are not located at mid-depth. This is because the method relies on the assumption that all parts of the bridge cross-section bend about a single neutral axis which is generally taken to be the centroid of the deck. Variability of neutral axis depth, when significant, results in the incorrect representation by a grillage analysis of the behaviour of the bridge deck.

O'Brien & Keogh (1998) proposed two new methods for the analysis of structures in which the neutral axis is not at a constant depth, namely the upstand grillage and upstand FEA methods. The methods were developed for use on slab bridge decks with wide transverse cantilevers, and were also tested for use on voided slab bridge decks. The upstand grillage is similar to a standard grillage except that each grillage member is located in a plane containing the centroid of the relevant portion of bridge. The grillage members in different planes are then connected by rigid vertical beams with infinite flexural rigidities. This results in a three dimensional idealisation of the structure, as shown in Figure 2.20.

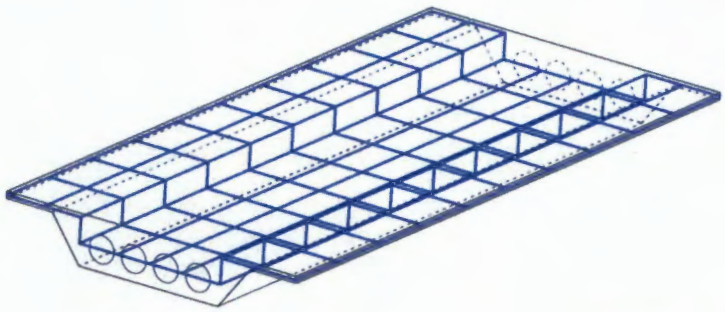

Figure 2.20 - Three-dimensional grillage model of a voided slab with wide transverse cantilevers (Diaz *et al.*, 2010).

Longitudinal stress results for the upstand grillage method of a wide transverse cantilever slab bridge were found to be more accurate than a typical grillage model when compared to a 3D finite element analysis, however poor stress predictions in regions of in-plane shear distortion were found (O'Brien & Keogh, 1998). O'Brien & Keogh (1998) proposed that this problem can be overcome by the use of a three-dimensional analysis method which can account for in-plane forces, and one which does not require all members representing parts of the deck to bend about a pre-assumed neutral axis position. However, three-dimensional methods are generally excessively complex for everyday use in a design office, therefore O'Brien and Keogh (1998) developed a simplified finite element method called upstand FEA.

The upstand FEA method is similar to the upstand grillage method, however grillage beams are replaced by finite elements. Simple finite elements are located in different planes, according to the geometry of the bridge deck, which coincide with the centroid of the part of the bridge they are representing. These planes of elements are connected once again by vertical beams with infinite flexural rigidity. The model can account for in-plane forces and deformations as well as out-of plane bending. Results from an upstand FEA for a wide transverse cantilever bridge compared accurately with a normal 3D model, with reduced computational effort.

2.3. Examples of Voided Bridge Deck Slab Analysis

Numerous studies have been conducted to determine the accuracy of the various methods mentioned above regarding the analysis of voided slab bridge decks. Results from selected studies are presented below to illustrate these methods for the analysis of voided slab bridge decks.

Oline & Sen (1987)

Oline & Sen (1987) conducted research to determine the effect of the void to cross-sectional area ratio on stresses and displacements of a prestressed voided bridge deck slab using finite element analysis. Two simply supported spans each with a length of 50ft (15.24m), a width of 26.25ft (8m), and an overall depth of 31.67in (804mm) were modelled. A horizontal radius of curvature of the centreline of the slab of 127.3ft (38.8m) was also used. Five 24.8in (629mm) central voids, and two 19.2in (487mm) voids, one at each end, were chosen in order to achieve a void to overall cross-sectional area ratio of 33%. This percentage was chosen as it closely matches the typical Canadian design for voided slab bridges. Table 2.3 and Figure 2.21 below give a summary of the cross-sectional parameters used. A second model with a void to cross-sectional area of 11.5% was also created in order for comparison.

Table 2.3 - Cross-section parameters of the voided slab deck with a 33% void to cross-sectional area ratio (Oline & Sen, 1987).

Parameter	Dimension
Large void diameter	24.8in (629mm)
Small void diameter	19.2in (487mm)
Spacing between larger voids	37.8in (960mm)
Spacing between larger and smaller voids	34.7in (880mm)
Side Cantilever length	47.3in (1200mm)
Side Cantilever Depth	12.0in (305mm)

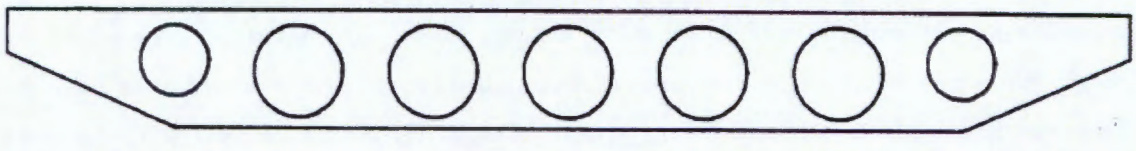

Figure 2.21 - Cross-section of the voided slab bridge with a 33% void to cross-sectional area ratio (Oline & Sen, 1987).

Due to geometric longitudinal symmetry, only one span of the bridge was modelled. The boundary conditions consisted of simple supports on either side. The end support condition was modelled at each node along the bottom end of the cross-section. The centre support was modelled by specifying a simple support at the bottom centre node of the cross-section. For longitudinal symmetry reasons, rotation about a radial line of nodes at the centre support was restricted. The voids were omitted near the end and centre supports resulting in a solid section. The length of the end solid section was 0.0695 of the span length and 0.20725 of the span length for the centre solid section, which is typical of a Canadian voided slab bridge design (Oline & Sen, 1987).

Six-sided, eight node solid elements were used for the finite element analysis of the bridge deck. Thin plate elements were also attached to the top and bottom of the cross-section in order to enable an easier determination of stress variations on the top and bottom surfaces. The longitudinal post-tensioning was modelled using six straight sagged steel truss elements. Straight profiles were used as opposed to parabolic profiles as they showed more accurate results. These cables began at the location corresponding to the top of the voids at the supported end of the slab, and sagged to the bottom of the voids location at the centre of the span. The completed structural finite element model consisted of 1904 nodes, 768 thin plate elements, 2170 solid elements and 96 truss elements, and is shown in Figure 2.22.

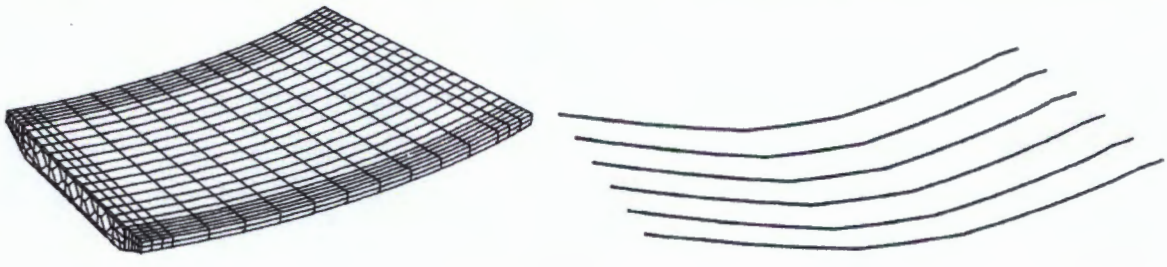

(a) (b)

Figure 2.22 - Finite element model of the (a) voided slab and (b) the longitudinal prestressing (Oline & Sen, 1987).

Three static load cases for the model were considered, namely, gravity loading, longitudinal posttensioning, and transverse posttensioning. Longitudinal posttensioning forces were generated in each of the six truss elements by decreasing the temperature in the elements, and the transverse posttensioning was generated by applying a force to the slab at each division line between the elements around the horizontal curve. All load cases were analysed using linear analysis.

The stress and displacement results for the 11.5% and 33% void to cross-sectional area were obtained and compared. The maximum deflections due to gravity loading were reduced from 1.363in (34.6mm) to 0.84883in (21.6mm) with the increase in void ratio. The maximum longitudinal tensile stresses on the bottom surface of the slab were reduced from 1019lb/in2 (7.03MPa) to 796.7lb/in2 (5.5MPa) under gravity loading.

Due to the longitudinal post-tensioning load the maximum upward deflection increased from 5.281×10^{-5} in (.00013mm) to 3.8975×10^{-3} in (0.099mm), while the maximum compressive stress on the bottom surface of the slab increased from 9.125lb/in2 (0.063MPa) to 11.34lb/in2 (0.078MPa) with the increase in void ratio.

From these results it could be concluded that a longitudinal post-tensioning load of 268,517lb (1.19kN) is required to overcome the effect of gravity for the 33% void ratio model. The 11.5% void ratio model required a longitudinal post-tension load of 426,807lb (1.9kN) to overcome the gravitational load. Therefore a reduction of 37% in the amount of prestressing is required to overcome the dead weight of the structure with a void ratio of 33% compared with a void ratio of 11.5%. The effects of

transverse post-tensioning on the stresses and displacements did not vary much from the 11.5% void model to the 33% void model, which illustrates that transverse stiffness is still present in the 33% void model and is not significantly affected by increasing the ratio of the voids.

O'Brien & Keogh (1998)

O'Brien & Keogh (1998) investigated the accuracy of the upstand FEA method proposed in Section 0 for the analysis of a voided slab bridge with wide transverse cantilevers. A two-span bridge deck incorporating longitudinal voids with solid sections above the end and central supports to simulate the presence of diaphragm beams was used in the model. A typical 3D finite element model was also created in order to draw comparisons with the upstand FEA results. Figure 2.23 shows a longitudinal section and cross-section through the voided part of the bridge deck, as well as an approximation of how the voids were modelled in the typical 3D model. As most FE software utilizes finite elements with straight sides, the circular voids were approximated by octagonal voids.

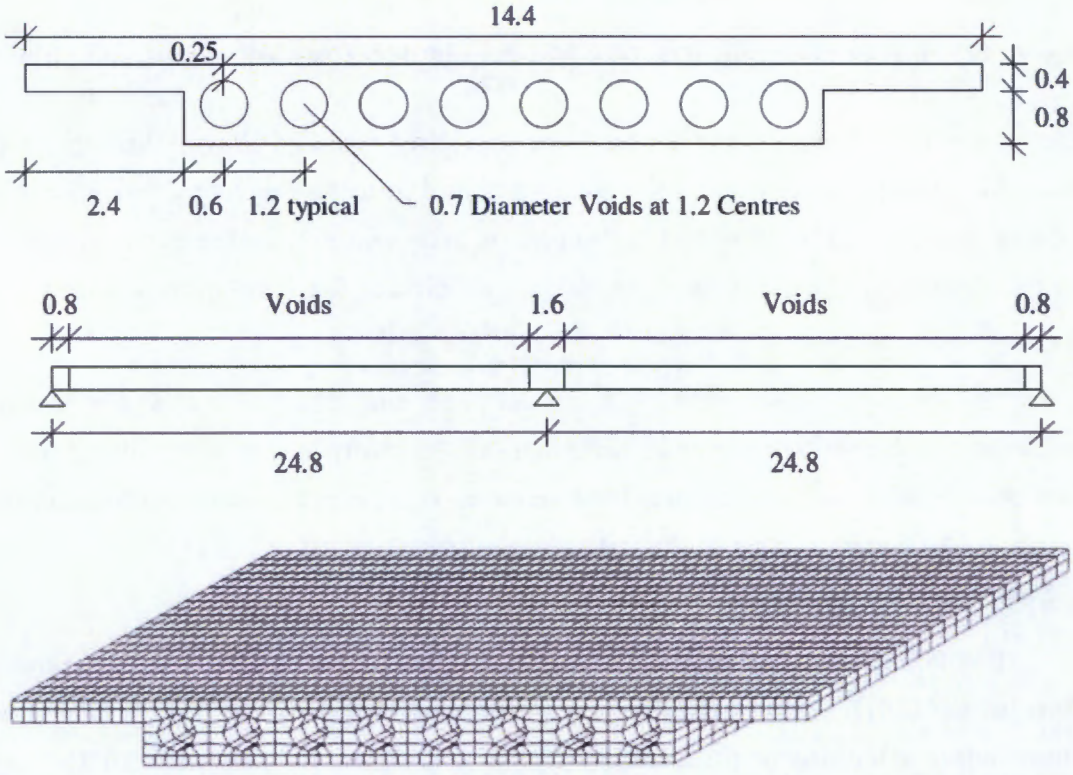

Figure 2.23 - Cross-section, longitudinal elevation, and 3D FE model of the voided slab deck (O'Brien & Keogh (1998).

The voided slab in the upstand FE model was modelled using isotropic elements based on plate theory. The use of isotropic elements meant that the transverse stiffness was equal to the longitudinal. This assumption was based on works by Hambly (1991), where it was found that slabs with a void diameter less than 60% of the slab depth can be modelled as isotropic. For an isotropic element, only the depth is required to define the stiffness. However, due to the presence of the voids, an equivalent depth had to be

calculated. This equivalent depth is that which gives a moment of inertia for the equivalent solid slab equal to the moment of inertia of the voided section which it represents. It is clear however that the area of such an equivalent element is not equal to that of the corresponding voided section. This is not normally a problem in a two-dimensional plane analysis, as in-plane axial forces are not modelled. However, in-plane axial forces do exist in an upstand FEA, therefore it is essential that the upstand FEA idealisation of the voided slab has both the correct area and moment of inertia (O'Brien & Keogh, 1998).

For this model, the elements were modelled with a depth that resulted in the correct cross-sectional area. However, this depth does not account for the voids effects on the moment of inertia. This was accounted for by the addition of extra longitudinal beams to make up the shortfall in moment of inertia. The additional beams allows for the cross-sectional area and moment of inertia to be defined separately, resulting in an equivalent solid slab.

Figure 2.24 shows a comparison of the top longitudinal stress from the upstand FEA and the typical 3D FEA. The predictions from the two models compare well to each other, with only a small disagreement at the central support. The disagreement can be accounted for by the complexity incurred by the rapid change from a voided to solid section (O'Brien & Keogh, 1998). The results show that the accuracy of the upstand FEA method is in good agreement with a typical 3D FEA, and the results can be obtained with less computation effort than a typical 3D finite element model.

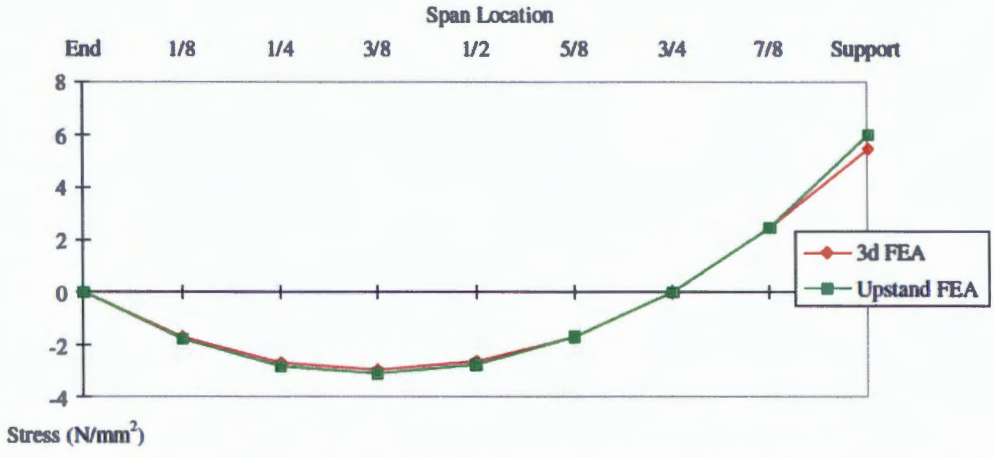

Figure 2.24 - Comparison of the top longitudinal stresses of a voided slab modelled using a typical 3D FEA and an upstand FEA (O'Brien & Keogh (1998).

Diaz *et al.* (2010)

Diaz *et al.* (2010) developed a code linked to a commercial finite element package that can be used to model the behaviour of voided slab bridge decks. The code is based on the orthotropic plate analogy described in Section 2.2.1. In this approach, a comparison is established between the actual concrete voided slab, which consists of an isotropic material, and an equivalent solid slab with the same height as the actual one, but made of an anisotropic material. The slab can then be modelled using shell elements under bending to analysis the deck behaviour. Post-tensioning cables can also be defined with one

dimensional beam elements connected directly to the slab. The finite element idealisation of a voided slab by Diaz *et al.* (2010) can be summarised with the following elements:

- The voided slab can be modelled using a layer of orthotropic shell elements, which are located in the centre of gravity of the voided slab. In solid sections at the abutments and intermediate piers, the deck elements can be defined as isotropic.
- Side cantilevers can be modelled as a layer of isotropic shell elements placed at their neutral axis.
- Elements of infinite rigidity are used to connect the layers located in different planes ensuring the transmission of forces between elements. This approach is similar to the upstand FEA proposed by O'Brien & Keogh (1998).
- Beam elements are used to model the post-tensioning layout, connected to the orthotropic elements of the slab with rigid bar elements of variable length.

Figure 2.25 below shows the finite element idealisation of the voided slab bridge deck using this methodology. The blue elements represent the orthotropic shell elements of the voided section of the deck, the green elements represent the isotropic shell elements of the side cantilevers, the red elements represent the post-tensioning beam elements, and the orange elements represent the rigid vertical beam elements.

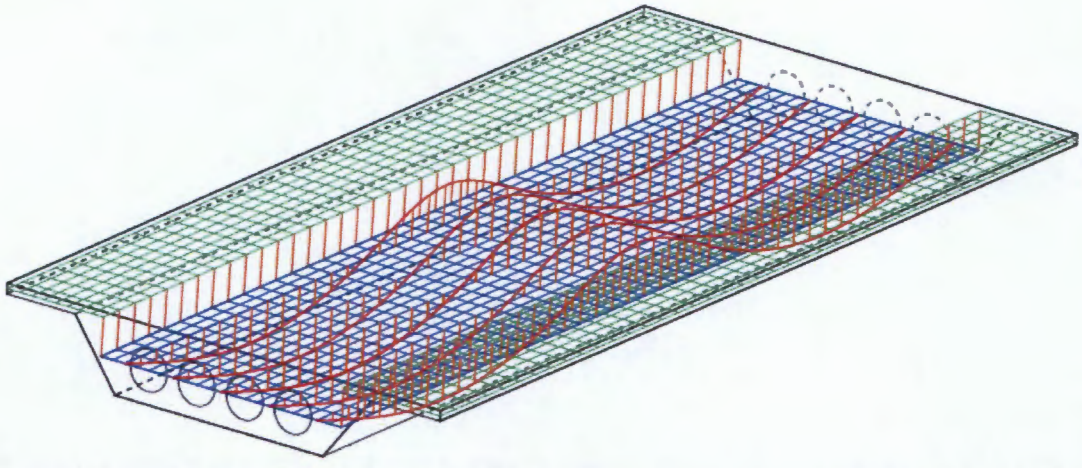

Figure 2.25 - Three-dimensional finite element model of a voided slab deck using shell and beam elements (Diaz *et al.*, 2010).

Diaz *et al.* (2010) developed a programme using a commercial finite element package based on the proposed orthotropic plate analogy. The purpose of this programme was to simplify the finite element process which can be complex and time consuming, while still maintaining the accuracy of a 3D model. The characteristic of the programme includes a graphical user interface that allows designers to define the geometrical and mechanical properties of the structural model, post-tensioning layouts, and loading, as well as providing a graphical and numerical output of the structural response, stresses and displacements.

In order to verify the accuracy of the orthotropic slab analogy and its implementation for the analysis of voided slabs, Diaz *et al.* (2010) produced a finite element model using the above methodology and compared it to the FEA results obtained by O'Brien and Keogh (1998). The longitudinal elevation and cross-section of the voided slab together with the finite element model are shown in Figure 2.26. The blue regions represent the orthotropic shell elements, the red regions represent the isotropic shell elements of the solid sections and side cantilevers, and the white represents the rigid vertical beams. The maximum element size was chosen to be 0.8m resulting in 2663 elements and 2174 nodes. The only load considered was the dead load, and no post-tensioning was modelled.

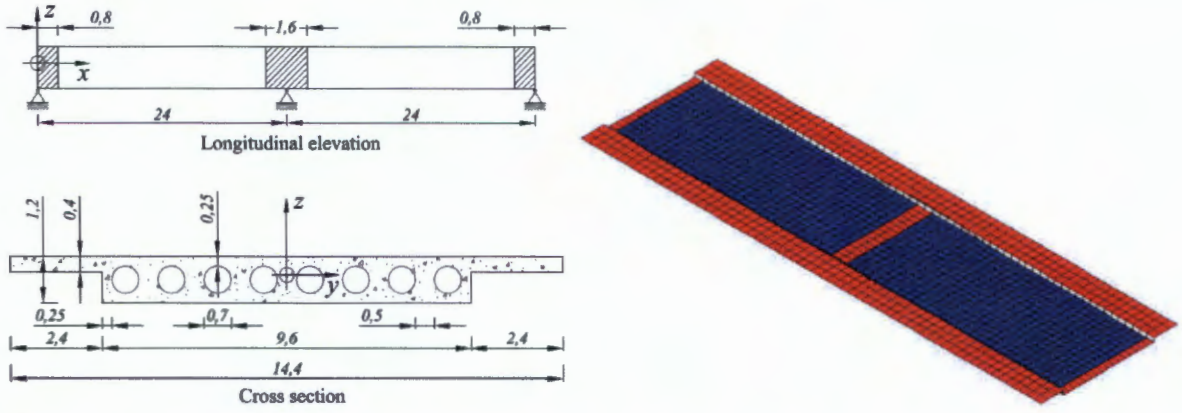

Figure 2.26 - Longitudinal elevation, cross-section, and finite element model of the voided slab bridge deck (Diaz *et al.*, 2010).

Figure 2.27 shows the comparison of the top stress results in the longitudinal direction for the first span between the orthotropic slab model and those of O'Brien and Keogh (1998). As expected, the maximum sagging stress is located at 3/8 of the span length, and the maximum hogging stress is located at the central support. As can be seen, the results are in accordance with each other with the difference being below 5%.

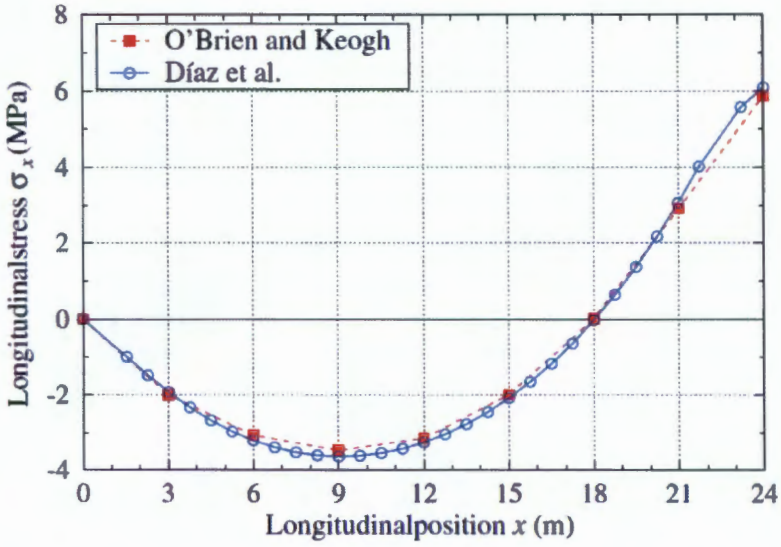

Figure 2.27 - Comparison of the longitudinal stress results on the top fibre of the first span between O'Brien and Keogh (1998) and Diaz *et al.* (2010) (Diaz *et al.*, 2010).

A second example was carried out by Diaz *et al.* (2010) in order to compare the results from the orthotropic plate model with a grillage model. The longitudinal elevation and cross-section of the voided slab used for the comparison are shown in Figure 2.28. No side cantilevers were considered in this example as they can result in inaccuracies in grillage models.

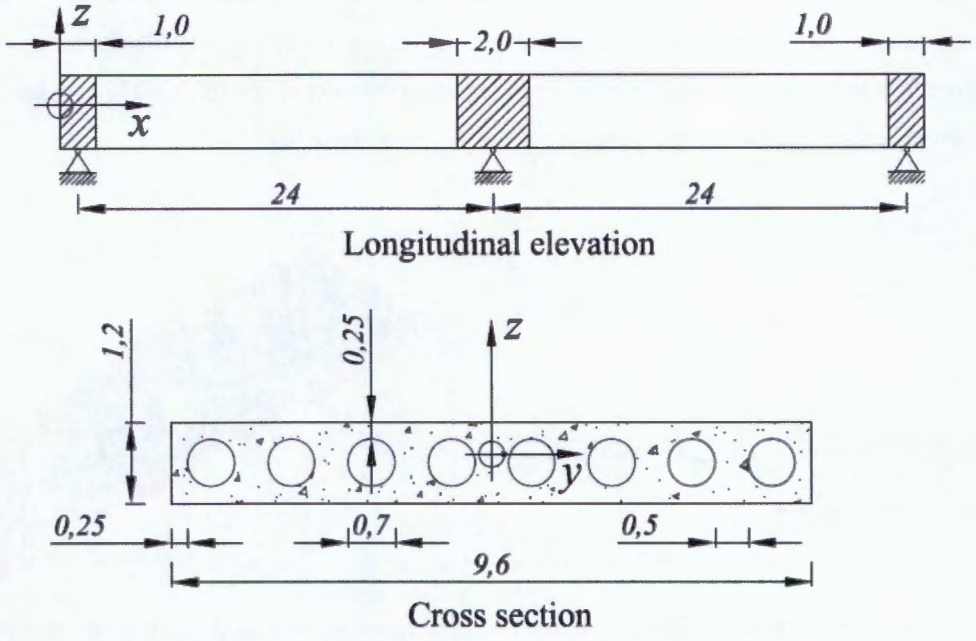

Figure 2.28 - Longitudinal elevation and cross-section of the voided slab used in the grillage comparison study (Diaz *et al.*, 2010).

Two load cases were considered, the first being symmetric, with the self-weight plus a live load of 4kN/m^2 equally distributed along the top surface of the deck. The second load case, which was selected to study the torsional behaviour of the bridge and the transverse response, had a live load distributed in alternate lanes along the deck in each span. The self-weight was also considered, along with an isolated live load of 600kN placed at mid-span in the outer lane of the first span. Eighteen post-tensioned cables each with a jack force of 2500kN were also modelled. The grillage and finite element models used for the comparison study are shown in Figure 2.29.

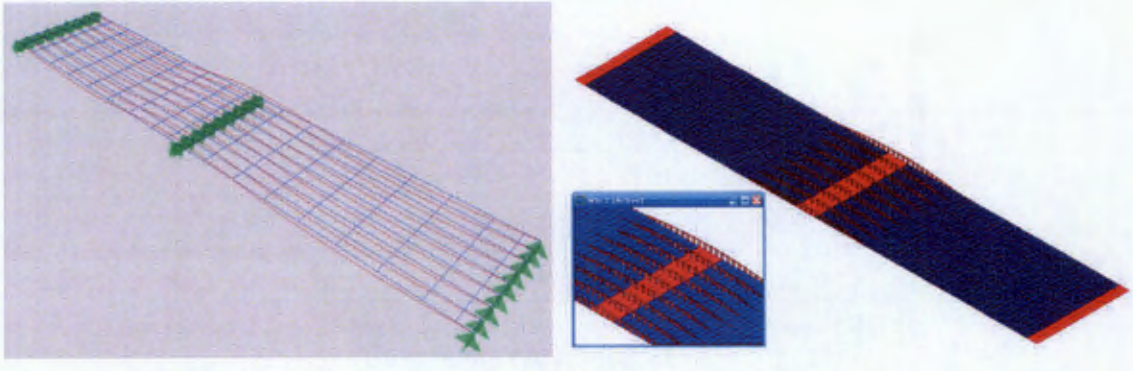

(a) **(b)**

Figure 2.29 – (a) Grillage and (b) finite element models used to compare analysis methods (Diaz *et al.*, 2010).

Figure 2.30 below shows the comparison of the vertical displacements in the longitudinal direction of the first span for the FE orthotropic plate and grillage models for the two different load cases. As can be seen, the results do not differ significantly and it was concluded that neither model stands out over the other in this aspect.

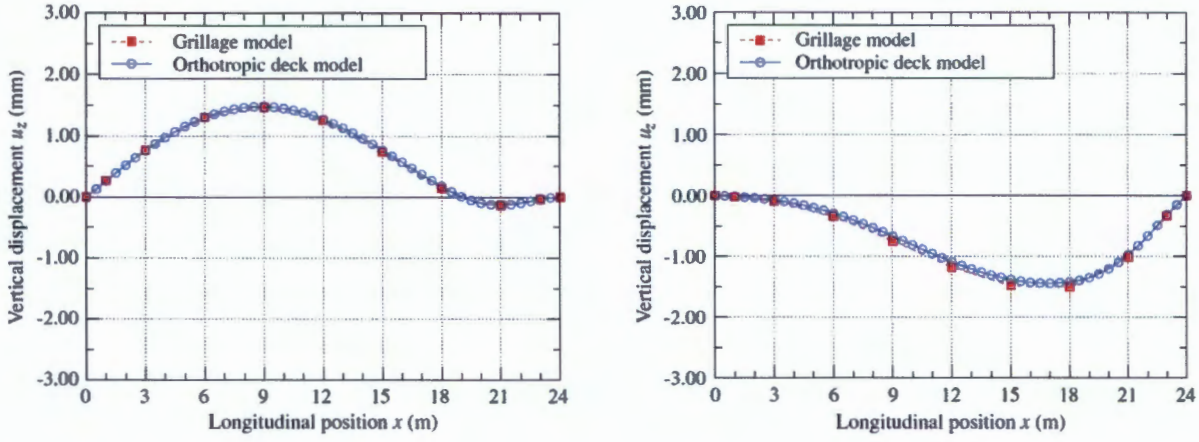

Figure 2.30 - Comparison of the vertical displacements for the grillage and orthotropic FE model for (a) load case 1 (b) and load case 2 (Diaz *et al.*, 2010).

Figure 2.31 shows the comparison of the vertical displacements in the transverse direction of the first span for the FE orthotropic plate and grillage models for the two different load cases. For the first load case, a small discrepancy could be noted between the two models. This variation was below 5% and was therefore not deemed significant. For the second load case, the relative error increases up to 74% at the edges of the deck. This is due to the poor performance of modelling unsymmetrical loads in grillage models. From the results, Diaz *et al.* (2010) concluded that the performance of orthotropic plate model and the grillage analogy for voided slabs are in good agreement, however the orthotropic plate model produces better results for unsymmetrical load cases when considering the vertical displacement in the transverse direction.

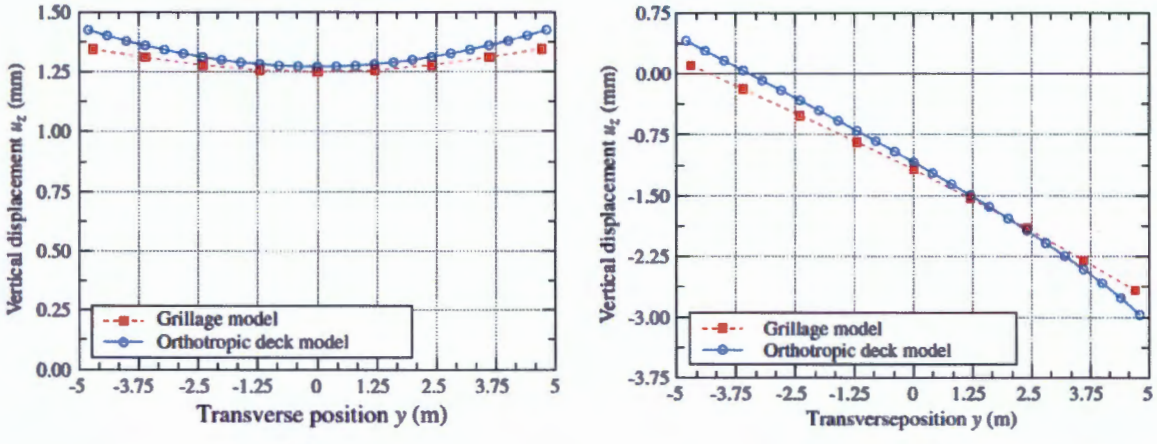

Figure 2.31 - Comparison of the vertical displacements of the transverse section at mid-span for the grillage and orthotropic model for (a) load case 1 and (b) load case 2 (Diaz *et al.*, 2010).

The results from Diaz *et al.* (2010) shows that a post-tensioned voided slab concrete bridge deck can be modelled in a more precise way using three-dimensional finite element meshes made up of orthotropic shell elements. This approach is more precise than the well-known grillage model, it performs well with asymmetrical loading and local effects, and it does not complicate the analysis excessively, as with typical 3D finite element models (Diaz *et al.*, 2010).

Sen *et al.* (1994)

Sen *et al.* (1994) conducted a study in order to evaluate the validity of the use of equivalent orthotropic plate parameters in predicting the elastic response of straight and curved, continuous post-tensioned voided slab bridges using orthotropic plate theory. The proposed equivalent plate parameters to be validated by Sen *et al.* (1994) for the analysis of voided slab bridge decks, which are similar to the plate parameters in Table 2.1, are expressed as follows:

$$D_x = E\left(\frac{t^3}{12} - \frac{\pi d^4}{64s}\right) \tag{2.27}$$

$$D_y = \frac{Et^3}{12}\left[1 - 0.95\left(\frac{d}{t}\right)^4\right] \tag{2.28}$$

$$D_{xy} = D_{yx} = \frac{Gt^3}{6}\left[1 - 0.84\left(\frac{d}{t}\right)^4\right] \tag{2.29}$$

In order to validate the proposed parameters, results from two-dimensional finite element models using the parameters were compared to 1:4 scale experimental results. Both straight and curved models were used. Each concrete model consisted of a two 8m span continuous deck, with solid sections over the end and central supports. The cross-section consisted of four central 0.216m diameter voids, a 0.127m diameter void on either end, a total width of 2m, and a span to depth ratio of 28. The centreline of the curved model in plan subtended an arc of 40° on a radius of curvature of 22.92m. The loading consisted of both dead load and live load using HS20-44 AASHTO truck loading. The models were both longitudinally and transversely prestressed.

The finite element models were created using four node quadrilateral shell elements in ANSYS. The solid sections were modelled using isotropic plate elements, and the voided sections were modelled using orthotropic plate elements with the parameters suggested above. As the plate elements cannot be defined by the parameters directly, the modulus of elasticity and moment of inertia per unit width were separately specified. This was accomplished by assuming a constant plate thickness and solving for the equivalent moduli in the longitudinal and transverse direction based on the plate thickness and the rigidity factors.

As the stress results from the FE model relate to the stresses in the equivalent orthotropic plate, two factors were used to convert the stresses from the equivalent plate model to the actual voided slab. The two factors included a material factor (MF), which was used to take into account the reduced stiffness of the equivalent plate, and a distance factor (DF), which allowed for the variation in the neutral

axis between the voided section and its orthotropic idealisation due to the different slab thicknesses. The factors were defined as follows:

$$MF = \frac{E}{E_e} \text{ and } DF = \frac{d_v}{d_e} \tag{2.30}$$

Where E is the modulus of elasticity of concrete for the voided deck, E_e is the modulus of elasticity of the equivalent orthotropic plate in the relevant direction (E_x or E_y), and d_v and d_e are the distances from the neutral axis of the voided and equivalent plate sections, and depend on the location where the stresses are to be determined.

Comparison of the results from the finite element models and 1:4 scale model for the stresses, reactions and deflections were found to be in good agreement for the straight model, with a variation of less than 5%. The test stress results for the curved model were in reasonable agreement with the finite element model, however the reactions and deflections comparison were poor. The finite element model deflection was found to be 25% larger than the test results, suggesting that the equivalent stiffness parameters underestimate the stiffness of a curved voided slab.

Sen *et al.* (1994) concluded that the equivalent plate parameters proposed can be used with reasonable accuracy to predict the response of straight continuous voided slab bridges, however their application to curved voided bridges is uncertain. The proposed factors to convert the stresses from the equivalent plate to the voided slab were found to be satisfactory.

Sen *et al.* (1993) used the same quarter scale models as Sen *et al.* (1994) to assess the ultimate load predictions of post-tensioned voided slab bridges. The two models consisted of the straight and curved voided slabs, and loading was simulated using AASHTO truck loading. Two separate analyses were conducted to predict the collapse load, namely one-dimensional beam analysis and two-dimensional grillage analysis, which would then be compared to the quarter scale test collapse loads. Bending failure, shear/torsion failure, and bending/torsion failure where considered for determining the collapse load.

For the test slabs, loading was stopped when the total load on the slab was 645kN for the straight bridge, and 782.3kN for the curved bridge, with deflections of 89mm and 177.8mm respectively. In both models, the failure was initiated by the formation of plastic hinges at the centre support, and collapse occurred with the formation of a second hinge at the maximum sagging moment location at 0.4 of the span length.

For the one dimensional analysis, the voided slab was idealised as a beam with equivalent bending and torsional stiffness determined from the uncracked cross-section and ignoring the contribution of the reinforcement. For the straight deck, the predicted collapse load was calculated to be 808kN for a bending failure mode. For the curved model, which was idealised as a number of straight elements, the predicted collapse load was calculated to be 807kN for a bending failure mode.

The grillage model of the straight bridge consisted of 9 longitudinal and 18 transverse members, and the curved bridge consisted of 7 longitudinal and 29 transverse members. For the straight bridge, the predicted collapse load was calculated to be 781kN for a bending failure mode. For the curved model, which was idealised as a number of straight elements, the predicted collapse load was calculated to be 700kN for a bending failure mode.

The failure load predicted by one-dimensional beam analysis was found to be somewhat greater than the observed failure loads from tests. Sen *et al.* (1993) concluded that an estimate of the failure load may be obtained by reducing the calculated value from beam analysis by 10%. The failure loads were accurately predicted by two-dimensional grillage analysis. The grillage analysis was found to provide a lower estimate of the collapse load than from the one-dimensional analysis as the latter tends to overestimate the stiffness of the deck by providing continuous support across the width. Sen *et al.* (1993) concluded that a grillage analysis is preferred to a one dimensional beam analysis for predicting the ultimate limit state behaviour of voided slab bridge decks.

Jofriet *et al.* (1973)

Jofriet *et al.* (1973) conducted a study to determine the extent to which a simple two-dimensional bending and plane stress finite element analysis could be used to model a post-tensioned, voided bridge slab. The two-dimensional model in question was based on the orthotropic plate theory. In order to perform the study, two-dimensional finite element model results were compared to those of an experimental 1:36 scale Plexiglass model of a voided slab bridge.

The bridge deck used for the study was 50ft (15.2m) wide, and consisted of a centre span of 148ft (45.1m) and two back spans of 118ft (36.0m). The deck thickness was 52in (1321mm) with void diameters of 41in (1041.4mm) resulting in a void diameter ratio of 0.79. The voids extended to 5ft (1.5m) from the centerlines of each support to allow for solid sections over the supports. The deck was prestressed using eight sets of four post-tensioning cables arranged in the webs between the voids.

The finite element model made use of Clough-Felippa general quadrilateral compatible displacement elements with five nodes and three degrees of freedom. As the governing equations of the element type apply to a solid homogenous slab, Jofriet *et al.* (1973) proposed the following equation to relate the stress-strain of the voided slab to an equivalent orthotropic solid slab:

$$\begin{pmatrix} \sigma_x \\ \sigma_y \\ \tau_{xy} \end{pmatrix} = \begin{pmatrix} D_{11} & D_{12} & 0 \\ D_{21} & D_{22} & 0 \\ 0 & 0 & D_{33} \end{pmatrix} \begin{pmatrix} \varepsilon_x \\ \varepsilon_y \\ \lambda_{xy} \end{pmatrix} \tag{2.31}$$

The above equation reduces the elastic moduli in the x and y directions, where the amount of reduction is proportional to the reduction in cross-sectional area and moment of inertia for plane stress analysis and bending analysis respectively. Jofriet *et al.* (1973) proposed the following reduction factors for plane stress analysis to be used in the above equation:

$$D_{11} = \frac{E}{1-\nu^2}\frac{A_x}{A} \qquad D_{22} = \frac{E}{1-\nu^2}\frac{A_y}{A} \qquad D_{12} = D_{21} = \nu\sqrt{D_{11}\,D_{22}} \qquad D_{33} = \frac{1-\nu}{2}\sqrt{D_{11}\,D_{22}} \quad (2.32)$$

Where A is the cross-sectional area of the solid slab, A_x is the reduced area in the x direction of the voided slab, and A_y is the reduced area in the y direction of the voided slab. Similar factors can be used for bending analysis where I, I_x, and I_y replace A, A_x, and A_y respectively. As these equations allow for the stress and strains in the equivalent orthotropic plate to be determined, an equation to relate the stresses in the voided slab is required. Jofriet *et al.* (1973) proposed the following equation to obtain the stresses in the voided slab from the equivalent orthotropic results:

$$\{\sigma\} = [C]\,[F]\,[C]^{-1}\,\{\sigma'\} \quad (2.33)$$

Where σ and σ' are the stresses in the voided and equivalent solid slab respectively, C is the stress transformation matrix, and F is given by the following matrix for plane stress analysis:

$$[F] = \begin{bmatrix} A/A_x & 0 & 0 \\ 0 & A/A_y & 0 \\ 0 & 0 & A/\sqrt{A_x A_y} \end{bmatrix} \quad (2.34)$$

A similar equation can be used for bending analysis where I, I_x, and I_y replace A, A_x, and A_y respectively. A_y and I_y are simple to calculate as the voids are constant along the length of the deck, and can be calculated per unit width. In the transverse direction, an approximate value needs to be obtained as the area is not constant across the voids. Jofriet *et al.* (1973) proposed that A_x should be 60% of A_y. This assumption is based on plane strain finite analysis results of a solid and voided beam. I_x can be assumed to be equal to I_y, which is based on a study of voided beams and square slabs by Aster (1968).

Another error that can lead to inaccuracies using this methodology is the assumption that the neutral axis of the voided slab is flat and lies at mid-depth. The flexural rigidity of regions where the neutral surface is not at mid-depth is underestimated by this mid-plane assumption. This will result in an underestimation of the stiffness and an overestimation of the longitudinal stresses and deflections. The solution to this problem is to either assume a more realistic neutral axis location based on experience or experiment, or to use a neutral axis location that lies between mid-depth and that obtained by beam theory (Jofriet *et al.*, 1973). In the second method, stress results may be bracketed by the values obtained from the two neutral axis positions. A comparison of experimental results, and numerical results based on mid-depth neutral axis and an adjusted neutral axis found that the adjusted mid-depth results were closer to the experimental results. However, the average difference between the two sets of results was 10%, with the mid-depth results yielding more conservative results.

The results from the study indicated good agreement between numerical and experimental results for longitudinal stresses in the centre region of the bridge. The numerical stress results for the two different neutral axis positions were found to diverge at the edge of the slab in the transverse direction,

however in most cases the experimental results were found to lie between the numerical results. The reason for the divergence is due to the effect of the side cantilevers on the neutral axis. From these results, Jofriet *et al.* (1973) concluded that using a neutral axis midway between the mid-depth and beam theory neutral axis would be a good assumption. Comparisons between the numerical and experimental results for the transverse stresses were also found to be in good agreement. The research concluded that a two-dimensional finite element model using orthotropic plate elements is sufficiently accurate for predicting stresses in prestressed voided slab bridges.

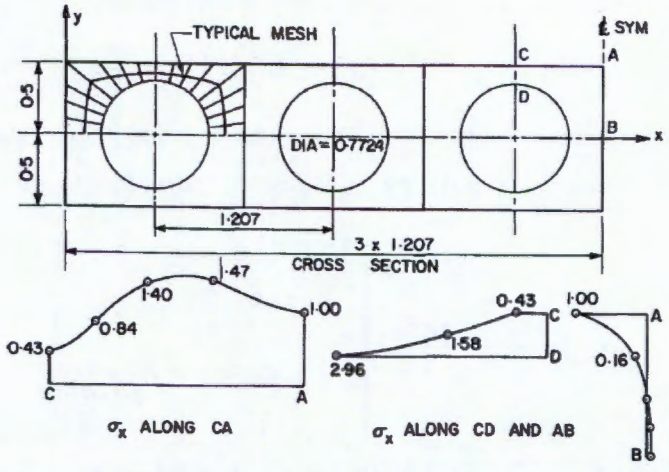

Figure 2.32 - Model for transverse effective area study and resulting stress variations in a voided slab cross-section (Jofriet *et al.*, 1973).

In addition, Jofriet *et al.* (1973) performed an investigation into the stress variations in the cross-section of the bridge resulting from the effect of the voids. From the results, it was found that the voids have a considerable stress raising effect, where the maximum stress occurring directly above the voids was almost three times greater than the average stress in the centre of the web. The stress distribution is shown in Figure 2.32. This is an indication of local moments in the top flange due to Vierendeel truss behaviour. It is evident that a three-dimensional analysis would be extremely valuable to analysis the distribution of the stress raising effect of the voids (Jofriet *et al.*, 1973).

Elliot & Clarke (1982)

Elliot & Clarke (1982) performed a study in order to determine the longitudinal and transverse bending stiffness rigidities of voided slab bridge decks modelled as solid orthotropic plates. The stiffness's were derived from the finite element analyses of cross-sections of voided slabs, with voids symmetrical with respect to the slab mid-depth. The finite element analysis assumed uncracked and linear elastic concrete and ignored the stiffness contributions of the reinforcement. The results of the FEA were compared with experimental stiffness's obtained from tests on epoxy resin models of voided slabs having different void sizes and spacing.

Both the tests and the analyses were based on plate bending theory formulation where the stiffness's were obtained by the imposition of only one constant bending moment in either the

longitudinal or transverse direction at a time. The determination of the parameters was carried out by using a two-dimensional plane strain finite element analysis of the cross-section of a voided slab. Degrees of freedom were chosen to allow for a linear variation of strain parallel to the voids with respect to the depth of the deck. Boundary conditions were also employed which allowed for only a quarter of a single cell between two webs of the voided cross-section to be modelled.

The flexural rigidity in the direction of the voids was determined using the moment of inertia and the elastic modulus, calculated in the conventional manner by subtracting the voided regions from that of a solid slab. The flexural rigidity perpendicular to the voids was calculated using the FEA of a quarter of a cell of the voided slab by applying a unit curvature. One solid and three voided epoxy resin slabs were tested in order to compare the experimental results with those from the theoretical approaches. The voided slabs had void diameter to slab thickness ratios ranging from 0.47 to 0.81 and void spacing ratios of 0.75 to 1.09. A moment was applied to the slabs in directions parallel and perpendicular to the voids in order to create the unit curvature.

From the results, Elliot & Clarke (1982) determine that the following rigidity factors could be used when using a solid orthotropic plate to idealise a voided slab:

$$D_x = \left[\frac{t^3}{12} - \frac{\pi d^4}{64}\right] \tag{2.35}$$

$$D_y = E\left[1 - \left(\frac{d}{t}\right)^4\right] \tag{2.36}$$

$$D_x = E\left[1 - 0.85\left(\frac{d}{t}\right)^4\right] \tag{2.37}$$

The rigidity factors were found to be dependent on the void diameter to thickness ratio. The void spacing was found to have little effect on the rigidities, and therefore do not feature in the equations. Elliot & Clarke (1982) also stated that the factors should only be used for voided slabs with void diameter to thickness ratios of less than 0.81.

The research concluded that in terms of design, a voided slab can be considered to behave essentially like a solid slab, however this result is dependent on the void diameter ratio. Elliot & Clarke (1982) also noted that the analysis did not account for transverse shear and the associated deformations. When a voided slab is used in a practical situation such as a bridge, the loading will induce shear forces, resulting in shear deformation. These deformations can be insignificant in a direction parallel to the voids, but could be significant in a direction perpendicular to the voids. Elliot & Clarke (1982) proposed that a shear stiff thin plate can be used to account for these effects.

Donohoe & Keogh (2000)

Donohoe & Keogh (2000) conducted a study to compare results of a two-dimensional finite element analysis using a solid plate consisting of isotropic and orthotropic elements for the idealisation of voided bridge deck slabs. Slabs with varying void to thickness ratios were used, which were then compared to results from identical slabs analysed using three-dimensional finite element models. The orthotropic elements were defined using orthotropic plate theory, and the equivalent plate parameters suggested by

Elliot & Clarke (1982). The scope of the research was to determine the applicability of using isotropic and orthotropic elements for the determination of transverse moments and stresses of voided slabs with increasing orthotropic behaviour.

For the two-dimensional plate models, the longitudinal rigidity was calculated using a slab depth based on the moment of inertia of the voided slab being represented, and the modulus of elasticity defined the equivalent plate parameter. The transverse rigidity was made equal to the longitudinal rigidity in the isotropic models and was calculated using the equivalent plate parameter proposed by Elliot & Clarke (1982) for the orthotropic models.

The voided slab modelled consisted of a cross-section with a width of 10m and a void spacing of 1.0m. Single spans as well as two span continuous bridges were considered, with spans of 24m in both cases. A range of void diameter to slab depth ratios were considered, namely 0.6, 0.65, 0.7, and 0.75. The minimum void ratio of 0.6 was considered as it signifies the expected change from isotropic to orthotropic behaviour suggested by Hambly (1991). The centre support for the two span bridge consisted of two bearings situated 3m from the deck edge in order to generate high transverse moments at this location. A uniformly distributed load of $8kN/m^2$ was used in all of the models.

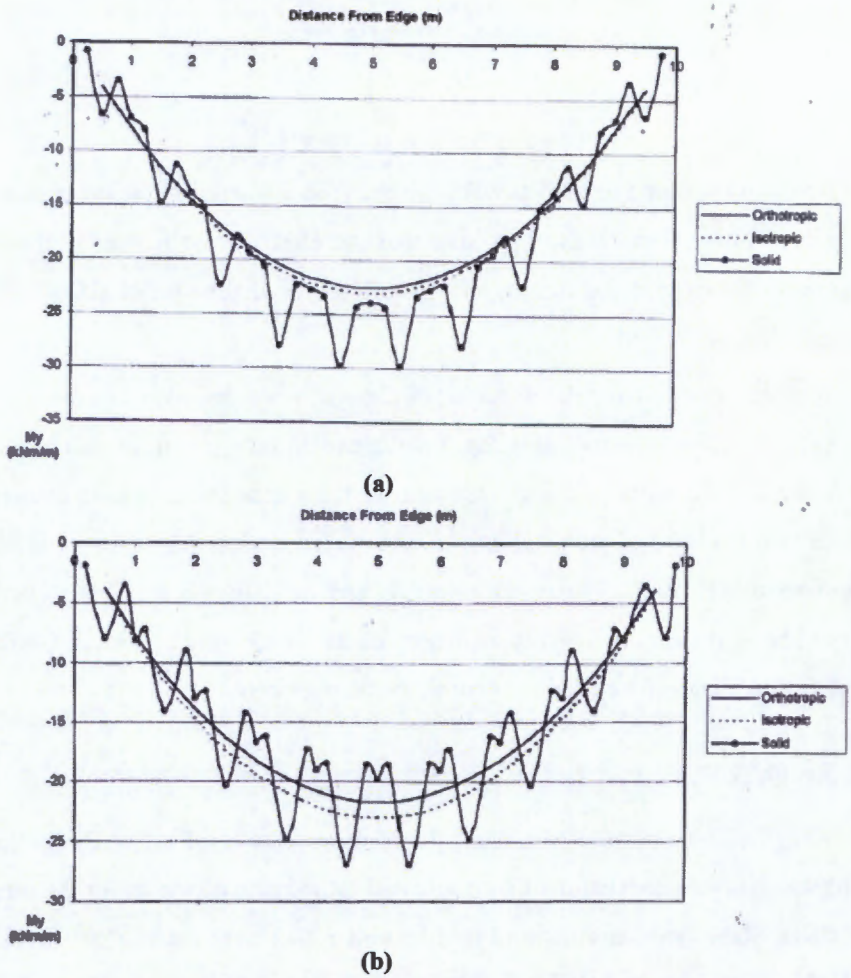

Figure 2.33 - Transverse moments per unit breadth at mid-span of the single span bridge for (a) 0.6 void diameter ratio (b) 0.75 void diameter ratio (Donohoe & Keogh, 2000).

Figure 2.33 shows the transverse moments at mid-span for the single span bridge for the two-dimensional orthotropic and isotropic models, and the three-dimensional solid element model with 0.6 and 0.75 void diameter ratios. The intermediate results for 0.65 and 0.7 void diameter ratio models are not shown as they lie between the other two results. The results show that the three-dimensional solid element model has several peaks which coincide with the centre of the voids, while the isotropic and orthotropic elements average out the moments across the width of the slab. These peaks in the moments indicate local bending in the flanges above the voids, which cannot be predicted using a simplified two-dimensional model. In a two-dimensional model, the effect of the voids is averaged or smeared across the width of the bridge and particular points, such as between or above the voids, are not specifically modelled. It can also be seen that there is very little difference between the isotropic and orthotropic results for the 0.6 void ratio models. This is consistent with the assumption by Hambly (1991). The difference between the isotropic and orthotropic two models is more pronounced in the 0.75 model, suggesting increasing orthotropic behaviour.

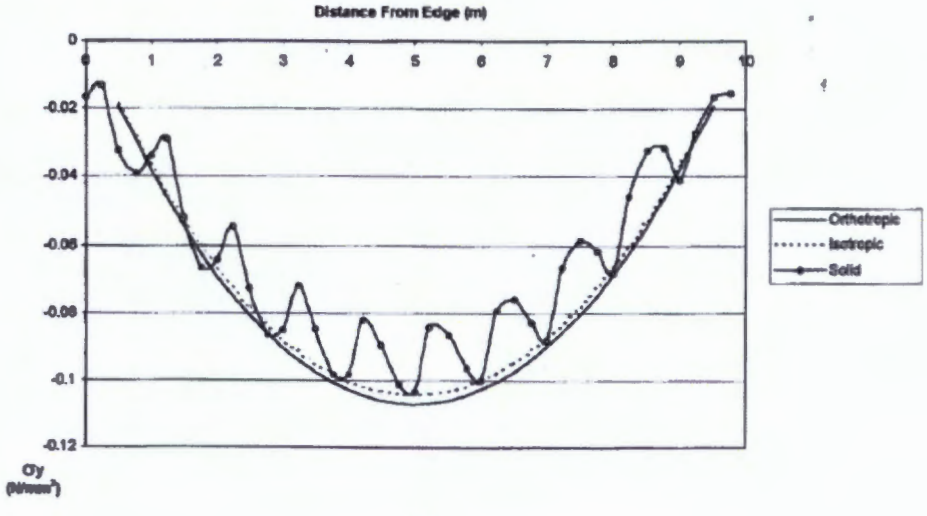

(a)

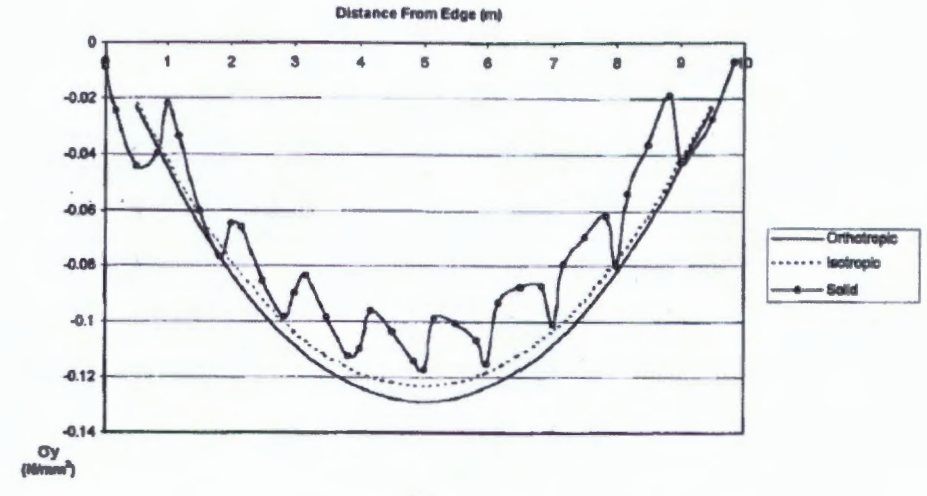

(b)

Figure 2.34 - Transverse stresses per unit breadth at mid-span of the single span bridge for (a) 0.6 void diameter ratio (b) 0.75 void diameter ratio (Donohoe & Keogh, 2000).

Figure 2.34 shows the transverse stresses at the top of the slab for the three models in Figure 2.33. It was noted that the stress at the centre of the voids decreased in the three-dimensional solid element model, despite having an increased moment. This was considered to be due to the fact that the stresses do not reduce through the depth of the deck to the same extent as it does in the two-dimensional idealisation.

Figure 2.35 shows the transverse stresses on the top of the deck at the centre support for the two span bridge for the two-dimensional orthotropic and isotropic models, and the three-dimensional solid element model with 0.6 and 0.75 void diameter ratios. It is evident from the results that the three-dimensional model predicts a higher peak stress at points along the cross-section than the isotropic or orthotropic model due to the local bending above the voids. The orthotropic model predicts a slightly higher peak stress than the isotropic model with a 0.75 void ratio and is therefore in better agreement with the three-dimensional model. This indicates an inaccuracy in the isotropic elements with increasing void ratio.

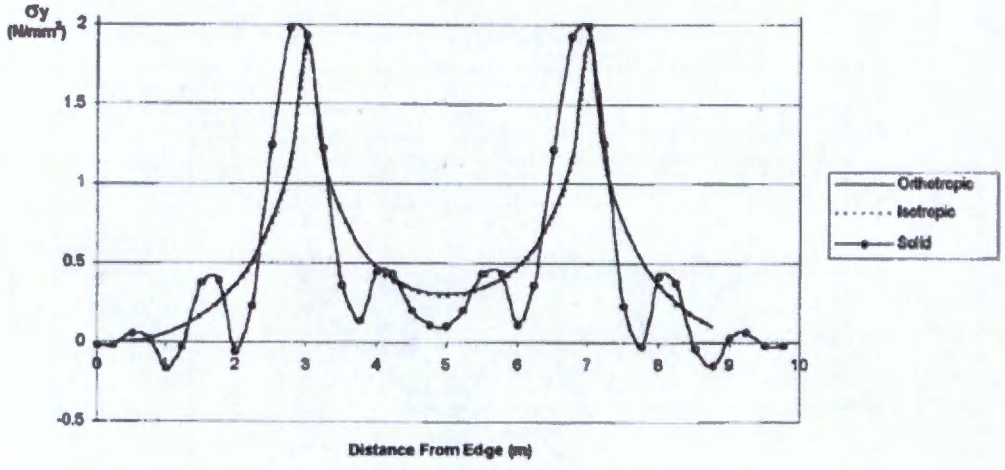

(a)

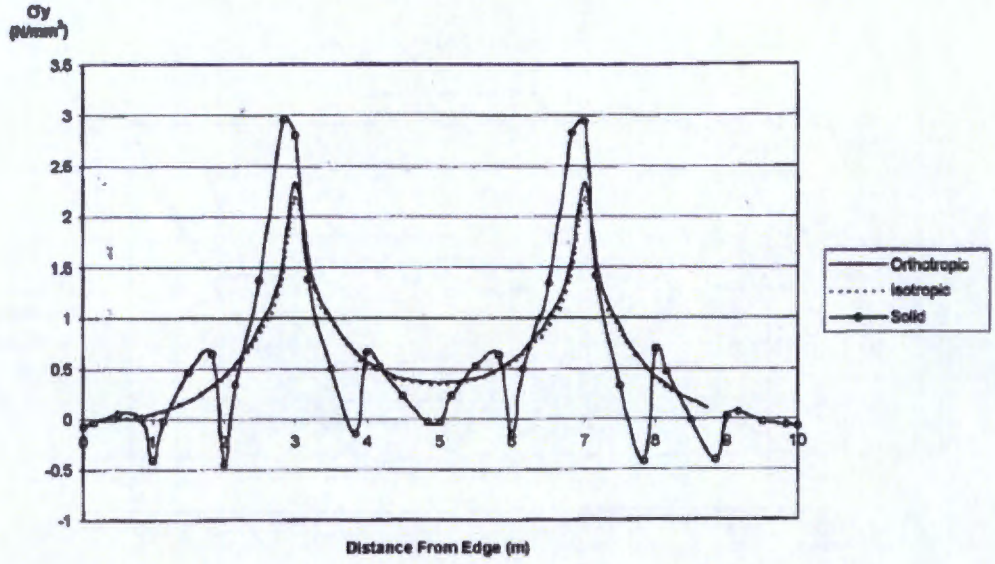

(b)

Figure 2.35 - Transverse stresses per unit breadth at the centre support of the two span bridge for (a) 0.6 void diameter ratio (b) 0.75 void diameter ratio (Donohoe & Keogh, 2000).

Donohoe & Keogh (2000) also performed an analysis in order to compare the results obtained by defining the transverse stiffness based on the transverse cross-sectional area at the centre of a void, and at the centre of a web. These two results should provide an upper and lower bound solution respectively as they represent the minimum and maximum cross-sectional area respectively. Figure 2.36 shows the transverse stresses at the top of the slab at mid-span for these two models, as well as the results from the three-dimensional solid model. It can be seen that the stresses from the three-dimensional model lies within the results for the other two models for most of the deck, which is an expected result. The localised decrease of stress above the voids does not fall within these limits. This indicates that the lower bound solution still does not account for the local moments above the voids, and alternative methods of analysis need to be used.

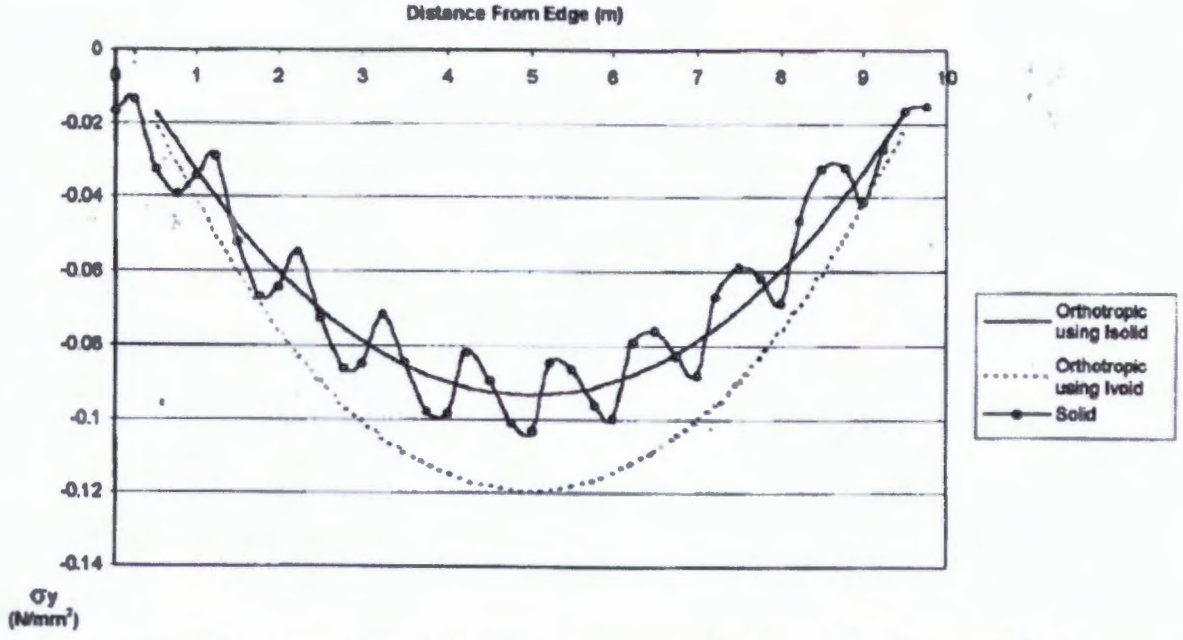

Figure 2.36 - Transverse stresses per unit breadth at mid-span of the single span bridge for different values of I_y (Donohoe & Keogh, 2000).

Donohoe & Keogh (2000) concluded by stating that isotropic elements are suitable for a void diameter ratio of less than 0.6. For greater void diameters, orthotropic elements are more suitable, however they are still unable to account for the local stresses and moments in the flanges above the voids. A three-dimensional analysis should be used for critical designs where the transverse moments or stresses above the voids are of a particular concern.

Clarke & Thorogood (1994)

In order to verify the formation of shear and flexure cracking of voided slabs with various shear reinforcement arrangements, Clarke & Thorogood (1994) tested ten transverse strips of voided slabs using a two point loading system. The details for the transverse strips specimens are shown in Figure 2.37 below. The left hand span was left solid to ensure failure occurred in the right hand section, allowing only one section to be instrumented.

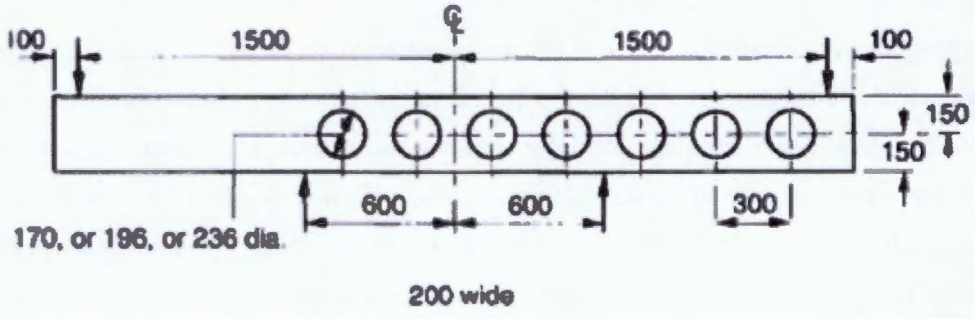

Figure 2.37 - Dimensions of transverse strip test specimens (Clarke & Thorogood, 1994).

Each transverse strip was tested with the reinforcement details provided in Table 2.4. In addition short lengths of bars were provided to represent the longitudinal reinforcement in the slab.

Table 2.4- Reinforcement details for the transverse strip specimens (Clarke & Thorogood, 1994).

Strip	Void dia. (mm)	Reinforcement		
		Top*	Bottom*	Web links
TS1	196	5T5	5T5	5R6
TS2	196	5T5	5T5	5R6
TS3	196	3T5	3T5	2R3
TS4	196	8T5	8T5	3T2.5
TS5	236	5T5	5T5	-
TS6	170	5T5	5T5	-
TS7	196	5T5	5T5	-
TS8	196	10T5	10T5	4T2.5
TS9	236	5T5	5T5	5T2.5
TS10	170	5T7	5T7	3T2.5

Strip TS1 and TS2 were identical, except that TS2 was loaded over the voids rather than the webs. TS3 was designed to investigate whether the occurrence of diagonal cracks, initiating from the inside of a void, would cause immediate failure. Strip TS4 was intended to investigate whether two layers of flange reinforcement would raise the shear capacity above that at which shear cracking would occur. In each flange, five of the eight main bars were in the outer layer and three in the inner layer. Vertical web reinforcement was designed to resist the shear force at which the inner layer of flange reinforcement was predicted to yield. TS5 and TS6 had varying void diameters and no web reinforcement. The remaining strips consisted of a variety of the reinforcement from the other strips in order to test the failure mechanisms.

The results showed that extreme fibre strains occurred over the voids on the tension face, and strains on the compressive face were generally small at all load stages. Strains were also found to be negligible prior to diagonal cracking, but increased rapidly after diagonal cracking in the web, irrespective of the reinforcement. Clarke & Thorogood (1994) suggested there is a need either to prevent diagonal cracking at the serviceability limit state or to control it by providing inclined web reinforcement.

The loads at which cracking occurred at various locations are given in Table 2.5. The shear forces at which diagonal cracks were first observed in each strip were found to be greater than those calculated using a standard shear failure mechanism for a solid slab. It is believed that this is due to the conservative assumption in the calculation method that all of the shear is resisted by the compression flange, whereas some shear is actually resisted by the tension flange. Clarke & Thorogood (1994) also emphasised that, for voided strips with web reinforcement, the diagonal shear cracks did not cause immediate failure. Thus, it is suggested that control of diagonal shear cracking should be considered in terms of the serviceability limit state and not at the ultimate limit state.

Table 2.5 - Summary of loading resulting in transverse shear cracking (Clarke & Thorogood, 1994).

Strip	Cube strength (N/mm^2)	Flex. cracking load (kN)	Other cracks		Failure load (kN)		Test Calc	Failure mode +	
			Load (kN)	Location *	Test	Calc.		Test	Predicted
TS1	35.5	5.8	9.0 10.0	C T	20.0	18.9	1.06	T	F
TS2	39.9	7.5	12.0 16.0	C,T W	26.2	23.0	1.14	F	F
TS3	42.1	6.1	6.3 6.9 9.0	T C W	12.4	7.6	1.63	F	L
TS4	40.9	7.5	14.0	C,T	21.0	17.9	1.24	L	L
TS5	28.4	4.0	5.5	C,T,W	6.2	4.9	1.27	H	H
TS6	25.2	7.0	11.0 13.0	C T	18.7	8.2	2.28	S	H
TS7	27.1	6.0	10.0	C,T,W	13.8	11.7	1.18	H	H
TS8	38.5	7.5	16.0	C,T,W	27.5	22.6	1.22	L	L
TS9	38.4	3.5	7.0	C,T	14.2	16.5	0.86	L	L
TS10	34.9	7.0	14.0 16.0 18.0	T W C	30.7	22.6	1.36	L	L

* C: compression flange
T: tension flange
W: web

\+ T: combined global bending and Vierendeel bending of tension flange
F: flexure
L: horizontal crack causing yield of links
H: horizontal crack
S: conventional solid beam shear

Three strips failed in flexural modes and the other seven failed in shear modes as shown in Table 2.5. Of the three flexural failures, two (TS2 and TS3) were pure flexural failures within the constant moment zone, and the third (TS1) was a local failure of the tension flange due to combined global and Vierendeel bending. With the exception of TS6, the shear failures were all initiated by the formation of horizontal cracks in the webs. Diagonal cracking did not result in immediate failure. Hence, it is necessary to control the diagonal cracks at the serviceability limit state, rather than consider their formation as a criterion of failure at the ultimate limit state. However, from ultimate limit state considerations, web reinforcement needs to be provided in order to prevent failure due to the formation of horizontal cracks.

The exception to this behaviour was strip TS6, which had the smallest void ratio (0.567) and no web reinforcement. This strip failed suddenly in a conventional solid beam shear manner. However, strip TS10, which also had a void ratio of 0.567 but had two layers of flange reinforcement, failed by the formation of horizontal cracks.

Clarke & Thorogood (1994) concluded that the tests indicated that diagonal web cracks do not initiate failure, but these cracks do widen rapidly with an increase in load, and they need to be controlled by web reinforcement. The shear behaviour of voided slabs is also similar to a solid slab for low void diameter ratios.

2.4. Examples of BubbleDeck Slab Analysis

As the structural behaviour of voided slab bridge decks and BubbleDeck slabs are both dictated by the ratio of the void diameter to the thickness of the slab, examples of the methods of analysis employed for BubbleDeck slabs will also be considered.

Ibrahim *et al.* (2012)

Ibrahim *et al.* (2012) conducted an experiment in order to determine the influence of the ratio of void diameter to slab thickness on the flexural behaviour on biaxial BubbleDeck slabs. Six slabs were tested comprising two conventional solid slabs and four BubbleDeck slabs with varying void diameter to slab thickness ratios. The properties of the slabs are listed in Table 2.6 below.

Table 2.6 - Properties of slab specimens used to determine the influence of the void diameter to slab thickness ratio on structural behaviour of BubbleDeck slabs (Ibrahim et al., 2012).

No.	Specimen name	Length (mm)	Width (mm)	Slab thickness H (mm)	Bubble diameter B (mm)	B/H	No. of plastic spheres	f'_c (MPa)	ρ (%)
1	SD2	1000	1000	100	--	-	--	33.13	0.443
2	BD2-bu 64				64	0.64	144	34.66	
3	BD2-bu 80				80	0.80	100	33.34	
4	SD3			125	--	--	--	32.14	0.285
5	BD3-bu 64				64	0.51	144	34.66	
6	BD3-bu100				100	0.80	64	33.34	

The slabs were simply supported at all edges using steel beams and were tested using a five-point load system in order to distribute the load and avoid punching shear failure. The load was increased in increments of 10kN and deflections and strains on the compressive side at mid-span were measured. The results of the experiment are summarised in Table 2.7.

Table 2.7 - Test results for the BubbleDeck slab specimens including ultimate load, maximum deflection and strains (Ibrahim *et al.*, 2012).

Slab name	Weight (kg)	% Decrease in Weight	Pu (kN) Ultimate Load	$\Delta_{0.7Pu}$ (mm)	% Increase in $\Delta_{0.7Pu}$	Δ_u(mm) Ultimate Deflection	$\frac{Pu}{Pu\ solid}$ %
SD2	253	---	552	9.8	---	25.4	100
BD2-bu64	190	25	550	11.5	17	27.0	100
BD2-bu80	179	29	491	12.5	28	24.3	89
SD3	314	---	707	9.1	---	21.1	100
BD3-bu64	240	24	704	10.3	13	23.0	100
BD3-bu100	221	30	634	12	32	20.5	90

From the results, it can be seen that the slabs with the void diameter to slab thickness ratio of 0.51 and 0.64 had a negligible difference in ultimate load when compared to the solid slabs, with a decrease in weight of 24% and 25% as a result of the voids. The slabs with a void diameter ratio of 0.8 showed a lower ultimate load than the solid slabs by around 10%. Figure 2.38 shows the load versus displacement for the slab specimens.

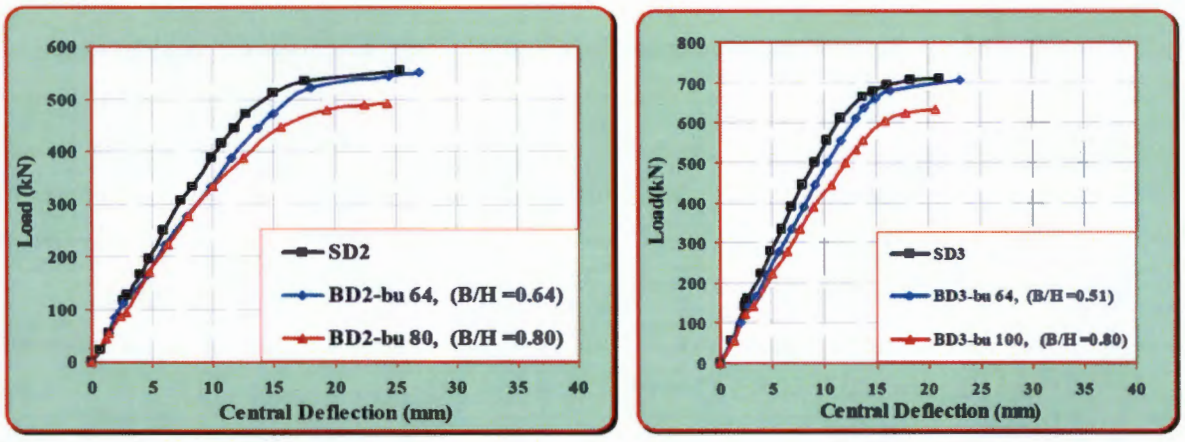

(a) (b)

Figure 2.38 - Load versus deflection relationship for (a) 100mm slab and (b) 125mm slab (Ibrahim et al., 2012).

From the graphs, it can be seen that the deflection under service load of the BubbleDeck specimens were higher than those of an equivalent depth solid slab. These differences between the two deflections become more pronounced after flexural cracking and yielding of reinforcement has occurred. Figure 2.39 shows the load versus maximum compressive strain for the slab specimens. The BubbleDeck slabs also show an increase in the maximum concrete compressive strain under service load over those of an equivalent depth solid slab, which is due to the reduced concrete volume in the compression zone. All specimens displayed diagonal flexural crack patterns initiating from mid-span and moving towards the slab corners. The BubbleDeck slabs with 0.8 void diameter to slab thickness ratio also displayed small longitudinal cracks. This may be due to the relatively thin slab thickness in the bottom slab under the voids.

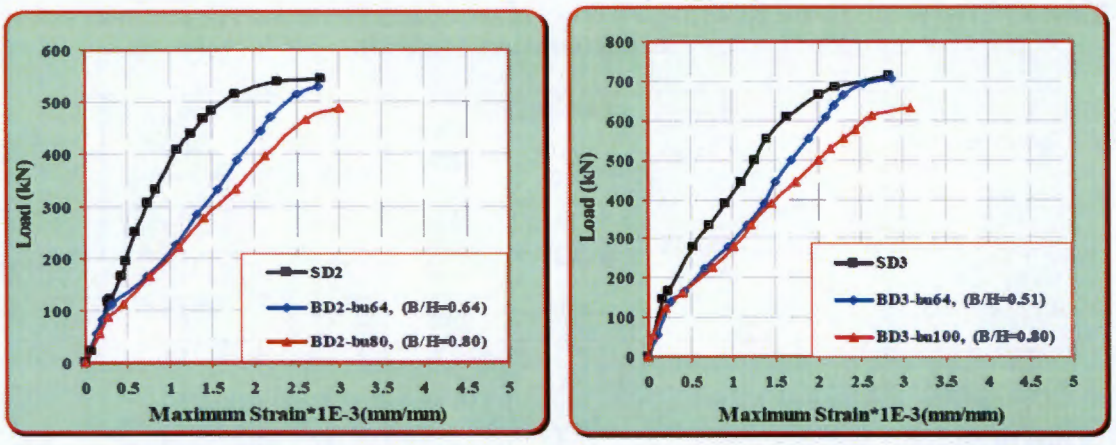

(a) (b)

Figure 2.39 - Load versus maximum concrete compressive strain relationship for (a) 100mm slab and (b) 125mm slab (Ibrahim et al., 2012).

In view of the results, Ibrahim *et al.* (2012) concluded that biaxial BubbleDeck slabs can be considered to act like conventional solid slabs in flexure and the effect of the voids on the flexural behaviour is dependent on the void diameter to slab thickness ratio.

Lai (2010)

Lai (2010) performed an analysis to compare the structural response of BubbleDeck slabs to solid slabs. Two finite element models were created of an office floor slab that was 120ft (36.6m) long, 120ft (36.6m) wide, and 17.75in (450mm) thick with 14.17in (360mm) voids. The slab was composed of nine bays, with each bay being 40ft (12.2m) by 40ft (12.2m), supported on four columns. Bubbles within three bubble diameters of the columns were removed and replaced with concrete for shear considerations. The solid slab was modelled as a thick shell of solid concrete while the BubbleDeck slab was modelled as a layered shell, with a rectangular layer of high density polyethylene sandwiched in between two thin layers of concrete. Both models were subjected to a 100-psf (4.8kN/m^2) live load in addition to their self-weight.

Table 2.8 below summarises the moments, shear forces, in-plane stresses, and deflections results for the BubbleDeck and solid slabs. The results show that the moments, shear forces and in-plane stresses are 30-40% less than those of the solid slab, which can be contributed to the decrease in dead load. The BubbleDeck slab showed a 10% increase in deflection, which is the result of the decrease in stiffness.

Table 2.8 - Comparison of structural response of BubbleDeck and solid slabs (Lai, 2010).

STATIC RESPONSE - OFFICE SLAB									
	M11	M22	M12	V13	V23	S11Top	S22Top	S12Top	U3
	(kNm/m)	(kNm/m)	(kNm/m)	(kN/m)	(kN/m)	MPa	MPa	MPa	mm
Solid Slab	-906.8	-906.9	-166.6	-2158.8	-2157.7	26.8	26.8	4.9	-18.9
BubbleDeck	-598.5	-598.6	99.5	1309.8	1309.8	17.7	17.7	3.5	-20.9
% Difference	-34%	-34%	-40%	-39%	-39%	-34%	-34%	-29%	-10%

Lai (2010) also performed an analysis to determine the application of BubbleDeck slabs for a light weight pedestrian bridge. The bridge used was 16ft (4.9m) wide and 200ft (61m) long. The depth of the slab was 9.25in (235mm) with 180mm diameter bubbles being used. The 200ft long deck was made up using 12.5 bays of slab that were 16ft (4.9m) long by 16ft (4.9m) wide, with each bay being simply supported on columns. A finite element model of the bridge was created in order to analyse the structural response. An identical solid slab model was also created for comparison. Both decks were loaded with a pedestrian live load of 100-psf (4.8kN/m^2) and analysed for static and dynamic response.

Table 2.9 below summarizes the moments, shear forces, in-plane stresses and deflections results for the BubbleDeck and solid slab. The maximum moment and internal stresses of the BubbleDeck were found to be 64% higher than the solid deck, while the maximum shear was approximately the same in both models. The deflection was 68% greater in the BubbleDeck slab than in the solid slab. Lai (2010) deduced that the decreased performance of the BubbleDeck slab was due to the continuity of the slab, which resulted in the slab acting more like a one-way spanning slab rather than a biaxial slab.

Table 2.9 - Comparison of structural response for BubbleDeck and Solid Slab for pedestrian bridge application (Lai, 2010).

STATIC RESPONSE - BRIDGE SLAB									
	M11	M22	M12	V13	V23	S11Top	S22Top	S12Top	U3
	(kNm/m)	(kNm/m)	(kNm/m)	(kN/m)	(kN/m)	MPa	MPa	MPa	mm
Solid Slab	23.3	-123.6	20.8	-1856.7	1857.4	-2.5	13.4	-2.3	-3.2
BubbleDeck	38.2	-143.8	24.2	-1863.3	1867.9	-4.2	15.6	-2.6	-5.3
% Difference	64%	16%	16%	0%	1%	64%	16%	16%	68%

Lai (2010) concluded that BubbleDeck technology is more efficient than a traditional biaxial concrete slab in an office floor system, where it acts in a similar manner to a solid biaxial slab. However, further studies are required to understand the behaviour of BubbleDeck technology in a bridge application.

2.5. Summary of the Structural Analysis of Voided Slabs

The structural behaviour and analysis of voided slab bridge decks has been the subject of extensive research in the past. This research has found that the structural behaviour of voided slabs is mainly influenced by the ratio of the void diameter to slab thickness, where the behaviour changes from biaxial solid slab behaviour to more like a cellular structure behaviour as the void ratio exceeds 60%.

With an increase in void diameter ratio, the voided slab starts to behave in a similar manner to a cellular structure. This behaviour is characterised by the deformable nature of the cross-section due to transverse shear, which results in the flanges and webs of the cross-section bending about their own neutral axes. This results in increased moments in the flanges, resulting in an increase in the transverse

stresses. Many authors have stressed that a form of analysis which can account for the effect of cellular distortion should be used for the analysis of voided slabs.

Past research has focused on modelling voided slabs using two-dimensional forms of analysis such as grillage models and solid orthotropic plate models, and three-dimensional finite element models. One-dimensional forms of analysis utilizing beam theory are rarely used for the analysis of voided slab bridges as they do not provide an appreciation of the actual two-dimensional plate behaviour and can lead to erroneous conclusions for the transverse distribution of longitudinal stresses, and the omission of transverse stresses.

Grillage models have been shown to be a simple yet accurate method for modelling voided slab bridges. The longitudinal stiffness can be calculated by subtracting the moment of inertia of the voided section from the solid section based on a mid-depth neutral axis. The transverse stiffness, which requires complex calculations to determine accurately, is simply assumed to be equal to the longitudinal stiffness, which was found to be an accurate assumption by Oline & Sen (1987). However, the accuracy of grillage models decreases for large void diameter ratios, as the analysis neglects the effects of cellular distortion. O'Brien & Keogh (1998) found grillage models to be inaccurate methods of analysis for decks consisting of wide transverse cantilevers, such as a twin spine voided decks. Inaccuracies were also found in grillage models subject to unsymmetrical loading, and their inability to predict local effects around point loads.

Two-dimensional finite element analysis using shell elements based on orthotropic plate theory has been shown to provide accurate results for the analysis of voided slabs. The method involves modelling the voided deck as a solid slab consisting of an anisotropic material which accounts for the effects of the voids. The effect of the voids on the longitudinal and transverse stiffness is considered by using equivalent plate parameters in the orthogonal directions. Several equivalent plate parameters have been proposed by various authors, with accurate results being obtained when compared to scale tests and three-dimensional finite element analysis results. These parameters reduce the rigidity of the slab in each direction, and are therefore considered to be able to predict the effects of cellular distortion. However, no conclusive study has been performed to compare the various plate parameters proposed by different authors in the past. Some authors also propose that factors are required to convert the stresses obtained in equivalent orthotropic plate models to the stresses in the actual voided slabs, while others mention no requirement of such parameters.

Three-dimensional finite element models made of solid elements, which are considered to give the most accurate idealization of the structural behaviour, are rarely used for the analysis of voided slab decks. This is because the high computational costs and the complexity of the model make three-dimensional finite element models unfeasible for everyday use. However three-dimensional finite element models can be useful to analysis the stress raising effects of the voids, to determine the effect of the varying neutral axis depth, and to analyse local moments in the flanges due to cellular distortion.

3. FINITE ELEMENT MODELLING OF VOIDED SLABS

The finite element method is a numerical procedure for the approximate solution of problems in continuum mechanics in which the actual structure is represented as an assemblage of finite elements interconnected at a finite number of nodal points (Abdelraouf & Matlock, 1972). The entire procedure of the finite element method involves subdividing the structure into an equivalent system of finite elements, choosing a suitable displacement function, deriving a stiffness matrix using the principles of mechanics, formulating a global stiffness matrix for the entire structure, solving the resulting differential equations to determine the displacements of the nodes, and computing the stresses and strains from the nodal displacements (Ryall, 2008).

In this study, the structural behaviour of voided slab bridge decks will be modelled using the finite element program ABAQUS Version 6.13, which is a general purpose finite element code developed by HKS. ABAQUS has a wide variety of tools that have been successfully used to attain solutions through the entire behavioural range of reinforced concrete, and will therefore be able to attain the outcomes required in this study.

A complete analysis using ABAQUS requires a detailed description of the model which includes the element type, material properties, boundary conditions, loading configuration, and type of analysis. This chapter provides an overview of the salient features required to create a finite element model of a voided slab bridge deck in ABAQUS.

3.1. Constituent Materials

The finite element method works well for many structural materials such as steel and aluminium, which have well-defined constitutive properties. For complex materials such as reinforced concrete, in which discrete cracking and yielding of steel reinforcement occurs, there are major factors that limit the capabilities of the finite element method (Chen *et al.*, 1993). When performing an analysis of reinforced concrete with finite elements, it is essential to understand the underlying theory of reinforced concrete behaviour.

When concrete is loaded in compression, it initially exhibits elastic response. As the stress is increased, the concrete exhibits plastic behaviour and the response becomes non-linear. The plastic behaviour is characterised by stress hardening followed by some non-recoverable inelastic straining resulting in the softening of the material response beyond the ultimate stress. If the load is removed at some point after inelastic straining has occurred, the unloading response is softer than the initial elastic response, and the elasticity has been reduced. Upon further loading the material loses strength until it can no longer carry any stress, and yielding of compression reinforcement and crushing of the concrete occurs, resulting in a brittle failure.

When a uniaxial concrete specimen is loaded in tension, it responds elastically until the cracking stress is exceeded, after which cracking occurs. The local effects of cracking result in a softening of the stress-strain response and a drastic decrease of stiffness, leading to the redistribution of forces and moments to stiffer regions (Engström, 2011). Upon further loading, tensile reinforcement if present will start to yield resulting in an increase in deformation and plastic redistribution until failure. The uniaxial behaviour of plain unreinforced concrete is shown in Figure 3.1.

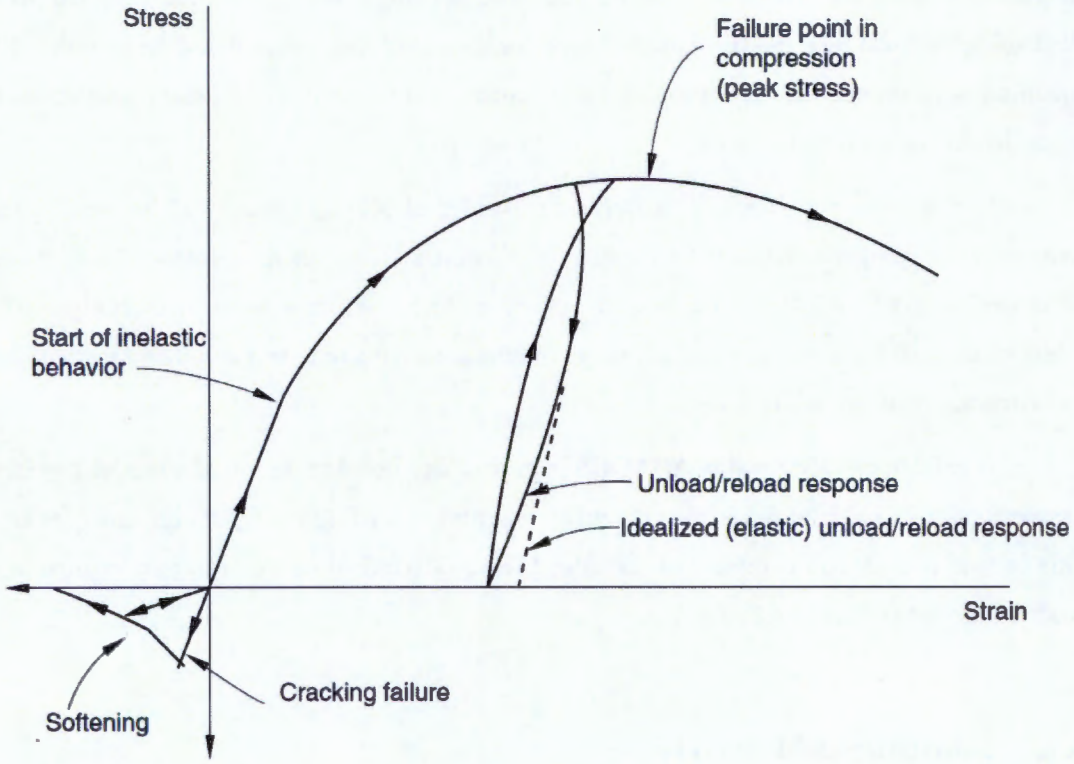

Figure 3.1 - Uniaxial behaviour of plain unreinforced concrete (ABAQUS, 2013)

ABAQUS has various models that can be used to model reinforced concrete behaviour which include the non-linear effects, the concrete and steel reinforcement bond interface as well as the effect of discrete concrete cracking. When modelling the behaviour of concrete, a decision must be made whether the full behaviour range of the concrete will be modelled, or whether only the linear range of the concrete will be considered. The linear range of an isotropic concrete material can be defined using two independent parameters, namely the elastic modulus and Poisson's ratio. For the full range of concrete behaviour, the non-linear response of the material has to be defined, making the preprocessing on the finite element model more complex as well as increasing the computational requirements.

3.1.1. Orthotropic Material Models

Linear orthotropic behaviour can be defined in ABAQUS using a number of different material models. The choice of the model employed depends on a number of factors, namely if plane stress conditions are required, the type of element used, and the parameters that are available in order to define the orthotropic response of the material. Some of the material models in ABAQUS that can be used to define an orthotropic material are discussed below:

Defining Orthotropic Elasticity using Engineering Constant

A linear elastic orthotropic material can most easily be defined in ABAQUS by inputting several engineering constants, which are used to define a three-dimensional orthotropic material, and is suitable for most element types in ABAQUS. The engineering constants consist of three elastic moduli, E_x, E_y, and E_z, three Poisson's ratios, v_{xy}, v_{xz}, and v_{zy}, and the three shear elastic moduli, G_{xy}, G_{zy}, and G_{zy}, which are associated with the materials principal directions. These moduli define the elastic compliance in accordance with the matrix in Figure 3.2

$$\begin{Bmatrix} \varepsilon_{11} \\ \varepsilon_{22} \\ \varepsilon_{33} \\ \gamma_{12} \\ \gamma_{13} \\ \gamma_{23} \end{Bmatrix} = \begin{bmatrix} 1/E_1 & -\nu_{21}/E_2 & -\nu_{31}/E_3 & 0 & 0 & 0 \\ -\nu_{12}/E_1 & 1/E_2 & -\nu_{32}/E_3 & 0 & 0 & 0 \\ -\nu_{13}/E_1 & -\nu_{23}/E_2 & 1/E_3 & 0 & 0 & 0 \\ 0 & 0 & 0 & 1/G_{12} & 0 & 0 \\ 0 & 0 & 0 & 0 & 1/G_{13} & 0 \\ 0 & 0 & 0 & 0 & 0 & 1/G_{23} \end{bmatrix} \begin{Bmatrix} \sigma_{11} \\ \sigma_{22} \\ \sigma_{33} \\ \sigma_{12} \\ \sigma_{13} \\ \sigma_{23} \end{Bmatrix}.$$

Figure 3.2 - Matrix to define orthotropic behaviour using engineering constant in ABAQUS (ABAQUS, 2007).

The quantity v_{xy} has the physical interpretation of the Poisson's ratio that characterises the transverse strain in the y direction, when the material is stressed in the x direction. In general, v_{xy} is not equal to v_{yx} in an orthotropic material, and are normally related by the following expression:

$$\frac{v_{xy}}{E_x} = \frac{v_{yx}}{E_y} \tag{3.1}$$

This method requires a total number of nine independent constants to be specified to define orthotropic behaviour. The degree of orthotropy depends on the relationship between the independent constants (ABAQUS, 2007).

Defining Transversely Isotropic Elasticity

A subclass of orthotropy is transverse isotropy, which can be used to characterise a plane of isotropy at every point in a material. Assuming the x-y plane to be the plane of isotropy at every point, transverse isotropy requires that $E_x = E_y = E_p$, $v_{zx} = v_{zy} = v_{tp}$, $v_{xz} = v_{yz} = v_{pt}$, and $G_{xz} = G_{yz} = G_t$, where p and t stand for in-plane and transverse to the isotropic plane respectively. The value that defines E_3, which is the

elastic modulus in the z direction, characterises the degree of orthotropy of the material. v_{tp} has the physical interpretation of the Poisson's ratio that characterises the strain in the plane of isotropy resulting from stress normal to it, v_{pt} characterises the transverse strain in the direction normal to the plane of isotropy resulting from stress in the plane of isotropy. The stress-strain laws can then be reduced to the stiffness matrix in Figure 3.3.

$$\begin{Bmatrix} \varepsilon_{11} \\ \varepsilon_{22} \\ \varepsilon_{33} \\ \gamma_{12} \\ \gamma_{13} \\ \gamma_{23} \end{Bmatrix} = \begin{bmatrix} 1/E_p & -\nu_p/E_p & -\nu_{tp}/E_t & 0 & 0 & 0 \\ -\nu_p/E_p & 1/E_p & -\nu_{tp}/E_t & 0 & 0 & 0 \\ -\nu_{pt}/E_p & -\nu_{pt}/E_p & 1/E_t & 0 & 0 & 0 \\ 0 & 0 & 0 & 1/G_p & 0 & 0 \\ 0 & 0 & 0 & 0 & 1/G_t & 0 \\ 0 & 0 & 0 & 0 & 0 & 1/G_t \end{bmatrix} \begin{Bmatrix} \sigma_{11} \\ \sigma_{22} \\ \sigma_{33} \\ \sigma_{12} \\ \sigma_{13} \\ \sigma_{23} \end{Bmatrix}$$

Figure 3.3 - Matrix to define orthotropic behaviour using transversely isotropic elasticity in ABAQUS (ABAQUS, 2007).

The following expression can also be used to reduce the number of terms required to define the stiffness matrix:

$$G_p = \frac{E_p}{2(1+v_p)} \tag{3.2}$$

This method means that only a total number of five independent constants need to be specified to define orthotropic behaviour. This model is also suitable for three-dimensional stress strain analyses, and can be used with most element types (ABAQUS, 2007).

Defining Orthotropic Elasticity in Plane Stress Conditions

Under plane stress conditions, only the values of E_x, E_y, v_{xy}, G_{xy}, G_{yz}, and G_{xz} are required to define an orthotropic material. The shear moduli G_{xz} and G_{yz} are included because they may be required for modelling transverse shear deformation in shell elements. If shear deformations are not required, the stress-strain relations for the in-plane components are in the form of the matrix in Figure 3.4.

$$\begin{Bmatrix} \varepsilon_1 \\ \varepsilon_2 \\ \gamma_{12} \end{Bmatrix} = \begin{bmatrix} 1/E_1 & -\nu_{12}/E_1 & 0 \\ -\nu_{12}/E_1 & 1/E_2 & 0 \\ 0 & 0 & 1/G_{12} \end{bmatrix} \begin{Bmatrix} \sigma_{11} \\ \sigma_{22} \\ \tau_{12} \end{Bmatrix}$$

Figure 3.4 - Matrix to define orthotropic behaviour for plane stress conditions in ABAQUS (ABAQUS, 2007).

Using this method, only four independent constants need to be defined for orthotropic behaviour if shear deformations are not required. This model cannot be used for three-dimensional analysis, and is usually employed for two-dimensional shell element analyses (ABAQUS, 2007).

Defining Orthotropic Elasticity using an Elastic Stiffness Matrix

Linear elasticity in an orthotropic material can also be defined by giving the nine independent elastic stiffness parameters. This model allows for two orthogonal symmetric planes with elastic properties. In this case, the stress-strain relations are of the form of the matrix in Figure 3.5.

$$\begin{Bmatrix} \sigma_{11} \\ \sigma_{22} \\ \sigma_{33} \\ \sigma_{12} \\ \sigma_{13} \\ \sigma_{23} \end{Bmatrix} = \begin{bmatrix} D_{1111} & D_{1122} & D_{1133} & 0 & 0 & 0 \\ & D_{2222} & D_{2233} & 0 & 0 & 0 \\ & & D_{3333} & 0 & 0 & 0 \\ & & & D_{1212} & 0 & 0 \\ & sym & & & D_{1313} & 0 \\ & & & & & D_{2323} \end{bmatrix} \begin{Bmatrix} \varepsilon_{11} \\ \varepsilon_{22} \\ \varepsilon_{33} \\ \gamma_{12} \\ \gamma_{13} \\ \gamma_{23} \end{Bmatrix} = [D^{el}] \begin{Bmatrix} \varepsilon_{11} \\ \varepsilon_{22} \\ \varepsilon_{33} \\ \gamma_{12} \\ \gamma_{13} \\ \gamma_{23} \end{Bmatrix}$$

Figure 3.5 - Matrix to define orthotropic behaviour using the elastic stiffness matrix in ABAQUS (ABAQUS, 2007).

In Figure 3.5, the flexural rigidities are defined as functions of the elastic moduli and Poisson's ratio in the relevant directions. This model requires the nine independent flexural rigidity constants to be defined (ABAQUS, 2007).

Defining Fully Anisotropic Elasticity

For fully anisotropic elasticity, twenty one independent elastic stiffness parameters are required to be defined. The stress-strain relations are shown in the matrix in Figure 3.6.

$$\begin{Bmatrix} \sigma_{11} \\ \sigma_{22} \\ \sigma_{33} \\ \sigma_{12} \\ \sigma_{13} \\ \sigma_{23} \end{Bmatrix} = \begin{bmatrix} D_{1111} & D_{1122} & D_{1133} & D_{1112} & D_{1113} & D_{1123} \\ & D_{2222} & D_{2233} & D_{2212} & D_{2213} & D_{2223} \\ & & D_{3333} & D_{3312} & D_{3313} & D_{3323} \\ & & & D_{1212} & D_{1213} & D_{1223} \\ & sym & & & D_{1313} & D_{1323} \\ & & & & & D_{2323} \end{bmatrix} \begin{Bmatrix} \varepsilon_{11} \\ \varepsilon_{22} \\ \varepsilon_{33} \\ \gamma_{12} \\ \gamma_{13} \\ \gamma_{23} \end{Bmatrix} = [D^{el}] \begin{Bmatrix} \varepsilon_{11} \\ \varepsilon_{22} \\ \varepsilon_{33} \\ \gamma_{12} \\ \gamma_{13} \\ \gamma_{23} \end{Bmatrix}.$$

Figure 3.6 - Matrix to define fully anisotropic elasticity in ABAQUS (ABAQUS, 2007).

The model is able to capture the changes in the preferred material directions with deformation, and therefore allows for multiple plains of orthotropy (ABAQUS, 2007).

3.2. Type of Analysis

ABAQUS provides numerous analysis procedures that can be used to solve finite element problems. Among these procedures, static stress analysis and dynamic stress analysis are the most common. In this study, a static stress/displacement analysis of a voided slab bridge deck will be considered. A static stress procedure is one in which inertia effects are neglected.

Static stress analysis procedures in ABAQUS are solved using either the direct linear equation solver or the iterative linear equation solver, which relies on convergence to obtain a solution. Many factors must be carefully weighed before deciding to use the iterative solver in ABAQUS/Standard, such as element type, contact and constraint equations, material and geometric non-linearity's, and material properties, all of which can impact robustness and performance of the analysis. The two static stress procedures available in ABAQUS that are relevant to this study are a static analysis and a quasi-static analysis.

A static stress procedure is used for stable problems in which inertia effects are neglected. The analysis can account for both linear and non-linear behaviour. It ignores time-dependant material effects, however rate-dependent plasticity can be included if necessary (ABAQUS, 2007).

A quasi-static analysis is used to define a procedure that occurs infinitely slowly, and is primarily interested in determining the final static response of a structure. These problems typically show monotonic strain behaviour, and inertia effects are introduced primarily to improve convergence behaviour. A quasi-static analysis is used to analyse the transient response of structures considering time-dependant material behaviour. Inertia effects are neglected, and both linear and non-linear behaviour can be considered (ABAQUS, 2007).

Although the analysis involved in this study will be static, there are dynamic procedures, in which inertia effects are considered, that are relevant to obtaining a static solution to unstable problems through improved convergence. These include implicit and explicit dynamic analysis.

Implicit dynamic analysis, using direct integration, can be used to study quasi-static responses in which considerable energy dissipation provides stability and improved convergence behaviour for determining an essentially static solution. Quasi-static applications in implicit dynamic applications are solved using the backward Euler operator. The time integration operators used are implicit, which means that the operator matrix must be inverted and a set of simultaneous non-linear dynamic equilibrium equations must be solved at each time increment. The principal advantage of these operators is that they are unconditionally stable for linear systems and there is no mathematical limit on the size of the time increment that can be used to integrate a linear system. This eliminates impractically small time steps that can occur in explicit methods, and therefore reduces the amount of computation required (ABAQUS, 2007).

In explicit dynamic analysis, which uses the central difference operator, the global stiffness matrices do not need to be formed and inverted for each time increment, and therefore each increment is relatively inexpensive compared to an implicit analysis. The size of the time increment is limited however as the central difference operator is not unconditionally stable. This method is computationally attractive for problems in which the total dynamic response time is only a few orders of magnitude longer than its stability limit, which is closely related to the time required for a stress wave to cross the smallest element in the model. However, the computer time involved in running a quasi-static analysis can be very large as the simulation cost is directly related to the number of increments. Many of the advantages of dynamic explicit procedures apply to slower quasi-static processes where mass scaling can be used to reduce wave speeds and therefore the computation time (ABAQUS, 2007).

All of the above procedures can be used to obtain the static solution to a stress/displacement analysis. The choice of the procedure used will depend on the specific characteristics of the model, and the ability to converge on a solution. Once the procedure to be used has been chosen, it must be decided if the analysis will be considered linear, or if non-linear effects will be included.

A linear analysis assumes linear behaviour and infinitesimally small displacements and strains. Linear analysis disregards the redistribution due to concrete cracking and the stiffness contribution from steel reinforcement (Engström, 2007). A linear analysis of reinforced concrete is valid if the structure is uncracked. At high stresses, and once the elastic limit has been exceeded, the accuracy of linear analysis is reduced and other forms of analysis should be considered, such as plastic or non-linear analysis.

In a non-linear analysis, the non-linear response of a structure is accounted for in the analysis. Sources of non-linearity in stress analysis problems can include material, geometric and boundary non-linearity. The majority of non-linear problems are characterised by large deformations and/or non-linear material response, including the reduction and redistribution of stiffness as a result of concrete cracking and yielding of reinforcement (Jukic & Ekfeldt, 2012). The challenge in non-linear problems is to obtain a convergent solution in the least computational time. ABAQUS analyses non-linear problems using Newton's method, or a variant of it, where the solution is obtained by considering a series of time increments, with iterations to obtain equilibrium within each increment. Non-linear analysis is complex and time consuming, and for this reason non-linear effects are often neglected.

3.3. Element Type

Bridge deck behaviour is governed predominantly by flexural behaviour, which is best modelled using shell elements. By assuming a shell structure, the bridge deck components can be treated as two-dimensional surfaces rather than as three-dimensional solids. Consequently, the case of plane stress is assumed where the stresses in the direction normal to the middle surfaces of the shell are considered to be of negligible effect (Abdelraouf & Matlock, 1972). This assumption is valid for voided slabs if a two-

dimensional model in which the effect of the voids is accounted for by the use of factored rigidities using equivalent plate parameters. If a high degree of accuracy is required to idealise the effects of the voids, three-dimensional solid elements will need to be considered, which reduces the assumption required when modelling the complex geometry. ABAQUS provides a rich library of shell and solid elements which have been tested numerically to evaluate their ability to accurately model bridge decks.

Given the wide variety of element types available, it is important to select the correct element for the particular application. Choosing an element for a specific analysis can be simplified by considering specific element characteristics such as first or second-order, full or reduced integration, and element shape. By considering each of these aspects carefully, the element most appropriate for a given analysis can be selected.

Displacements are calculated at the nodes of an element. At any other point in the element, the displacement is obtained by interpolating from the nodal displacements using either linear or quadratic interpolation. First order elements are elements that have nodes at their corners only and use linear interpolation, whereas second order elements, which have additional nodes on the middle of each side, use quadratic interpolation, thus allowing for curvature in individual elements. ABAQUS uses numerical techniques to integrate various quantities over the volume of each element to allow complete generality in material behaviour. A reduced integration option is also available, which uses a lower-order integration to form the element stiffness, which can be used to reduce computation times. These aspects will be used to determine appropriate elements to be used in the model.

Solid Elements

Solid continuum elements are the standard volume elements in ABAQUS, which are defined by the shape and the number of nodes used. For a three-dimensional analysis, hexahedral shaped elements should be used as they give the most accurate results at minimum cost. The shape of the element should be kept as rectangular as possible, which will be determined by the size of the mesh employed. These elements can be used to model both linear and complex non-linear behaviour (ABAQUS, 2007).

For bending dominated problems using solid elements, second-order quadratic elements are preferred to first order linear plane strain elements as they are able to capture stress concentration more effectively and are better for modelling geometric features. Second-order reduced integration solid elements in ABAQUS also generally yield more accurate results than the corresponding fully integrated elements due to shear and volumetric locking effects. For first-order elements, the accuracy achieved with full versus reduced integration is largely dependent on the nature of the problem, and hourglass control should also be considered if mesh distortion occurs (ABAQUS, 2007).

Incompatible mode elements, which are first order elements that are enhanced by incompatible modes to improve their bending behaviour, can also be considered as they achieve very accurate results

in problems dominated by bending (ABAQUS, 2007). Examples of solid elements with different shapes and number of nodes are shown in Figure 3.7. The degrees of freedom are calculated at the locations of the nodes highlighted in Figure 3.7.

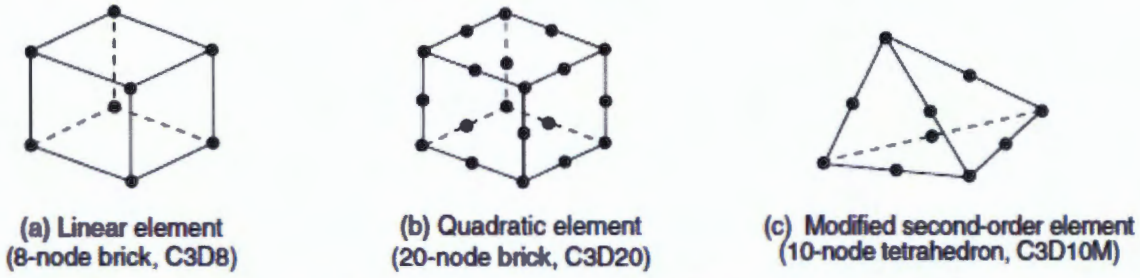

Figure 3.7 - Examples of solid elements with different nodal locations (ABAQUS, 2007).

Shell Elements

Shell elements are used to model structures in which one dimension, the thickness, is significantly smaller than the other dimensions. Conventional shell elements use this condition to discretise a three-dimensional body by defining the geometry at a reference surface. ABAQUS shell elements consist of varying nodal numbers, degrees of freedom, and shapes, and can therefore be used for a wide range of applications (ABAQUS, 2007).

As with solid elements, shell elements can make use of either linear or quadratic interpolation, and reduced integration can also be used on both first order and second order elements to reduce computation time. ABAQUS shell elements are valid for both thick and thin shell problems, using Kirchhoff's constraint and Mindlin's shell formulation respectively. Therefore the effects of transverse shear deformation can be modelled. In ABAQUS there is a choice of five or six degrees of freedom at all nodes. The elements that use five degrees of freedom can be more economical, however they are only available for thin shell applications (ABAQUS, 2007).

Shell elements behaviour is calculated using Simpson's rule or Gauss quadrature. Gauss quadrature typically requires fewer section points than Simpson's rule, and thus requires less computational time and storage space. However, more complex non-linear calculations may require more section points using Simpsons rule. Shell elements may also require numerical integration over the section. Numerical integration allows the cross-sectional behaviour to be calculated through the shell thickness, thus providing complete generality in material modelling, and is generally used when non-linear behaviour is experienced in the shell section (ABAQUS, 2007). An example of the nodal locations where degrees of freedom are calculated in shell elements is shown in Figure 3.8.

Continuum Shell Elements

Continuum shell elements can also be used to discretise a three-dimensional body, where the shell thickness is determined from the element nodal geometry. From a modelling point of view continuum shell elements look like three-dimensional continuum solids, but their kinematic and constitutive behaviour is similar to conventional shell elements. These elements include the effects of transverse shear deformation, thickness changes, and can include non-linear effects. Continuum shell elements employ first-order layer-wise composite theory, and estimate through-thickness section forces from the initial elastic moduli (ABAQUS, 2007). The primary differences between conventional shell and continuum shell elements are highlighted in Figure 3.8.

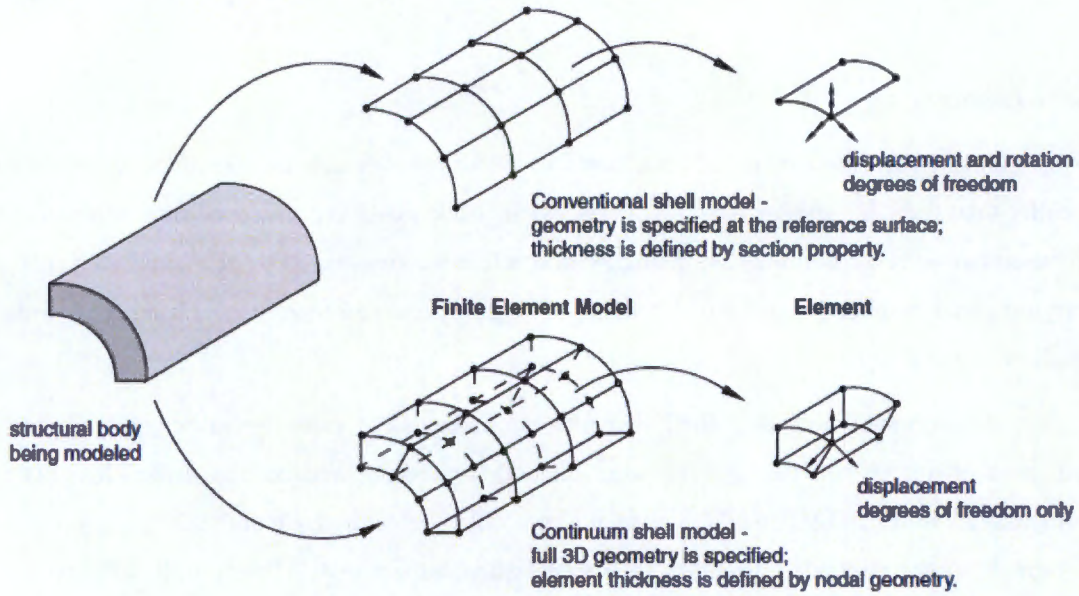

Figure 3.8 - Difference between conventional shell and continuum shell elements (ABAQUS, 2007).

4. METHODOLOGY: FINITE ELEMENT MODELLING

4.1. Introduction

This study will focus on the use of two-dimensional finite element analysis methods in order to accurately idealise voided slab bridge decks. From the literature review, three factors were identified as crucial to the outcome of the study. These include:

- The influence of the void diameter to slab thickness ratio on the structural behaviour of the voided slab.
- The influence of the void spacing on the structural behaviour of the voided slab.
- The use of orthotropic plate parameters in order to model a voided slab as a solid plate, by accounting for the effect of the voids through reduced elastic moduli.

In order to determine the effect of each of the above mentioned factors, three-dimensional finite element modelling will be used, with a separate phase being used to study each of the critical factors. A general finite element model of a voided slab bridge will be created. In each phase, the parameters in question will be isolated and varied keeping all other parameters constant in order to determine their influence on the structural behaviour. This section provides a detailed description of the modelling parameters used to create the finite element models, including a description of the boundary conditions, element types, loading conditions, material properties and analysis types used in each of the models. The models will be developed using the commercial finite element package ABAQUS 6.14.

4.2. Description of Modelling Phases

The finite element modelling was divided into three phases, with each phase being used to study the effect of an individual parameter. This section describes the purpose of each phase, and the modelling methods employed in order to achieve the necessary outcome. A detailed description of the finite element models used in each phase is given in Section 4.3.

Phase 1 – Influence of the Void Diameter Ratio

Phase 1 was used in order to determine the effect of the void diameter to slab depth ratio on the structural behaviour of a voided slab bridge deck. In order to determine this effect, five voided slabs with varying void diameter to slab depth ratios ranging from 0.5 to 0.9 were modelled. In each of these models, all parameters were kept constant apart from the varying void diameter ratios, which were varied by changing the void diameters and keeping the depth constant. The purpose of these models was to identify the variations in structural behaviour, predominantly on the longitudinal and transverse stresses, that are brought on by a variation in the void diameter ratio.

This phase also included modelling five solid slabs that idealised the corresponding voided slabs with varying void diameter ratios. These solid slabs were modelled with a reduced depth to give the same moment of inertia as the corresponding voided slabs. In each of these models, all parameters were kept constant apart from the depth of the solid slab. The purpose of the solid slab models was to determine the effect of the void diameter ratio on the variation between a voided slab, and an equivalent reduced depth solid slab.

Phase 2 – Influence of Void Spacing

Phase 2 was used in order to determine the effect of the void spacing on the structural behaviour of a voided slab bridge deck. In order to determine this effect, nine voided slabs with varying void spacing's ranging from 0.9m to 2.7m, which represent the logical minimum and maximum void spacing (O'Brien & Keogh, 1999), were modelled. In each of these models, all parameters were kept constant apart from the varying void spacing. The purpose of these models was to identify the variations in structural behaviour, predominantly on the longitudinal and transverse stresses, that are brought on by a variation in the void spacing.

This phase also included modelling nine solid slabs that idealised the corresponding voided slabs with varying void spacing. As with Phase 1, these solid plates were modelled with a reduced depth to give the same moment of inertia as the corresponding voided slabs. In each of these models, all parameters were kept constant apart from the depth of the solid slab. The purpose of the solid slab models was to determine the effect of the void spacing on the variation between a voided slab, and an equivalent reduced depth solid slab.

Phase 3 – Comparison of Orthotropic Plate Parameters

The purpose of this phase was to analyse and compare voided slabs idealised as solid slabs with a reduced elastic moduli to account for the effect of the voids. The elastic moduli were obtained using the equivalent orthotropic plate parameters listed in Table 2.1. In order to do this, the plate parameters and methodologies from different authors will be used to model the same voided slab deck. The results will then be compared to determine the suitability of the suggested parameters.

The results will also be compared to results from three-dimensional models of equivalent voided slabs in order to determine the suitability of each suggested method. As the factors are dependent on the void diameter ratio, each different methodology in question will be used to model five slabs with void diameter ratios ranging from 0.5 to 0.9.

4.3. System Geometry

Each phase of modelling consisted of the same typical arrangement of a voided slab bridge deck. This arrangement consisted of a single span of 20.0m in length and a width of 12.0m. This span length was chosen as it is in the typical range for voided slabs. The first 1.0m section at each end was kept solid for shear requirements, which is consistent with the literature. A deck depth of 1.0m was used, which is in the typical range for voided slabs. The void configuration consisted of nine 800mm voids with a spacing of 1.2m. This configuration resulted in internal webs of 400mm wide and end webs of width 200mm. The general arrangement of the voided slab bridge is shown in Figure 4.1 below.

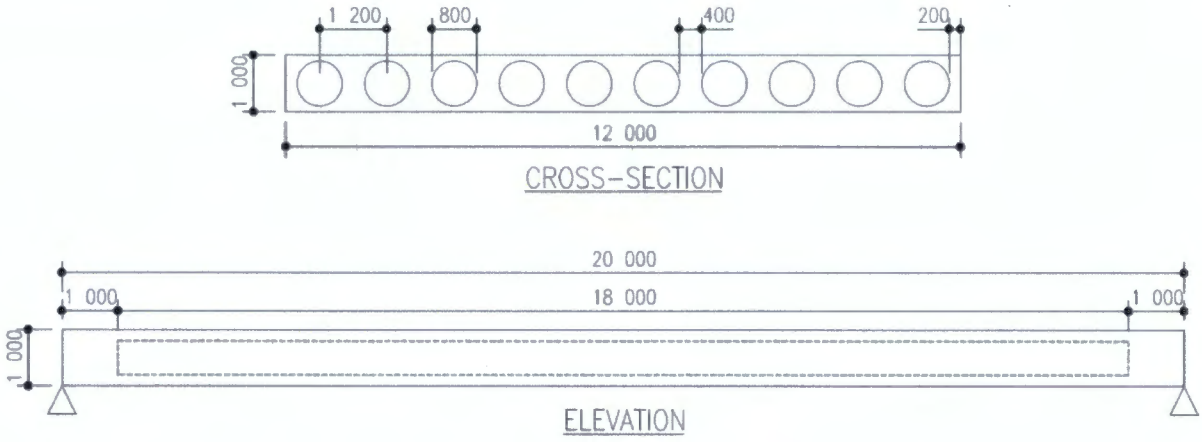

Figure 4.1 - Cross-section and elevation of the typical voided slab used for finite element modelling.

The finite element model of the typical voided bridge created in ABAQUS is shown in Figure 4.2.

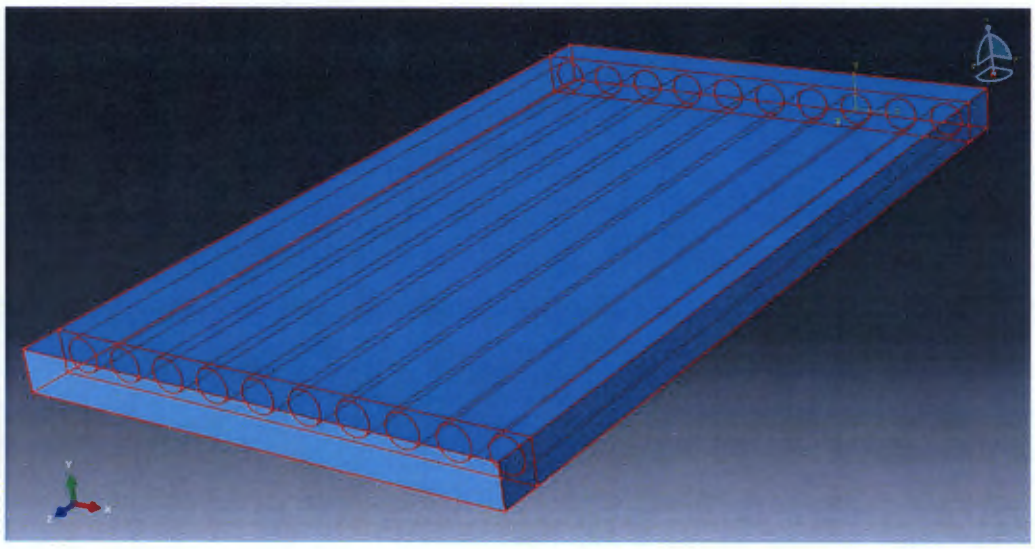

Figure 4.2 – Finite element model of the typical voided slab.

The general form of the structure was varied during each modelling phase in order to isolate and evaluate the effect of the required parameters. The following sections discuss the variations to the general form of the structure that were made during each modelling phase.

Phase 1 – Influence of the Void Diameter Ratio

During *Phase 1*, five voided slab finite element models were created with void diameter to slab thickness ratios varying from 0.5 to 0.9. The lower range of the void diameter ratio was selected as it is the suggested point where the voids begin to affect the structural behaviour of the slab. The higher range was selected as it represents the maximum void diameter that can be used that still allows for a flange above and below the voids. The only variations that were made from the general arrangement of the voided slab were to the void diameters in order to achieve the specified void diameter ratio. Therefore the depth of the slab was kept constant in each model. Table 4.1 below provides a summary of the geometry of the cross-section and span configuration of the voided slab models used for *Phase 1*.

Table 4.1 - Geometry of the cross-section and span configuration of the voided slab models used for Phase 1.

Model Name	Void Diameter (m)	Slab Thickness (m)	Void Diameter Ratio	Void Spacing (m)	Slab Length (m)	Slab Width (m)	No. of Voids (No.)
A1	0.5		0.5				
B1	0.6		0.6				
C1	0.7	1.0	0.7	1.2	20.0	12.0	9
D1	0.8		0.8				
E1	0.9		0.9				

The variations made to the general arrangement of the typical voided slab model for the five equivalent solid slabs modelled in *Phase 1* were to omit the voids, and reduce the slab thickness. The reduced depth was obtained by ensuring the same moment of inertia was obtained between the voided slab and the corresponding equivalent solid slab model. The moment of inertia was used to calculate the reduced depth as opposed to the cross-sectional area as this study will focus on the stresses primarily resulting from bending, and not those resulting from in-plane forces. Table 4.2 below provides a summary of the geometry of the cross-section and span configuration of the equivalent solid models used for *Phase 1*. Model A2 represents the equivalent solid slab used to idealise the voided model A1.

Table 4.2 - Geometry of the cross-section and span configuration of the solid slab models used for Phase 1.

Model Name	Void Diameter (m)	Slab Thickness (mm)	Idealised Void Diameter Ratio	Idealised Void Spacing (m)	Slab Length (m)	Slab Width (m)	No. of Voids (No.)
A2	0.5	0.989	0.5				
B2	0.6	0.978	0.6				
C2	0.7	0.959	0.7	1.2	20.0	12.0	0
D2	0.8	0.927	0.8				
E2	0.9	0.878	0.9				

Phase 2 – Influence of Void Spacing

During *Phase 2*, nine voided slab models were created with void spacing ranging from 900mm to 2700mm, which represent the logical minimum and maximum void spacing. The variations that were made to the general arrangement of the typical voided slab model was to the void spacing, which resulted in an increase or decrease in the number of voids in order to obtain the required void spacing. The void spacings were obtained by varying the number of voids from 5 to 13, while keeping the end webs in each model constant at 200mm wide. A void diameter ratio of 0.8 was employed in this phase as it already introduces a degree of orthotropy into the structure which is more likely to increase with the variation in void spacing. Table 4.3 below provides a summary of the geometry of the cross-section and span configuration of the voided slab finite element models created for *Phase 2*.

Table 4.3 - Geometry of the cross-section and span configuration of the voided slab models used for Phase 2.

Model Name	Void Diameter (m)	Slab Thickness (m)	Void Diameter Ratio	Void Spacing (m)	Slab Length (m)	Slab Width (m)	No. of Voids (No.)	Internal web width (mm)
F1				2.70			5	1900
G1				2.16			6	1316
H1				1.80			7	1000
I1				1.54			8	743
J1	0.8	1.0	0.8	1.35	20.0	12.0	9	550
K1				1.20			10	400
L1				1.08			11	308
M1				0.98			12	181
N1				0.90			13	100

The variations made to the general arrangement of the typical voided slab model or the nine equivalent solid slabs modelled in *Phase 2* were to omit the voids, and reduce the slab thickness. As with *Phase 1*, the reduced depth was obtained by ensuring the same moment of inertia was obtained between the voided slab and the corresponding equivalent solid slab model. Table 4.4 provides a summary of the geometry of the cross-section and span configuration of the solid plate models used for *Phase 2*. Model F2 represents the equivalent solid slab used to idealise the voided model F1.

Table 4.4 - Geometry of the cross-section and span configuration of the solid slab models used for Phase 2.

Model Name	Void Diameter (m)	Slab Thickness (m)	Idealised Void Diameter Ratio	Idealised Void Spacing (m)	Slab Length (m)	Slab Width (m)	No. of Voids (No.)	Internal web width (mm)
F2		0.965		2.70				1900
G2		0.958		2.16				1316
H2		0.951		1.80				1000
I2		0.943		1.54				743
J2	0.8	0.936	0.8	1.35	20.0	12.0	0	550
K2		0.928		1.20				400
L2		0.920		1.08				308
M2		0.912		0.98				181
N2		0.904		0.90				100

Phase 3 – Comparison of Orthotropic Plate Parameters

Phase 3 of the finite element modelling focused on the suitability of using equivalent orthotropic plate parameters suggested in Section 2.2.1 for the idealisation of voided slabs as solid orthotropic slabs. In order to investigate the suitability of these parameters, the various plate parameters and the accompanying methods employed by different authors were used to idealise a range of voided slabs with different void diameter to slab depth ratios. Methods utilising orthotropic plate theory from six different authors were used in this phase, with each method being used with five different void diameter to slab depth ratios ranging from 0.5 to 0.9. A range of void diameter to slab depth ratios were used in order to determine in what range the plate parameters produce accurate results. A total of thirty solid orthotropic finite element models were generated for this phase.

The seven authors whose methods will be compared in this phase include Aster (1968), Bakht (1981), Jofriet *et al.* (1973), Pama *et al.* (1975), Elliot & Clarke (1982), Diaz *et al.* (2010), and Sen *et al.* (1994). Each of these methods use equivalent plate parameters to define an orthotropic material in order to account for the effect of the voids, and differ only in the values of the equivalent plate parameters and the need for stress conversions from the equivalent orthotropic slab to the actual voided slab. The definitions of each authors suggested equivalent plate parameters are given in Table 2.1.

In order to apply the equivalent plate parameters in the finite element models, it was decided to model the voided slabs as solid volumes, with an anisotropic material being used to account for the orthotropic behaviour. The equivalent plate parameters are used to calculate the flexural rigidity of the slab in each direction. As the flexural rigidity is defined as the product of the moment of inertia and the elastic modulus, the depth of the slab and the elastic modulus are required to determine the flexural rigidity. The depth of the slab was defined as the depth required for the solid slab idealisation to give the

same moment of inertia as the actual voided slab, resulting in a constant moment of inertia in each direction. The elastic modulus in the longitudinal and transverse directions could then be obtained by dividing the flexural rigidity defined by the equivalent plate parameters by the moment of inertia based on the depth of the equivalent solid slab. A summary of the slab depth, moment of inertia, flexural rigidities, and elastic moduli for the finite element models in *Phase 3* are summarised in Table 4.5

Table 4.5 - Summary of the slab depth, moment of inertia, flexural rigidities, equivalent plate parameters and anisotropic material properties used for the solid orthotropic finite element models in *Phase 3*.

Author	Void Diameter Ratio	Depth (m)	I (m^4)	D_x (10^9 N/m^2)	D_y (10^9 N/m^2)	D_{xy} (10^9 N/m^2)	E_x (GPa)	E_y (GPa)	E_{xy} (GPa)	Use of Stress Multi-plier
Aster (1968)	0.5	0.99	0.97	29.08	29.08	12.12	30.00	30.00	12.50	-
	0.6	0.98	0.94	28.09	28.09	11.70	30.00	30.00	12.50	
	0.7	0.96	0.88	26.46	26.46	11.03	30.00	29.99	12.50	
	0.8	0.93	0.80	23.97	23.96	9.98	30.00	29.99	12.50	
	0.9	0.88	0.68	20.34	20.32	8.47	30.00	29.98	12.50	
Bakht (1981)	0.5	0.99	0.97	29.08	28.22	12.12	30.00	29.11	12.50	-
	0.6	0.98	0.94	28.09	26.31	10.53	30.00	28.09	11.25	
	0.7	0.96	0.88	26.46	23.16	9.08	30.00	26.25	10.29	
	0.8	0.93	0.80	23.97	18.33	6.89	30.00	22.94	8.63	
	0.9	0.88	0.68	20.34	11.30	4.19	30.00	16.67	6.19	
Jofriet *et al.* (1973)	0.5	1.00	1.00	29.08	29.08	5.82	29.08	29.08	5.82	Yes
	0.6	1.00	1.00	28.09	28.09	5.62	28.09	28.09	5.62	
	0.7	1.00	1.00	26.46	26.46	5.29	26.46	26.46	5.29	
	0.8	1.00	1.00	23.97	23.97	4.79	23.97	23.97	4.79	
	0.9	1.00	1.00	20.34	20.34	4.07	20.34	20.34	4.07	
Pama *et al.* (1975)	0.5	0.99	0.97	29.08	26.25	11.81	30.00	27.08	12.19	-
	0.6	0.98	0.94	28.09	23.52	10.80	30.00	25.12	11.53	
	0.7	0.96	0.88	26.46	19.71	9.56	30.00	22.34	10.84	
	0.8	0.93	0.80	23.97	14.64	8.10	30.00	18.32	10.14	
	0.9	0.88	0.68	20.34	8.13	6.41	30.00	11.99	9.46	
Elliot & Clarke (1982)	0.5	0.99	0.97	29.08	28.13	11.84	30.00	29.02	12.21	-
	0.6	0.98	0.94	28.09	26.11	11.12	30.00	27.89	11.88	
	0.7	0.96	0.88	26.46	22.80	9.95	30.00	25.84	11.28	
	0.8	0.93	0.80	23.97	17.71	8.15	30.00	22.17	10.20	
	0.9	0.88	0.68	20.34	10.32	5.53	30.00	15.22	8.16	
Diaz *et al.* (2010)	0.5	1.00	1.00	29.08	29.08	12.12	29.08	29.08	12.12	Yes
	0.6	1.00	1.00	28.09	28.09	11.70	28.09	28.09	11.70	
	0.7	1.00	1.00	26.46	26.46	11.03	26.46	26.46	11.03	
	0.8	1.00	1.00	23.97	23.97	9.99	23.97	23.97	9.99	
	0.9	1.00	1.00	20.34	20.34	8.47	20.34	20.34	8.47	
Sen *et al.* (1994)	0.5	0.99	0.97	29.08	28.22	12.12	30.00	29.11	12.50	Yes
	0.6	0.98	0.94	28.09	26.31	10.53	30.00	28.09	11.25	
	0.7	0.96	0.88	26.46	23.16	9.08	30.00	26.25	10.29	
	0.8	0.93	0.80	23.97	18.33	6.89	30.00	22.94	8.63	
	0.9	0.88	0.68	20.34	11.30	4.19	30.00	16.67	6.19	

From Table 4.5 it can be seen that the slab depth and elastic modulus in the longitudinal direction suggested by Aster (1968), Bakht (1981), Pama *et al.* (1975), Elliott & Clarke (1982), and Sen *et al.* (1994) are all the same. This is because the calculation of the flexural rigidity in the longitudinal direction is simple to calculate due to the constant cross-section, and uses the moment of inertia based on the slab depth and the elastic modulus of the actual material. The difference in these methods arises from the transverse flexural rigidity used to define the transverse elastic modulus.

The exception to this rule is the method of Jofriet *et al.* (1973) and Diaz *et al.* (2010), where the depth of the solid slab is unchanged from that of the voided slab, and a decrease in longitudinal elastic modulus is used to account for the decrease in the moment of inertia due to the voids. The transverse elastic modulus is assumed to be equal to the longitudinal elastic modulus, resulting in an isotropic material. A stress multiplier is also employed in these methods, which is used to convert the stresses from the solid slab idealisation to those of the actual voided slab. The advantages of such magnifiers are that they can be used in conjunction with existing simplified methods such as the orthotropic plate methods, in order to adjust the stress results to account for effects such as cellular distortion, which are neglected in the simplified analysis. The stress multipliers are different in the longitudinal and transverse directions due to orthotropic behaviour of voided slab bridge decks.

The multipliers suggested by Diaz *et al.* (2010) are based on the depth of the neutral axis and the thickness of the flanges above and below the voids. The derivation of these equations is described in detail in Section 2.3. The multipliers suggested by Jofriet *et al.* (1973) are based on the moment of inertia of the actual voided slab to that of the solid slab idealisation. The multiplier is assumed to be the same in the orthogonal directions due to the difficulty in obtaining the transverse moment of inertia. The formulae and values of the longitudinal and transverse stress multipliers used for this study are given in Table 4.6.

Table 4.6 - Stress multipliers used for orthotropic idealisations of voided slab bridge decks recommended by Diaz *et al.* (2010) and Jofriet *et al.* (1973).

Author	Void Diameter Ratio	Longitudinal Stress Multiplier		Transverse Stress Multiplier	
		Formula	Value	Formula	Value
Diaz *et al.* (2010)	0.5	$\frac{h_t h^2}{6 I_{r,y}} \sigma_{f,x,b,t}$	1.03	$\frac{2 h_t h^2}{e_1{}^3 + e_2{}^3 + 12\left[e_1\left(h_1 - \frac{e_1}{2}\right)^2 + e_2\left(h_2 - \frac{e_2}{2}\right)^2\right]} \sigma_{f,y,b,t}$	1.14
	0.6		1.07		1.28
	0.7		1.13		1.52
	0.8		1.25		2.05
	0.9		1.48		3.69
Jofriet *et al.* (1973)	0.5	$\frac{I_{solid}}{I_{voided}}$	1.03	$\frac{I_{solid}}{I_{voided}}$	1.03
	0.6		1.07		1.07
	0.7		1.13		1.13
	0.8		1.25		1.25
	0.9		1.48		1.48

The method suggested by Sen *et al.* (1994) also recommended the use of a stress multiplier. The authors suggest that the stress multiplier is required as the solid slab and voided slabs have different depths, and therefore have different neutral axis positions. Sen *et al.* (1994) suggests that stress multipliers are required to account for the difference in distance between the extreme fibres of the slab and the neutral axis of the solid and voided slabs. Other than the use of stress multipliers, the method recommended by Sen *et al.* (1994) is no different from that of Bakht *et al.* (1982). It should be noted that Bakht *et al.* (1982) makes no mention of the requirement of stress multipliers.

The stress multiplication suggested by Sen *et al.* (1994) is calculated by using two correction factors, namely a material and a distance factor, and the following equation:

$$\sigma_{voided} = \sigma_{orthotropic} * MF * DF \tag{4.1}$$

The material factor takes into account the reduced stiffness of the equivalent orthotropic model, and the distance factor allows for the variation in the neutral axis between the voided slab and solid orthotropic idealisation. The distance factor depends on the location of where the stresses are being calculated through the depth of the slab. The following equations can be used to determine the material and distance factors:

$$MF = \frac{E_{voided}}{E_{orthotropic}} \tag{4.2}$$

$$DF = \frac{d_{voided}}{d_{orthotropic}} \tag{4.3}$$

Where d is the distance to the neutral axis from the position in the depth of the slab where the stresses are being determined. The values of the multipliers used for this study based on the equations recommended by Sen *et al.* (1994) are shown in Table 4.7. It can be seen that the multipliers have the greatest influence on the transverse stresses, which is predominantly due to the material factor. The longitudinal stress multipliers are smaller in magnitude than the transverse stress multipliers, and are less than unity on the top fibre, which is due to the distance factor.

Table 4.7 - Stress multipliers used for orthotropic idealisations of voided slab based on the recommendations of Sen *et al.* (1994)

Void Diameter Ratio	Transverse Stress Multiplier		Longitudinal Stress Multiplier	
	Top Fibre	Bottom Fibre	Top Fibre	Bottom Fibre
0.5	1.02	1.04	0.99	1.01
0.6	1.04	1.09	0.98	1.02
0.7	1.01	1.19	0.96	1.04
0.8	1.21	1.40	0.93	1.07
0.9	1.58	2.02	0.88	1.12

4.4. Element and Analysis Type

In each phase of the finite element modelling, three-dimensional twenty node second order brick elements (C3D20R) with reduced integration were used. These elements were chosen as they are well suited for bending applications, provide a reasonable solution convergence time, and were able to match the shape of the voided cross-section sufficiently well (ABAQUS, 2007).

The voids within the slab cross-section increased the complexity of the mesh formation as quadrilateral elements had to be used to mesh around the circular form. The circular form meant that automated meshing techniques in ABAQUS could not be employed directly as a highly distorted and non-symmetric mesh resulted. The distorted and non-symmetric mesh meant that additional steps were required to improve the quality of the mesh. Figure 4.3 shows the resulting mesh of the voided cross-section created using automated meshing techniques.

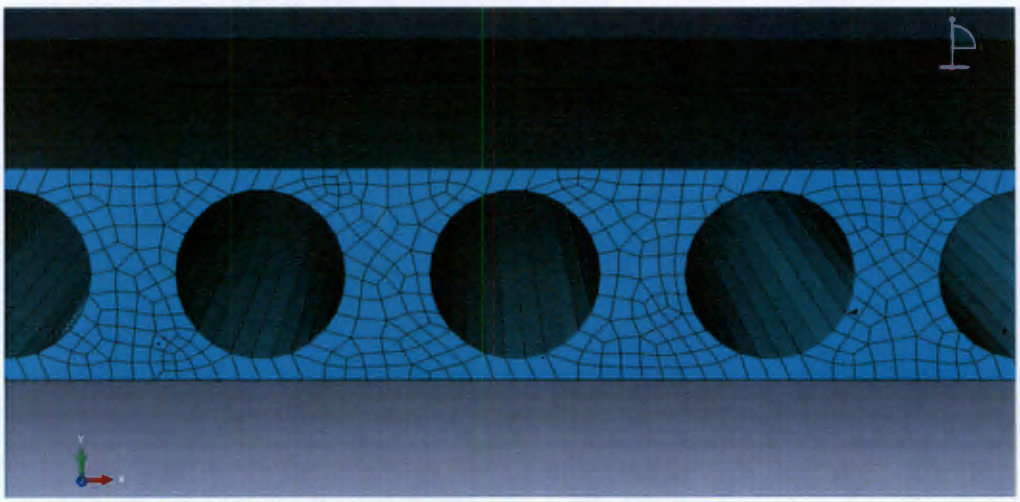

Figure 4.3 - Distorted mesh of the voided cross-section resulting from automated meshing in ABAQUS.

Manual meshing of the numerous models employed in this study was seen as unfeasible due to the amount of time required, therefore a method of making better use of the automated meshing techniques in ABAQUS was sought. The chosen method involved partitioning each voided cell into quarters. The automated Structural meshing technique in ABAQUS could then be employed to create the mesh. This method resulted in an undistorted and symmetric mesh which could be produced in a suitable amount of time. The partition technique and the resulting mesh are shown in Figure 4.4 and Figure 4.5 respectively. No partitioning was required for the solid slab models.

An element size of 0.1m x 0.1m x 0.1m was chosen. Although this small element size increased the processing time of the model to converge on a solution, a small element size was required to ensure that a suitable number of elements were able to fit in the flange above the voids. This was an important requirement as the stresses directly above the voids were critical to the objectives of this study. The resulting mesh consisted of 223 270 elements. A convergence study was used in order to determine the

accuracy of the mesh with varying element sizes. The resulting mesh was sufficiently dense to converge on an accurate solution with reasonable stress distributions in a suitable time frame.

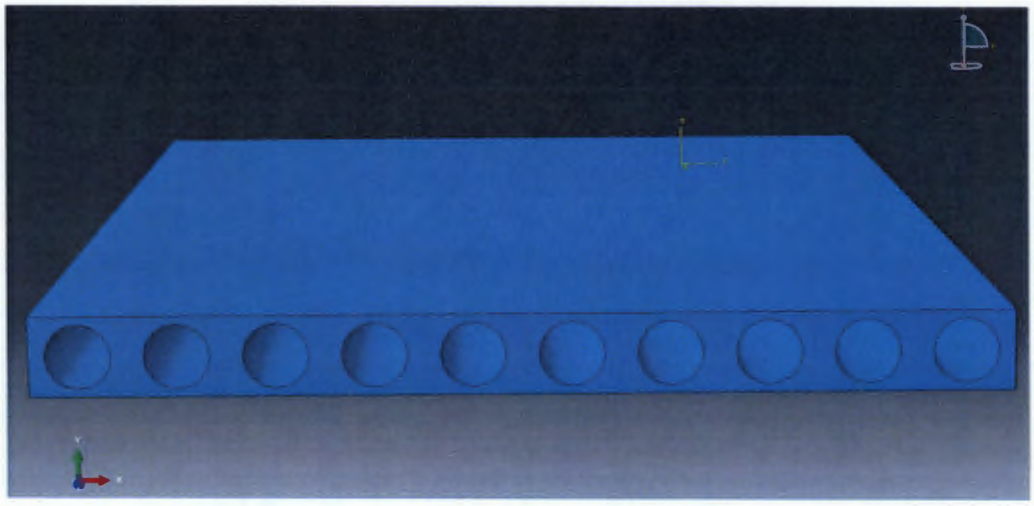

(a)

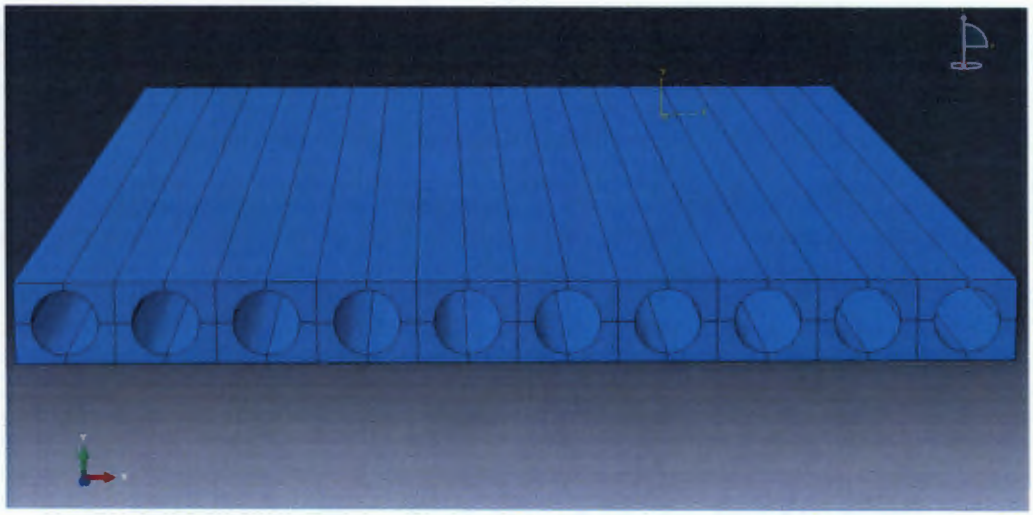

(b)

Figure 4.4 - Finite element model of the voided cross-section (a) before and (b) after partitioning.

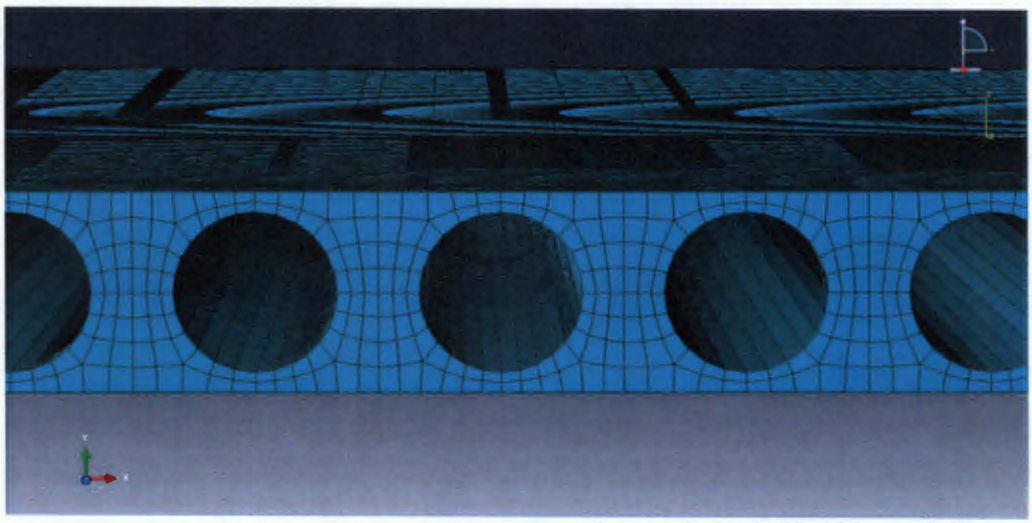

Figure 4.5 - Resulting mesh of the voided cross-section after using partitioning and automated meshing.

The same element type and size was employed in each phase of the modelling. This was done in order to reduce the effect of varying modelling techniques when comparing the models. A static stress displacement analysis type was used in each phase of modelling.

4.5. Boundary and Loading Conditions

The support and loading conditions remained constant in all phases of the modelling in order to reduce the effect of varying modelling techniques when comparing models. The supports were modelled as simply supported by fixing the middle of each edge of the slab from translation in the x, y and z directions, with no fixity of rotation. Although this method is not an accurate idealisation of a simple support as in reality the bridge deck would be supported on bearings with a tangible size and not a line with no zero width, it provided a simple method of creating the required support conditions.

The pinned support was modelled by fixing the middle of the slab and not the bottom of the slab in order to reduce the effect of the boundary conditions on the stress distribution. Fixing of the bottom edge of either end of the slab was found to alter the position of the neutral axis, resulting in its position not being at mid-depth, which was the result of different fixities of the top and bottom of the slab. This method also resulted in high mesh distortion near to the supports, resulting in distorted stress distributions near the supports. Modelling the support on the middle of the slab was found to reduce both the effect on the neutral axis and the stress concentrations. The modelling of the support conditions in ABAQUS is shown in Figure 4.6. This support condition was employed in all phases of modelling.

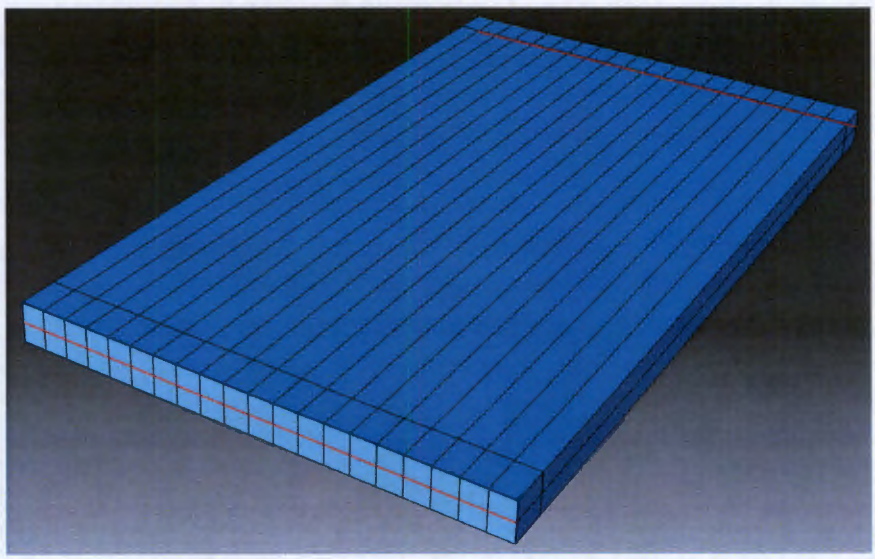

Figure 4.6 - Modelling of boundary conditions as pinned supports in the finite element model.

The loading employed in all phases of the modelling consisted of a uniformly distributed load of 8kN/m^2 applied directly to the top surface of the deck. This approach is adopted from O'Brien & Keogh (1998). While this may not be the most severe loading that bridges are subjected to in their service life, it enables

comparisons of results obtained in this study to previous studies. A uniformly distributed load was also employed, as typical traffic loading patterns can influence the cross-section distortion of cellular decks. Therefore the loading employed allowed the parameters in question to be isolated and compared without the effect of traffic loading patterns. The uniformly distributed load applied to the finite element model in ABAQUS is shown in Figure 4.7.

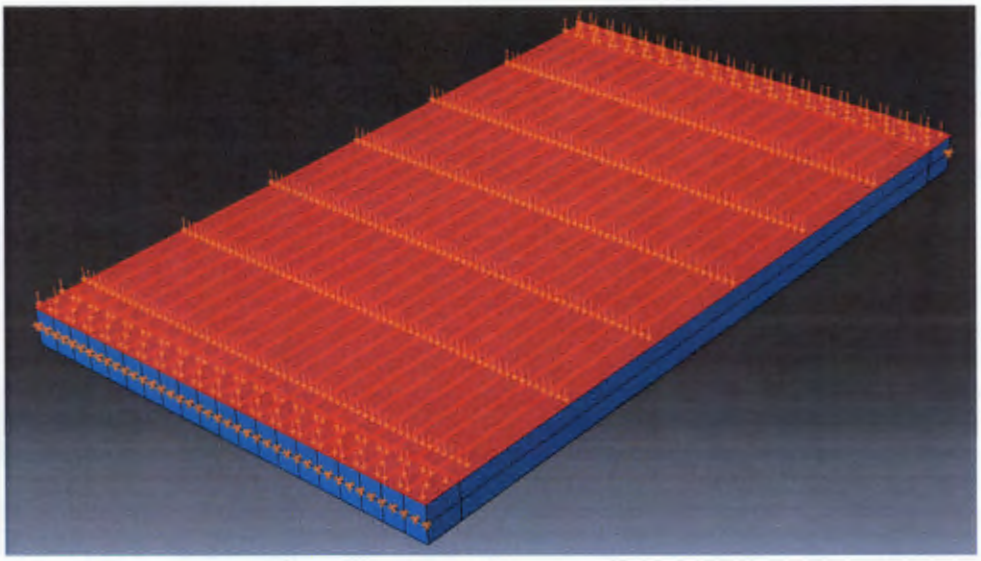

Figure 4.7 - Modelling of the uniformly distributed load in the finite element model.

4.6. Material Properties

In *Phase 1* and *Phase 2,* the concrete was modelled using a linear elastic isotropic material with an elastic modulus of 30GPa and a Poisson ratio of 0.2. No attempt was made to account for the cracking of concrete or for the presence of steel with the concrete, which is typical for linear forms of analysis specified in design codes such as TMH7 and Eurocodes. The use of linear material simplified the preprocessing required and the running time of the model.

During *Phase 3*, different elastic moduli in the longitudinal and transverse directions where required in order to idealise the orthotropic behaviour. Several material models are available in order to idealise orthotropic behaviour in ABAQUS as discussed in Section 0. The plate parameters suggested by the authors in the literature review only defined three parameters, namely E_x, E_y, and G_{xy}, along with a Poisson ratio. The plane stress orthotropic definition requires the input of only these parameters, however it cannot be used with the three-dimensional elements used in this study, and was therefore disregarded. The anisotropic and orthotropic stiffness matrix definitions were also disregarded as they required the definition of twenty one and nine independent rigidities respectively for which no definitions could be obtained from the equivalent plate parameters.

For this study, it was therefore decided to utilise the engineering constant definition in order to define the material parameters, which required the definition of nine independent material parameters. These included three elastic moduli, E_x, E_y, and E_z, three Poisson's ratios, ν_{xy}, ν_{xz}, and ν_{zy}, and the three shear elastic moduli, G_{xy}, G_{zy}, and G_{zy} associated with the materials principal directions. E_x, E_y, and G_{xy} were defined using the equivalent plate parameters defined in Table 2.1. The three Poisson's ratios are unaffected by the presence of the voids, and were therefore defined as $\nu_{xy} = \nu_{xz} = \nu_{zy} = 0.2$ as per the recommendation by Elliott & Clarke (1982).

This left E_z, G_{xz}, and G_{yz} to be defined, the definitions of which are not mentioned in the literature. It was decided to make $E_z = 30$GPa, as the effect of the voids on the stiffness of the slab in the direction of the slab thickness is minimal. G_{xz} and G_{yz} were made equal to 12.5MPa, which is based on the following equation for the shear modulus of a linear material with an elastic modulus of 30GPa:

$$G = \frac{E}{1+\nu} \tag{4.2}$$

A sensitivity study was performed in order to determine the effect of these values on the longitudinal and transverse stress results on the finite element model. The results of the sensitivity study showed that the longitudinal and transverse stress results were unaffected by these parameter definitions, therefore these definitions of the engineering constants were considered to be accurate for this study.

The voided section of the deck, which is between 1m and 19m along the length, was modelled as an orthotropic material using the equivalent plate parameters to define the engineering constant. The solid sections of 1.0m in width over the supports were modelled as an isotropic linear material. The modelling of an equivalent orthotropic solid slab using different material types in ABAQUS is shown in Figure 4.8.

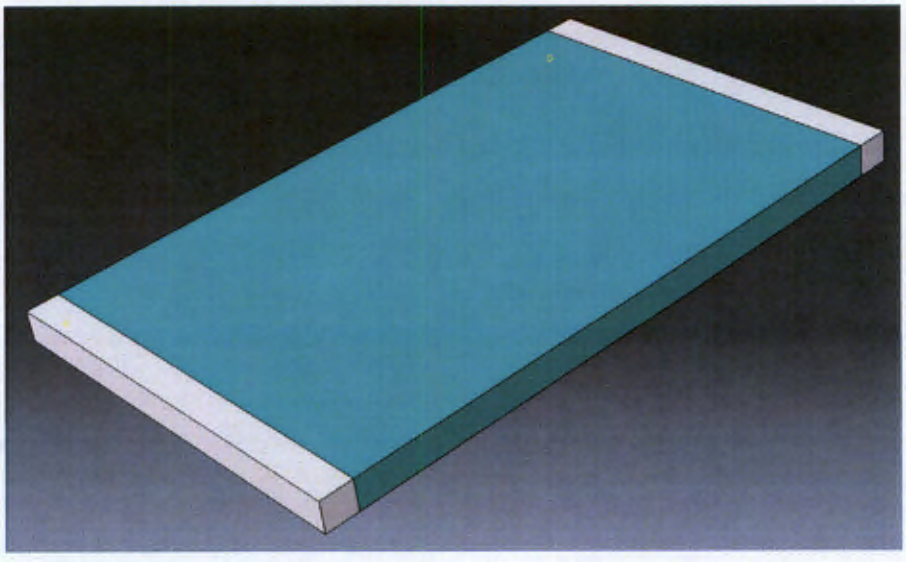

Figure 4.8 - Modelling of isotropic (white) and orthotropic (green) materials in finite element model of an equivalent orthotropic solid slab.

5. RESULTS AND DISCUSSION

This chapter presents the results of the finite element modelling outline in Chapter 4, as well as the analysis and discussion thereof. This study will focus on the stress distribution and stress raising effect of the voids in a voided slab, therefore the results presented from the finite element models will consist of the longitudinal and transverse stresses at critical locations. These critical locations include:

- A transverse line at mid-span on the extreme compression fibre of the cross-section.
- A transverse line at mid-span on the extreme tension fibre of the cross-section.
- A longitudinal line along the centreline of the deck on the extreme compression fibre.
- A longitudinal line along the centreline of the deck on the extreme tension fibre.
- A transverse line at the transition from the voided to the solid cross-section on the extreme compression fibre of the cross-section.

The location of these critical locations is shown in Figure 5.1.

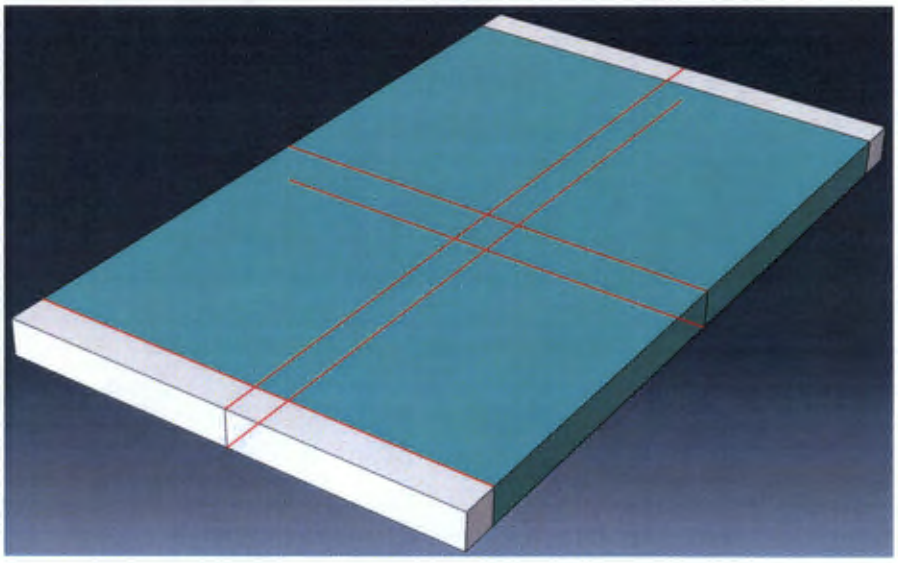

Figure 5.1 - Location of the critical stress result locations from the finite element models.

It was decided to present the results of the stresses as opposed to the moments as the stress results could be directly output from ABAQUS, whereas the moments could only be obtained through integration. The stresses were also chosen as the stress multipliers required in *Phase 3* are directly applied to the stresses, and not the moments. Therefore in order to draw comparisons between the different models, the stress results were deemed to be a more appropriate output than the moments.

The incorporation of the voids within a slab can affect the stress results primarily due to the reduction of the moment of inertia, and the distortion of the cross-section. The discussion of results that follows will therefore seek to analyses the effect of the reduced moment of inertia and the cross-section distortion on the longitudinal and transverse stresses, which can be used to determine the stress raising effect of the voids.

5.1. General Finite Element Results of a Voided Slab

This section presents the longitudinal and transverse stress results from the finite element of a voided slab model with a void diameter ratio of 0.8 and a void spacing of 1.2m, which represent dimensions of a typical voided slab (O'Brien and Keogh, 1998 and Diaz *et al.*, 2010). The purpose of this section is to study the effects of the introduction of the voids to the stress distributions of a slab type bridge deck.

Figure 5.2 shows the longitudinal stress distribution of the finite element model on the extreme compression and tension fibre of the deck. The longitudinal stress varies from zero at either end of the deck to a peak stress in the middle of the deck, with compression and tension on the top and bottom of the deck respectively.

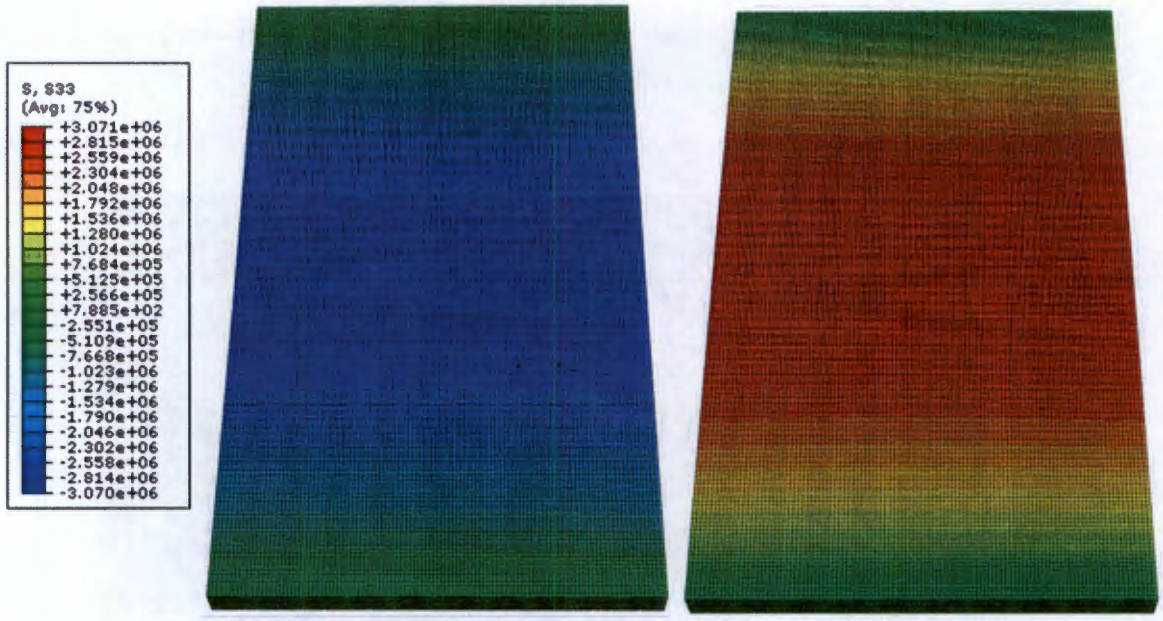

Figure 5.2 - Longitudinal stress distribution from a voided slab finite element model on (a) the extreme compression fibre and (b) the extreme tension fibre of the deck.

The longitudinal stress distribution on the top and bottom of the deck cross-section at mid-span is shown in Figure 5.3. The longitudinal stress on the webs in between the voids varies linearly between compression and tension on the top and bottom of the deck respectively. The neutral axis is located at mid-depth of the deck, and is consistent with the linear material used in the finite element model.

These results show that the addition of the voids does not create any significant variations to the longitudinal distribution of stresses on a slab. The primary effect will be the decrease in moment of inertia due to the reduction in cross-section due to the voids, which will result in an increase in the longitudinal stresses. However, the distribution of the longitudinal stresses is unaffected by the presence of the voids.

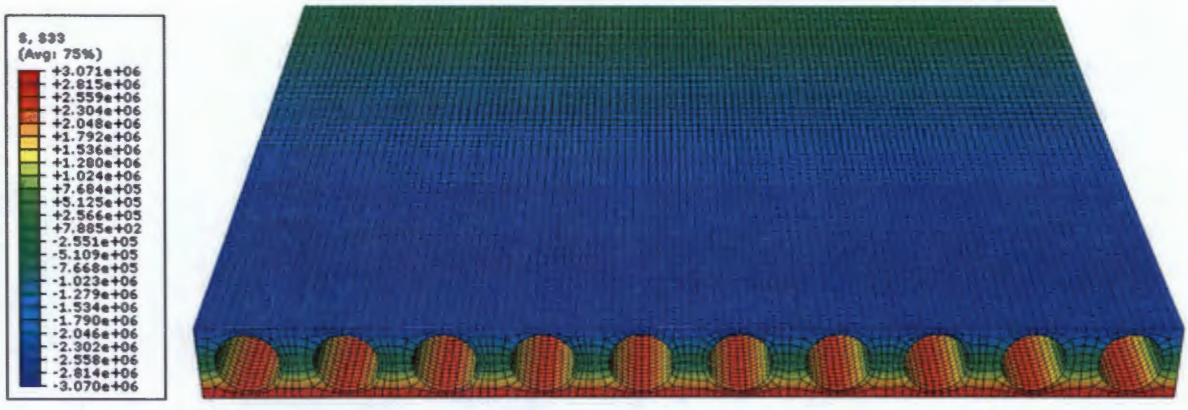

(a)

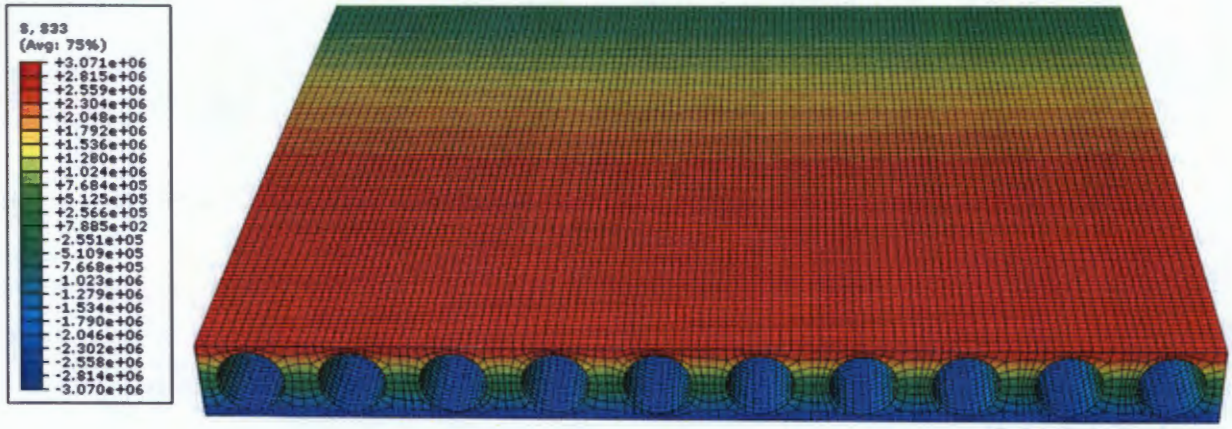

(b)

Figure 5.3 - Longitudinal stress distribution on the cross-section of the voided slab finite element model on (a) the extreme compression fibre and (b) the extreme tension fibre of the deck, with a transverse cut at mid-span.

The distribution of transverse stresses on the extreme compression and tension fibre of the deck is shown in Figure 5.4. The transverse stress is zero at the supports and increases parabolically in the longitudinal direction resulting in a peak transverse stress at mid-span. The transverse stresses also increase from zero on either side of the deck to a peak transverse stress along the centreline of the deck. The transverse stresses are in compression and tension on the top and bottom of the deck respectively.

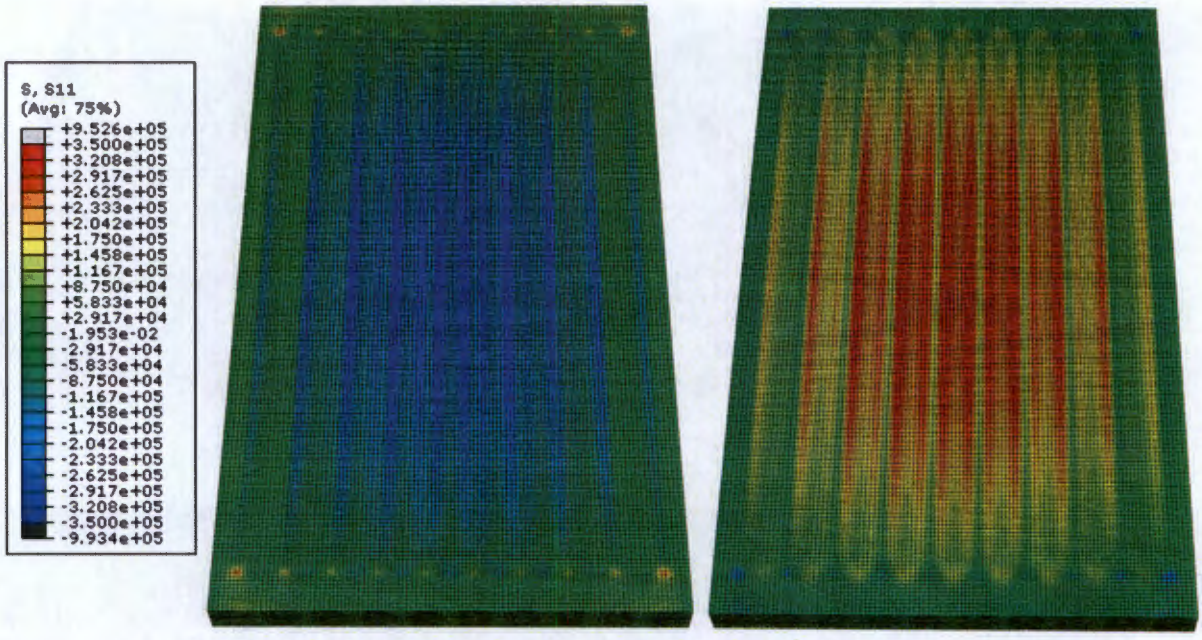

(a) **(b)**

Figure 5.4 - Transverse stress distribution from voided finite element model on (a) the extreme compression fibre and (b) the extreme tension fibre of the deck.

The effect of the voids on the transverse stresses can clearly be seen, resulting in longitudinal bands of high stress concentrations that are distributed transversely across the deck. Figure 5.5 shows a close up of the transverse stress distribution on the middle four voids with a transverse cut at mid-span. It can be seen that the peak stresses resulting in the concentration of stresses on the top and bottom of the slab are located on either side of the centre of each void.

At the centre of the voids on both the top and bottom of the deck, the transverse stress decreases to a local minimum in between the peak stresses on either side of each void. There is also a decrease in stress at the webs on both the top and bottom of the deck. The transverse stresses are mainly concentrated in the flanges above and below the voids. The stresses in the flanges are also not able to reduce through the depth of the deck to the same extent as in the web portions of the deck. Therefore there is minimal vertical distribution of transverse stresses, resulting in low stresses at the neutral axis position at the webs, and a concentration of stresses in the flanges.

A concentration of stresses can be seen on each of the void's perimeter at the top and bottom of the void centreline. These transverse stresses, which represent the maximum transverse stresses in the cross-section, are indicated by the blue and red colours in Figure 5.5 with compression and tension at the top and bottom of the slab respectively. These stresses distribute at an angle of 45 degrees through the flange to the location of the peak stresses on the extreme compression and tension fibre of the deck.

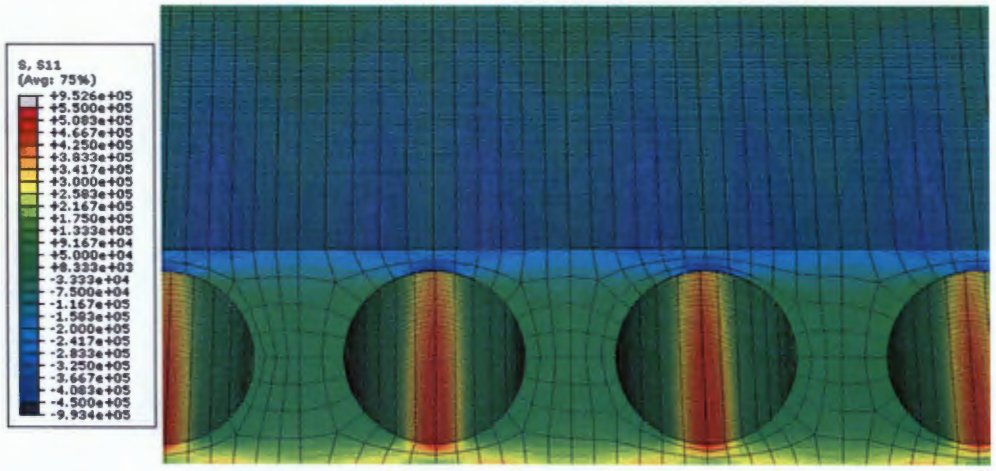

(a)

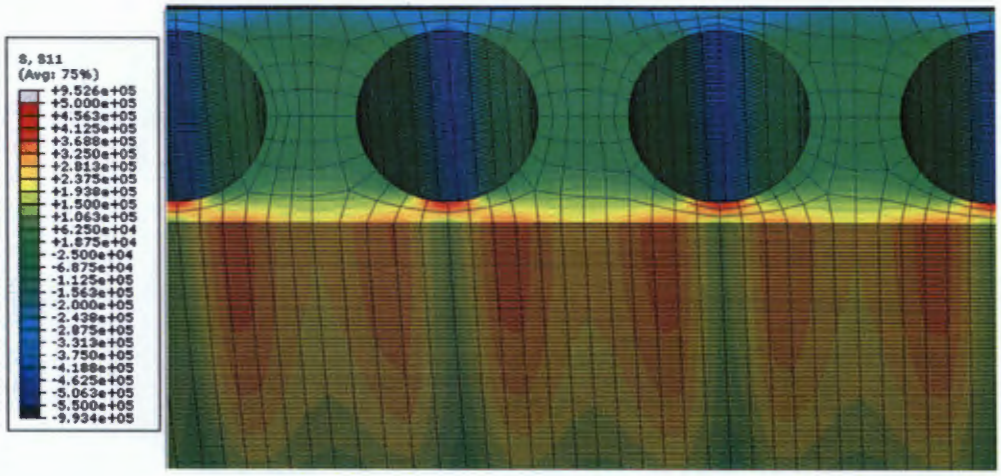

(b)

Figure 5.5 - Close up of transverse stress distribution of the central voids on (a) the extreme compression fibre (b) the extreme tension fibre of the finite element model along a transverse cut at mid-span.

The above results show that the greatest influence of the addition of the voids on the slab is on the transverse stress distribution. In order to understand the effect of the voids on the transverse stress distribution, the transverse stress distributions on the extreme compression and tension fibres of a voided and solid slab are shown in graphical form in Figure 5.6. The solid model has a depth which gives the same moment of inertia as the voided slab. The vertical lines of the graph indicate the centre of each void.

By comparing the results from the solid and voided models, it is clear that the addition of the voids causes large variations to the transverse stresses across the width of the slab. For the solid model, the transverse stress distribution follows a parabolic shape across the width of the deck, with a maximum transverse compressive and tensile stress occurring at the centre of the deck on the top and bottom of the deck respectively. For the voided model, the transverse stress distribution follows the same parabolic shape as the solid model, with large deviations to the parabolic shape of the graph as a result of the voids. The longitudinal and transverse stress distributions of the solid model are shown in Figure 5.7 and Figure 5.8.

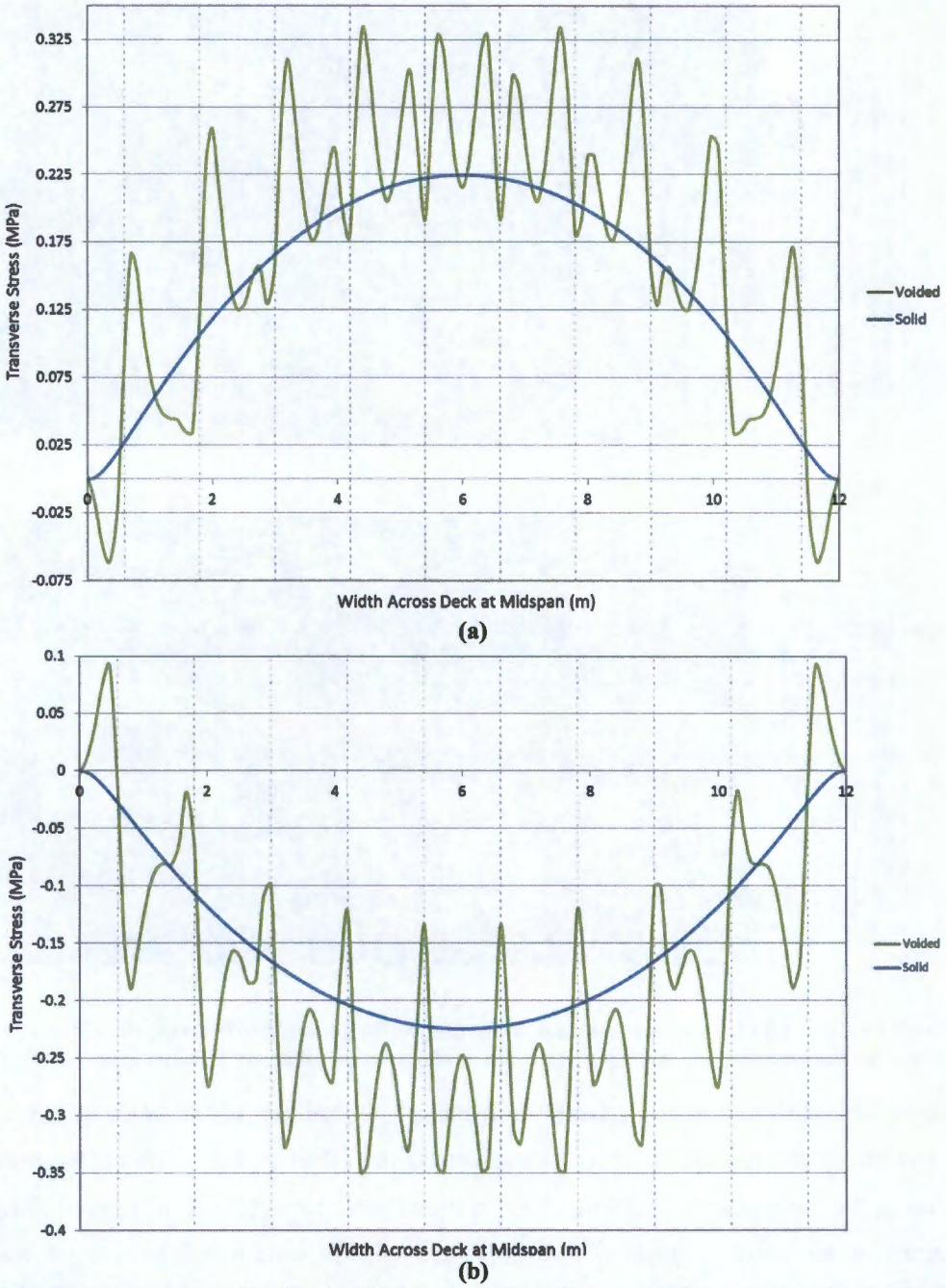

Figure 5.6 - Transverse stress distribution along a transverse line on (a) the extreme compression fibre (b) the extreme tension fibre of the voided and solid slab models at mid-span.

The large peaks in transverse stress on either side of the void centres on the top and bottom of the slab can clearly be seen in Figure 5.6, which result in the bands of high stress concentrations in Figure 5.4. The peak stresses are almost double in magnitude compared to the transverse stress of the solid slab at each peak stress location. The peak stresses on the top and bottom of the slab are also shown to be in the same vertical plane.

On the extreme compression fibre of the voided slab, there is a local decrease in stress at the location of the centre of the voids. The decrease in stress at the centre of the voids results in the lowest stresses across the width of the slab. At the locations of the webs on the extreme compression fibre, the

transverse stresses of the voided model converge to a local minimum stress at each web. The local minimum stresses at the location of the webs compare favourably with the transverse stresses of the solid slab.

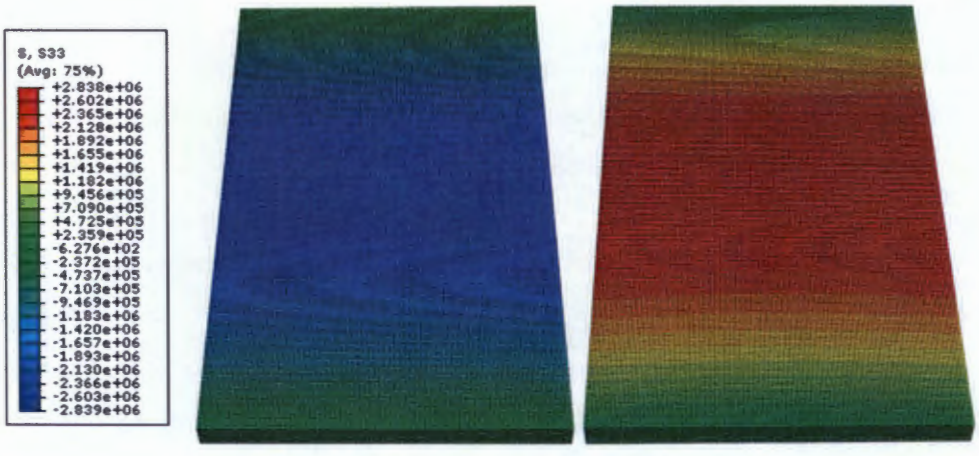

(a) (b)

Figure 5.7 - Longitudinal stress distribution from a solid slab finite element model on (a) the extreme compression fibre and (b) the extreme tension fibre of the deck.

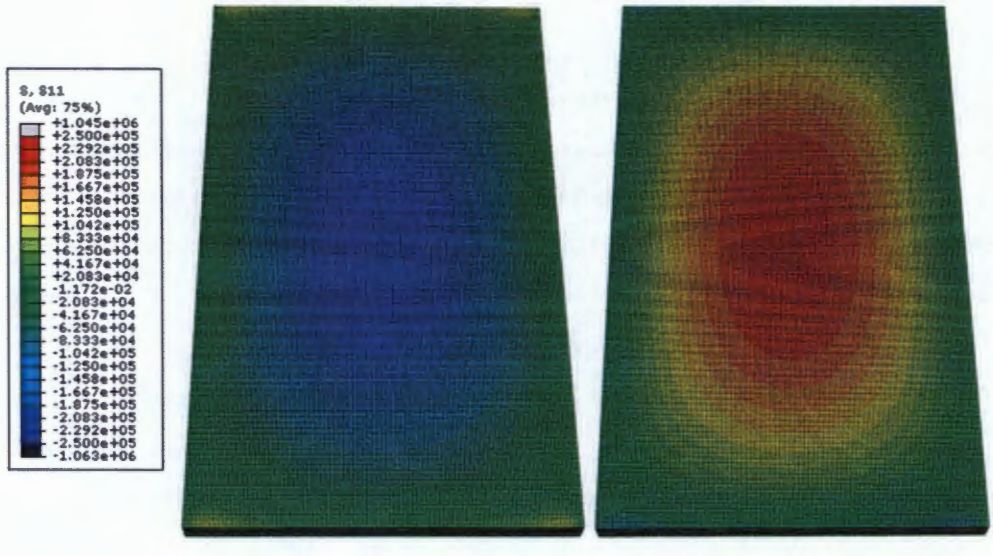

(a) (b)

Figure 5.8 - Transverse stress distribution from a solid slab finite element model on (a) the extreme compression fibre and (b) the extreme tension fibre of the deck.

On the extreme tension fibre of the voided slab, there is the same local decrease in transverse stress at the location of the centre of the voids as on the extreme compression fibre. The variation between the stresses at the centre of the voids and the peak stresses is much greater on the extreme tension fibre than the extreme compression fibre. The transverse stress on the tension fibre of the voided model converges to a local minimum at the location of the webs, however the transverse stresses compare less favourably with the solid model than on the extreme compression fibre, with the voided model having the greater transverse stresses.

Therefore it can be seen that the addition of the voids leads to peak transverse stresses on both the extreme compression and tension fibre of the deck on either side of the centre of each void. There is

a decrease in the transverse stresses from the peak stresses to the location of the centre of the voids, and this decrease is greater on the extreme tension fibre. The transverse stresses at the web locations compare most favourably with the transverse stresses of the solid model.

The reason for this distribution of transverse stresses can be explained by considering the distortion of the cross-section, and the bending of the flanges above and below the voids about their local axes. As the top flange above the voids bends about its local axis, the stresses caused by local bending result in a reduction in the transverse stresses due to global bending of the slab at the centre of the void. The local bending results in an increase in the transverse stresses in the flange on either side of the void centre, which results in the peak transverse compression stresses. A large compression stress is also present at the top of the void perimeter, which is again due to local bending of the flange above the void.

As the bottom flange bends about its local axis, it causes a reduction in the global tension stress on the bottom fibre of the deck at the centre of the void. As with the top flange, the local bending results in an increase in the transverse stresses in flange on either side of the void centre, resulting in the peak transverse tension stresses. A large tension stress is also present at the base of the void perimeter. These effects can be seen by focusing on the transverse stress results at the centre of the slab in Figure 5.5 and Figure 5.6.

The webs between the voids are relatively stiff when compared to the flanges, and therefore undergo very little bending, which leads to the transverse stresses comparing favourably with the transverse stresses of the solid slab. The flanges over the voids are less stiff than the webs, and therefore undergo local bending about their local neutral axis. This bending causes the stress peaks where the transverse stress deviates from the parabolic function. As the solid models have no flanges to undergo local bending, there are no stress peaks in the transverse stress distribution, and the stresses follow the parabolic shape.

The voided model also experiences a tension stress on the top fibre at either end of the deck. This tension stress occurs in the flange above the voids, and is the result of the tension stress caused by local bending in the flange overcoming the compression stress due to the global bending of the slab, resulting in a net tension stress. The tension stresses are only present at the edge of the slab where compression stresses due to global bending are small. The same argument can be used to explain the compression stresses on the bottom fibre of the slab at either end of the slab.

The transverse stresses of the voided model are higher than the transverse stresses of the solid model across most of the deck. The solid model accounts for the decrease in moment of inertia due to the addition of the voids in the voided model through a reduced depth. Therefore it can be concluded that the increase in stresses is more than the expected increase from the decrease in moment of inertia, and there is a stress raising effect associated with the voids of a voided deck cross-section. This stress raising effect has the greatest influence on the transverse stresses, and is primarily due to the distortion of the cross-section.

Transition Zone

The rapid change in cross-section from the voided to the solid section of the deck can result in a complex stress distribution. The transverse stress distribution along the width on the top fibre of the deck at the point of transition for the voided model is shown in Figure 5.9 below. Results of the transverse stresses 0.5m on either side of the transition zone of the voided model, and where the transition zone would be in the solid model, are also presented for comparison.

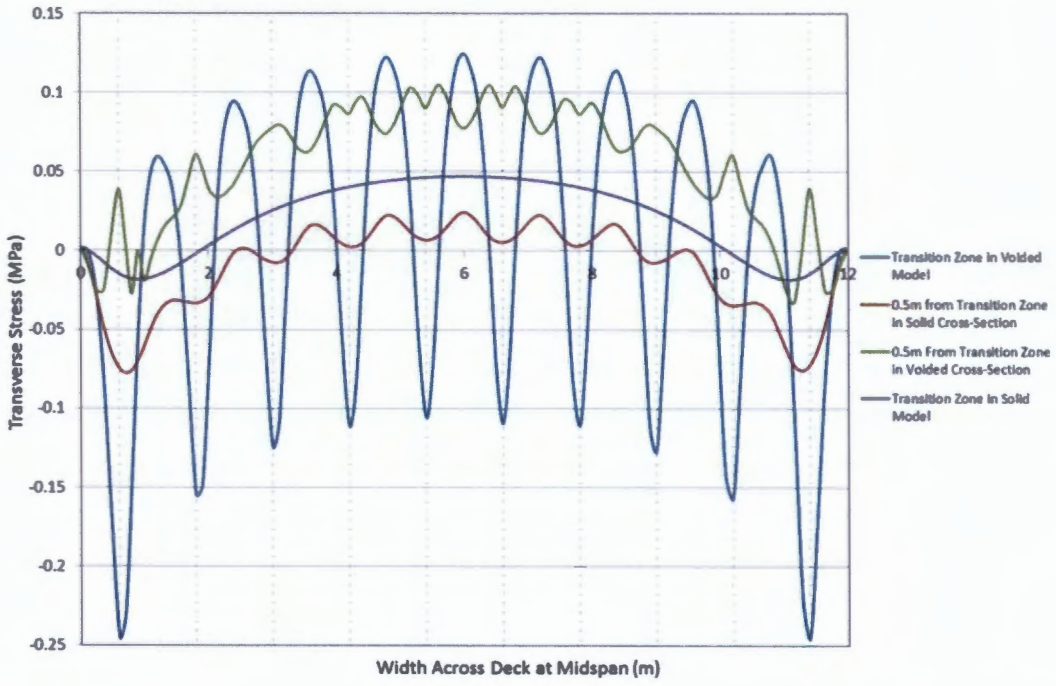

Figure 5.9 - Transverse stress distribution along a transverse line at the transition zone along the extreme compression fibre for the voided and solid FE models.

It can be seen that the transverse stress distribution at the transition zone of the voided model follows the same shape as the transverse stresses at mid-span, with variations in the typical parabolic shape due to the presence of the voids. The transverse stress also reverses continually along the width of the deck in the voided model, resulting in compression and tension stresses on the top of the deck.

The transverse stress distribution in the solid model at the point of transition follows a parabolic function, with no variation to this shape as with the voided models. The stress distribution consists of a negative stress on either end of the deck, and a maximum positive stress at the centre of the deck. Comparing the maximum transverse compression stresses for the voided and solid models shows that the transverse compression stresses are on average more than double in the voided model at the transition zone.

The transverse stresses 0.5m from the transition zone in the voided part of the cross-section are almost entirely in compression across the width of the deck, apart from either end of the deck. The magnitude of the maximum transverse stresses are 25% less than those of the maximum compression stresses at the transition zone, with no stress reverse present like at the transition zone. It has been shown

in Figure 5.4 that the transverse stresses increases in the longitudinal direction from zero at the supports to a maximum value at mid-span. The transverse stresses 0.5m from the transition zone in the voided part of the cross-section being less than the transverse stresses at the transition zone contradicts this result, indicating there is a local concentration of stresses at the transition zone.

It is also noted that the transverse stress distribution 0.5m from the transition zone in the solid part of the cross-section follows the same shape as that of the transverse stress distribution in the voided section, and does not follow a typical parabolic distribution like that of the solid model. This shows that the voids affect the distribution of stresses within the solid cross-section on either end of the deck. The magnitude of the maximum transverse stresses are also on average 80% less than the maximum transverse compressive stress at the transition zone.

A comparison of the stresses at the transition zone to the stresses at 0.5m either side of the transition in the voided model shows that there is an increase in stress at the change in cross-section. This result shows that the transition zone results in a high concentration of stresses, which is due to the complex behaviour brought on by the discontinuous geometry at the point of transition. Although the transition zone results in an increase in the transverse stresses than what would be expected, the transverse stresses at mid-span are greater than those at the transition zone and are therefore more critical for the analysis of voided slabs.

5.2. Effect of Void Diameter Ratio

This section will focus on the results of the finite element models used in *Phase 1*, where five voided slab models with void ratios ranging from 0.5 to 0.9 were analysed in order to determine the effect of the void diameter ratio on the structural behaviour of voided slab bridge decks.

Table 5.1 shows the moment of inertia of each of the five voided slab models used in this phase, as well as the percentage variation between the moment of inertia of each model compared to the 0.5 void diameter model. Figure 5.10 shows the exponential decrease in moment of inertia with an increase in void diameter ratio. As the flexural stresses are inversely proportional to the moment of inertia, the decrease in moment of inertia due to the increase in void diameter ratio will lead to an exponential increase in the longitudinal and transverse stress results, consequently it is the quantity which is examined in this section. The stress raising effect of the voids due to cross-sectional distortion will also be demonstrated.

Table 5.1 - Decrease in moment of inertia with increasing void diameter ratio for the models in *Phase 1*.

Model Name	Void Diameter Ratio	Moment of Inertia (m^4)	Percentage Variation (%)
A1	0.5	0.969	-
B1	0.6	0.936	3.4
C1	0.7	0.882	9.0
D1	0.8	0.798	17.6
E1	0.9	0.678	30.0

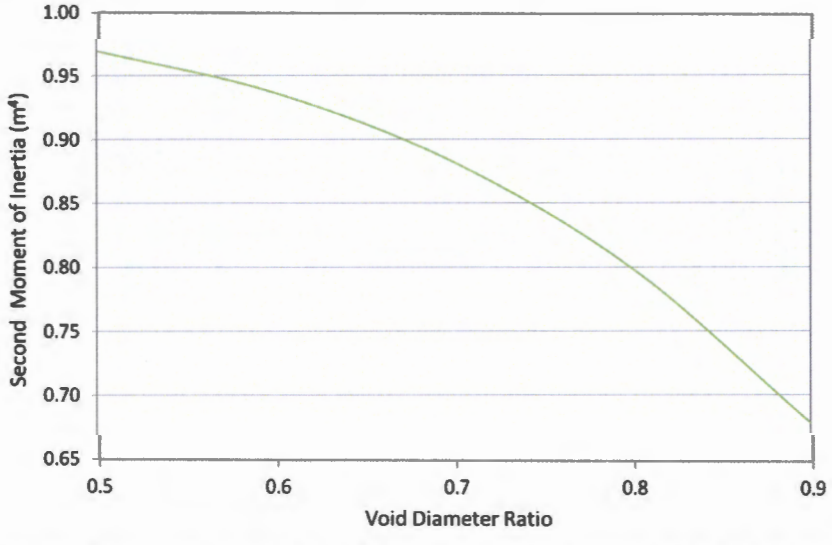

Figure 5.10 - Decrease in moment of inertia with increasing void diameter ratio for the models in *Phase 1*.

In order to determine the effect of the void diameter ratio on the longitudinal and transverse stresses of a voided slab, the stresses along the four critical locations were obtained from each of the finite element models. The effect of the void diameter ratio is demonstrated through comparisons of the stress results at these critical locations from each of the five finite element models.

Transverse Stresses along a Transverse Grid Line

Figure 5.11 presents a comparison of the transverse stress distribution for the five voided slab FE models and the five corresponding solid slab FE models along a transverse line at the mid-width along the extreme compression fibre of the deck. Each of the solid and voided models follows the same respective transverse stress distributions as discussed in Section 5.1, with the solid slab models following a parabolic shape, and the voided slab models exhibiting local variations to the parabolic shape.

Comparing the results from the models, it can be seen that the transverse stresses of both the solid and voided models increase with an increase in the void diameter ratio. The stress increase for the solid models occurs across the width of the deck with an increase in void diameter ratio. For the voided models, the increase in void diameter ratio results in an increase in the peak stresses. However, the stresses at the centre of the voids and the webs typically remain relatively constant. These stress increases are attributed to the decrease in moment of inertia and increase in cellular distortion associated with an increase in void diameter ratio. All of the voided models experience a tension stress at either end of the deck, with the 0.9 void diameter ratio model experiencing a tension stress between the first and second void from either end of the slab. These tension stresses are the result of local bending in flanges, which increases with an increase in void diameter ratio.

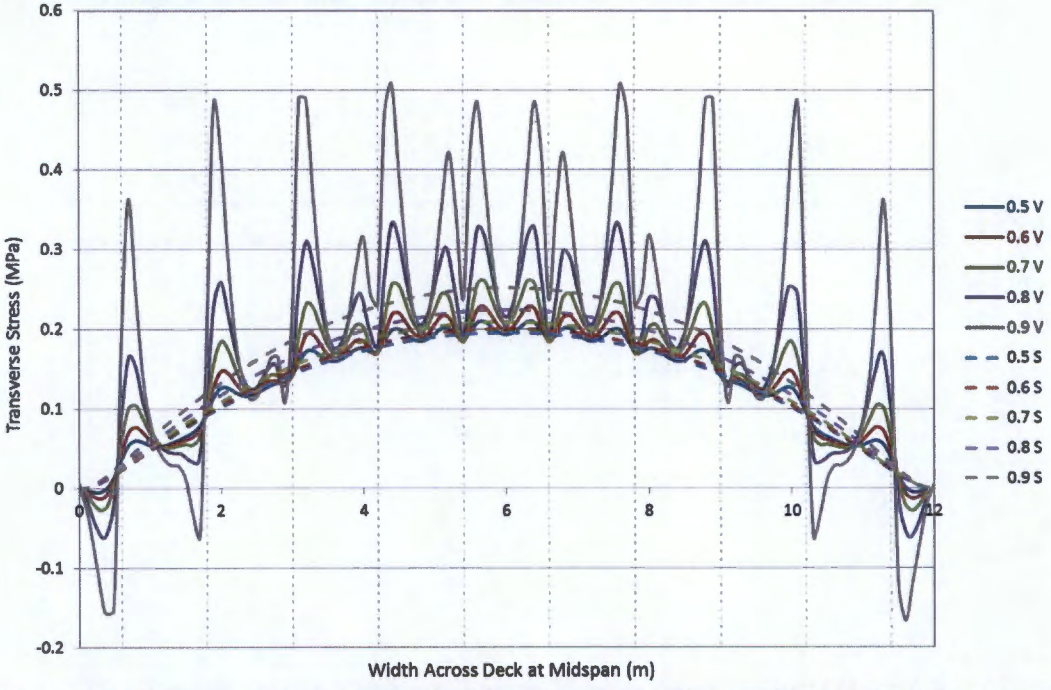

Figure 5.11 – Transverse stress distribution along a transverse line at mid-span along the extreme compression fibre for the Voided and Solid FE Models.

Figure 5.12 shows the transverse stress distribution for five voided slab FE models and the corresponding solid slab FE models along a transverse line at mid-width along the extreme tension fibre of the deck. As with the transverse stresses on the compression fibre, the transverse stresses on the bottom fibre of the voided and solid models increase with an increase in void diameter ratio. For the voided models, the increase in void diameter ratio results in an increase in the peak stresses, as with the stresses on the compression fibre. However, the stresses at the centre of the voids and webs decrease and

increase respectively with the increase in void diameter ratio. All of the models experience a compression stress at either end of the deck, which is due to the same reason as the tension stresses developed on the compression fibre described above.

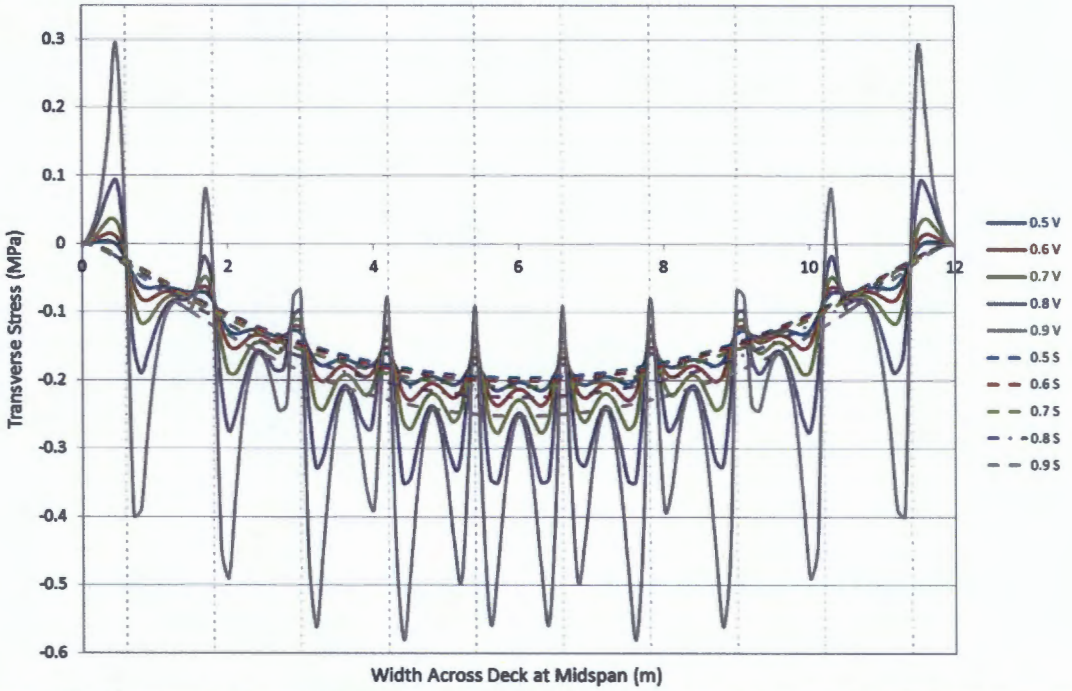

Figure 5.12 - Transverse stress distribution along a transverse line at mid-span along the extreme tension fibre of the deck for the Voided and Solid FE Models.

In order to study the effects of the voids, and an increase in the void diameter ratio, the stresses at three key locations along the compression and tensions fibres of the transverse line were studied. These locations included the centre of the middle web, the centre of the middle peak stress, and the centre of the middle void, as shown in Figure 5.13. A comparison of the transverse stresses for the solid and voided models at these key locations are summarised in Table 5.2.

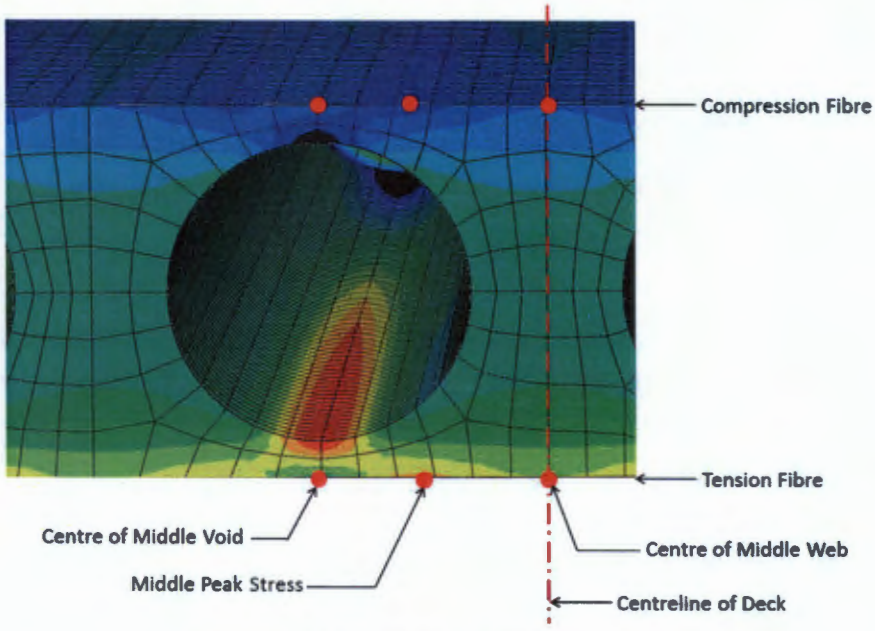

Figure 5.13 - Locations of critical stress results.

Table 5.2 - Transverse stresses at key locations on the top and bottom fibres of the voided and solid FE models.

Void Diameter Ratio	Location of stresses	Voided Slab			Solid Slab		
		Stress at centre of middle web (MPa)	Stress at centre of middle void (MPa)	Stress at centre of middle peak (MPa)	Stress at centre of middle web (MPa)	Stress at centre of middle void (MPa)	Stress at centre of middle peak (MPa)
0.5	Top	0.193	0.187	0.210	0.196	0.194	0.195
	Bottom	-0.203	-0.176	-0.215	-0.196	-0.194	-0.195
0.6	Top	0.199	0.184	0.228	0.201	0.199	0.200
	Bottom	-0.213	-0.166	-0.237	-0.201	-0.199	-0.200
0.7	Top	0.207	0.184	0.261	0.209	0.207	0.209
	Bottom	-0.228	-0.154	-0.277	-0.210	-0.207	-0.209
0.8	Top	0.215	0.191	0.328	0.225	0.222	0.224
	Bottom	-0.248	-0.133	-0.350	-0.225	-0.222	-0.224
0.9	Top	0.203	0.238	0.486	0.252	0.250	0.252
	Bottom	-0.251	-0.092	-0.557	-0.252	-0.250	-0.252

It is evident from Figure 5.11 and Figure 5.12 that an increase in void diameter ratio causes large variations to the transverse stresses across the width of the deck. Table 5.3 shows a comparison between the stresses at the centre of the middle void, and the centre of the middle peak to the stress at the centre of the middle web for the voided and solid models.

The top fibre stresses at the centre of the void are 3.2%, 8.2%, 12.5%, 12.6% and -14.7% smaller than the top stresses at the centre of the middle webs for the 0.5 to 0.9 void diameter ratio models. The top fibre stresses at the middle peaks are 8.1%, 12.7%, 20.7%, 34.5% and 58.2% greater than top stresses at the centre of the middle webs. It can be seen that the top fibre stresses at the centre voids and at the middle peaks decrease and increase respectively when compared to the stresses at the centre of the middle voids, which is the result of the local bending of the flange above the voids. A discrepancy was noted on the 0.9 void diameter ratio model, where the top fibre stress is greater at the centre of the middle void than the web, which is attributed to the thin flange above the void.

The bottom fibre stresses at the centre of the middle void are 15.3%, 28.3%, 48.1%, 86.5% and 172.8% smaller than bottom fibre stresses at the centre of the middle webs. The bottom stresses at the peaks are 5.6%, 10.1%, 17.7%, 29.1% and 54.9% greater than bottom stresses at the centre of the voids. Therefore the bottom fibre stresses follow the same trend as the top fibre stresses in this regard. These variations, which can clearly be seen in Figure 5.11 and Figure 5.12, are as a result of the local bending of the flanges which is shown to increase with increasing void diameter ratio. It can also be seen from Table 5.3 that the stresses are relatively constant at each location in the solid models.

Table 5.3 - Comparison of transverse stresses at the centre of the middle void and middle peak stress to the stress at the middle web for the voided and solid FE models.

Void Diameter Ratio	Location of stresses	Comparisons of transverse stresses (Void and Peak) to centre web stresses			
		Voided Slab		Solid Slab	
		Void	Peak	Void	Peak
0.5	Top	3.2	-8.1	1.0	0.5
	Bottom	15.3	-5.6	1.0	0.5
0.6	Top	8.2	-12.7	1.0	0.5
	Bottom	28.3	-10.1	1.0	0.5
0.7	Top	12.5	-20.7	1.0	0.0
	Bottom	48.1	-17.7	1.4	0.5
0.8	Top	12.6	-34.5	1.4	0.4
	Bottom	86.5	-29.1	1.4	0.4
0.9	Top	-14.7	-58.2	0.8	0.0
	Bottom	172.8	-54.9	0.8	0.0

In order to determine the effect of the void diameter ratio on the transverse stresses, the transverse stresses at each different void diameter ratio were compared to the results of the 0.5 void diameter ratio model at each key location. The results of these comparisons are shown in Table 5.4.

Table 5.4 – Comparison of top and bottom transverse stresses for the voided and solid FE models for different void diameter ratios.

Void Ratio	Location of stresses	Voided Slab			Solid Slab		
		Comparison at centre of middle web (%)	Comparison at centre of middle void (%)	Comparison at centre of middle peak (%)	Comparison at centre of middle web (%)	Comparison at centre of middle void (%)	Comparison at centre of middle peak (%)
0.5	Top	-	-	-	-	-	-
	Bottom	-	-	-	-	-	-
0.6	Top	3.0	-1.6	7.9	2.5	2.5	2.5
	Bottom	4.7	-6.0	9.3	2.5	2.5	2.5
0.7	Top	6.8	-1.6	19.5	6.2	6.3	6.7
	Bottom	11.0	-14.3	22.4	6.7	6.3	6.7
0.8	Top	10.2	2.1	36.0	12.9	12.6	12.9
	Bottom	18.1	-32.3	38.6	12.9	12.6	12.9
0.9	Top	4.9	21.4	56.8	22.2	22.4	22.6
	Bottom	19.1	-91.3	61.4	22.2	22.4	22.6

As the void diameter ratio increases from 0.5 to 0.9, the top fibre transverse stresses at the middle web are relatively constant, and differ by 10.2%. The top fibre stresses at the centre of the middle void increase by 1.6%, 1.6%, 2.1%, and 21.4% as the void diameter ratio increases from 0.5 to 0.9. The top fibre stresses at the centre of the peaks increase by 7.9%, 19.5%, 36.0%, and 56.8% as the void diameter ratio increases from 0.5 to 0.9. It is noted that the top fibre stresses increase exponentially at the peak locations with an increase in void diameter ratio. The stresses at the centre of the voids is relatively constant, with a discrepancy noted in the 0.9 void diameter ratio model.

These results show that the webs are relatively stiff compared to the flanges and therefore undergo very little bending. The flanges undergo bending about their local axes resulting in a high stress concentration, which shows that the least stiff part of the cross-section attracts higher moments. The increase in stresses at the peaks is due to both local bending and the decrease in moment of inertia, both of which increase with increasing void diameter ratio. The transverse stresses in the solid models increase with an increase in voided diameter ratio, and this increase is constant at each location. This increase is the result of the decrease in the moment of inertia.

The bottom fibre stresses at the centre of the middle web increase by 4.7%, 11.0%, 18.1%, and 19.1% as the void diameter ratio increases from 0.5 to 0.9. The bottom fibre stresses at the centre of the middle void decrease by 6.0%, 14.3%, 32.3%, and 91.3% as the void diameter ratio increases from 0.5 to 0.9. The bottom fibre stresses at the centre of the middle peak increase by 9.3%, 22.4%, 38.6%, and 61.4% as the void diameter ratio increases from 0.5 to 0.9. It is noted that the bottom fibre stresses at the centre of the voids and the peak locations increase exponentially with an increase in void diameter ratio.

The bottom fibre stresses at the middle webs increase in a similar manner to the solid model stress results, indicating that the stress increase is related to the decrease in moment of inertia and not cross-section distortion. The increase in stress at the location of the peaks is due to the reduction in moment of inertia and cellular distortion, which increases exponentially with an increase in void diameter ratio. The stresses at the centre of the voids decrease exponentially with an increasing void diameter ratio. This decrease shows that local bending, which causes a reduction in tension stresses along the bottom of the slab at the centre of the voids as explained in Section 5.1, increases with increasing void diameter ratio. As with the top fibre stresses, the bottom fibre stresses in the solid model increase by the same amount at each location with increasing void diameter, and are only influenced by the moment of inertia.

Table 5.5 compares the top and bottom fibre stresses of the solid and voided models at each of the key locations. The top fibre stresses in the voided models at the centre of the middle web are 4.9%, 6.6%, 9.2%, 13.3%, and 19.1% lower than the bottom for each respective void diameter ratio. The top stresses in the voided models at the centre of the middle void are 6.3%, 10.8%, 19.5%, 43.6%, and 158.7% higher than the bottom for each respective void diameter ratio. The top and bottom stresses at

the middle peak of the voided model are relatively constant and differ by between 2.3% and 12.7%, with the bottom stresses being greater than the top stresses.

These results show that for a constant void diameter ratio, the presence of the voids causes the bottom flange to be more stressed than the top flange at the centre of the webs and at the peak stresses. The top flange is more stressed at the centre of the voids than the bottom flange for each void diameter ratio.

Table 5.5 – Comparison of top and bottom stresses for the voided and solid FE models at key locations

Void Ratio	Voided Slab			Solid Slab		
	Comparison at centre of middle web (%)	Comparison at centre of middle void (%)	Comparison at centre of middle peak (%)	Comparison at centre of middle web (%)	Comparison at centre of middle void (%)	Comparison at centre of middle peak (%)
0.5	4.9	-6.3	2.3	0.0	0.0	0.0
0.6	6.6	-10.8	3.8	0.0	0.0	0.0
0.7	9.2	-19.5	5.8	0.5	0.0	0.0
0.8	13.3	-43.6	6.3	0.0	0.0	0.0
0.9	19.1	-158.7	12.7	0.0	0.0	0.0

In order to compare the effects of the presence of the voids, the stresses at each of the key locations of the voided models were compared to those of the solid models. These comparisons are shown in Table 5.6.

The top fibre stresses at the centre of the middle web of the voided models are 1.6%, 1.0%, 1.0%, 4.7%, and 24.1% lower than the top stresses in the solid models for the respective void diameter ratios. The top fibre stresses at the centre of the middle void of the voided models are 3.7%, 8.2%, 12.5%, 16.2%, and 5.0% lower than the top stresses in the solid models for the respective void diameter ratio. The top stresses at the middle peak in the voided models are 7.1%, 12.3%, 19.9%, 31.7%, and 48.1% higher than the top stresses in the solid models for the respective void diameter ratio. It is noted that the addition of the voids causes a reduction in top stress at the centre of the webs and the voids, and these stresses decrease exponentially with increasing void ratio. As the solid models have a reduced moment of inertia that corresponds to the reduction in moment of area of the corresponding voided models, the stress variations can be attributed to the effect of the voids.

The bottom fibre stresses at the middle webs in the voided models are 3.4%, 5.6%, 7.9%, 9.3%, and 0.4% higher than the bottom fibre stresses in the solid models for the respective void diameter ratio. It is assumed that the outlying result of the 0.9 void diameter ratio model is due to the unreasonably thin webs resulting from the high void diameter ratio. The bottom stresses at centre of the webs of the voided models are shown to be in good agreement to the solid models, with a difference of less than 10%. The bottom fibre stresses at the middle void in the voided models are 10.2%, 19.9%, 34.4%, 66.9%, and

171.7% lower than the top fibre stresses in the solid models for the respective void diameter ratio. The bottom fibre stresses at the middle peak in the voided models are 9.3%, 15.6%, 24.5%, 36.0%, and 54.8% higher than the top fibre stresses in the solid models for the respective void diameter ratio.

Table 5.6 – Comparison of voided and solid FE results at key locations, and comparison of peak and void stresses to web stresses.

Void Ratio	Location of stresses	Comparison of voided and solid slab stresses		
		Comparison at centre of middle web (%)	Comparison at centre of middle void (%)	Comparison at centre of middle peak (%)
0.5	Top	-1.6	-3.7	7.1
	Bottom	3.4	-10.2	9.3
0.6	Top	-1.0	-8.2	12.3
	Bottom	5.6	-19.9	15.6
0.7	Top	-1.0	-12.5	19.9
	Bottom	7.9	-34.4	24.5
0.8	Top	-4.7	-16.2	31.7
	Bottom	9.3	-66.9	36.0
0.9	Top	-24.1	-5.0	48.1
	Bottom	-0.4	-171.7	54.8

It is noted that the addition of the voids causes a reduction in the bottom fibre stresses at the centre of the voids, which increase exponentially with increasing void ratio. The bottom stress at the centre of the webs of the voided models compares favourably with the stresses in the solid models.

The comparison of the peak stress values between the solid and voided models in Table 5.6 gives an indication of the variation of the transverse stress from the average value that may be expected in the cross-section of a solid slab. It is evident that transverse stresses over the voids can be much greater than the average transverse stresses in a solid slab, which can be attributed to the local bending in the flanges.

The effect of the voids on the transverse stresses along a transverse line at mid-span can be summarised as follows:

- The addition of the voids causes large transverse stress increases at 0.4m offsets from the centre of the voids on both the top and bottom fibres of the deck.
- In general, the transverse stresses on the top and bottom fibres increase rapidly with an increase in void diameter ratio. This is due to the reduced moment of inertia and local bending of the flanges.
- The transverse stresses along the top fibre of the voided models are smaller than the transverse stresses along the bottom fibre both at the centre of the webs and at the location of the peak stresses. The transverse stresses along the top fibre of the voided models are greater than the

transverse stresses along the bottom fibre at the centre of the voids. These variations increase rapidly with increasing void diameter ratio.

- For a constant void diameter ratio, the transverse stresses along the top and bottom fibres of the voided models are smaller than the transverse stresses of the solid models at the centre of the webs and voids. The discrepancy to this rule is the transverse stresses along the bottom fibre at the centre of the webs, which are greater in the voided model compared to the solid model. These effects increase with increasing void diameter ratio.

Longitudinal Stresses along a Transverse Grid Line at Mid-span

Figure 5.14 shows the longitudinal stress distribution on the extreme compression fibre along a transverse line at mid-span for the five voided slab FE models and corresponding solid slab FE models. The longitudinal stress distribution of each model follows a linear progression across the width of the deck, with a maximum variation of 6% between the ends of the deck. The stress distribution is therefore linear across the width of the deck for both the solid and voided slab models.

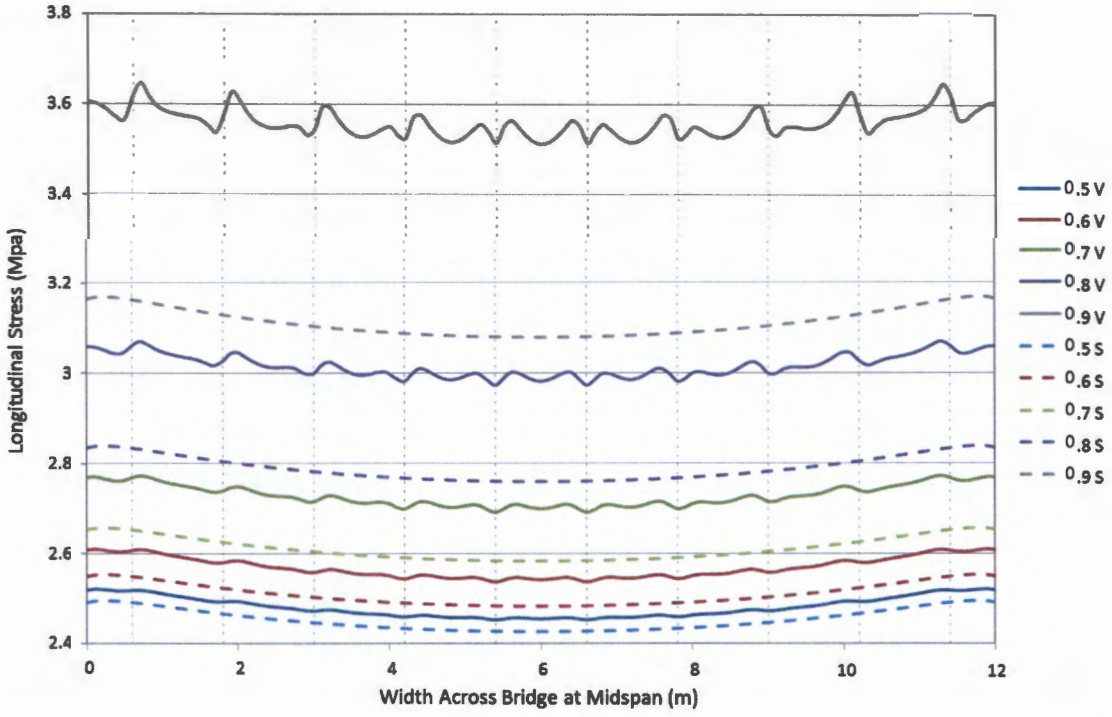

Figure 5.14 - Longitudinal stress distribution along the extreme compression fibre at mid-span for the voided and solid FE models.

The effect of the presence of the voids on the longitudinal stress distribution can be seen by comparing the results of the voided models with corresponding solid models. The voids cause the stresses to vary from the parabolic shape, resulting in localised peaks and dips across the width of the slab. However, these peaks and dips vary less than 6% than the average longitudinal stress of the models, thus the voids have a negligible effect on the shape of the longitudinal stress distribution.

Table 5.7 summarises the peak longitudinal stresses at the centre of the deck along the top fibre for the solid and voided models. Percentage comparisons are also shown between the peak stresses of the voided models to the 0.5 void diameter ratio, as well as a comparison between the peak stresses of the voided and solid models.

Table 5.7 - Longitudinal stresses at the centre of the slab on the top fibre of the voided and solid FE models, as well as comparisons between the voided model results, and solid and voided model results.

Void Diameter Ratio	Location of stresses	Peak Stress at centre of voided slab (MPa)	Peak Stress at centre of solid slab (MPa)	Comparison of peak stress to 0.5 void ratio model (%)	Comparison of voided and solid stresses (%)
0.5	Top	2.45	2.43	-	0.8
0.6	Top	2.54	2.48	3.5	2.4
0.7	Top	2.70	2.58	9.3	4.7
0.8	Top	2.98	2.76	17.8	8.5
0.9	Top	3.51	3.08	30.2	14.0

Using Table 5.7 and Figure 5.14, the effect of the void diameter ratio on the longitudinal stresses is evident. There is an exponential increase in longitudinal stress with an increase in void diameter ratio. As the void diameter ratio increases from 0.5 to 0.9, the top fibre longitudinal stresses increase by 3.5%, 9.3%, 17.8%, and 30.2% respectively. The exponential increase in longitudinal stress with increasing void diameter ratio is clear in Figure 5.14.

The effect of the voids on the longitudinal stresses becomes more evident with comparisons between the solid and voided models. The longitudinal stresses in the voided models are 0.8%, 2.4%, 4.7%, 8.5%, and 14.0% higher than the longitudinal stresses in the solid models for the respective void diameter ratio. As the solid models have a reduced moment of inertia that equals that of the corresponding voided slab, the increased stress of the voided models compared to the solid slabs is due to the presence of the voids.

The longitudinal stresses along the bottom fibre of the models follow the same distribution and magnitude as the longitudinal stresses on the top of the slab, with the only difference being tension as opposed to compression. For this reason, the longitudinal stress distribution on the tension fibre is not shown. The effect of the voids on the longitudinal stresses along a transverse line at mid-span can be summarised as follows:

- Local bending in the flanges causes local variations in the parabolic shape of the longitudinal stress distribution, however these variations are negligible.
- The longitudinal stresses increase rapidly with an increase in void diameter ratio. This is due to the reduced moment of inertia, and the stress raising effect of the voids.

- For a constant void diameter ratio, the longitudinal stresses of the voided model are greater than those of the solid slab model. Since the solid models account for the decreased moment of inertia, there is a stressing effect associated with the incorporation of the voids.
- The longitudinal stresses in the top and bottom flanges are equal in magnitude and opposite in sign in both the voided and solid models.

Transverse Stresses along a Longitudinal Grid Line

Figure 5.15 shows the transverse stress distribution for the five voided slab FE models and the five corresponding solid slab FE models along the centreline of the extreme compression fibre of the deck. For each model, the transverse stress distribution follows a parabolic shape across the width of the deck, with the stresses being in compression along the length of the deck. A peak transverse stress occurs at 1.0m from either end of the deck in the voided models, which does not occur in the solid models. This variation is incurred by the rapid change from voided to solid section at this location, which gives rise to a stress variation, which is not present in the solid models.

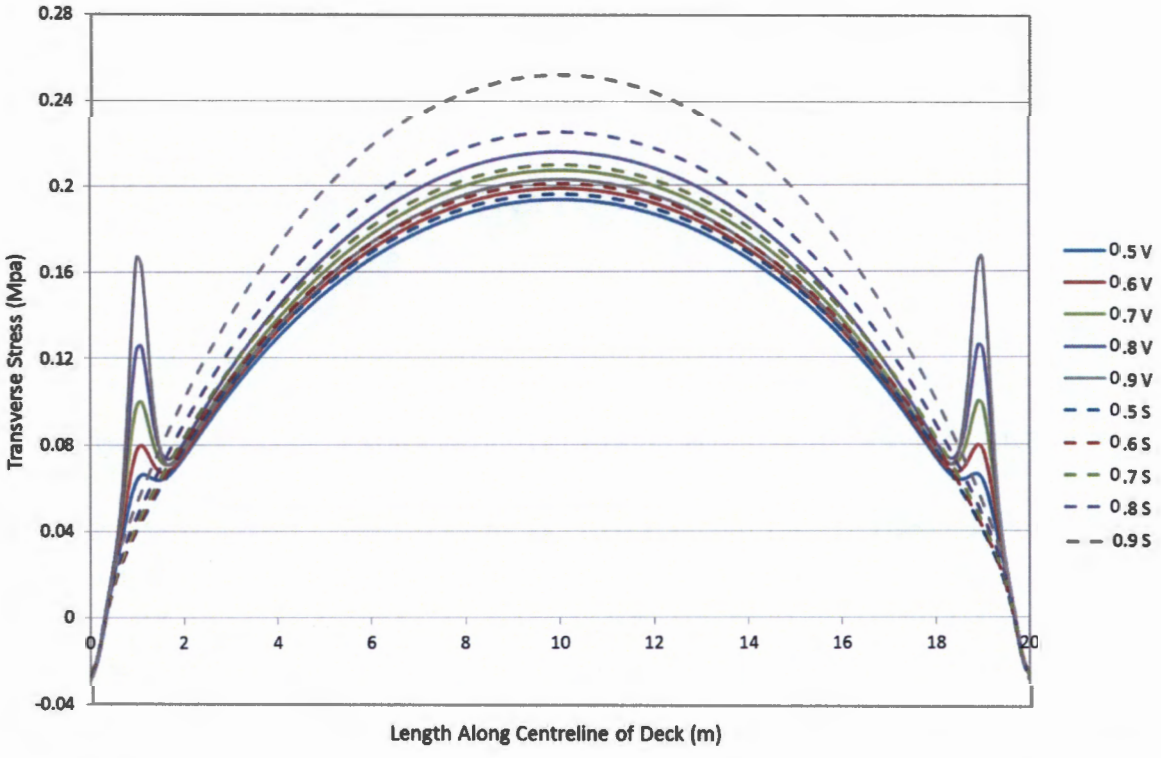

Figure 5.15 - Transverse stress distribution along the centreline of the compression fibre for the voided and solid FE models.

The top transverse stress increases with an increase in void diameter ratio for both the solid and voided models, apart from the 0.9 void diameter model where the stress decreases causing the results to lie between the 0.6 and 0.7 void diameter models. The reason for this decrease in the 0.9 void diameter ratio can be explained by studying the transverse distribution of stresses along the mid-width of the deck

shown in Figure 5.11. The voided models predict stresses that are less than the corresponding solid models. It can also be seen that the variation between the voided and solid models increases with increasing void diameter ratio.

Figure 5.16 shows the transverse stress distribution for five voided slab FE models and the corresponding solid slab FE models along the centreline of the extreme tension fibre. The graphs follow the same parabolic shape as the top transverse stress distribution, with the stresses being reversed from compression to tension.

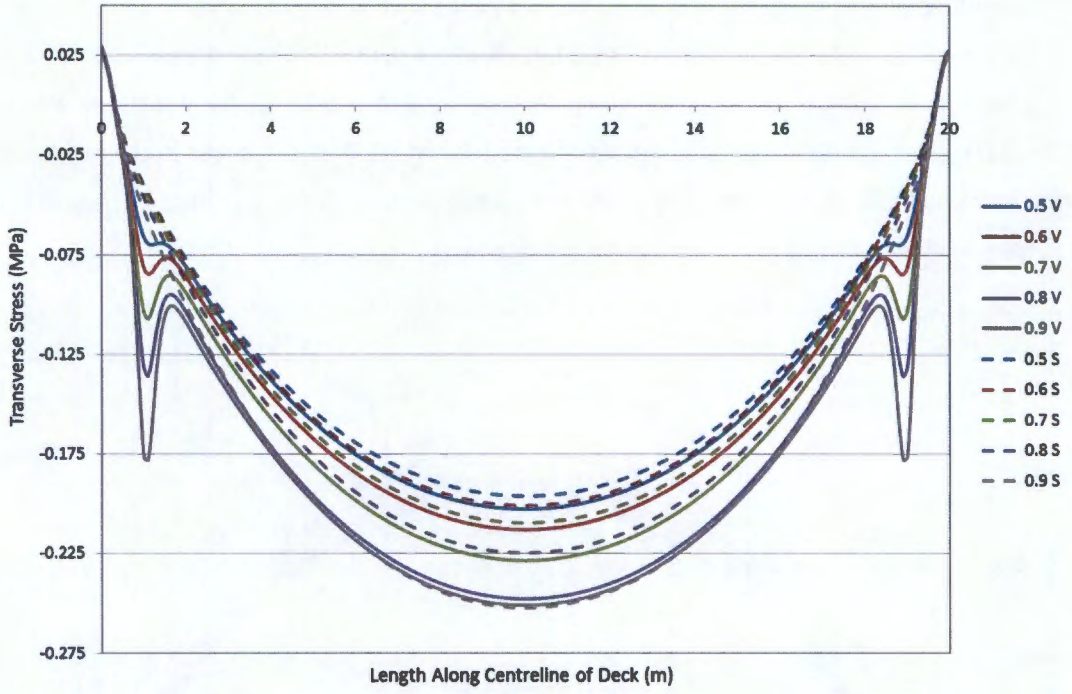

Figure 5.16 - Transverse stress distribution along the centreline of the tension fibre for the voided and solid FE models.

The transverse stresses on the tension fibre increase with an increase in void diameter ratio. The voided models also predict transverse stresses which are greater than those predicted by the solid models, which is the opposite for the transverse stresses along the compression fibre. The variation between the voided and solid models also increases with an increase in void diameter ratio, apart from the 0.9 void diameter model where the voided and solid models are in good agreement.

It can be seen that the voids cause a reduction in the stresses on the compression fibre, and an increase in stresses in the bottom flange when compared to the results of the solid models. These variations have been shown to increase with increasing void diameter ratio in Figure 5.15 and Figure 5.16. It should be noted that the centreline of the slab lies at the position of a web within the voided cross-section, and the stress results are in agreement with the trends discussed above for the transverse stresses along a transverse line at mid-span. It can be concluded that the transverse stress distribution along a longitudinal line is highly dependent on the location of where the results are presented.

The effect of the voids on the transverse stress distribution along the centreline of the bridge can be summarised as follows:

- The stresses along the tension fibre increase at a greater rate than the stresses along the compression fibre for each void diameter ratio, and this variation increases with increasing void diameter ratio.
- For a constant void diameter ratio, the stresses in the top flange of a voided model are lower when compared to a solid model. The stresses in the bottom flange of the voided model are greater when compared to a solid model with the same void diameter ratio. This is due to direction of localised bending in the flanges.
- The transverse stresses along both the compression and tension fibres increase with an increase in void diameter ratio. This is due to the reduced moment of inertia and the stress raising effect of the voids.

Longitudinal Stresses along a Longitudinal Grid Line

Figure 5.17 shows the longitudinal stress distribution for the five voided slab FE models and the five corresponding solid slab FE models along the centreline of the compression fibre of the deck. For each model, the longitudinal stress distribution follows a parabolic shape across the length of the deck, with the stress being in compression across the width of the deck. The longitudinal stresses of all the models converge at 1.0m from either end of the deck, which is due to the solid sections at each end of the deck. As the solid sections are the same on all the models, the results converge at these sections.

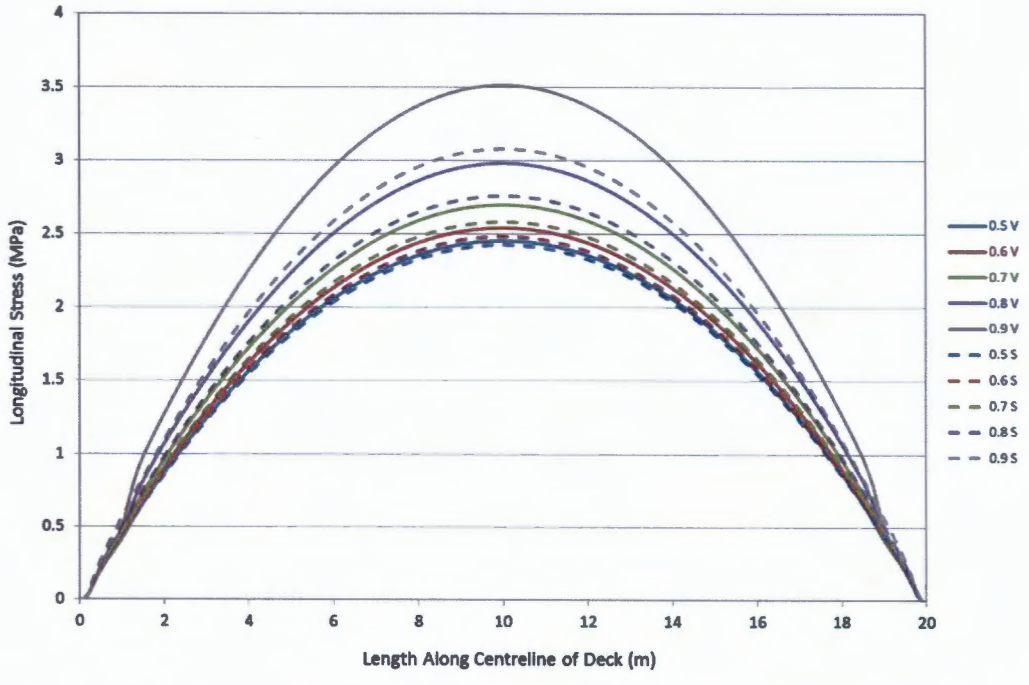

Figure 5.17 - Longitudinal stress distribution along the centreline of the compression fibre for the voided and solid FE models.

It can be seen that the longitudinal stress increases exponentially with an increase in void diameter ratio. The voided models predict longitudinal stresses which are greater than those predicted by the solid models. The variation between the voided and solid models increases with the increase in void diameter ratio. As the solid models have a reduced moment of inertia that equals that of the corresponding voided slab, the longitudinal stress increase in the voided models is due to the stress raising effect of the voids.

The longitudinal stresses along the bottom fibre of the deck are equal in magnitude and opposite in sign to the longitudinal stresses along the top fibre of the deck. Therefore these results are of little interest and are not presented here.

The effect of the voids on the longitudinal stresses along the centreline of the bridge can be summarised as follows:

- The longitudinal stresses along the top and bottom fibres increase exponentially with an increase in void diameter ratio. This is due to the reduced moment of inertia, and the stress raising effect associated with the voids.
- The variation between the longitudinal stresses predicted by voided and solid models increases with an increase in void diameter ratio.

5.3. Effect of Void Spacing

This section will focus on the results of the finite element models used in *Phase 2*. Nine voided slab models with void spacing ranging from 0.9m to 2.7m were analysed in order to determine the effect of void spacing on longitudinal and transverse stress distributions of a voided slab.

Table 5.8 shows the moment of inertia of each of the nine models used in this phase, as well as the percentage variation between the moment of inertia of each model compared to the 1.2m void spacing model. It can be seen that the moment of inertia is not as sensitive to variations in void spacing as to the void diameter ratio. The moment of inertia varies by 2.5% with the addition of each void, which is used to obtain the required spacing of the voids. The effect of the void spacing on the moment of inertia is shown in Figure 5.18.

Table 5.8 – Variation in moment of inertia with different void spacing for the FE models in *Phase 2*.

Model Name	Void Diameter Ratio	Void Spacing (m)	Number of Voids	Moment of Inertia (m^4)	Percentage Difference of Moment of inertia (%)
O	0.8	0.90	13	0.739	-7.55
N	0.8	0.98	12	0.759	-5.03
R	0.8	1.08	11	0.779	-2.52
C	0.8	1.20	10	0.799	-
L	0.8	1.35	9	0.819	2.52
M	0.8	1.54	8	0.839	5.03
K	0.8	1.80	7	0.859	7.55
P	0.8	2.16	6	0.879	10.07
Q	0.8	2.70	5	0.899	12.58

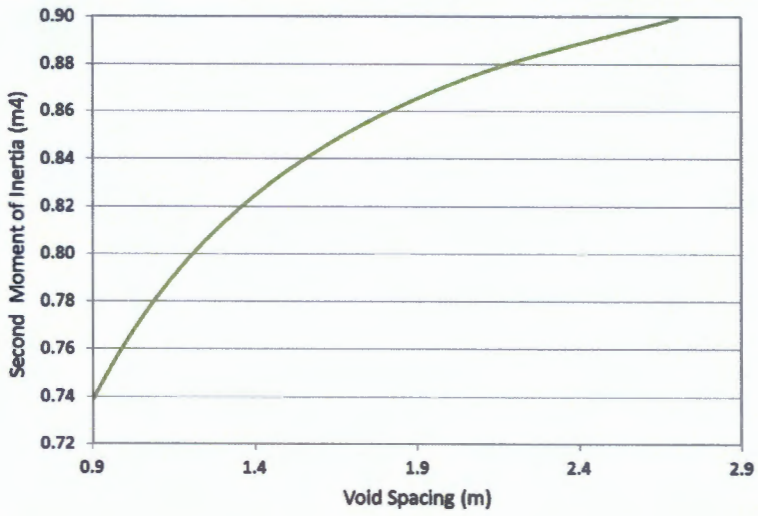

Figure 5.18 - Variation in moment of inertia for different void spacing for the models in *Phase 2*.

In order to determine the effect of the void spacing on the longitudinal and transverse stresses of a voided slab, the stresses along the four critical locations were obtained from each of the finite element models. The stresses at these critical locations are discussed below.

Transverse Stresses along a Transverse Grid Line

Figure 5.19 shows the transverse stress distribution along a transverse line at mid-span on the extreme compression fibre for the voided and corresponding solid slabs with an odd number of voids, with the 1.35m void spacing model used as baseline for comparison. As the locations of the voids in each model vary, so do the locations of the peak stresses, making it difficult to identify trends. For this reason, the models with an odd and even number of voids have been separated and compared to a baseline to allow for an easier interpretation of the results. The centre of the width of the deck represents the centre of a void for the models with an odd number of voids, and the centre of a web in the models with an even number of voids. Figure 5.20 shows the transverse stress distribution along a transverse line at mid-span on the extreme compression fibre for the voided and corresponding solid slabs with an even number of voids, with the 1.2m void spacing model used as baseline for comparison.

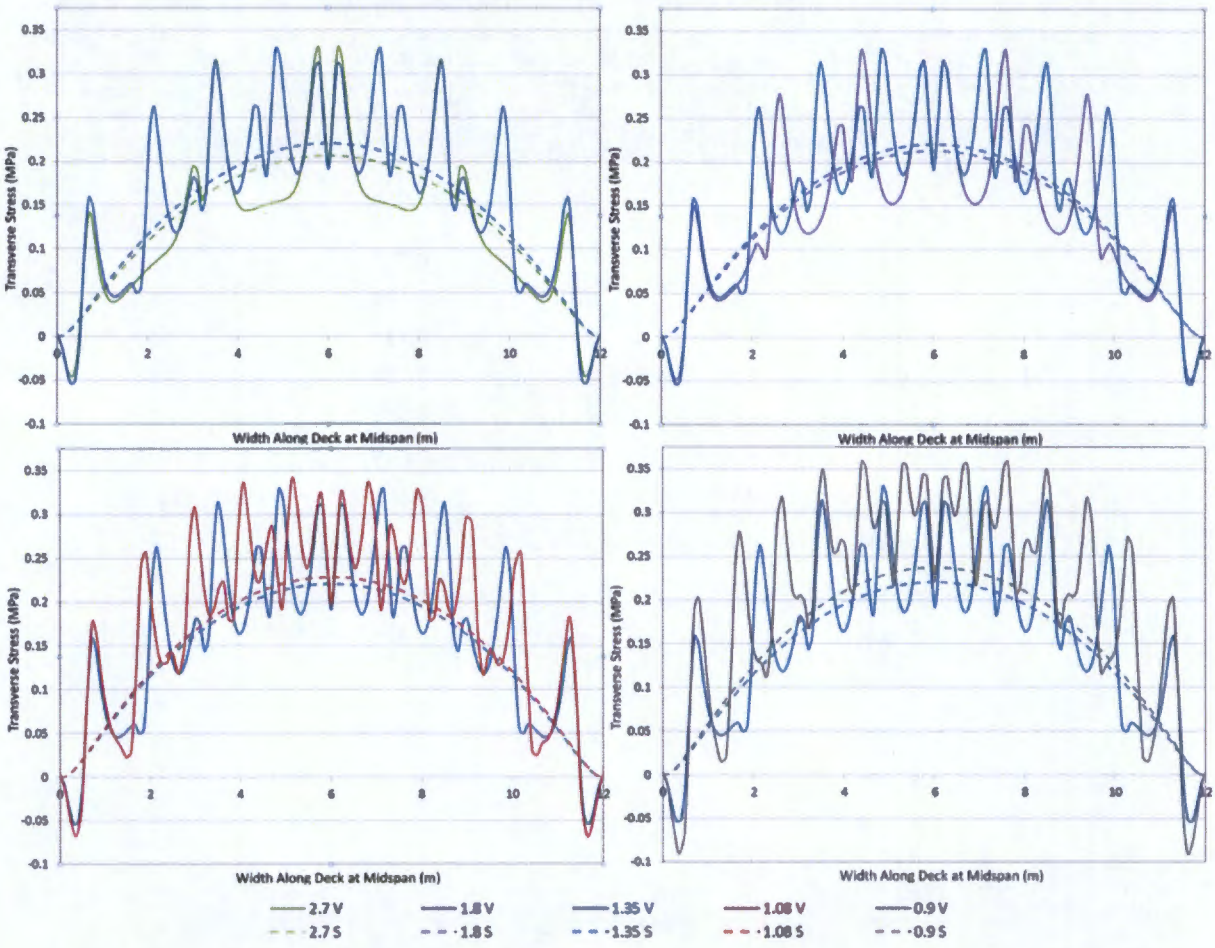

Figure 5.19 - Transverse stress distribution on the compression fibre along a transverse line at mid-span for the voided and solid FE models with an odd number of voids (1.35m void spacing model used as a baseline for comparison).

Comparing the results from the models in Figure 5.19, it can be seen that the transverse stress distributions of the voided models with different void spacing are similar. The general trend of the results show that there is an increase in stress with a decrease in void spacing, however the increase is minor. By comparing the stress at similar locations, such as the centre of the voids or the peak stresses, it

can be seen that the transverse stresses predicted are similar to each other with minor variations. This is in contrast to the models with different void diameter ratios, where clear variations in the models were observed. This shows the transverse stress distribution is less sensitive to the void spacing than the void diameter ratio. The solid models also show a minor increase in transverse stress with decreasing void spacing, which is attributed to the change in moment of inertia. All the models show a similar transverse stress distribution 1.5m from either end of the deck as the width of the end webs is constant for all models. The same can be concluded for the models with an even number of voids in Figure 5.20.

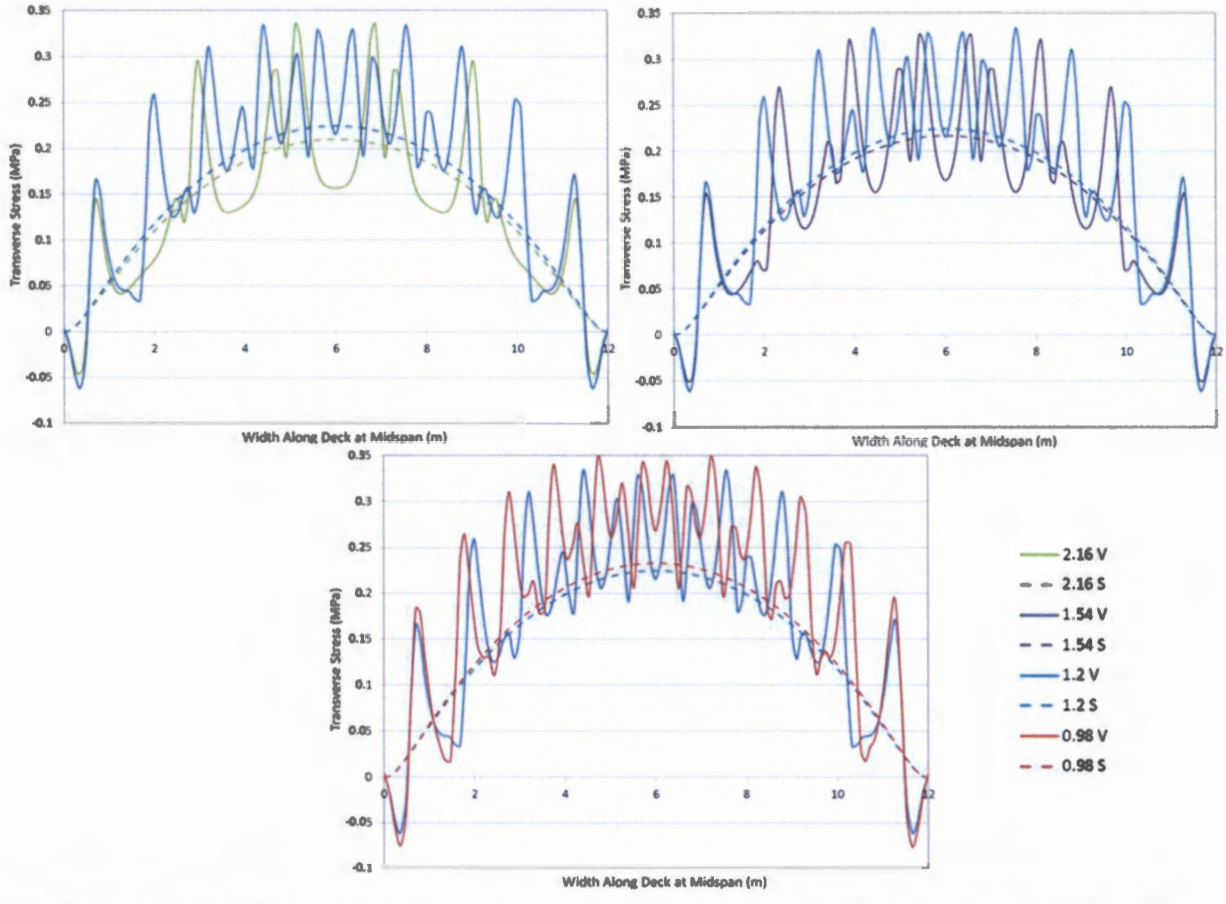

Figure 5.20 - Transverse stress distribution on the compression fibre along a transverse Line at mid-span for the voided and solid FE models with an even number of voids (1.2m void spacing model used as a baseline for comparison).

In order to evaluate the effect of the void spacing on the transverse stress distribution, transverse stresses from each model at key locations were compared. These key locations include the centre of the middle web, the centre of the middle void, and the location of the peak stress in the middle of the deck. The position of these key locations varies in each model according to the void spacing, thus the key locations are not constant for each model. Table 5.9 shows the transverse stresses at each of the key locations on the extreme compression and tension fibres for both the voided and the equivalent solid models with varying void spacing.

Table 5.9 - Transverse stresses at key locations on the tension and compression fibre for the voided and solid FE models for different void spacing.

Void Spacing (m)	Number of Voids (No.)	Location of stresses	Voided Slab			Solid Slab		
			Stress at centre of middle web (MPa)	Stress at centre of middle void (MPa)	Stress at centre of middle peak (MPa)	Stress at centre of middle web (MPa)	Stress at centre of middle void (MPa)	Stress at centre of middle peak (MPa)
0.9	13	Top	0.296	0.222	0.341	0.237	0.236	0.236
		Bottom	-0.350	-0.246	-0.374	-0.237	-0.236	-0.236
0.98	12	Top	0.269	0.206	0.335	0.232	0.231	0.232
		Bottom	-0.306	-0.152	-0.373	-0.232	-0.231	-0.232
1.08	11	Top	0.239	0.198	0.326	0.229	0.227	0.228
		Bottom	-0.290	-0.141	-0.347	-0.229	-0.227	-0.228
1.2	10	Top	0.215	0.192	0.316	0.225	0.222	0.224
		Bottom	-0.248	-0.134	-0.348	-0.225	-0.222	-0.224
1.35	9	Top	0.186	0.192	0.312	0.221	0.222	0.222
		Bottom	-0.214	-0.132	-0.340	-0.221	-0.222	-0.222
1.54	8	Top	0.168	0.190	0.326	0.217	0.214	0.216
		Bottom	-0.191	-0.128	-0.338	-0.217	-0.214	-0.216
1.8	7	Top	0.152	0.192	0.316	0.213	0.208	0.211
		Bottom	-0.167	-0.129	-0.338	-0.213	-0.208	-0.211
2.16	6	Top	0.157	0.191	0.335	0.210	0.203	0.206
		Bottom	-0.163	-0.127	-0.355	-0.210	-0.203	-0.206
2.7	5	Top	0.151	0.198	0.330	0.207	0.197	0.204
		Bottom	-0.150	-0.133	-0.353	-0.207	-0.197	-0.204

It can be seen that the transverse stress at the centre of the middle webs decreases as the void spacing increases, with the stress halving as the void spacing increased from 0.9m to 2.7m. The stress along the bottom fibre is also higher than the stress along the top fibre at a lower void spacing, but the stresses converge to equal each other as the void spacing increases.

The transverse stress at the centre of the middle voids also decreases with increasing void diameter ratio on both the top and bottom fibres of the slab. This decrease is rapid as the void diameter increases from 0.9m to 1.2m, but becomes relativity constant with the change in void diameter ratio from 1.2m to 2.7m. The peak transverse stresses also decrease with increasing void spacing, however the decrease is small, and therefore the peak stresses are relatively constant within the void spacing range.

The decrease in transverse stresses with increasing void spacing is most notably due to the variation in geometric properties including the increase in moment of inertia, and the reduction in cellular distortion due to an increase in the size of the webs between the voids. It is noted that the transverse stresses are most sensitive to variations within the void spacing range of 0.9m to 1.2m. A void spacing of less than 1.2m can be considered to be unreasonable as it results in thin webs between the

voids. It can therefore be concluded that the stresses at the centre of the voids is not sensitive to the spacing of the voids, provided a reasonable void spacing is provided.

The transverse stresses in the solid model are constant at each of the key locations, and decrease with increasing void spacing. The decrease in stress is the same for each void spacing interval as the decrease in moment of inertia is the constant due to the additional void being added to obtain the required void spacing. The transverse stresses on the top and bottom fibre are also equal in the solid models.

Table 5.10 shows a percentage comparison of the transverse stresses at each key location to the transverse stress for the 1.2m void spacing model. The 1.2m void spacing model has been chosen as the base model as it represents a reasonable void spacing, and will therefore be used to make comparisons.

Table 5.10 - Comparison of transverse stresses at key locations for the voided and solid slab with varying void spacing.

Void Spacing	Number of Voids	Location of stresses	Voided Slab			Solid Slab		
			Comparison at centre of middle web	Comparison at centre of middle void	Comparison at centre of middle peak	Comparison at centre of middle web	Comparison at centre of middle void	Comparison at centre of middle peak
0.9	5	Top	-37.7%	-15.6%	-7.9%	-5.3%	-6.3%	-5.4%
		Bottom	-41.1%	-83.6%	-7.5%	-5.3%	-6.3%	-5.4%
0.98	6	Top	-25.1%	-7.3%	-6.0%	-3.1%	-4.1%	-3.6%
		Bottom	-23.4%	-13.4%	-7.2%	-3.1%	-4.1%	-3.6%
1.08	7	Top	-11.2%	-3.1%	-3.2%	-1.8%	-2.3%	-1.8%
		Bottom	-16.9%	-5.2%	0.3%	-1.8%	-2.3%	-1.8%
1.2	8	Top	-	-	-	-	-	-
		Bottom	-	-	-	-	-	-
1.35	9	Top	13.5%	0.0%	1.3%	1.8%	0.0%	0.9%
		Bottom	13.7%	1.5%	2.3%	1.8%	0.0%	0.9%
1.54	10	Top	21.9%	1.0%	-3.2%	3.6%	3.6%	3.6%
		Bottom	23.0%	4.5%	2.9%	3.6%	3.6%	3.6%
1.8	11	Top	29.3%	0.0%	0.0%	5.3%	6.3%	5.8%
		Bottom	32.7%	3.7%	2.9%	5.3%	6.3%	5.8%
2.16	12	Top	27.0%	0.5%	-6.0%	6.7%	8.6%	8.0%
		Bottom	34.3%	5.2%	-2.0%	6.7%	8.6%	8.0%
2.7	13	Top	29.8%	-3.1%	-4.4%	8.0%	11.3%	8.9%
		Bottom	39.5%	0.7%	-1.4%	8.0%	11.3%	8.9%

The comparison of the transverse stresses at the centre of the middle web shows that the percentage difference in stresses to the 1.2m void spacing varies from around -41% to 40% for stresses on both the top and bottom fibre. This variation is much less than the maximum percentage differences experienced from the models in *Phase 1* with varying void diameter ratios, which varied by more than 100% in some cases. This confirms that the transverse stress is more sensitive to the void diameter ratio than the void spacing. It is noted that the transverse stress variation to the 1.2m model is 41% with a void spacing

range of 0.3m from 0.9m to 1.2m, and 40% with a void spacing range of 1.5m from 1.2m to 2.7m. This shows that the transverse stress is more sensitive to the void spacing at lower void spacing.

For the transverse stresses at the centre of the middle void, the percentage difference to the 1.2m model is 15.6% and 83.6% for the top and bottom fibre stresses respectively for the 0.9m void spacing. For the void spacing range between 1.2m and 2.7m, the maximum percentage variation is 4.5%. It can therefore be assumed that the transverse stresses at the centre of the voids is relatively unaffected by a void spacing of more than 1.2m. The maximum variation between the peak stresses to the 1.2m is 7.9%, with an average of less than 5%. The peak stresses are therefore constant across the void spacing range.

Figure 5.21 and Figure 5.22 show the transverse stress distribution along a transverse line at mid-span on the extreme tension fibre for the voided and corresponding solid models with an odd and even number of voids respectively. The models with a void spacing of 1.35m and 1.2m are used as a baseline for comparison in each case. As with the transverse stresses on the compression fibre, the transverse stresses on the bottom fibre undergo minor variations with the change in void spacing. The greatest effect of the change in the void spacing is on the transverse stresses at the webs, particularly at the centre of the deck Figure 5.22, which represents the centre of the middle web. As with the top fibre transverse stresses, the transverse stress on the bottom fibre is unaffected by the void spacing, which can be seen at the centre of the deck in Figure 5.21. Small variations in peak stresses can be seen in both Figure 5.21 and Figure 5.22, which shows they are not sensitive to the spacing of the voids.

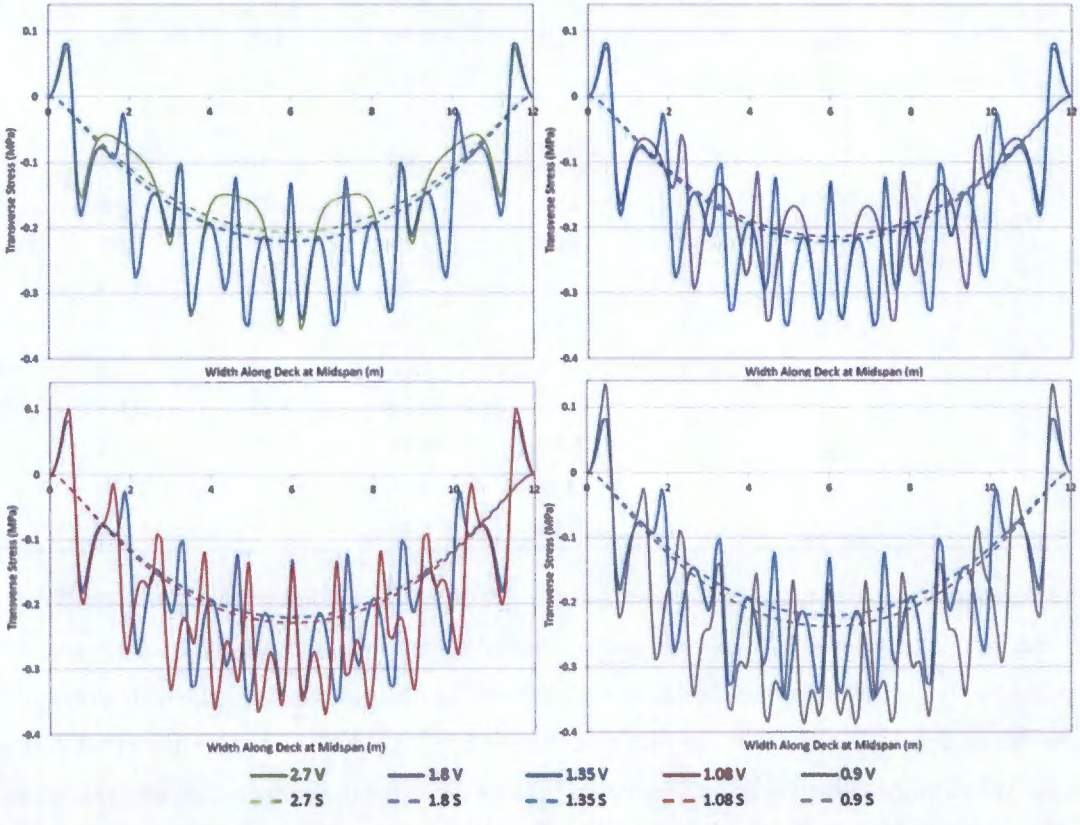

Figure 5.21 - Transverse stress distribution on the tension fibre along a transverse Line at mid-span for the voided and solid FE models with an odd number of voids (1.35m void spacing model used as a baseline for comparison).

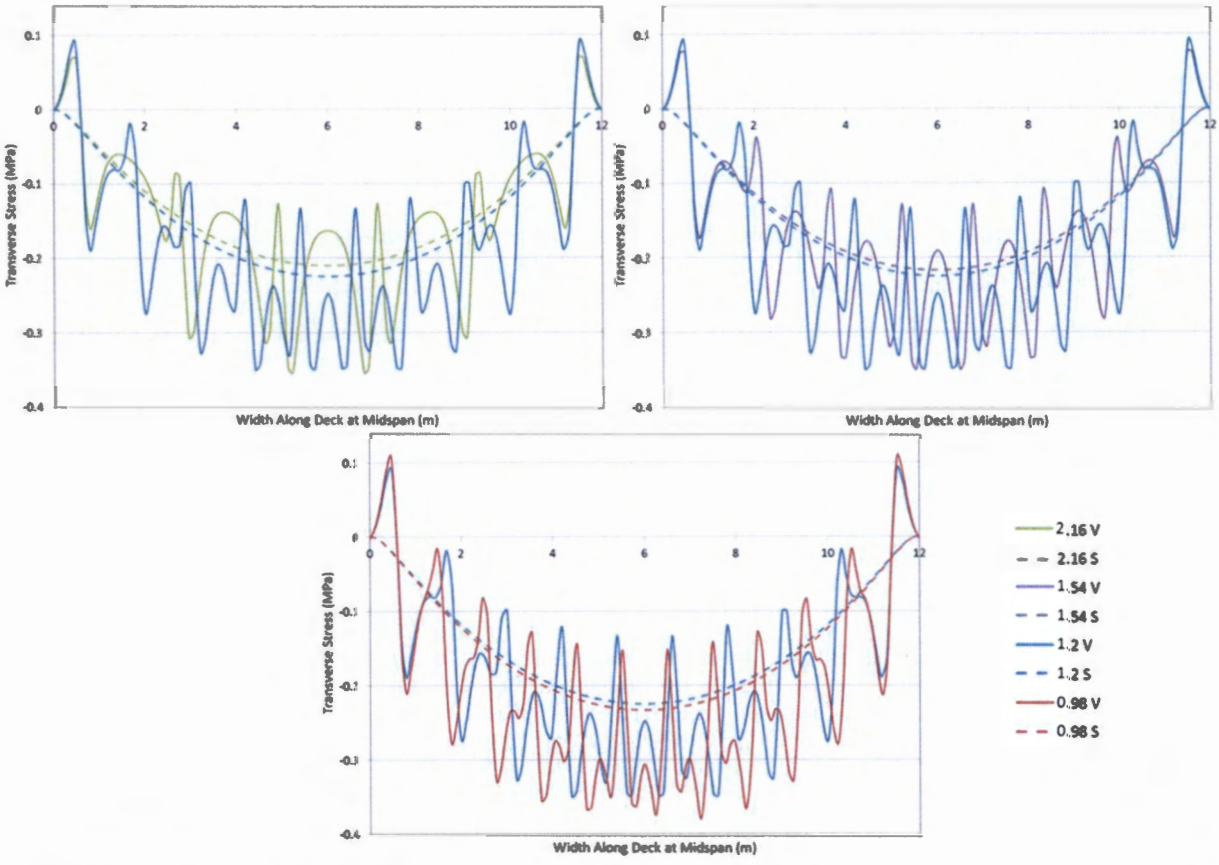

Figure 5.22 - Transverse stress distribution on the tension fibre along a transverse Line at mid-span for the voided and solid FE models with an even number of voids (1.2m void spacing model used as a baseline for comparison).

The effect of the void spacing on the transverse stress distribution along a transverse grid line can be summarised as follows:

- An increase in void spacing leads to a decrease in transverse stresses across the full width of the deck. This is due to the increase in moment of inertia which increases with an increase in void spacing.
- At a void spacing of more than 1.2m, the transverse stresses at the centre of the voids and the peak stresses are unaffected by the void spacing. At a void spacing of less than 1.2m, the transverse stresses and peak stresses are sensitive to changes in void spacing. This is due to the increase in cellular distortion due to the thin webs in between the voids at low void spacing.
- The stresses at the centre of the webs experience large variations within the full void spacing range studied. These variations in stress were more than the variation in moment of inertia due to change in void spacing predicted by the solid models.

Longitudinal Stresses along a Transverse Grid Line

The longitudinal stresses along a transverse line at mid-span on the extreme compression fibre of the deck for the voided and corresponding solid models are shown in Figure 5.23. It can be seen that the longitudinal stresses increase with a decrease in the void spacing, which is due to the decrease in moment of inertia with decreasing void spacing. The longitudinal stresses increase from 2.64MPa to 3.22MPa as the void spacing decreases from 2.7m to 0.9m, which is a percentage variation of 22%. The variation between the longitudinal stresses of the voided models with different void spacing also increases as the void spacing decreases.

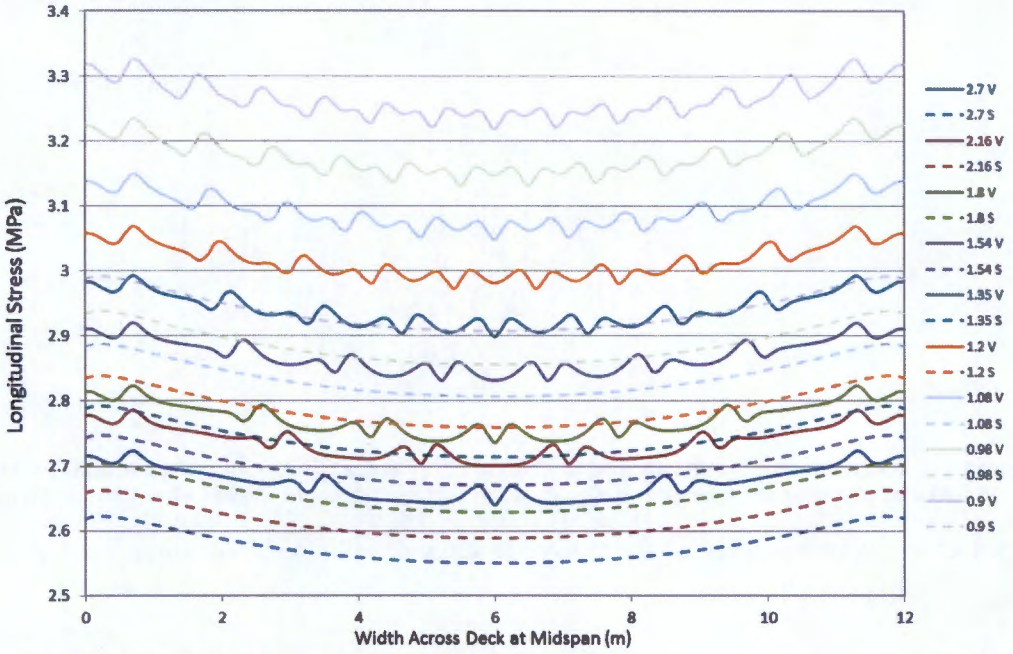

Figure 5.23 - Longitudinal stress distribution on the compression fibre along a transverse Line at mid-span for the voided and solid FE models.

The solid models underestimate the longitudinal stresses across the width of the deck when compared to the corresponding voided model for each void spacing. The variation between the longitudinal stresses of the solid models is constant between each void spacing, which is due to the constant variation in moment of inertia to obtain the required void spacing. It is therefore noted that the longitudinal stresses in the solid models are directly proportional to the moment of inertia, while the longitudinal stresses of the voided models are not, and increase more than the decrease in moment of inertia at low void spacing. This is attributed to the increase in cellular distortion.

Table 5.11 shows the longitudinal stresses for the voided and solid models, a percentage comparison between the voided and solid models, and a comparison between the voided models to the model with a 1.2m void spacing. It can be seen that at a void spacing of 2.7m, the solid models underestimate the longitudinal stress by 3.4% when compared to the 3D voided model, and this variation increases to 9.7% with a void spacing of 0.9m. As the solid models account for the decrease in moment

of inertia at each void spacing, the variation between longitudinal stresses of the solid and voided models is due to the stress raising effect of the voids.

It is noted that this stress raising effect results in an increase in longitudinal stress of 3.4% to 9.7% as the void spacing decreases from 2.7m to 0.9m when comparing the solid and voided models. It can be concluded that a decrease in void spacing can result in an increase in cellular distortion, and an increase in longitudinal stresses. It is also noted that for a logical void spacing of between 1.2 and 1.8m, the variation between the longitudinal stresses is minimal. It can therefore be concluded that the longitudinal stresses are not sensitive to variations in void spacing for a logical void spacing.

Table 5.11 – Longitudinal stresses and comparisons for the voided and solid FE models

Void Spacing (m)	Stress at centre of voided model (MPa)	Stress at centre of voided model (MPa)	Comparison between solid and voided model (%)	Comparison between 1.2m void spacing model (%)
0.9	3.22	2.91	9.7%	7.4%
0.98	3.15	2.86	9.3%	5.2%
1.08	3.05	2.81	7.9%	2.1%
1.2	2.98	2.76	7.4%	-
1.35	2.90	2.71	6.4%	-2.6%
1.54	2.83	2.67	5.7%	-4.7%
1.8	2.74	2.63	3.9%	-7.6%
2.16	2.70	2.59	4.2%	-8.7%
2.7	2.64	2.55	3.4%	-10.6%

The longitudinal stresses along a transverse line at mid-span on the extreme tension fibre of the deck for the voided and corresponding solid models are equal in magnitude and opposite in sign compared to the longitudinal stresses on the extreme tension fibre, and are therefore not presented here.

The effect of the void spacing on the longitudinal stress distribution along a transverse grid line can be summarised as follows:

- An increase in void spacing leads to a decrease in longitudinal stresses across the width of the deck. This is due to the increase in moment of inertia which increases with an increase in void spacing.
- The longitudinal stresses are underestimated by the solid models when compared to the voided models, which account for the decrease in moment of inertia.
- The variation between the longitudinal stresses of the voided and solid models increases as the void spacing decreases due to an increase in cellular distortion.

Transverse Stresses along a Longitudinal Grid Line

The transverse stresses on the extreme compression fibre along the centreline of the deck for the voided and solid models with an odd number of voids are shown in Figure 5.24. The voided models predict a transverse stress distribution consisting of a peak tension stress at either end of the deck, with a peak compression stress at mid-span. The solid models predict a transverse stress distribution which consists of a peak compression stress at mid-span only. The negative peak stress at either end of the voided models is due to the change from the solid to voided section of the deck, which results in a concentration of stresses which is not present in the solid models. The solid models show a more even distribution of stress along the length of the deck, whereas the voided models have a steep transition from a positive to a negative stress, with a more gradual transition between 2m and 18m.

The voided models predict transverse stress distributions which coincide with each other, with the exception of the 0.9m void spacing model showing a slightly higher peak stress at mid-span. Ignoring the 0.9m, the void spacing is shown to have no effect on the transverse stresses along the centre line of the voided model. The solid models show a gradual increase in transverse stresses at mid-span as the void spacing decreases, which relates to the change in moment of inertia.

The variation between the solid and voided models can be explained by considering the location of the stress results relative to the position of the voids. As the voided models shown in Figure 5.24 all have an odd number of voids, there is a void located along the centreline of the deck. From Figure 5.19, the transverse stresses at the centre of a void experience a local minimum transverse stress. This results in the solid models overestimating the transverse stresses compared to the voided models at the centre of the deck.

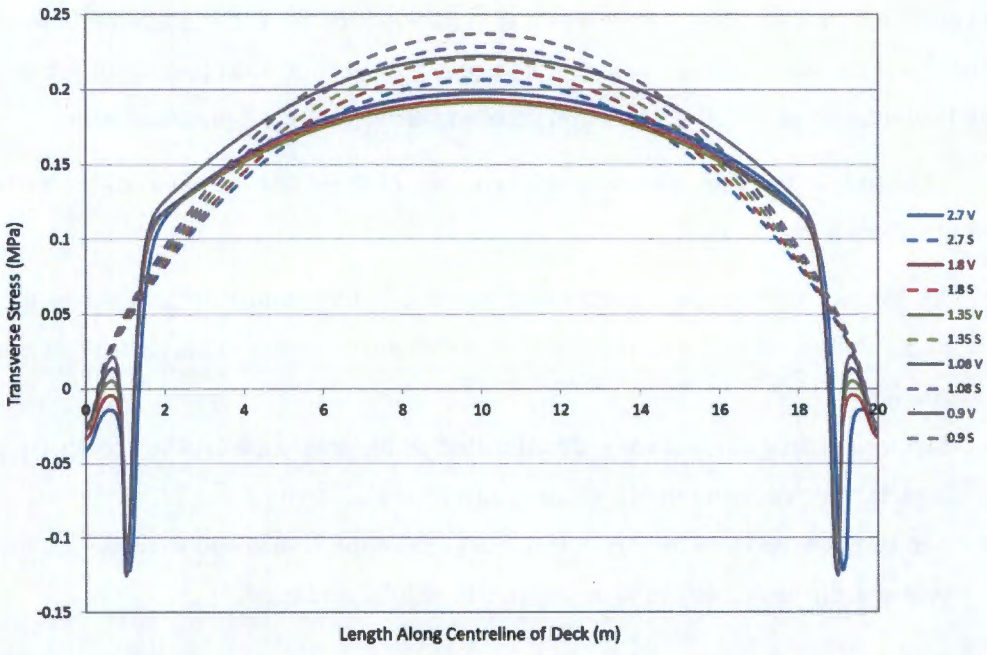

Figure 5.24 - Transverse stress distribution on the compression fibre along the centreline of the deck for the voided and solid FE models with an odd number of voids.

Figure 5.25 shows the transverse stresses on the extreme compression fibre along the centreline of the deck for the voided and solid models with an odd number of voids. The general trend of the transverse stresses is similar to those along the compression fibre, with an inversion of the sign of the stress. It is noted that the variation between the solid and voided model results is greater for the stresses on the tension fibre.

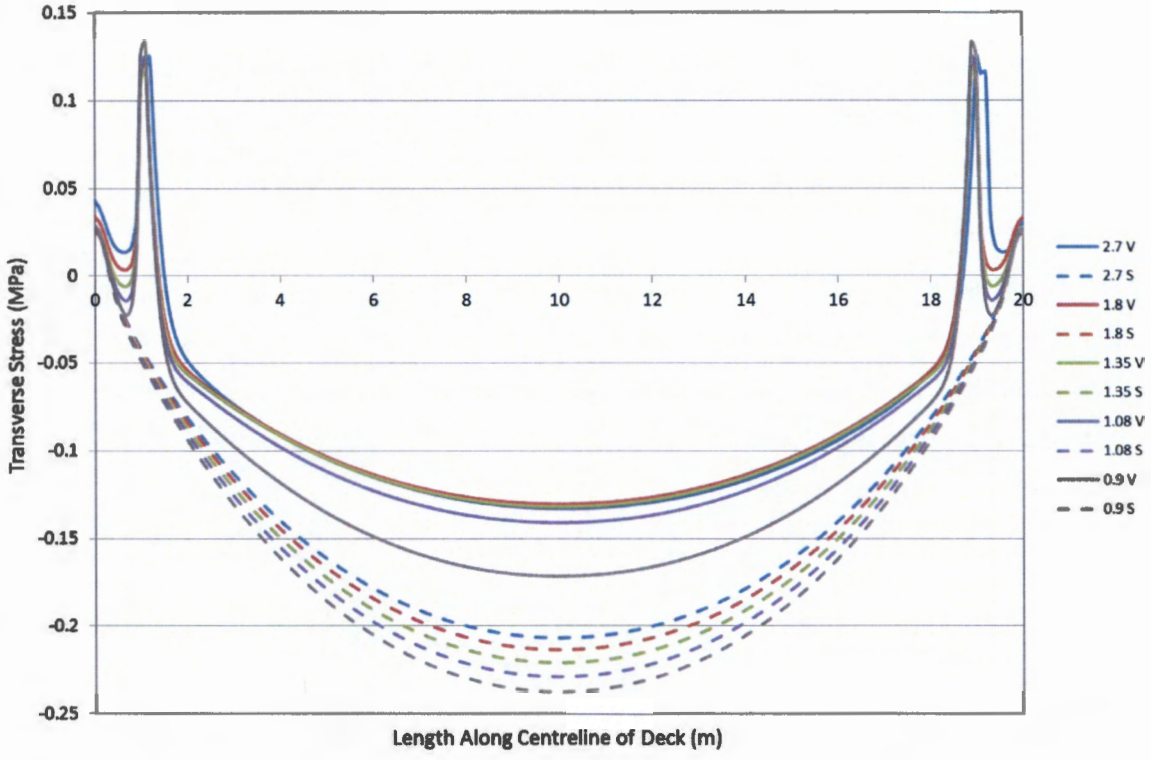

Figure 5.25 - Transverse stress distribution on the tension fibre along the centreline of the deck for the voided and solid FE models with an odd number of voids.

As with the transverse stresses on the compression fibre, the voided models predict similar stress distributions, with the exception of the 0.9m void spacing model which predicts a higher transverse stress than the other voided models. The solid models show the same gradual increase in transverse stress at mid-span as the void spacing decreases. The solid models again show a gradual transition between the peak stresses, while the voided models have a steep stress transition at either end of the deck, and a gradual transition between 2m and 18m. The solid models overestimate the transverse stresses compared to the voided models again due to the decrease in transverse stresses at the centre of a void in the voided models.

The consistent results obtained from the voided models shows that the void spacing has minimal effect on the transverse stress distribution on the centreline of the deck. The increasing variation between the solid and voided models is the result of the inability of the solid model to predict local effects near the voids, and is thus not related to the void spacing.

The effect of the void spacing on the transverse stress distribution along a longitudinal grid line can be summarised as follows:

- The transverse stress on both the compression and tension fibre are affected by variations in void spacing, however the effect is small.
- The transverse stress distribution depends on the location of the longitudinal grid line that the results are reported on relative to the position of the voids. This results in the variation between the voided and solid model stresses. It is noted that the void spacing could have an effect on the transverse stress results if they are reported on an alternative longitudinal gridline.

Longitudinal Stresses along a Longitudinal Grid Line

The longitudinal stresses on the extreme compression fibre along the centreline of the deck for the voided and solid models with different void spacing are shown in Figure 5.26. It is noted that there is an increase in longitudinal stress with decreasing void spacing. It can also be seen that the solid models underestimate the longitudinal stresses along the full length of the bridge when compared to the voided model with the same void spacing.

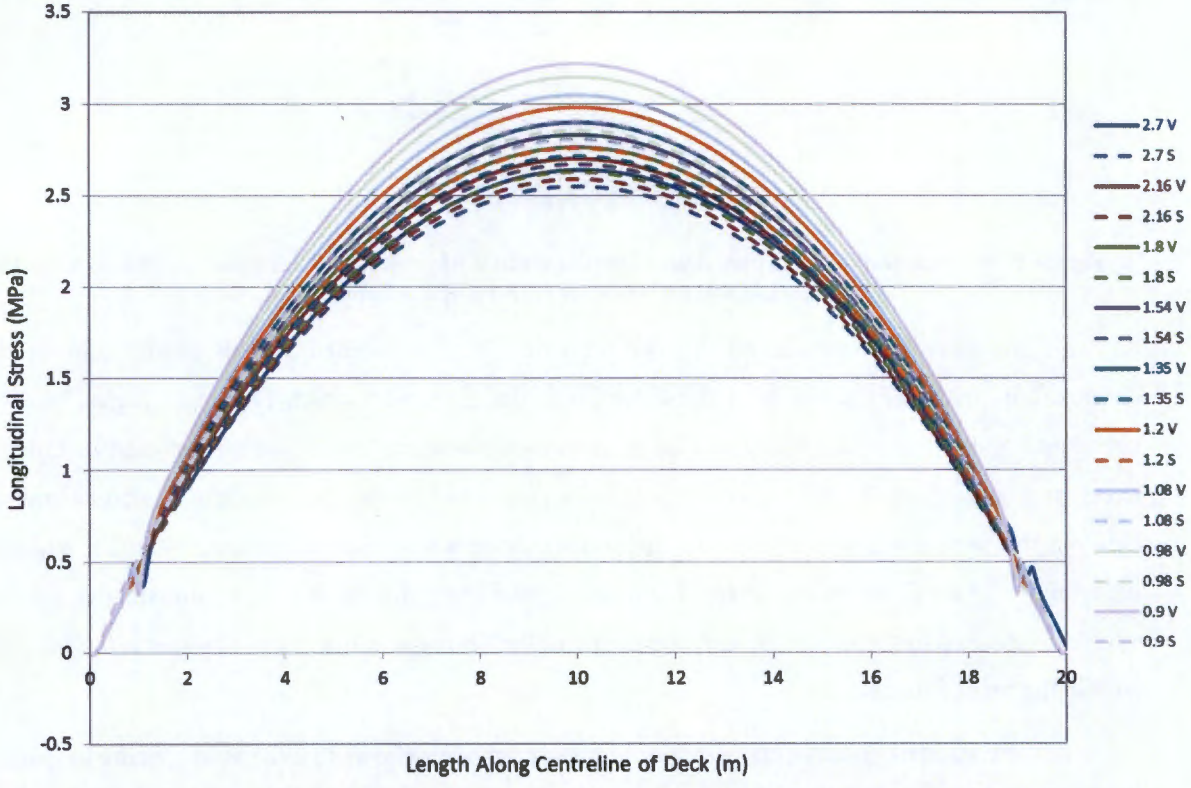

Figure 5.26 - Longitudinal stress distribution on the compression fibre along the centreline of the deck for the voided and solid FE models.

The longitudinal stresses of the voided models increase from 2.64MPa to 3.22MPa at mid-span as the void spacing decreases from 2.7m to 0.9m, which is a percentage variation of 22%. The variation between the longitudinal stresses of the voided models with different void spacing also increases as the

void spacing decreases. The longitudinal stresses of the solid models increase from 2.55MPa to 2.91MPa as the void spacing decreases from 2.7m to 0.9m, which is a percentage variation of 14%. The variation between each of the solid models is relatively constant for each voids spacing increment.

These results indicate that there is a stress raising effect due to the voids along the length of the deck. This stress raising effect results in the longitudinal stresses being between 3.4% and 9.6% greater at mid-span in the voided models than the solid models as the void spacing decreases from 2.7m to 0.9m. Therefore it can be suggested that a decrease in the void spacing results in an increase in the stress raising effect on the longitudinal stresses on the extreme compression fibre of the deck. The same can be concluded for the longitudinal stresses on the tension fibre of the deck.

The effect of the void spacing on the longitudinal stress distribution along a longitudinal grid line can be summarised as follows:

- A decrease in void spacing leads to an increase in longitudinal stresses across the length of the deck on the extreme compression fibre. This is primarily due to the decrease in moment of inertia with a decrease in void spacing.
- The longitudinal stresses are underestimated by the solid models when compared to the voided models, which account for the decrease in moment of inertia.
- The variation between the longitudinal stresses of the voided and solid models increases as the void spacing decreases due to an increase in cellular distortion.

5.4. Orthotropic Plate Parameter Comparison

This section will focus on the results of the finite element models used in Phase 3. A range of voided slab bridges were modelled with different void diameter to slab depth ratios using orthotropic plate theory and the plate parameters suggested in Table 2.1 to model the effect of the voids. Results from three-dimensional models and solid isotropic models are also presented in order to draw comparisons with the orthotropic models.

Transverse Stress along a Transverse line at Mid-span

Figure 5.27 and Figure 5.28 show the transverse stresses on the extreme compression fibre at mid-span for the voided slab models with void diameter ratios of 0.5 and 0.9 respectively. The stress results are shown for the seven solid orthotropic plate models, the solid isotropic model, and the three-dimensional voided model. The stress results for the 0.6 to 0.8 void ratio models are not shown here as they fall between these two sets of results.

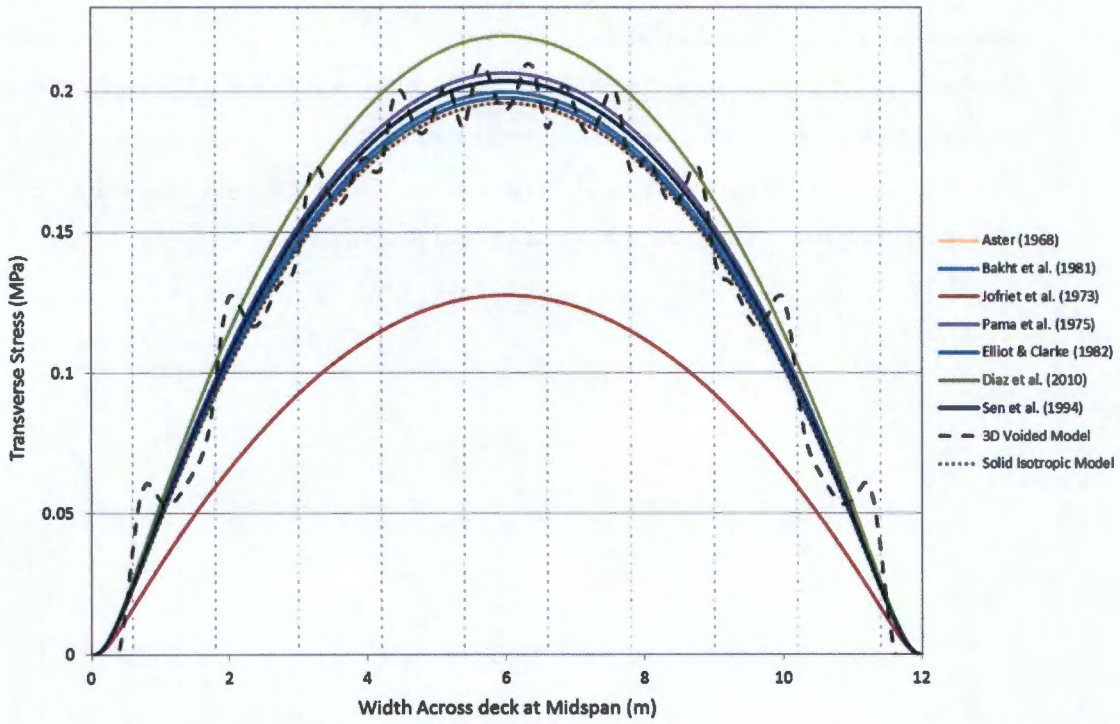

Figure 5.27 - Comparison of transverse stress results on the extreme compression fibre along a transverse line at mid-span for the 0.5 void diameter ratio models obtained using orthotropic plate theory.

It is noted that the effect of the voids is averaged or smeared across the width and depth of the slab in the solid orthotropic and isotropic models. The actual geometery of the cross-section, such as the webs and flanges around the voids, is not specifically modelled, resulting in the transverse stresses following a parabolic function. This is in contrast to the three-dimensional model, where the stresses have local peaks and dips along the width of the deck. These maximum and minimum stresses can only be obtained by using elaborate forms of analysis such as three-dimensional finite element models, which are capable of modelling cellular behaviour. The general trend of the orthotropic models is similar to that of the 3D

model, with the stresses falling in between the maximum and minimum stresses predicted by the 3D model.

In Figure 5.27, the stresses predicted by Diaz *et al.* (2010) and Jofriet *et al.* (1973) show the largest variation to those predicted by the three-dimensional model, with the stresses being over and underestimated respectively. Both of these methods involve using an isotropic model in conjunction with a stress multiplier to obtain the effect of the voids. The remainder of the models, which use an anisotropic material, compared well to the 3D model.

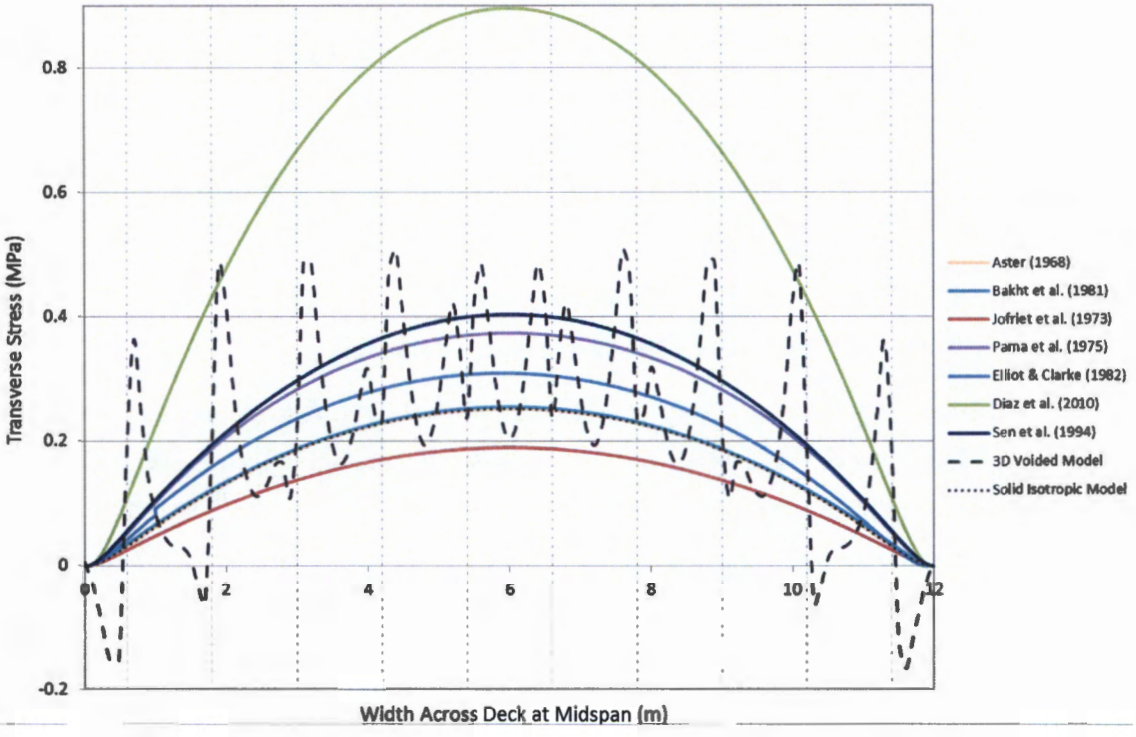

Figure 5.28 - Comparison of transverse stress results on the extreme compression fibre along a transverse line at mid-span for the 0.9 void diameter ratio models obtained using orthotropic plate theory.

The method of Diaz *et al.* (2010) involves modelling the slab as an isotropic slab of full depth, with a stress multiplier being used to account for the effect of the voids. The stress multiplier is based on theoeritcal principals using force equilibruim between the solid and voided slab under plane stress and flexure. Many authors suggest that the stress variations in a voided slab are the result of cellular distortion due to transverse shear, therefore the use of a flexural theory to obtain the stress multiplier is open to question. The modelling of the slab as full depth and with an isotropic material, which is inconsistent with most of the literature, could also lead to the variation in results compared to the 3D model. The results of Diaz *et al.* (2010) decrease in accuracy with an increase in void diameter ratio, resulting in a further overestimation of the stress results at high void diameter ratios. The most accurate results are obtained for the 0.5 void diameter ratio model, where the stress results compare favourably with the peak stresses of the 3D model. However, this method results in an overestimation of most of the results across the width of the deck, and is therefore considered to be too conservative.

The method of Jofriet *et al.* (1973) predicts results which increase in accuracy with increasing void diameter ratio. However, the results tend to underestimate the stress, with only the 0.9 void diameter ratio giving results similar to that of the 3D model. As with Diaz *et al.* (2010), the method of Jofriet *et al.* (1973) involves modelling the slab as an isotropic slab of full depth, with a stress multiplier being used to account for the effect of the voids. The large variation between these two sets of results is due to the stress multipliers employed. It is noted that the methodology employed by Diaz *et al.* (2010) and Jofriet *et al.* (1973) using a full depth isotropic slab and stress multiplication is not seen as an accurate method of modelling voided slabs.

The isotropic model and orthotropic models with a reduced depth and no stress multiplication are shown to be in agreement with the results of the 3D model across the full range of void diameter ratios. The method proposed by Pama *et al.* (1975) and Sen *et al.* (1994) predict closer stress results to the 3D model at the location of the peak stresses, while the other 2D orthotropic methods predict more accurate results at the centre of the webs. This is because the methods proposed by Pama *et al.* (1975) and Sen *et al.* (1994), which account for increased amounts of orthotropic behaviour, predict higher stress results which compare more favourable with the peak stresses.

The method proposed by Aster (1968) compares well with the isotropic model across the full range of void diameter ratios. This is the result of the small variation to the transverse elastic modulus due to the suggested plate parameter, resulting in an essentially isotropic deck. The results of Bakht *et al.* (1981) also produces results which are similar to the isotropic model, however the similarity decreases with increasing void ratio. This suggests that the plate parameters proposed by Bakht *et al.* (1981) do introduce some degree of orthotropic behaviour.

The method employed by Sen *et al.* (1994) is a combination of the orthotropic parameters suggested by Bakht *et al.* (1982) and stress multipliers proposed by Sen *et al.* (1994). The results of this method compare more favourably with the results of the 3D model than those obtained by Bakht *et al.* (1982), which differ only in the use of stress multipliers, which suggests that a stress multiplier is required to convert the results from the orthotropic models to the actual voided model. This method predicts higher stresses than the other orthotropic and isotropic models, which results in an overestimation of the stresses across the width of the slab, apart from the peak stresses, compared to the 3D model. This is a conservative result, and considered to be the most accurate as they account for the stress raising effect of the voids. Consistent comparisons are obtained with increasing void diameter ratio, which shows that this method accurately accounts for an increase in orthotropic behaviour.

Figure 5.29 and Figure 5.30 show the percentage difference between the transverse stress on the top fibre of the deck for each of the 2D modelling methods compared to the 3D model for the 0.5 and 0.9 void diameter ratios respectively. The variation between the 3D model which predicts the local peak stress and the 2D models which average the stresses is clear from the graphs. Another trend that can be seen is that the percentage difference in transverse stresses increases with increasing void diameter ratio.

The percentage difference is at most 40% at the centre of the deck for the 0.5 the void diameter ratio model, and increases to over 100% for the 0.9 void diameter ratio model, excluding the results of Diaz *et al.* (2010). The models with a 0.9 void diameter ratio indicate a more significant difference between the predictions of the 2D and 3D models. This shows that the 2D models predict the transverse stresses with less accuracy with increasing void diameter ratio. This is in keeping with Hambly (1991), who stated that the degree of orthotropy becomes significant when the void diameter ratio exceeds 0.6.

For the 0.5 void diameter ratio models in Figure 5.29, all methods predict stresses at the centre of the deck which are within 20% of the 3D model, apart from the results from Jofriet *et al.* (1973) which has an average deviation of 35%. The greatest deviations from the 3D model stresses occur at the location of the peak stresses, which is due to the averaging out of the stresses in the 2D models. The stresses at the centre of the voids and webs coincide with negligible difference. The percentage difference also varies between positive and negative values, which indicates the 2D models are averaging out the peak stress and not wholly underestimating or overestimating the transverse stresses. The exception to this are the results of Jofriet *et al.* (1973) which underestimates the transverse stresses across the whole width of the bridge. The method of Diaz *et al.* (2010) also results in an overestimation of most of the results. Large deviations from the 3D model occur at either end of the deck, which are as a result of the negative stress predicted in the 3D model, and have therefore been excluded from Figure 5.27 to allow for a better scale to view the results.

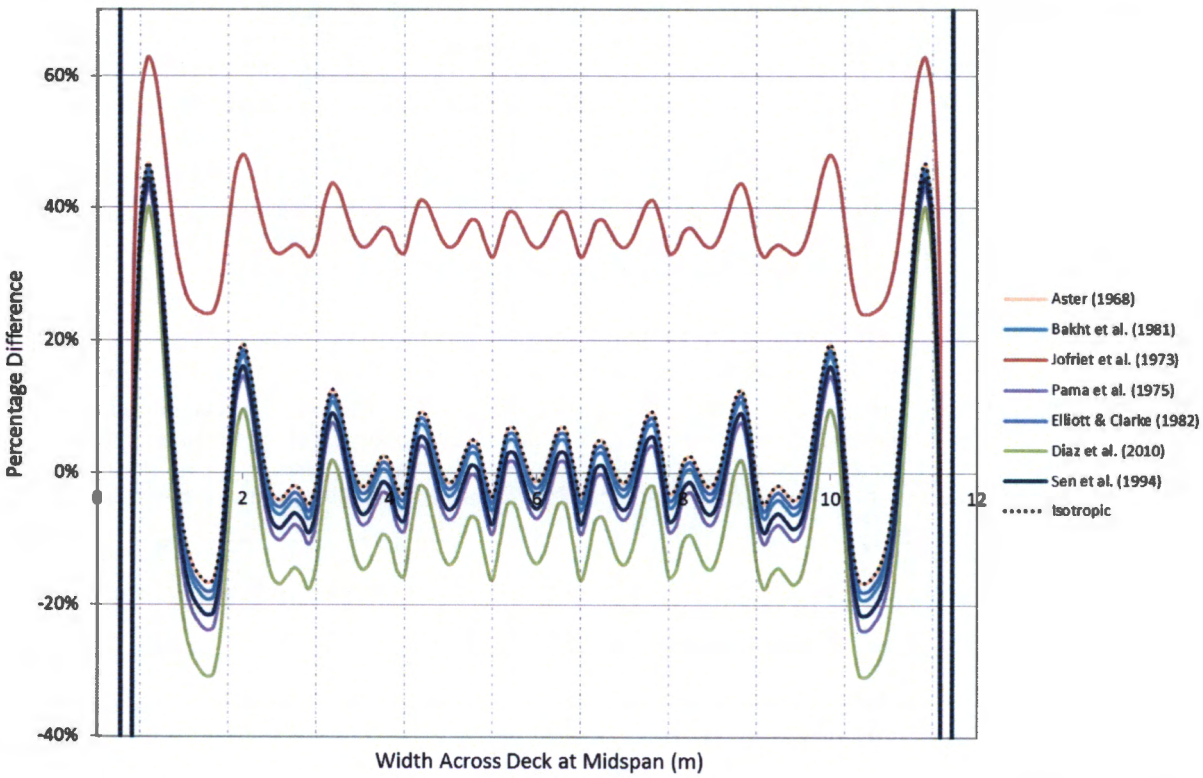

Figure 5.29 - Percentage difference comparison between the top fibre transverse stresses at mid-span of the 2D solid models and the 3D voided FE model for a 0.5 void diameter ratio.

The deviation in transverse stress of the 2D models from the 3D model becomes more significant in Figure 5.30, which shows the percentage deviations to the 3D model for the 0.9 void diameter ratio models. The maximum peak stress deviation varies from 80% to -100% for the 2D models at the centre of the deck, apart from the results of Diaz *et al.* (2010) which overestimates the transverse stresses by as much as 300%. The results indicate the increase in orthotropic behaviour with increasing void diameter ratio, and the inability of 2D methods to account for the increased orthotropic effects. The skew in percentage variation to negative results indicates that the 2D models are underestimating the transverse stresses compared to the 3D model. The results from Jofriet *et al.* (1973) compare more favourable with the 3D model in the 0.9 void diameter ratio model, which indicates that their method is more applicable to higher void diameter ratios.

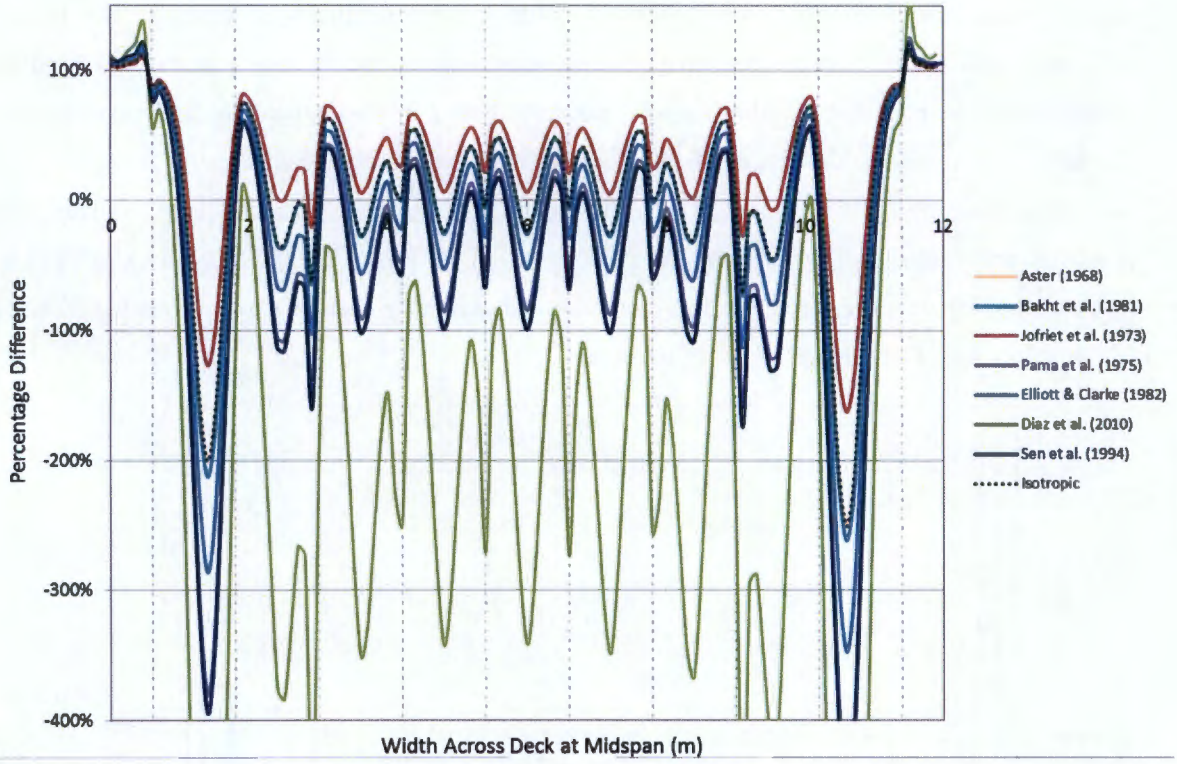

Figure 5.30 - Percentage difference comparison between the top fibre transverse stresses at mid-span of the 2D solid models and the 3D voided FE model for a 0.9 void diameter ratio.

Figure 5.31 shows the transverse stress on the extreme tension fibre along a transverse line at mid-span for the 3D and 2D voided slab models with a void diameter ratio of 0.5. The stress results are shown for the seven orthotropic plate models, the solid isotropic model, and the three-dimensional voided model.

The 0.5 void ratio models in Figure 5.32 show a similar trend to the transverse stresses on the compression fibre, with the 2D model results falling in between the maximum and minimum stresses of the 3D model. The method of Jofriet *et al.* (1973) underestimates the transverse stresses across the width of the deck. The results of Diaz *et al.* (2010) compare favourably with the peak stress results of the 3D model. The results from Aster (1968) once again compare favourably to the isotropic results.

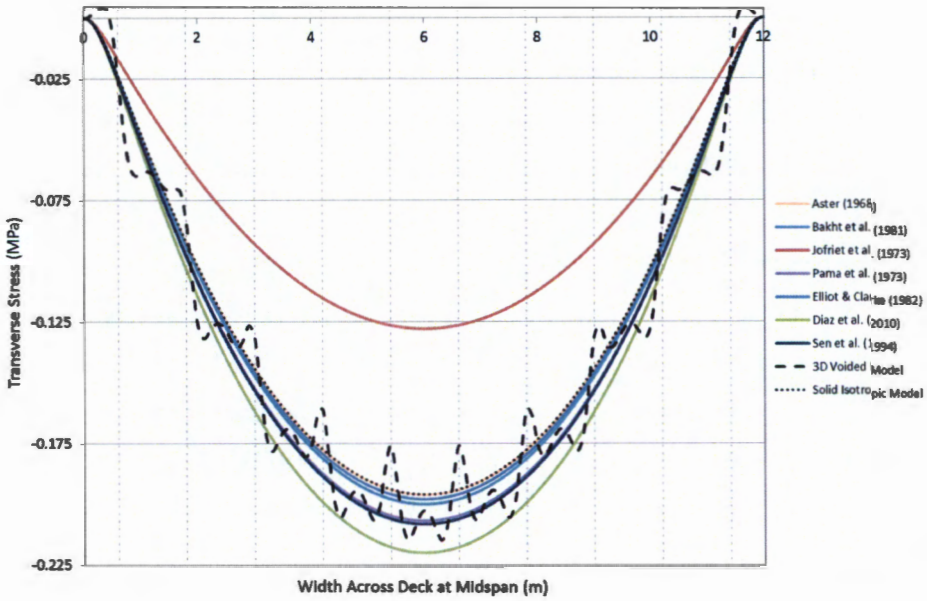

Figure 5.31- Comparison of transverse stress results on the extreme compression fibre along a transverse line at mid-span for the 0.9 void diameter ratio models obtained using orthotropic plate theory.

Figure 5.32 shows the percentage difference between the transverse stress on the bottom fibre of the deck for each of the 2D modelling methods compared to the 3D model for the 0.5 void diameter ratio. The percentage differences are similar to the transverse stresses on the top fibre, with the greatest variations to the 3D model occuring at the location of the centre of the voids and the peak stresses. The transverse stresses are underestimated in the 2D models at the location of the peaks and overestimated at the centre of the voids. The majority of the models predict stresses that are within 20% of the 3D model results. The method of Jofriet *et al.* (1973) results in an average underestimation of the transverse stress by 35% at the centre of the deck. Comparing Figure 5.29 and Figure 5.32, it can be seen that the 2D models compare more favourably with the top fibre stresses than the bottom fibre stresses.

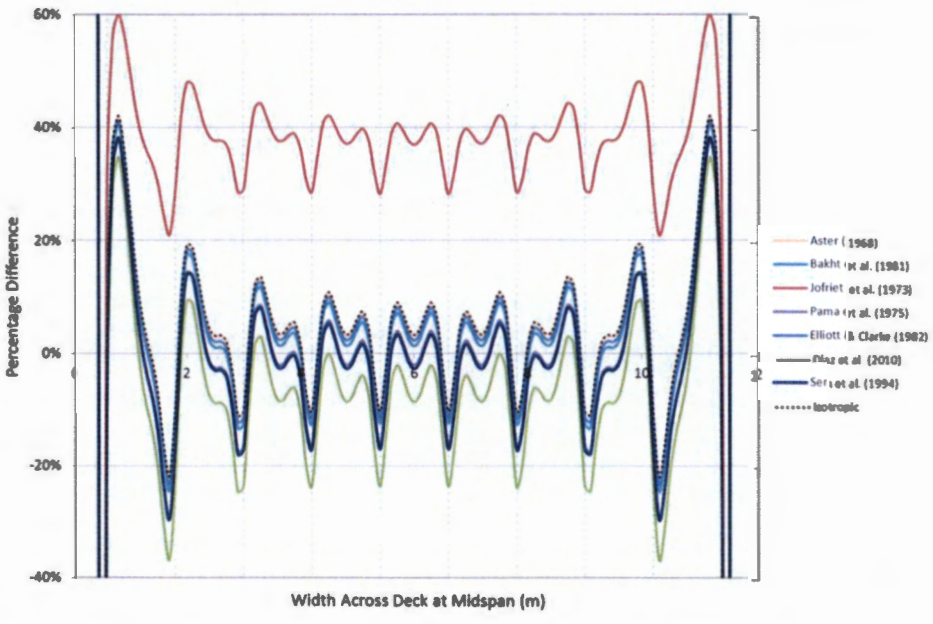

Figure 5.32 - Percentage difference comparison between the bottom fibre transverse stresses at mid-span of the 2D solid models and the 3D voided FE model for a 0.5 void diameter ratio.

Figure 5.33 shows the transverse stress on the extreme tension fibre along a transverse line at mid-span for the 3D and 2D voided slab models with a 0.9 void diameter ratio. It can be seen that the isotropic model, and the methods of Aster (1968), Bakht *et al.* (1981), and Elliot & Clarke (1982) produce results that compare less favourably with the 3D model at a void diameter ratio of 0.9 than 0.5, and are therefore unable to account for the increase in orthotropic behaviour. The method of Pama *et al.* (1975) produces results which represent a good comparison to the average of the 3D model, as the results lie between the maximum and minimum peaks. The method of Sen *et al.* (1994) predicts results which compare favourably with the peak stresses of the 3D model, and therefore can be considered as conservative. The results from Diaz *et al.* (2010) once again overestimate the transverse stresses, and are therefore considered to be too conservative. Results from Jofriet *et al.* (1973) increase in accuracy with increasing void diameter ratio, however underestimate the transverse stresses.

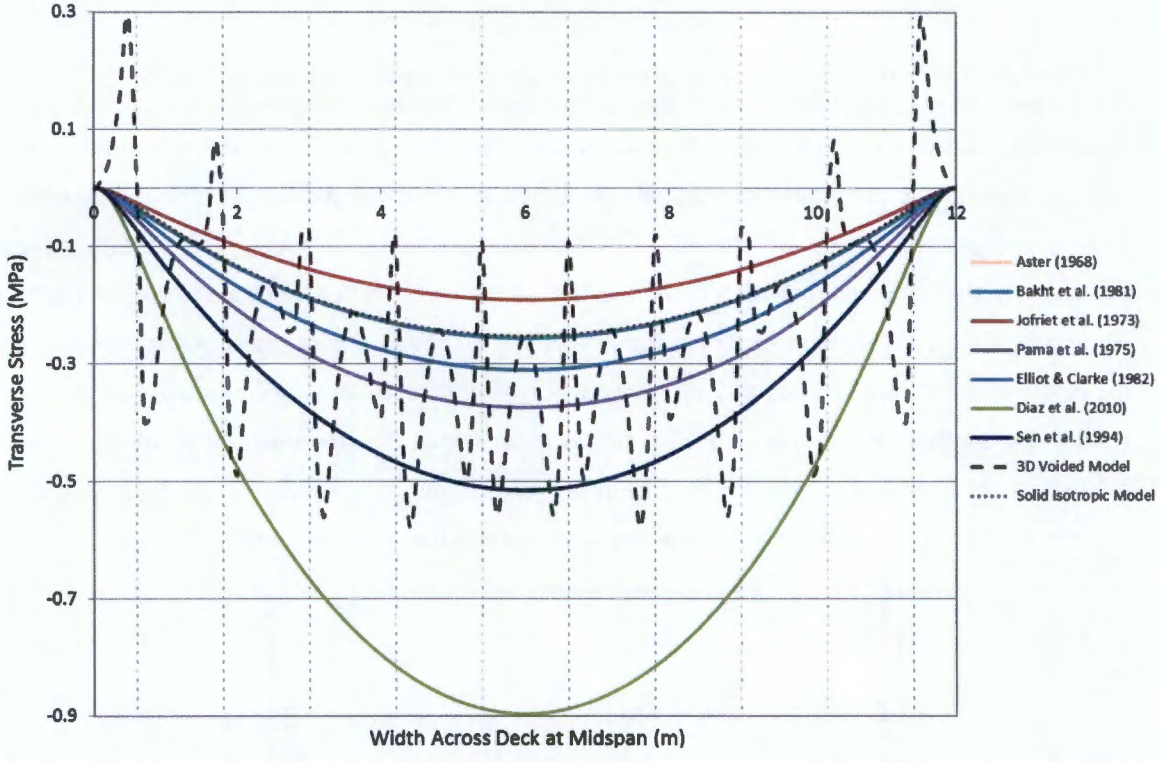

Figure 5.33 - Comparison of transverse stress results on the extreme tension fibre along a transverse line at mid-span for the 0.9 void diameter ratio models obtained using orthotropic plate theory.

Figure 5.34 shows the percentage difference between the transverse stress on the bottom fibre of the deck for each of the 2D modelling methods compared to the 3D model for the 0.9 void diameter ratio. The methods of Jofriet *et al.* (1973) and Diaz *et al.* (2010) underestimate and overestimate the transverse stress by an average of 50% and 175% respectively. The results from Diaz *et al.* (2010) results in an overestimation of the transverse stresses at the centre of the webs by 250%. The rest of the models predict stresses that are within 100% of the 3D model stresses at the centre of the bridge. The average percentage differences between the orthotropic models and the 3D voided model has increased from 20% to 100% with the increase in void diameter ratio from 0.5 to 0.9.

The greastest variations to the 3D model occurs at the centre of the voids, where the stresses are overestimated in the 2D models. The reason why the percentage variation at the centre of the voids is so large is due to the large decrease in stresses at the centre of the voids of the 3D model, which is not predicted by the 2D models. The percentage difference results of Aster (1968), Bakht *et al.* (1981), and Elliott & Clarke (1982) are skewed towards a positive value, indicating that the transverse stresses are underestimated compared to the 3D model. The negative skew of the percentage differences for Pama *et al.* (1975) and Sen *et al.* (1994) shows that these methods predict stresses which are primarily overestimated compared to the 3D model, however, they still underestimate the transverse stresses at the location of the peak stresses in the 3D model. The method of Sen *et al.* (1994) shows the least variation to the 3D model, apart from the overestimation of the stresses at the centre of the voids, which has been omitted from Figure 5.34. This overestimation is due to the large magnitude of the stress multiplier at high void diameter ratios.

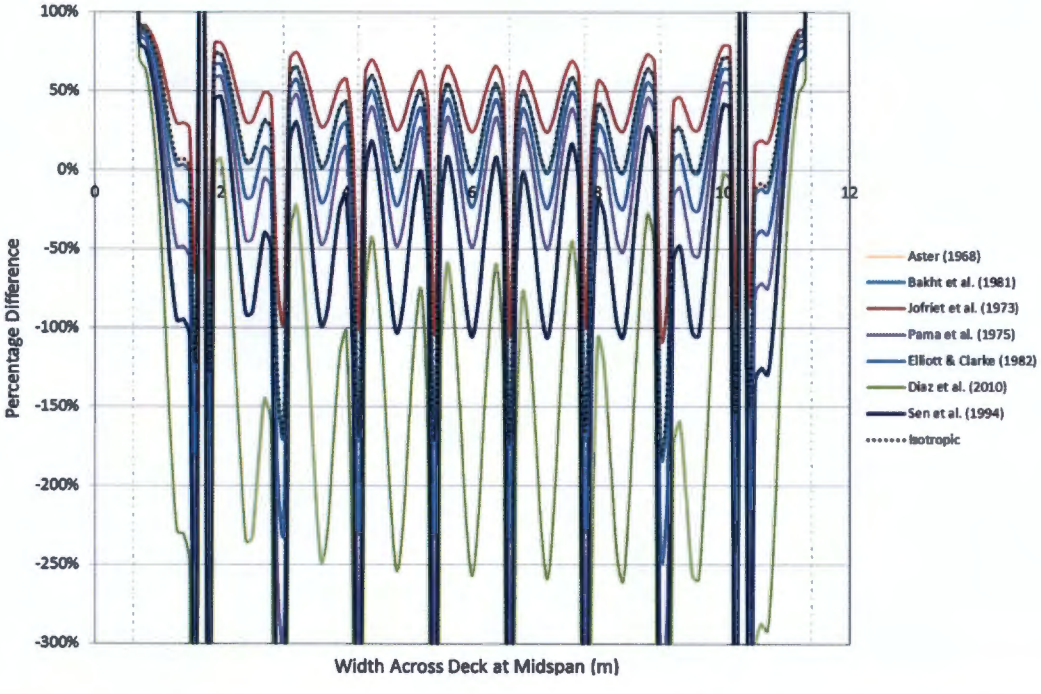

Figure 5.34 - Percentage difference comparison between the bottom fibre transverse stresses at mid-span of the 2D solid models and the 3D voided FE model for a 0.9 void diameter ratio.

Longitudinal Stress Along a Transverse Line at Mid-span

Figure 5.35 and Figure 5.36 show a comparison of the longitudinal stress results on the extreme compression fibre at mid-span for the 0.5 and 0.9 void diameter ratio models respectively. The longitudinal stresses are relatively constant across the width of the deck for each model. For the 0.5 void diameter ratio model, all of the orthotropic models predict a similar longitudinal stress distribution to each other, where the longitudinal stresses are underestimated by 2% compared to the 3D model along the width of the bridge.

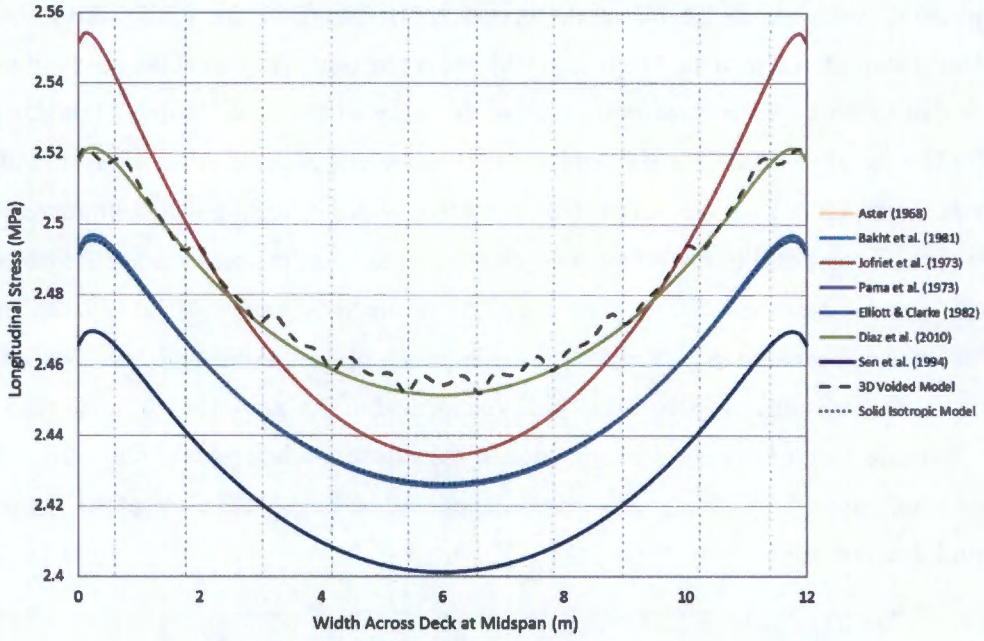

Figure 5.35 - Comparison of longitudinal stress results on the extreme compression fibre along a transverse line at mid-span for the 0.5 void diameter ratio models obtained using orthotropic plate theory.

The results of the 0.9 void diameter ratio models in Figure 5.36 show the longitudinal stresses are underestimated across the width of the bridge. The results from Aster (1968), Bakht *et al.* (1981), Pama *et al.* (1975), and Elliott & Clarke (1982), which all use a similar methodology, predict similar results with an underestimation of the longitudinal stresses by 12% compared to the 3D model. The results of Diaz *et al.* (2010) and Jofriet *et al.* (1973) predict results which are within 2% of the 3D model. The results of Sen *et al.* (1994) are shown to be the most inaccurate compared to the 3D model, with an underestimation of 25%, which is due to the stress multiplier which is less than unity.

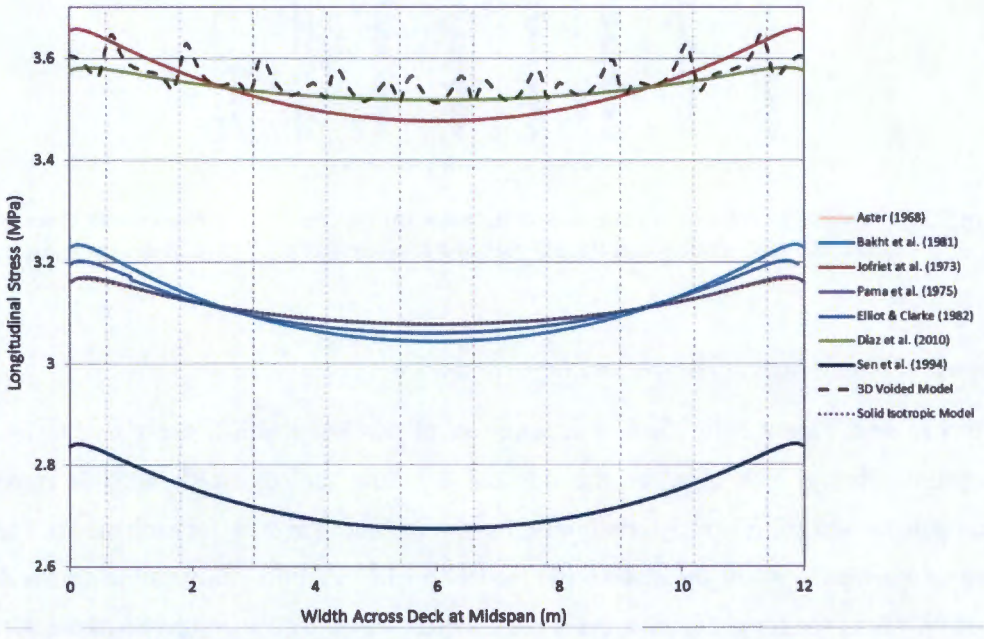

Figure 5.36 - Comparison of longitudinal stress results on the extreme compression fibre along a transverse line at mid-span for the 0.9 void diameter ratio models obtained using orthotropic plate theory.

From Figure 5.35 and Figure 5.36 it is noted that the methods of Aster (1968), Bakht *et al.* (1981), Pama *et al.* (1975), and Elliott & Clarke (1982) all produce similar results, and underestimates the longitudinal stress by 2% and 14% as the void ratio increases from 0.5 to 0.9 compared to the 3D model. These methods only account for the decrease in moment of inertia due to the voids in the slab, and do not account for the stress raising effect of the voids, resulting in an underestimation of the longitudinal stresses. The underestimation of the longitudinal stresses increases with increasing void diameter ratio, as the orthotropic behaviour becomes more pronounced.

The methods proposed by Jofriet *et al.* (1973) and Diaz *et al.* (2010) produce longitudinal stress results that compare most favourably with the 3D model, with a constant variation of 2% for void diameter ratios of 0.5 and 0.9. The methodology employed uses the same decrease in the moment of inertia as the methods above, but also allows for an increase in stress using stress multipliers. The theoretical basis of the longitudinal stress multiplier is considered sound due to the favourable comparison with the 3D model results. This excludes the multiplier proposed by Sen *et al.* (1994) which requires further consideration.

Transverse Stress Along a Longitudinal Line

Figure 5.37 and Figure 5.38 show a comparison of the transverse stress results on the extreme compression fibre along the centreline of the deck for the 0.5 and 0.9 void diameter ratio models respectively. All of the 0.5 void diameter ratio models predict a similar transverse stress distribtuion along the length of the bridge, with a percentage difference of less than 5% to the 3D model. This excludes the results from Diaz *et al.* (2010) and Jofriet *et al.* (1973) which overestimate and underestimate the transverse stresses by 34% and 14% respectively.

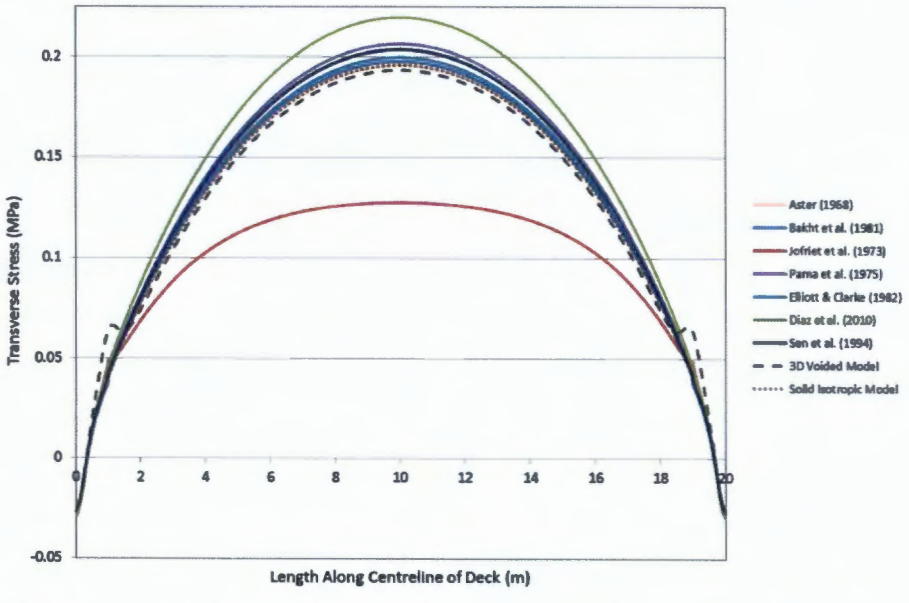

Figure 5.37 - Comparison of transverse stress results on the extreme compression fibre along the centreline of the deck for the 0.5 void diameter ratio models obtained using orthotropic plate theory.

For the 0.9 void diameter ratio models in Figure 5.38, the variation between the different models increases, resulting in a greater spread of results. All of the models overestimate the transverse stress along the length of the bridge. This is due to the fact that the stress results are given along the centreline of a web, where there is a local minimum in the 3D model stress results. As the orthotropic models average out the stresses across the width, the net stresses result in a magnitude which is greater than the local minimum over the centre of the webs.

The results from Diaz *et al.* (2010) overestimate the stresses by 342%. Aster (1968) predicts stresses similar to the isotropic model. The percentage difference of the transverse stresses to the 3D model ranges from 2% for Jofriet *et al.* (1973) to 53% for Sen *et al.* (1994). It can again be seen that the results from Jofriet *et al.* (1973) increase in accuracy when compared to the 3D model with an increasing void diameter ratio.

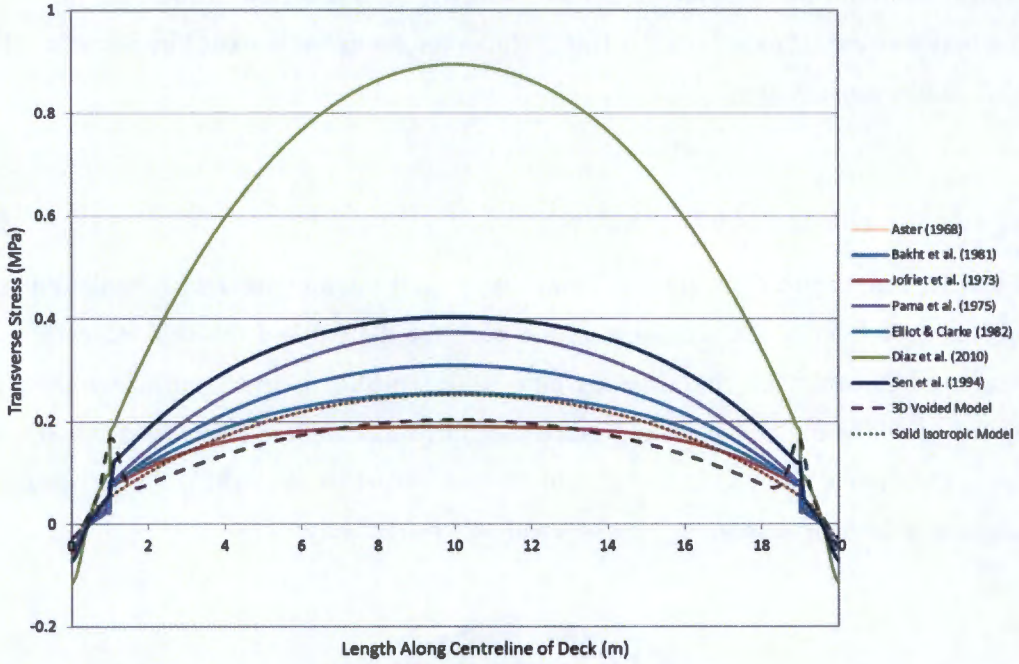

Figure 5.38 - Comparison of transverse stress results on the extreme compression fibre along the centreline of the deck for the 0.9 void diameter ratio models obtained using orthotropic plate theory.

Figure 5.39 and Figure 5.40 show a comparison of the transverse stress results on the extreme tension fibre along the centreline of the deck for the 0.5 and 0.9 void diameter ratio models respectively. As with the transverse stresses on the compression fibre, all of the 0.5 void diameter ratio models predict a similar transverse stress distribtuion along the length of the bridge, with a percentage difference of less than 8% to the 3D model. This excludes the results from Jofriet *et al.* (1973) which underestimate the transverse stresses by 37% at the centre of the bridge.

The transverse stress results from Aster (1968) and the isotropic model of the 0.9 void diameter ratio slab in Figure 5.40 are shown to compare favourably with the 3D model. This result indicates that the transverse stresses along the centreline of the deck are not affected by orthotropic behaviour, and can

be sufficiently accounted for using a decreased moment of inertia and an isotropic model. The remainder of the methods in Figure 5.40, excluding Jofriet *et al.* (1973), account for orthotropic behaviour which results in an overestimation of the transverse stresses. The results for Diaz *et al.* (2010) and Sen *et al.* (1994) are over conservative, and overestimate the transverse stresses by 250% and 79% respectively.

The overestimation of transverse stresses is the rest of the local minimum stress over the centre of the voids in the 3D model, which can be seen in the transverse distribution of stresses in Figure 5.33. It is noted that the accuracy of the orthotropic method will therefore depend on the transverse location of where the stresses are compared due to the variation of transverse stresses in the 3D model. The variation compared to the 3D model increases with increasing void diameter ratio due to decrease in minimum stress of the 3D model with increasing void diameter ratio.

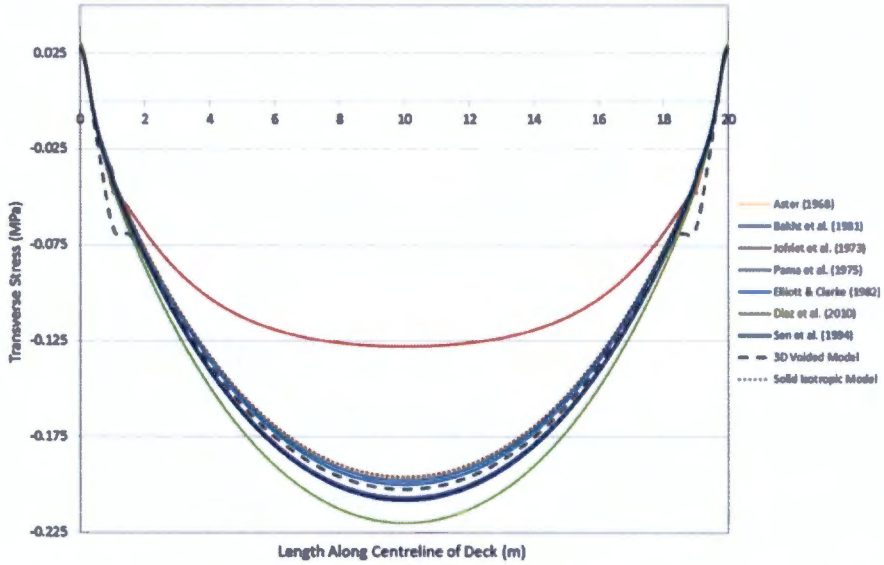

Figure 5.39 - Comparison of transverse stress results on the extreme tension fibre along the centreline of the deck for the 0.5 void diameter ratio models obtained using orthotropic plate theory.

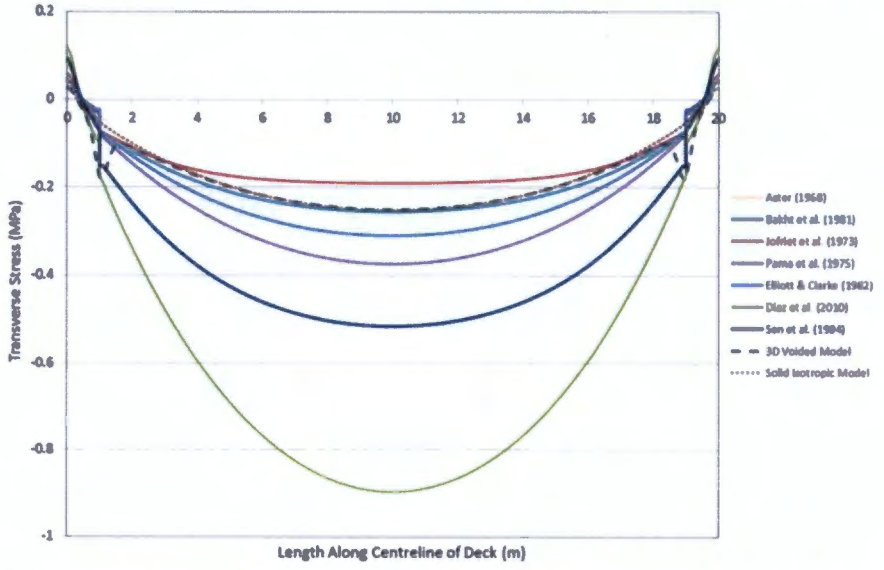

Figure 5.40 - Comparison of transverse stress results on the extreme tension fibre along the centreline of the deck for the 0.9 void diameter ratio models obtained using orthotropic plate theory.

Longitudinal Stress Along a Longitudinal Line

Figure 5.41 shows a comparison of the longitudinal stress results on the extreme compression fibre along the centreline of the deck for the 0.5 void diameter ratio models. All of the models predict a similar longitudinal stress distribtuion along the length of the bridge, which compare favourably with the 3D model.

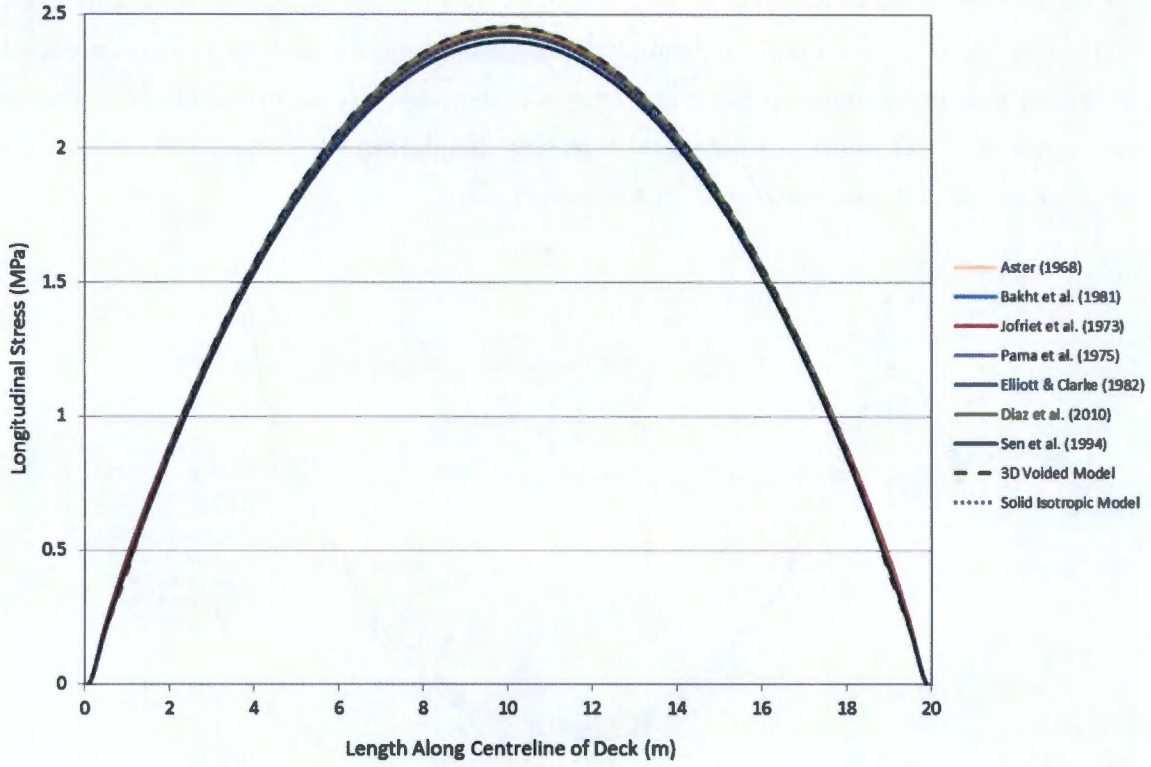

Figure 5.41 - Comparison of longitudinal stress results on the extreme compression fibre along the centreline of the deck for the 0.5 void diameter ratio models obtained using orthotropic plate theory.

Figure 5.42 shows a comparison of the longitudinal stress results on the extreme compression fibre along the centreline of the deck for the 0.9 void diameter ratio models. The variation of the longitudinal stress results has increased with increasing void diameter ratio, resulting in a greater spread of results, with the maximum variation between the results occurring at mid-span.

All of the models which account for the effect of the voids longitudinally using a reduced depth slab, namely Aster (1968), Bakht *et al.* (1982), Pama *et al.* (1975) and Elliott & Clarke (1982), result in an underestimation of 20% compared to the 3D model. This result indicates that the effect of the voids on the longitudinal stresses is more than the corresponding decrease in moment of inertia. The results from Jofriet *et al.* (1973) and Diaz *et al.* (2010), which make use of stress multipliers, are in good agreement with the 3D model, which emphasises the requirement of a stress multiplier to convert the stress from an equivalent solid slab to the actual voided slab, and to account for the stress raising effect of the voids. The results from Sen *et al.* (1994) underestimate the longitudinal stress at mid-span by 24%, which is due to the distance factor which is less than unity in the stress multiplier.

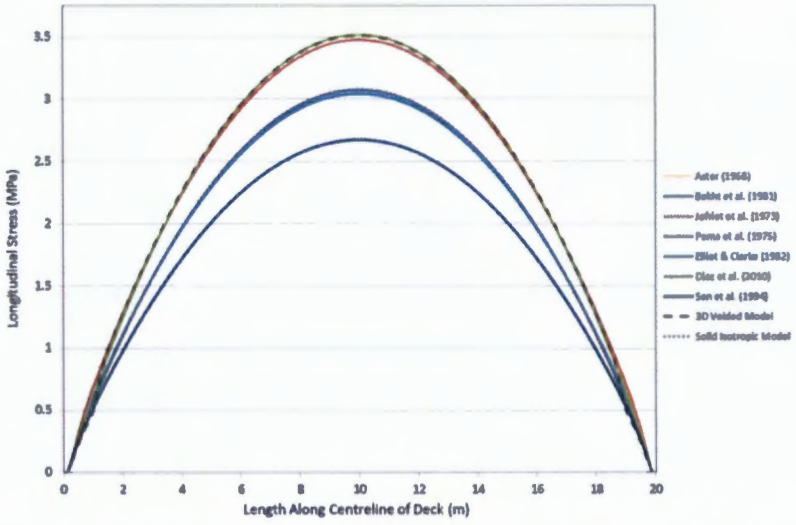

Figure 5.42 - Comparison of longitudinal stress results on the extreme compression fibre along the centreline of the deck for the 0.9 void diameter ratio models obtained using orthotropic plate theory.

Summary of Plate Parameter Model Results

The suitability of the various plate parameters methodoligies can be summarised as follows:

- Aster (1964)

The plate parameters suggested by Aster (1964) have a minimal impact on the material properties, resulting in a material that is essentially isotropic. For this reason, the results predicted using this method compared favourably with the isotropic model. This method therefore does not acount for any orthotropic behaviour, and only produces accurate results for low void diameter ratios.

- Bakht *et al.* (1981) and Elliott & Clarke (1982)

The plate parameters suggested by Bakht *et al.* (1981) and Elliott & Clarke (1982) account for increased orthotropic behaviour by decreasing the elastic modulus in the transverse direction. Both methods produce similar values for the transverse elastic modulus, with Elliott & Clarke accounting for more orthotropic behaviour. The reduced elastic modului used in these methods resulted in an increase in the transverse stresses compared to the isotropic model, which compared more favourably with the average transverse stresses of the 3D model. The transverse stress results of these methods fell in between the maximum and minimum transverse peaks of the 3D model, resulting in the stresses being overestimated and underestimated across the width of the deck. The accuracy of the results predicted using these methods decreased as the void diameter ratio increased. These methods also underestimated the longitudinal stresses for large void diameter ratios.

- Pama *et al.* (1975)

The plate parameters suggested by Pama *et al.* (1975) produced the lowest value of transverse elastic modulus, and therefore accounted for the greatest amount of orthotropic behaviour. The transverse stress results predicted using this method fell in between the maximum and minimum peaks of the

3D model, with a skew towards the maximum peak transverse stresses. Although this method resulted in an overestimation of the transverse stresses across most of the width of the deck, it resulted in an underestimation of the peak stresses of the 3D model. An underestimation of the longitudinal stresses for large void diameter ratios was also noted.

- Jofriet *et al.* (1973)

The method employed by Jofriet *et al.* (1973) does not employ an orthotropic material, but rather uses a full depth isotropic solid slab with stress multipliers to account for the effect of the voids. The results show that this method underestimates the transverse stresses across the full range of void diameter ratios tested. The underestimation of transverse stresses are a combined result of the full depth isotropic modelling method and an inaccuracy with regards to the transverse stress multiplier. This method provided an accurate prediction of the longitudinal stresses for both low and high void diameter ratios. Both stress multipliers are based on the ratio of the longitudinal moment of inertia of the voided models to the solid models. This assumption has been shown to be correct for the longitudinal stress multiplier, however, inaccurate results were obtained for the transverse stresses as the multiplier does not account for the stress raising effect of the voids. This method is not recommended for the structural idealisation of voided slabs due to the underestimation of transverse stresses.

- Diaz *et al.* (2010)

The method employed by Diaz *et al.* (2010) also uses a full depth solid isotropic slab with stress multipliers to account for the effect of the voids. The stresses predicted using this method resulted in an overestimation of the transverse stresses compared to the 3D model, which increased with an increase in void diameter ratio. The longitudinal stresses were shown to be in good agreement with the 3D model. The longitudinal and transverse stress multipliers employed are based on equilibruim of forces between a voided slab and the solid slab idealisation determined using first principles. The results show that the longitudinal stress multiplier can accurately account for the effect of the voids, while the transverse stress multiplier is overestimated. The reason for the overestimation is that the value of the transverse stress multiplier is obtained at the location of the centre of the voids. This assumption is conservative as it takes no account of the webs in between the voids, and assumes the voids are continious in the transverse direction. This method is not recommended for the structural idealisation of voided slabs as it results in over conservative results.

- Sen *et al.* (1994)

The method employed by Sen *et al.* (1994) uses a reduced depth orthotropic slab with the plate parameters suggested by Bakht *et al.* (1982). Stress multipliers are used as the authors suggest that stresses obtained from the equivalent orthotropic method are required to be converted to the actual voided slab stresses due to the change in the elastic modulus and position of the neutral axis between the two models. The transverse stress results predicted using this method compared the most

favourably with the 3D model for the range of void diameter ratios tested. The transverse stress results were also consistently more accurate to the 3D model than the results obtained by Bakht *et al.* (1982). This result suggests that the conversion of stresses between the actual and equivalent models is required. The longitudinal stresses predict using this method were shown to be inaccurate compared to the 3D model. The longitudinal stress multipliers therefore require further consideration.

The consequence of using a solid orthotropic slab to idealise a voided slab is the averaging out of the geometric properties across the width of the deck, as opposed to modelling the actual cellular form of the structure. This means that the results produced by the solid models will at some point either overestimate or underestimate the transverse stresses depending on the location that the stresses are analysed. A decision needs to be made whether the solid model should produce results that compare favourably with the peak stresses of the voided slab, and overestimate the transverse stresses throughout the rest of the deck, or whether the results predicted should be an average of the voided slab transverse stresses, with the peak stresses being accounted for in a seperate analysis.

The results from Pama *et al.* (1975) produced results that fell in between the minimum and maximum peaks of the 3D model results, and therefore provide an accurate indication of the average stresses of the voided slab. The method of Sen *et al.* (1982), which uses the same plate parameters as Bakht *et al.* (1982) in conjunction with stress multipliers, provided results that compared most favourably with the peak transverse stresses of the 3D model. Both methods are seen as producing accurate results, and the choice of the method employed will depend on whether average or peak stresses are required from the analysis.

The results in the above discussion show that a solid orthotropic slab, in conjunction with stress multipliers, present the most accurate method for simplifying the analysis of voided slabs. The method of Sen *et al.* (1994) predicted transverse stress results that compared the most favourably with the 3D model, and is therefore considered to be the most accurate method from this study. However, the underestimation of the longitudinal stresses requires further consideration.

The underestimation of longitudinal stresses occurred in all of the reduced depth orthotropic models used in this study. The methods of Jofriet *et al.* (1973) and Diaz *et al.* (2010) using full depth isotropic slabs in conjunction with stress multipliers produced accurate predictions of the longitudinal stresses. Both of these methods use a similar procedure to account for the voids in the longitudinal direction. The ratio of the decrease in moment of inertia between the voided and solid slabs is used to reduce the longitudinal elastic modulus or as a stress multiplier in the reduced and full depth models respectively, with the primary difference being the depth of the slab that is modelled. The variation in the accuracy results of these two methods highlights the need for a stress multiplier when the depth of the slab is decreased. Further research is required to derive a stress multiplier that can be employed in reduced depth orthotropic models to account for the underestimation of longitudinal stresses.

6. CONCLUSIONS & RECOMMENDATIONS

The objectives of this research were to investigate the effect of the void diameter ratio and void spacing on the structural behaviour of voided slab bridge decks, and to verify the suitability of using an orthotropic plate for their idealisation. The objectives were achieved by comparing various models based on the finite element approach.

Several finite element models were developed in ABAQUS, which consisted of a range of void diameter ratios and void spacing. In order to determine the validity of orthotropic plate idealisations, several solid orthotropic plate models were developed using the orthotropic plate parameters suggested by various authors, and compared to 3D finite element voided models.

The following conclusions were reached after evaluating the results of the finite element modelling:

i. The addition of the voids causes large variations to the transverse stress distribution from the typical parabolic stress distribution shape, leading to large peak transverse stresses in the flanges above and below the voids. These variations are due to the deformable nature of the cross-section. The voids also lead to a stress raising effect on the longitudinal stresses.

ii. The results presented have shown that the incorporation of voids begins to affect the structural behaviour of the slab once the void diameter ratio exceeds 0.6, and the orthotropic behaviour becomes considerable. The stress raising effect of the voids should be accounted for in the analysis of a voided slab once the void diameter ratio exceeds 0.6.

iii. An increase in void diameter ratio results in a rapid increase in both the longitudinal and transverse stresses. This stress increase exceeds the stress increase predicted from the decrease in moment of inertia, which shows that there is an increase in the deformation of the cross-section with an increase in void diameter ratio.

iv. It can be concluded that the optimal void diameter ratio is between 0.6 and 0.8. This range of void diameter ratios allow for greater efficiency due to reduced dead load and material use, without generating excessive stresses due to cellular distortion resulting from excessively thin and flexible flanges above and below the voids.

v. The spacing of the voids was found to have minimal effect on the stress distribution results for a logical void spacing. The optimal void spacing can therefore be chosen to allow for sufficiently sized webs between the voids. A void spacing of between 1.2m and 1.8m is recommended, depending on the void diameter, to allow for web thicknesses of between 250mm and 500mm.

These results show that the orthotropic behaviour and deformation of the cross-section are more sensitive to variations in void diameter ratio than the spacing of the voids. The void diameter ratio should

therefore form the basis of the equivalent plate parameters for the use of orthotropic plate theory. The following can be concluded regarding the comparison of the solid orthotropic plate methods:

i. The orthotropic models have been shown to be in better agreement to the 3D models than the isotropic models at predicting the transverse stresses. This can be attributed to the fact that the reduced stiffness in the transverse direction due to the presence of the voids has been considered. The orthotropic models compare more favourably with the 3D model than the isotropic models with increasing void diameter ratio.

ii. The transverse stresses predicted by the orthotropic models result in the averaging out of the effect of the voids, as geometry at particular points is not specifically modelled. Therefore the peak stresses exhibited by the 3D model are not predicted using solid orthotropic models.

iii. The method of Pama *et al.* (1975) produced results that compared the most favourably with the average transverse stress results of the 3D model. The method of Sen *et al.* (1994) produced results which compared the most favourably with the peak transverse stresses of the 3D model.

iv. The reduced depth orthotropic models resulted in an underestimation of the longitudinal stress results, which is the result of the change in neutral axis position of the reduced depth model compared to the actual voided model.

v. The method of using a reduced height orthotropic slab in combination with stress multipliers is considered to be the most accurate method of idealising voided slab bridge decks in order to account for orthotropic behaviour and deformation of the cross-section.

If a structure is to be analysed using a 2D orthotropic plate method, the equivalent plate parameters could have a significant effect on the accuracy of the analysis. These parameters should therefore model the actual structural behaviour as closely as possible without requiring complex calculations. Of the methods listed in this study, the most appropriate method for calculating the equivalent plate parameters is that of Pama *et al.* (1975), which accounts for the highest degree of orthotropic behaviour of the methods tested. However, the plate parameters suggest by Bakht *et al.* (1982) using the stress multipliers recommended by Sen *et al.* (1994) produced results which compared the most favourably with the transverse stress results of the 3D model. The analysis of a voided slab using orthotropic plate theory in combination with equivalent plate parameters can be summarised as follows:

- A solid slab is used to idealise the voided slab. The depth of the solid slab is defined to give the same moment of inertia as the voided slab.
- The rigidity of the slab in the longitudinal and transverse directions is calculated using equivalent plate parameters.
- The reduced elastic moduli in the longitudinal and transverse direction can be defined using the moment of inertia of the solid slab and the calculated rigidities.
- Stress multipliers, if required by the method employed, are then used to convert the stress results from the solid slab to the voided slab.

For the lower end of the void diameter ratios considered, the amount of orthotropic behaviour can be said to be minimal as there is little difference between the isotropic and orthotropic models. As the void diameter ratio increases, the difference between the isotropic and orthotropic models is considerable. It can therefore be concluded that when the void diameter ratio is less than 0.6, isotropic models are suitable for the idealisation of voided slabs. When the void diameter ratio is greater than 0.6, the transverse stiffness should be evaluated independently from the longitudinal stiffness, and orthotropic models are more suitable. For critical designs, or where the transverse stresses above the voids are of particular concerns, a three-dimensional analysis may be required.

The research presented in this study shows that an orthotropic plate provides reasonably accurate predictions for the structural idealisation of a voided slab. However, discrepancies between the longitudinal stresses of the 3D voided model and the 2D solid orthotropic models result in an underestimation of the actual longitudinal stresses along the length of the deck. This result highlights the need for further refinement of the orthotropic plate method. The results of this study are also limited by the scope of the research. Items which could be considered for future research, which were beyond the scope of this study, include:

- Experimental investigations in order to propose a new longitudinal stress multiplier that can be used in conjunction with the orthotropic plate methods in order to account for the underestimation of the longitudinal stresses.
- Experimental investigations where a voided model is subject to asymmetrical loading patterns which more accurately idealise real traffic loading, which has been suggested to increase the distortion of a voided cross-section.
- Research of voided slabs incorporating wide transverse cantilevers. Past research (O'Brien & Keogh, 1998) has indicated that wide transverse cantilevers have an effect on the vertical position of the neutral axis position of a voided slab. The assumption that all parts of the cross-section bend about the centroid of the deck is no longer valid, and an incorrect representation of a voided slab can be obtained using the orthotropic plate method.
- Analytical investigation to determine the effect of prestressing on the longitudinal and transverse stress distributions. Longitudinal prestressing can be used to control longitudinal tensile stresses, however minimal effect on the transverse stress distribution is expected. The effect of prestressing on the equivalent plate parameters will also be of interest.
- Experimental investigations to compare the deflections of a voided slab idealised as an orthotropic plate to a 3D finite element model.

7. REFERENCES

ABAQUS Inc (2006). *User's Manual: Version 6.6-1*. Dassaults Systems, Providence.

ABAQUS Inc (2007). *User's Manual: Version 6.7-3*. Dassaults Systems, Providence.

Abdelraouf, M., & Matlock, H. (1972). Finite-Element Analysis of Bridge Decks. *Development of Methods for Computer Simulation of Beam-Columns and Grid-Beam and Slab Systems.* Report Number 56-28, Centre For Highway Research, The University Of Texas, Austin.

Aster, H. (1968). The Analysis of Rectangular Hollow RC Slabs Supported on Four Sides. Approved doctoral thesis. Technological University of Stuttgart, Germany.

Bakht, B., Jaeger, L.G., & Cheung, M.S. (1981a). Cellular and Voided Slab Bridges. Journal of the Structural Division, American Society of Civil Engineers, 1797-1813.

Bakht, B., Jaeger, L.G., Cheung, M.S., & Mufti, A.A. (1981b). The State of the art in Analysis of Cellular and Voided Slab Bridge. Canadian Journal of Civil Engineering. 8, 376-391.

Bapat, A. (2009). *Influence of Bridge Parameters on Finite Element Modelling of Slab on Girder Bridges*. MSc Thesis, Virginia Polytechnic Institute and State University, Virginia.

Benaim, R. (2008). Solid slabs, Voided Slabs and Multi-Cell Box Girders. *Solid and Voided Slabs*, 1(11), 327-348.

Biswas, M. (1986). Precast Bridge Deck Design Systems. *PCI Journal*, 40-66.

Bokil, A.S. (2010). A Seminar on Voided Slab (BubbleDeck Technology).

BubbleDeck UK (2006). *BubbleDeck Voided Flat Slab Solutions*. Technical Manual & Documentation, 1(5).

Clark, L.A. (1983). Concrete bridge design to BS 5400, Harlow, Construction Press, 1983.

Clark, L.A., & Thorogood, P. (1994). Transverse Shear in RC Circular Voided Slabs. *The Structural Engineer, 72(12)*, 192-195.

Diaz, J., Hernandez, A., Fontan, A., & Romera, L. (2010). A Computer Code for Finite Element Analysis and Design of Post-Tensioned Voided Slab Bridge Decks with Orthotropic Behaviour. *Advances in Engineering Software, 41(2010)*, 987-999.

Donohoe, S., & Keogh, D. (2000). Orthotropic Analysis of Voided Slab Bridges. Computation Civil and Engineering, 71-79.

Elliott, G., & Clark, L.A. (1982). Circular Voided Concrete Slab Stiffnesses. Journal of Structural Division, 108(11), 2379-2393.

Faridoon, F.A.K., & Nazar, S. (2011). Development of More Robust Bridge Deck Slabs – Potentials of Ultra High Performance Fiber Reinforced Concrete. MSc Thesis, Chalmers University of Technology, Göteborg.

Fellinger, J., Stark, J., & Walraven, J. (2009). Shear and Anchorage Behaviour of Fire Exposed Hollow Core Slabs. *HERON, 50(4),* 279-301.

Gonzalez, A. (2010). Vehicle-Bridge Dynamic Interaction using Finite Element Modelling, Finite Element Analysis, David Moratal (Ed.), ISBN: 978-953-307-123-7, InTech.

Hambly, E.C. (1991). Bridge Deck Behaviour. ISBN 0 412 13190 0. 1st Edition.

Ibrahim, A.M., Ali, N.K., & Salman, W.D. (2013). Flexural Capacities of Reinforced Concrete Two-Way BubbleDeck Slabs of Plastic Spherical Voids. *Diyala Journal of Engineering Sciences, 6(2)*, 9-20.

Jackson, P. (2008). Design of Reinforced Concrete Bridges. *ICE Manual of Bridge Engineering*, 2nd Edition, Chapter 7, 49-112, ISBN 978-0-7277-3452-5.

Jofriet, J.C., McNeice, G.M., & Csagoly, P. (1973). Finite Element Analysis of Prestressed Concrete Voided Bridge Decks. *PCI Journal*, 51-66.

Jukic, A., & Ekfeldt, K. (2012). *Concrete Bridge Design with FEM: A Comparative Analysis Between 2D and 3D Frame Models*. MSc Thesis. Chalmers University of Technology, Göteborg,.

Kim, G.C., & Kang, J.W. (2012). Calculation of Voided Slabs Rigidities. *World Academy of Science, Engineering and Technology*, 65(1), 691-694.

Lai, T. (2010). Structural Behaviour of BubbleDeck Slabs and their Application to Lightweight Bridge Decks. MSc Thesis, Massachusetts Institute of Technology, Massaschusetts.

Latimer, M.G. (2011). Superstructures. SANRAL Construction Monitoring Manual for Bridges and Structures, 1st Edition, Chapter 12.

Mota, M. (2010). Voided Slabs: Then and Now. Concrete International, 41-45.

O'Brien, E.J., & Keogh, D.L. (1998). Upstand Finite Element Analysis of Slab Bridges. *Computers and Structures*, 69(6), 671-683.

O'Brien, E.J., Keogh, D.L. (1999). Bridge Deck Analysis. ISBN 0-419-22500-5

Oline, L., & Sen, R. (1987). Analytical and Experimental Evaluation of Stiffness Parameters of Voided Concrete Slab Bridges. Progress Report No. 4, Department of Civil Engineering and Mechanics, University of South Florida.

Pajari, M. (2009). Web Shear Failure in Prestressed Hollow Core Slabs. *Journal of Structural Mechanics, 42(4)*, 207-217.

Pama, R.P., Imsom-Somboon, S., & Lee, S.L. (1975) Elastic Rigidities of Circularly Voided Slabs. Building Science. 10, 207-212.

Qaqish, M., Akawwi, E., & Fadda, E. (2009). Comparison between Computed Shearing Forces by AASHTO Specifications and Finite Element Method of Two Continuous Spans of Voided Slab Bridge. WSEAS Transactions on Information Science and Applications, 4(6), 621-636.

Scollard, C.R., & Bartlett, F.M. (2004). Rehabilitation Criteria for Post-Tensioned Voided Slab Bridges. *Canada Journal Civ. Eng., 31(2004)*, 977-987.

Sen, R., Issa, M., Gergess, A., & Sun, X. (1993). Collapse Load Analysis of Continuous Post-Tensioned Voided Slab Bridge Models. *Journal of Structural Engineering, 119(6)*, 1825-1843.

Sen, R., Issa, M., Sun, X., & Gergess, A. (1994). Finite Element Modelling of Continuous Post-Tensioned Voided Slab Bridges. *Journal of Structural Engineering, 120(2)*, 651-667.

Shanmugan, N.E., & Narayanan, R. (2008). Structural Analysis, *ICE Manual of Bridge Engineering*, 2nd Edition, Chapter 3, 49-112, ISBN 978-0-7277-3452-5.

Timoshenko, S., Woinowsky-Krieger, S. (1959). Theory of Plates and Shells. 2nd Edition, McGraw-Hill Book Company, ISNB 0-07-064779-8.

Ward, K., & Cassel, A.C. (1974). Torsional Properties of Voided Slabs. Unpublished Report. Department of Civil Engineering, Imperial College, University of London, England.